



Durham E-Theses

Electroluminescence in zinc selenide

zsan, M. E.

How to cite:

zsan, M. E. (1976) *Electroluminescence in zinc selenide*, Durham theses, Durham University. Available at Durham E-Theses Online: <http://etheses.dur.ac.uk/8140/>

Use policy

The full-text may be used and/or reproduced, and given to third parties in any format or medium, without prior permission or charge, for personal research or study, educational, or not-for-profit purposes provided that:

- a full bibliographic reference is made to the original source
- a [link](#) is made to the metadata record in Durham E-Theses
- the full-text is not changed in any way

The full-text must not be sold in any format or medium without the formal permission of the copyright holders.

Please consult the [full Durham E-Theses policy](#) for further details.

ELECTROLUMINESCENCE IN ZINC SELENIDE

BY

M. E. ÖZSAN

Presented in candidature for the degree of

Doctor of Philosophy

in the

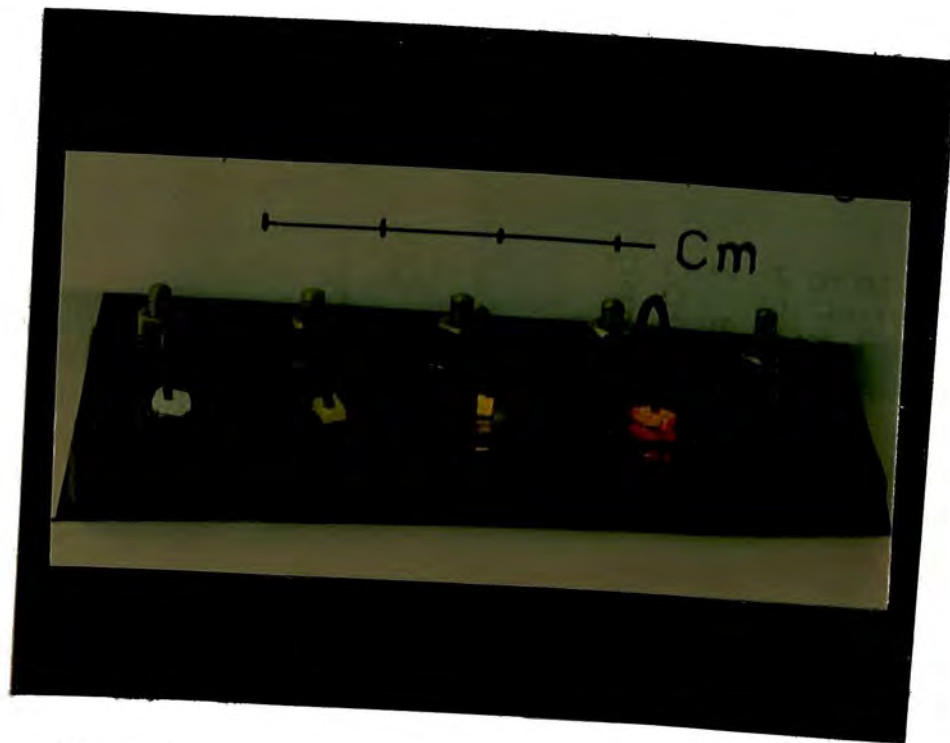
University of Durham

The copyright of this thesis rests with the author.
No quotation from it should be published without
his prior written consent and information derived
from it should be acknowledged.

May 1976



To my Parents



The photograph shows

a Red $\text{ZnSe:Mn,Cu,Cl,Zn,Al}$

a Yellow ZnSe:Mn,Cl,Zn

a Green $\text{ZnS}_{0.6}\text{Se}_{0.4}:\text{Zn,Al}$, and

a Blue ZnS:I,Zn,Al

light emitting diode.

ACKNOWLEDGEMENTS

I am most grateful to my supervisor, Dr. J. Woods, for his enthusiastic guidance and assistance during the course of this research project. I have also benefitted from many discussions with Dr. M.J. Morant.

I would like to thank Professor D.A. Wright for allowing me to use the facilities of the department and the workshop staff for their assistance. Thanks are due to Mr. N. Thompson for growing the crystals studied in this project.

I would also like to thank the British Council and the Turkish Ministry of National Education (M.E.B.) for the award of a grant.

Finally I would like to express my gratitude to my parents for their many sacrifices and their encouragement over the years.

ABSTRACT

The main purpose of the research reported was to study zinc selenide crystals with the object of developing red and yellow light emitting devices. Zinc sulphide and zinc sulpho-selenide mixed crystals were also studied to extend the colour range to green and blue.

Most of the electroluminescent devices were of the Schottky barrier type and were prepared on chemically etched crystal surfaces. Electroluminescence (EL) was always observed when such devices were reverse biased. Forward bias EL was only observed in diodes which contained a relatively thick ($\sim 200 \text{ \AA}$) semi-insulating layer under the Schottky contact.

Almost all ZnSe diodes free of intentionally added luminescent centres emitted a yellow-orange band (self-activated) when biased in the reverse or forward directions. The optimum brightness (e.g. 800 Ft-L with a conversion power efficiency of $4 \times 10^{-3} \%$) in the yellow region of the spectrum was obtained with reverse biased ZnSe:Mn diodes. The characteristic manganese emission in EL occurred at 5785 \AA , but was usually found to be swamped and broadened by the onset of self-activated emission which lies in the same region of the spectrum. A good red emission at 6400 \AA was obtained from reverse biased ZnSe:Mn,Cu,Cl diodes with a brightness of 200 Ft-L and a conversion power efficiency of $1.5 \times 10^{-3} \%$.

Free exciton and pair emission in the blue have also been observed in undoped forward biased ZnSe diodes. These emissions have been studied in the temperature range from 20 - 360 K. Excitons became bound to neutral donors, or acceptors at temperatures below 65 K. The pair emission observed at low temperatures was associated with donor and acceptor levels with ionization energies around 26 meV and 122 meV respectively.

The S.A. yellow-orange EL from ZnSe shifted to green and then to blue as the selenium was replaced by sulphur to make mixed Zn(S,Se) crystals. Green light emitting devices were prepared on mixed crystals containing 60% sulphur. However to obtain blue emitting devices, the sulphur concentration required was 90% or more. An optimum brightness of 200 - 300 Ft-L was achieved in the green (5450 Å) and the blue (4800 Å) with conversion power efficiencies of about $1 \times 10^{-3}\%$.

Different types of ZnSe:Mn electroluminescent diode have been run on life test for periods up to 1000 hours. It is shown that two major physical changes occur during ageing; the width of the semi-insulating interfacial layer increases and the uncompensated donor concentration in the barrier region decreases.

CONTENTS

CHAPTER 1	INTRODUCTION	1
CHAPTER 2	ELECTROLUMINESCENCE IN II-VI COMPOUNDS	5
2.1	ELECTRONIC BAND STRUCTURE	5
2.2	ELECTRICAL PROPERTIES	8
2.2.1	Introduction	8
2.2.2	Imperfections and Self-compensation	8
2.2.3	Effective Carrier Masses	10
2.2.4	Charge Carrier Mobility	10
2.3	LUMINESCENT PROPERTIES	12
2.3.1	Introduction	12
2.3.2	Edge Emission	13
2.3.3	Edge Emission in Zinc Selenide	17
2.3.4	The Deep Centre Luminescence	18
2.3.5	Deep Centre Luminescence in ZnSe, ZnS and Zn(S,Se)	23
2.4	ELECTROLUMINESCENCE	27
2.4.1	Introduction	27
2.4.2	Mechanisms of Electroluminescence in II-VI Compounds	27
2.4.3	The Schottky Barrier	31
2.4.4	Current Transport Processes in Schottky Barriers	39
2.4.5	Experimental determination of the barrier height in Schottky diodes	43
2.5	DIRECT CURRENT ELECTROLUMINESCENCE IN THE SINGLE CRYSTALS OF ZnS, Zn(S,Se) AND ZnSe	45
CHAPTER 3	CRYSTAL GROWTH	50
3.1	INTRODUCTION	50
3.2	CRYSTAL STRUCTURE AND BONDING IN II-VI COMPOUNDS	50
3.3	CRYSTAL GROWTH	51
3.3.1	Preparation and purification of the Starting Material	53
3.3.2	Vapour Growth	54
3.3.3	High Temperature Growth	56
3.3.4	Chemical Transport	56
3.4	HEAT TREATMENT FOR EXTRACTION OR INTRODUCTION OF 'IMPURITIES'	57
3.5	X-RAY POWDER ANALYSIS	59
3.6	RESULTS	60
3.7	DISCUSSION	62



CHAPTER 4	EXPERIMENTAL PROCEDURE	65
4.1	INTRODUCTION	65
4.2	DEVICE PRODUCTION	65
4.2.1	Surface Treatment	65
4.2.2	Ohmic Contacts	66
4.2.3	Schottky Barrier Formation	67
4.2.4	Vacuum System and Metal Film Deposition	67
4.3	ELECTRICAL MEASUREMENTS	69
4.3.1	Current-Voltage Characteristics as a function of emitted light (luminance) of the diodes	69
4.3.2	Capacitance - Voltage measurements	70
4.4	OPTICAL MEASUREMENTS	71
4.4.1	Apparatus	71
4.4.2	Emission Spectra	73
4.4.3	Photoresponse and Excitation Spectra	74
4.5	THE POWER EFFICIENCY OF THE DIODES	75
CHAPTER 5	ELECTRICAL PROPERTIES OF Au-ZnSe DIODES	76
5.1	INTRODUCTION	76
5.2	SURFACE PREPARATION	76
5.3	OHMIC CONTACTS	77
5.4	PHOTORESPONSE MEASUREMENTS	78
5.4.1	Photoresponse of Au-ZnSe Diodes	78
5.5	CAPACITANCE-VOLTAGE MEASUREMENTS	81
5.5.1	Introduction	81
5.5.2	C-V measurements on Au-ZnSe diodes doped with donors	82
5.5.3	C-V Results on Au-ZnSe diodes containing donors and acceptors	83
5.5.4	C-V Variation with Temperature	84
5.5.5	Surface Leakage and C-V Characteristics	86
5.6	THE FREQUENCY DEPENDENCE OF C-G-V PLOTS AND SURFACE STATES	86
5.6.1	Frequency Dependence of C-G-V Characteristics	86
5.6.2	G-V Measurements	89
5.7	DEVICE PARAMETERS	91
5.7.1	Introduction	91
5.7.2	The Diffusion Potential V_{BO}	91
5.7.3	The Depletion Layer Width, W	92
5.7.4	Maximum Electrical Field, E_{max} , and the Image Force Lowering $\Delta\phi$, at the Interface	92
5.7.5	Interfacial Layer Thickness, d	93
5.8	CURRENT VOLTAGE (I-V) CHARACTERISTICS	95
5.8.1	Introduction	95
5.8.2	Forward-Bias I-V Characteristics	95
5.8.3	The Reverse Current-Voltage Characteristics	98

5.9	AGEING AND THE ELECTRICAL PROPERTIES OF Au-ZnSe DIODES	100
5.9.1	Long Term Ageing in Au-ZnSe:Mn,Cl,Zn Prepared on Cleaved Surfaces of ZnSe	101
5.9.2	Long Term Ageing of Au-ZnSe Diodes Prepared on Chemically Cleaned Surfaces	103
5.9.3	Ageing a Chemically Cleaned Diode with thin slices cleaved from the sides	106
5.10	DISCUSSION	107
5.10.1	Ohmic Contacts	107
5.10.2	Photoresponse Measurements	108
5.10.3	Capacitance-Conduction-Voltage Measurements	109
5.10.4	The Current-Voltage Characteristics	111
5.10.5	Barrier Height	113
5.10.6	A Possible Model for the Au-ZnO-ZnSe System	114
5.10.7	Ageing Effects	115
CHAPTER 6	ELECTROLUMINESCENCE IN ZnSe DOPED WITH SUBSTITUTIONAL DONORS	118
6.1	INTRODUCTION	118
6.2	EL AND PL OF SCHOTTKY DIODES PREPARED ON NOMINALLY PURE ZnSe	118
6.2.1	Forward bias EL and PL	118
6.2.2	Reverse bias EL	124
6.3	EL AND PL FROM A ZnSe DIODE DOPED WITH INDIUM DONORS	125
6.3.1	Forward bias electroluminescence (FEL) and photoluminescence (PL)	125
6.3.2	Reverse bias electroluminescence (REL)	128
6.4	EL AND PL IN ZnSe CONTAINING ALUMINIUM OR GALLIUM DONORS ONLY	129
6.4.1	Forward EL and PL	130
6.4.2	Reverse bias EL	132
6.5	EL AND PL IN ZnSe CONTAINING CHLORINE OR IODINE ONLY	132
6.5.1	Forward bias EL and PL	133
6.5.2	Reverse bias EL	134
6.6	DISCUSSION	135
6.6.1	Mechanism for Electroluminescence	135
6.6.2	Spectral Distribution of the Luminescence	137

CHAPTER 7	ELECTROLUMINESCENCE IN ZnSe DOPED WITH LUMINESCENT CENTRES, i.e. MANGANESE OR COPPER	145
7.1	INTRODUCTION	145
7.2	ELECTROLUMINESCENCE AND PHOTOLUMINESCENCE OF ZnSe CONTAINING MANGANESE	145
7.2.1	Forward bias electroluminescence (FEL) and photoluminescence (PL)	146
7.2.2	Reverse bias Electroluminescence	147
7.2.3	Light output as a junction of temperature	150
7.2.4	Ageing of the light output in REL of ZnSe:Mn,Cl,Zn diodes	150
7.3	THE EFFECTS OF ADDING ALUMINIUM TO ZnSe:Mn,Cl DIODES	152
7.4	ELECTROLUMINESCENCE AND PHOTOLUMINESCENCE IN ZnSe CRYSTALS DOPED WITH COPPER AND ALUMINIUM	153
7.4.1	Forward electroluminescence and photoluminescence	154
7.4.2	Reverse bias electroluminescence	155
7.5	ELECTROLUMINESCENCE AND PHOTOLUMINESCENCE IN ZnSe CONTAINING MANGANESE, COPPER AND CHLORINE	155
7.5.1	Forward bias electroluminescence and photoluminescence	156
7.5.2	Reverse bias electroluminescence (REL)	157
7.6	DISCUSSION	158
7.6.1	Mechanism for EL	158
7.6.2	Luminescence Transitions in Diodes containing Manganese	160
7.6.3	The Effect of Doping ZnSe:Mn,Cl with Aluminium	163
7.6.4	Luminescence Transitions in Copper Doped Samples	163
7.6.5	Luminescence Transitions in ZnSe:Mn,Cu,Cl,Zn+Al Diodes	164
7.6.6	Ageing Effect in ZnSe:Mn,Cl,Zn Diodes	165
CHAPTER 8	ELECTROLUMINESCENCE IN SOLID SOLUTIONS OF Zn(S,Se) CRYSTALS	167
8.1	INTRODUCTION	167
8.2	SOME ELECTRICAL PROPERTIES OF Zn(S,Se) ELECTROLUMINESCENT DEVICES	167
8.2.1	Preparation of Schottky Barriers	167
8.2.2	Photoresponse and C-V measurements	169
8.3	EL AND PL IN ZnS_xSe_{1-x} MIXED CRYSTALS	171
8.3.1	Nominally pure ZnS_xSe_{1-x} crystals	171
8.3.2	Mixed crystals doped with aluminium or iodine	172

8.3.3	Mixed Crystals doped with Iodine and Aluminium	175
8.3.4	Mixed Crystals containing Manganese as a Luminescent Centre	179
8.4	THE MAINTENANCE OF Zn(S,Se) DIODES	181
8.5	DISCUSSION	181
8.5.1	Electrical Properties	181
8.5.2	Mechanism of EL	185
8.5.3	Luminescent transitions involved in ZnS Se _x diodes	187
CHAPTER 9	CONCLUSION	191
9.1	SUMMARY OF RESULTS	191
9.2	FUTURE WORK	196
REFERENCES		198

CHAPTER 1

INTRODUCTION

Irradiation of matter with electromagnetic radiation or high energy particles can lead to a variety of excitation processes. Extra energy can be transferred and stored to cause either electronic excitation, or atomic and structural changes within the matter. In the former process electrons are excited to higher energy states. Once such excited states are obtained the extra stored energy is relaxed either by electrons returning to lower energy states and emitting radiation or by generating phonons.

The term luminescence in general refers to the radiation of visible light which is not purely thermal in origin as in incandescence. The emission is called cathodoluminescence or radioluminescence when the excitation is achieved by bombardment with high energy electrons or nuclear particles. In chemiluminescence the excitation energy is derived from chemical reactions (e.g. dry electrolysis) at solid phase boundaries. In bioluminescence the light is emitted as a result of biological excitation. Triboluminescence can occur as a result of grinding or abrading solids. Photoluminescence occurs when the excitation is provided by photons with energies ranging from x-rays to infrared radiation. Electroluminescence (EL) which will be the main concern in this thesis is the direct conversion of electrical energy into visible radiation. Here the electrical energy derived from the applied field is used to excite the electrons to higher energetic states and the light is emitted after the radiative recombination process. Electrical excitation and radiative recombination are the two essential parts of EL.

The first observation of the phenomenon of EL was made by Round (1907) using a point contact on SiC. Lossev (1923) repeated this

observation and made an extensive study on SiC lasting many years. AC EL in powdered ZnS was discovered by Destriau (1936). The mechanism of EL in II-VI compounds is still not fully understood. However, the discovery and studies made in the 1950's of the basic principles of carrier injection at p-n junctions in Si and Ge have added much to our understanding of EL mechanisms. Lehovc et al (1951, 1953) described the light emission from SiC in terms of the injection of carriers across a p-n junction. In the meantime single crystals of III-V compounds have become attractive as EL diodes and injection laser sources. Today the III-V compounds and their ternary alloys (e.g. GaAs, GaP and $\text{GaAs}_x\text{P}_{1-x}$) form the most efficient light emitting diodes yet developed and marketed. Destriau type EL devices have proved less attractive mainly because they operate at high alternating voltages and have so far failed to achieve high brightness, good efficiency and good maintenance. However, interest in d.c. EL panels, which were neglected in the fifties, has recently been stimulated by the work of Vecht et al (1969).

Several II-VI compounds have long been used as cathodo- and photoluminescence phosphors. The luminescent centres in these direct gap materials are capable of producing radiation with wavelengths ranging from the ultra-violet to the infrared. Since the carrier mobilities in II-VI compounds are relatively high, the chalcogenides of zinc and cadmium and their solid solutions, have long been regarded as promising materials for efficient conversion of electrical energy to light. However, except for ZnTe which is p-type and CdTe which can be n- or p-type, all the other members of the II-VI group are inherently n-type and cannot readily be made p-type. Therefore it is difficult, if not impossible, to prepare p-n junctions from II-VI compounds with band gaps greater than 2.2 eV. EL from compounds with one type of conductivity mechanism can, however, be obtained by exploiting heterojunction and tunnel or

Schottky barrier devices, (Fischer, 1966). Unfortunately these structures cannot compete with p-n junction EL devices.

ZnSe and ZnS with band gaps at room temperature of 2.67 and 3.6 eV respectively, have been of considerable scientific and technological interest as possible materials from which to produce low cost, EL devices. In the present work, red, yellow, green and blue emitting Schottky barrier devices (as shown in the frontispiece) have been produced using single crystals of ZnSe, and ZnS and Zn (S,Se), and their electrical and luminescent properties are described in this thesis.

Following this brief introduction, some of the more general electrical and luminescent properties of the semiconductors of interest are discussed briefly in Chapter 2.

The single crystals of ZnSe, Zn(S,Se) and ZnS used for device preparation were all grown in this laboratory. Therefore, the purification of the starting material, techniques of crystal growth, heat treatment and measurement of lattice parameters have been described in Chapter 3.

In Chapter 4, the production of electroluminescent devices and the experimental techniques used in making the electrical and optical measurements are described in detail.

In Chapter 5, a detailed account of the electrical properties of ZnSe Schottky barrier and MIS devices and the effects of ageing on the device parameters is given.

In Chapter 6, the electroluminescent and photoluminescent characteristics of nominally pure ZnSe and ZnSe doped with substitutional donors are reported.

In Chapter 7, the electroluminescence in ZnSe doped with luminescent activators (e.g. manganese or copper or both) is described.

The effects of ageing on the light output of manganese doped ZnSe diodes are also discussed in detail.

In Chapter 8, the electrical, photoluminescent and electroluminescent properties of solid solutions of mixed $\text{Zn S}_x\text{Se}_{1-x}$ crystals are described.

Finally the present work is summarised in Chapter 9 and some suggestions for future work are put forward.

CHAPTER 2

ELECTROLUMINESCENCE IN II-VI COMPOUNDS

The electrical and luminescent, and hence the electroluminescent, properties of these II-VI compounds are strongly influenced by the presence of impurities.

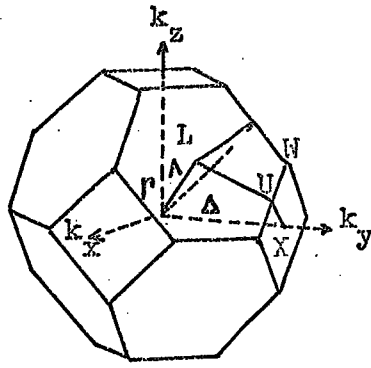
In the following sections a brief discussion will be given of the energy-band structures and the electrical, luminescent and electroluminescent properties of some of the II-VI compounds with special emphasis on ZnSe, ZnS and Zn (S,Se).

2.1 ELECTRONIC BAND STRUCTURE

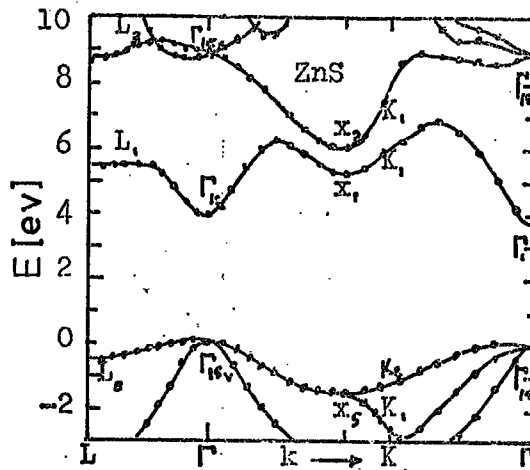
The electrical and luminescent properties of ZnSe and ZnS are strongly dependent on the structure of the energy bands of the materials. Both zinc selenide and zinc sulphide can crystallise in the stable zincblende and wurtzite structures. This is a result of tetrahedral bonding and covalency in most of the II-VI compounds. In this thesis special emphasis will be placed on the properties of cubic materials.

In general optical measurements provide the major data for energy band calculations. The band structures of some of the II-VI compounds have been calculated by various methods, including the empirical pseudopotential method by Cogen and Bergstresser (1966), Bergstresser and Cohen (1967). These authors described the band structures of 14 semiconductors with the diamond or zinc blende structures, including ZnS, ZnSe and ZnTe, for which they made use of the experimental work on photoemission by Aven et al (1961) and Cardona (1961).

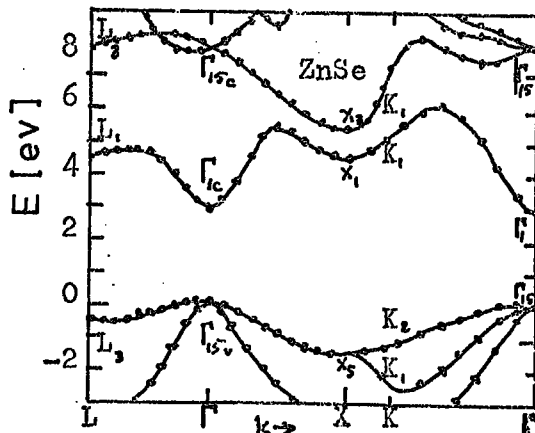
The Brillouin zone for the zinc blende lattice can be taken to be a truncated octahedron, see Figure 2.1(a). The high symmetry points are those at the zone centre (Γ) and the intersections (L,X,K) of the symmetry



(a) - The Brillouin zone for the lattice with the translational symmetry of a face centred cubic lattice



(b) - The band structure of ZnS



(c) - The band structure of ZnSe

Fig. 2.1 (a) The Brillouin zone, (b) & (c) Energy-band structure of ZnS and ZnSe along the (1,1,1), The (1,0,0) and the (1,1,0) symmetry axes calculated by pseudopotential method by Cohen and Bergstresser, 1966.

axes $(1,1,1)$, $(1,0,0)$ and $(1,1,0)$ with the zone faces. The shapes of the energy bands, i.e. the variation of E with K , for cubic ZnS and ZnSe along the $(1,1,1)$, $(1,0,0)$ and $(1,1,0)$ axes according to Cohen and Bergstresser (1966) are shown in Figure 2.1(b,c). The common features of these bands are that they all have two minima, Γ_{1c} and Γ_{15c} , in the conduction band at $k=0$. Γ_{1c} is thought to be made up primarily of anion s-like levels. However, the highest lying valence band level, Γ_{15v} , and the deepest lying conduction band level, Γ_{15c} , are thought to be made up of p-like levels. The subscripts c and v denote the conduction and the valence bands respectively. The other minima in the conduction band lie on the symmetry axes. These are L_1 and L_3 on the $(1,1,1)$ and X_1 and X_3 on the $(1,0,0)$ symmetry axes respectively. However, the energy separation is rather large along the $(1,0,0)$ symmetry axis. As in the rest of the II-VI compounds ZnS, ZnSe and ZnTe have their minimum vertical energy separation between the conduction and the valence bands (or direct bandgap) at the centre of the Brillouin zone (at $k=0$). Generally in II-VI compounds the band gaps tend to decrease with increasing atomic number. As one moves from the lighter to the heavier semiconductors (i.e. from ZnS to ZnTe) the Γ_{1c} energy level decreases rapidly in energy. Also the L_1 level decreases in energy with respect to X_1 . Table 2.1 lists various values of the theoretical energy levels in the energy band structures of cubic ZnS and ZnSe as calculated by Cohen and Bergstresser (1966). These values were found to be compatible with the values of the energy levels obtained by Stukel et al (1969) using self-consistent OPW and refined orthogonalised OPW energy band models.

Spin-orbit interaction in the zinc-blende structure has the profound effect of removing the degeneracy of the valence band (see for

LEVEL	ZnS	ZnSe
Γ_{15c}	8.9	7.9
Γ_{1c}	3.7	2.9
Γ_{15v}	0.0	0.0
X_{3c}	6.0	5.4
X_{1c}	5.2	4.5
X_{5v}	-1.5	-1.5
$X_{3v} - X_{5v}$	7.5	6.9
$X_{1c} - X_{5v}$	6.7	6.0
$X_{3c} - X_{1c}$	0.8	0.9
L_{3c}	8.7	7.9
L_{1c}	5.3	4.5
L_{3v}	-0.5	-0.5
$L_{3c} - L_{3v}$	9.2	8.4
$L_{1c} - L_{3v}$	5.8	5.0

TABLE 2.1: Theoretical energy level (eV) schemes for cubic ZnS and ZnSe (Cohen and Bergstresser, 1965)

example Permenter, 1955). The most important splitting is the splitting of the six-fold degenerate state Γ_{15v} at $k=0$, (see for example Segal, 1967). The splitting can be seen as two near-parabolic bands, Γ_7 and Γ_8 , with different curvatures touching at the centre of the Brillouin zone. As a consequence the four-fold degenerate state Γ_8 ($J=\frac{3}{2}$) state is split by an amount Δ_{SO} from the lower two-fold Γ_7 ($J=\frac{1}{2}$) state at $k=0$ (see Figure 2.2). The Γ_8 level splits into two bands V_1 and V_2 , which are the heavy and light hole bands respectively. The irreducible representations for the single groups (without spin) are given in brackets, the others are those for the double group. The broken curves in the upper valence band represent the effects of the small linear terms which reflect the lack of inversion symmetry in these materials.

Some of the experimental data relating to the band structure of ZnS and ZnSe are given in Table 2.2. Aven et al (1961) studied exciton absorption in ZnSe. They found very narrow and intense exciton absorption bands just below the absorption edge, indicating a direct band gap. The results of Reynolds et al (1961) on the edge emission of ZnSe were explained in terms of a direct band gap. Hite et al (1967), who studied the absorption edge and exciton emission in ZnSe found no evidence of indirect excitonic transitions. Furthermore, the electrical measurements of Aven and Segal (1963) and of Marple (1964) on n-type ZnSe could only be explained in terms of a direct band gap at $k=0$.

The band gap properties of ZnS have not been studied extensively. Reflectivity measurements at Lempicki et al (1961), exhibited characteristic exciton lines. The splitting of spectral lines in a magnetic field (Wheeler and Miklosz, 1964) suggested the material had a direct band gap at $k=0$.

The band structures of the various solid solutions which can be

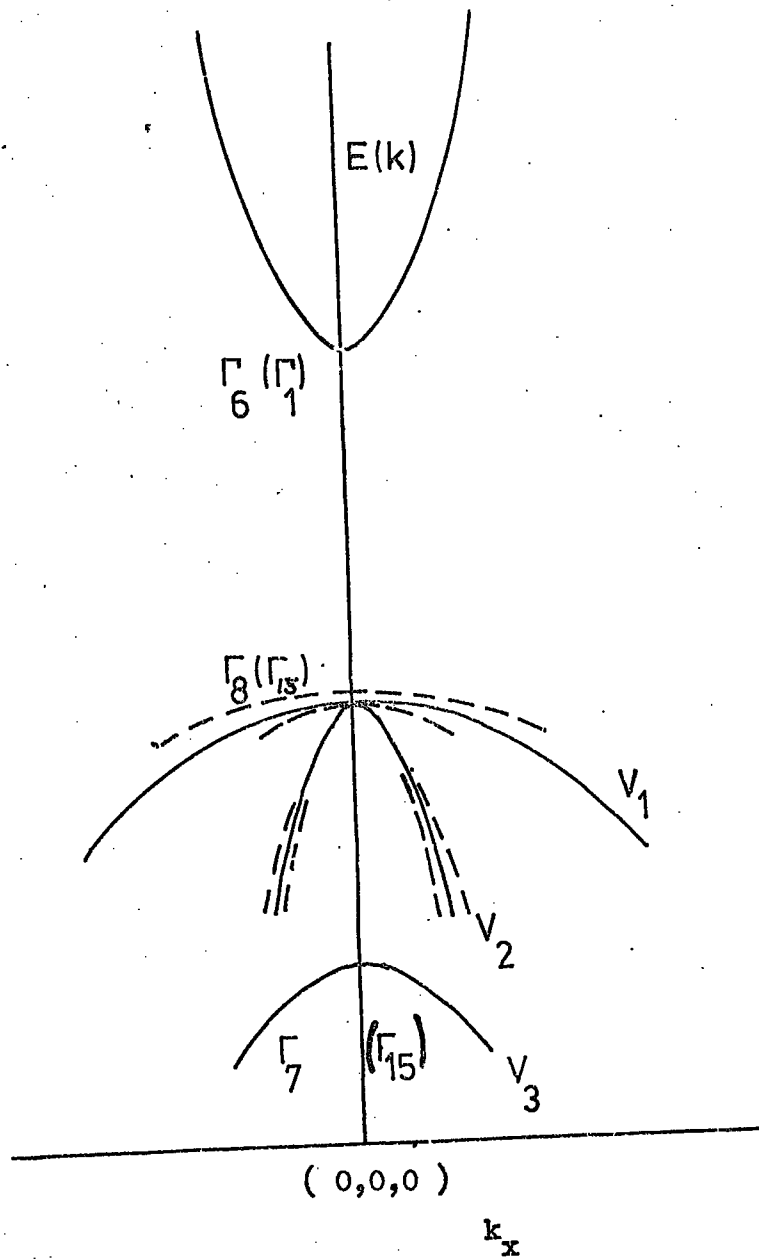


Fig. 2.2 The conduction and spin-orbit split valence bands of a zinc blende crystal around $k=0$.

prepared between the II-VI compounds, have not yet been investigated. However, if it is assumed that the bonding of the II-VI compounds is approximately ionic (i.e. the cation relates to the conduction band and the anion to the valence band) then a variation of composition from ZnS to ZnSe would imply a variation of the valence band edge, while the edge of the conduction band would remain a horizontally straight line (see for example Lehmann, 1966).

2.2 ELECTRICAL PROPERTIES

2.2.1 Introduction

Measurements of the electrical properties of II-VI compounds give valuable information about the energy band structure as well as about the type or number of carriers involved and the effective scattering processes.

2.2.2 Imperfections and Self-compensation

The most important lattice defects in II-VI compounds are lattice vacancies and interstitials. Anion (i.e. S, Se, Te) vacancies and cation (Zn, Cd) interstitials are expected to produce donor states in the forbidden gap. Similarly cation vacancies and anion interstitials introduce acceptor states. There has been considerable interest in the study of Zn and Cd vacancies and their complexes with foreign donors. Such complexes are thought to be responsible for the self-activated luminescence in II-VI compounds (Aven and Segal, 1963 and Merz et al, 1972). Impurity defects arise from the introduction of foreign elements such as the halogens (Cl, I, Br) substituting the anions, and group III elements (i.e. Al, Ga, In) substituting the cations. These impurities form shallow donor states in ZnS and ZnSe.

Most of the II-VI compounds are poor amphoteric semiconductors, i.e. ZnS and ZnSe can be made highly n-type, but p-type conductivity is very difficult to achieve, firstly because of the native tendency for automatic compensation, and secondly because the acceptor levels are deep. One possible consequence of compensation is that donors can form neutral pairs with acceptors and this phenomenon has been invoked to explain self-compensation in II-VI compounds. Aven and Halsted (1965) suggested that the V_{Zn}^D (D = shallow donors) vacancy complex was the major product of compensation in n-type ZnS or ZnSe, that is the addition of donor impurities (i.e. Al, Cl) would be compensated by the formation of the native defects (i.e. zinc vacancies or their complexes). The formation of compensating vacancies would depend on a simple energy balance. In other words, if the energy gained from compensation exceeds the energy required to form a vacancy, the vacancy would form, and compensation would occur. Therefore the energy levels of the added impurity and that of the compensating vacancy play the major role in compensation phenomena. If both levels are shallow, then the energy gained by carrier recombination could be almost as large as the band gap, which could be more than the energy needed to form a compensating vacancy, so a vacancy would form. Mandel (1964) has discussed this behaviour with a simple vacancy cavity model. It is possible to decrease the degree of compensation in ZnS and ZnSe doped with donors by heating them in molten zinc or zinc vapour, which removes the deep native acceptor levels (zinc vacancies). However, it is difficult, if not impossible, to prepare p-type samples. P-type ZnSe has been prepared by introducing acceptor-type dopants such as copper (Stringfellow and Bube, 1972), phosphorus (Reinberg et al, 1971), or by heating in selenium vapour (Yu and Park, 1972), but the conductivity of the resultant p-type samples was of the order of $10^{-8} - 10^{-10} \Omega^{-1} \text{ cm}^{-1}$.

2.2.3 Effective Carrier Masses

The motion of an electron in a semiconducting crystal, particularly at the bottom of the conduction band, resembles the motion of a free electron. The behaviour of the conducting electrons can be described in classical terms as though they were free electrons with an effective mass m^* . Kurik (1967) has calculated the effective mass of the current carriers of some of the II-VI compounds using Kane's (1957) theory of band structure. For cubic ZnS and ZnSe he found $m_e^* = 0.23 m_e$ and $m_e^* = 0.18 m_e$ respectively, (m_e = mass of free electron). Aven et al (1961) calculated the effective mass of electrons to be $0.1 m_e$ and holes $0.6 m_e$ in cubic ZnSe from experimental exciton emission data. From a study of infra-red reflectivity and Faraday rotation experiments Marple (1964) obtained an electron effective mass for cubic ZnSe of $m_e^* = 0.17 \pm 0.025 m_e$. Wheeler and Miklosz (1964) calculated an electron effective mass of $m_e^* = 0.27 m_e$ for ZnS using their data on optical spectra of excitons. (These values are tabulated in Table 2.2).

2.2.4 Charge Carrier Mobility

The electrical mobility of a charge carrier is described as the drift velocity per unit applied field. At higher temperatures the mobility in II-VI compounds is limited by the scattering of conduction electrons by fundamental lattice vibrations (Devlin, 1967). This limitation results from the interactions of the charge carriers with the quantised lattice vibrations (phonons). The lattice can vibrate both in optical and acoustical modes. Acoustic phonons deform the periodic potential of the lattice and they cause localised changes in the energy band structure (described in terms of the deformation potential). Charge carriers, as they pass through the crystal are then scattered.

Semi-conductor	$\Delta_{SO} (\Gamma_8 - \Gamma_7)$ (eV)	Band Gap Energy E_g (eV)	Free Exciton Energy (eV)	LO-Phonon Energy (eV)	Effective Carrier Masses	Mobility ($\text{cm}^2 \text{V}^{-1} \text{sec}^{-1}$)
ZnSe	0.45 (1)	2.82 (°K) (3)	2.81 (4 K) (1)	0.031 (4 K) (4)	$m_e^* = 0.1m$ (1)	$\mu_e = 530$ (300 K) (9)
		2.7 (300 K) (1)	2.799 (4 K) (5)		$m_h^* = 0.6m$ (1)	$\mu_e = 2,700$ (55 K) (9)
					$m_e^* = 0.17+0.025m$ (6)	
ZnS	0.072 (2)	3.84 (14 K) (3)	3.8 (14 K) (4)	0.044 (4 K) (4)	$m_e^* = 0.27m$ (7)	$\mu_e = 140$ (300 K) (10)
		3.58 (300 K) (8)	3.799 (14 K) (2)		$m_h^* = 0.58m$ (7)	

- (1) Aven et al (1961) (4) Halsted et al (1961) (7) Wheeler and Miklosz (1964)
- (2) Lempicki et al (1961) (5) Hite et al (1967) (8) Piper (1953)
- (3) Halsted et al (1965) (6) Marple (1964) (9) Woodbury and Aven (1962)
- (10) Aven and Mead (1965)

TABLE 2.2: Some experimental data related to the band structure

of ZnS and ZnSe.

Optical phonons are produced by the vibrations of adjacent atoms in antiphase. In compound semiconductors the adjacent atoms are oppositely charged which causes optical phonons to be associated with an electrostatic potential. The magnitude of this electrostatic force increases with the degree of ionicity of the bonding. Electron lattice interaction via optical phonon scattering is important in ionic crystals at high temperatures. At low temperatures ionised impurity scattering is usually dominant. There are other mobility limiting processes such as piezoelectric, neutral impurity or inter-valley scattering etc. but those processes are relatively unimportant in II-VI compounds. The expected variations of mobility with temperature and the effective carrier mass for various scattering mechanisms are listed in Table 2.3.

Little experimental work has been done on the transport properties of ZnS, partly because of the difficulty of growing single crystals with the required purity and resistivity. Aven and Mead (1965) measured the electrical properties of cubic ZnS doped with I and Al and found an electron mobility of $140 \text{ cm}^2 \text{ V}^{-1} \text{ sec}^{-1}$ at 300 K. Motossi et al (1966) gave the value as $165 \text{ cm}^2 \text{ V}^{-1} \text{ sec}^{-1}$. These experimental values are much lower than the predicted value of $285 \text{ cm}^2 \text{ V}^{-1} \text{ sec}^{-1}$ (see for example Rode, 1970). However, the measured variation of the mobility with temperature showed that considerable charged impurity scattering occurred, even at room temperature.

Compared with ZnS, ZnSe is more controllable. Aven et al (1961) studied the electrical properties of ZnSe crystals and measured the electron and hole mobilities. The values obtained were $\mu_e = 260 \text{ cm}^2 \text{ V}^{-1} \text{ sec}^{-1}$ at 300 K and $\mu_h = 15 \text{ cm}^2 \text{ V}^{-1} \text{ sec}^{-1}$. Subsequently Woodbury and Aven (1962) measured the electrical properties of ZnSe which had been heated in molten zinc. They obtained an electron mobility

Scattering Mechanism	Dependence of mobility on	
	Temperature (T)	Carrier effective mass m^*
Lattice scattering : Acoustic Mode (1)	$T^{-\frac{3}{2}}$	$m^{*\frac{-5}{2}}$
: Optical Mode (2)	$(\exp T^{-1})$	$m^{*\frac{-3}{2}}$
: Piezoelectric Mode (3)	$T^{-\frac{1}{2}}$	$m^{*\frac{-3}{2}}$
Inter Valley (4)	$T^{-\frac{3}{2}}$	-
Ionized Impurity (5)	$T^{\frac{3}{2}}$	$m^{*\frac{-1}{2}}$
Neutral Impurity (6)	m^*	-
Crystal Imperfection (Dislocations) (7)	T^{-1}	-

- (1) Bardeen and Shockley (1950)
- (2) Howarth and Sondheimer (1953)
- (3) Harrison (1956) and Zook (1964)
- (4) Herring (1955)
- (5) Conwell and Weisskopf (1950) and Brooks (1955)
- (6) Erginsoy (1950)
- (7) Dexter and Seitz (1952)

TABLE 2.3: The temperature dependence of mobility for the principle carriers scattering mechanisms in II-VI compounds.

of $530 \text{ cm}^{-2} \text{ V}^{-1} \text{ sec}^{-1}$ at 300 K and a maximum mobility of $2,700 \text{ cm}^2 \text{ V}^{-1} \text{ sec}^{-1}$ at 55.6 K. Later Aven and Segall (1963) investigated several undoped and donor doped samples of ZnSe. They concluded that the mobility was limited by optical mode scattering down to about 200 K. Fukuda and Fukai (1967) found a mobility maximum of about $3,000 \text{ cm}^2 \text{ V}^{-1} \text{ sec}^{-1}$ at 75 K. They analysed their results in terms of combined optical mode, ionised and neutral impurity and dipole scattering mechanisms. Recent work by Aven (1971) has shown that doubly charged defect centres are responsible for the impurity scattering. He showed that successive heating of ZnSe in molten zinc at temperatures between 850° and 650°C for a period of a week could increase the mobility. He obtained a highest value of electron mobility of $12,000 \text{ cm}^2 \text{ V}^{-1} \text{ sec}^{-1}$ at 50 K.

2.3 LUMINESCENT PROPERTIES

2.3.1 Introduction

The term "luminescence" is usually employed to describe the absorption of energy by a substance and its re-emission as visible or near-visible radiation. In general, luminescence occurs either as fluorescence or phosphorescence. The main distinction is concerned with the life times of the excited states of the luminescence centres. Luminescence emission during excitation is often referred to as fluorescence and is associated with decay times of the order of 10^{-8} seconds. Luminescence which persists after the excitation ends is referred to as phosphorescence (or after glow) and is associated with decay times of up to several seconds. Luminescence with intermediate values of decay time (i.e. 10^{-5} - 10^{-1} sec) is difficult to identify. In such cases the effects of changing the temperature enables the distinction

to be made. For example, the decay of fluorescence unlike phosphorescence is little dependent on temperature.

2.3.2 Edge Emission

The term edge emission in compound semiconductors is employed to describe the radiative recombination processes associated with transitions which occur within several tenths of an electron volt below that of the band gap. The fluorescent emission in the band edge region in II-VI compounds normally occurs with the simultaneous emission of photons and 0,1,2,3, longitudinal optical (LO) phonons. Equally spaced spectral lines were first observed in II-VI compounds by Ewles (1938) and Kröger (1940). The optical transitions in the band edge region became increasingly more efficient and particularly well resolved at liquid helium temperatures with the help of high intensity excitation. Three different recombination processes contributed to edge emission, namely free exciton, bound exciton and distant pair recombination, together with their phonon associates. The most extensive studies on edge emission in II-VI compounds have been made in cadmium sulphide crystals at 4.2 K (Klick 1953, Thomas and Hopfield 1962). They found that the high energy green edge emission of cadmium sulphide consisted of very narrow lines with half widths of approximately 0.005 eV. These lines were attributed to the recombination of free and bound excitons. The pair emission in cadmium sulphide (Pedrotti and Reynolds, 1960) was found to be associated with the recombination between an electron bound to a shallow donor ($E_d = 0.02$ eV), and a hole bound to an acceptor level ($E_a = 0.14$ eV) above the valence band. The edge emission in cadmium sulphide had also been observed in the electroluminescence at 77 K (Smith 1957).

(a) Exciton Emission

When a pure crystal is excited by absorbing energy exceeding the band gap, free electrons and holes are created in the conduction and valence bands. This process may lead to photoconductivity and can be regarded as photo-ionisation of an isolated atom. It is also expected that an excited but bound electron-hole pair, with a coulombic interaction between them, will exist with an energy just below that of the band gap. Such pairs can be excited with this energy and are called excitons. Excitons can be regarded as the excited states of crystals. Unlike the excited states of isolated atoms, excitons are not localised and have well defined wave vectors. Excitons are electrically neutral and have short life times (10^{-8} sec in CdS) at the end of which they recombine with photon emission. This radiative recombination in the vicinity of the band edge is called exciton emission. The structure of excitons can be complicated by the detailed energy band structures of the crystals. In II-VI compounds multiple series of exciton emission lines are expected because of the degeneracy of the valence band at $k = 0$. This degeneracy is due to spin-orbit interaction (see Section 2.2).

In general, excitons are either free or bound. The energy of the photon emitted when a free-exciton recombines, is equal to the band gap energy less the binding energy, E_{Bex} , of the exciton. The binding energy of the exciton can be calculated using a simple hydrogen model. Since the electron and the hole have comparable masses, the reduced mass $m_r = m_e^* / (m_e^* + m_h^*)$, of an exciton must be used, where m_e^* and m_h^* are the effective electron and hole masses respectively. The exciton energies are then given by

$$E_{exc} = E_G - 13.6 \left[\frac{m_r}{m_e \epsilon_s n^2} \right] \dots \dots (2.3.1)$$

where ϵ_s is the low frequency dielectric constant of the crystal and

$n = 1, 2, \dots$ define the ground and excited states of the exciton. The exciton spectrum therefore consists of a series of discrete lines on the long wavelength side of the band gap which can be explained in terms of the exciton energy diagram shown in Figure 2.3. The ground and excited states of an exciton can be found experimentally from absorption, reflection and emission measurements. Aven et al (1961) measured the absorption and the reflectivity of cubic zinc selenide at 23 K. They found that the excitons were formed from the holes in the Γ_8 valence band and the electrons in the Γ_6 conduction band at $k = 0$. The observed peaks were attributed to the transitions from Γ_8 to the ground ($n = 1$) and the first excited ($n = 2$) states. The $n = 1$ state lay 2.81 eV above the valence band and the energy separation of the ground and the first excited states was 0.02 eV. The reduced mass $m_r = 0.1 m$. They therefore suggested a band gap of about $E_g = 2.83$ eV at 23 K. Halsted et al (1965) gave the values of the bandgap as 2.82 eV for ZnSe at 4 K. They also attributed the higher value obtained by Aven et al to the presence of sulphur impurity in the ZnSe. Later Hite et al (1967) measured the normal reflectance spectra of zinc selenide crystals purified by heating in liquid zinc. They found the ground state absorption energy to be 2.799 eV at 4 K. They also suggest that the energies for maximum absorption were associated with the creation of direct excitons assisted by LO phonons with energies of 0.031 eV.

Lempicki et al (1961) measured the reflectance of cubic zinc sulphide crystals at 14 K. They found the characteristic direct exciton lines in the region of the onset of strong continuous absorption. They attributed the lower energy line (3.799 eV) to ground state ($n = 1$) excitons with the holes coming from Γ_8 valence bands, while the peak at 0.07 eV higher energy was associated with the split-off Γ_7 band.

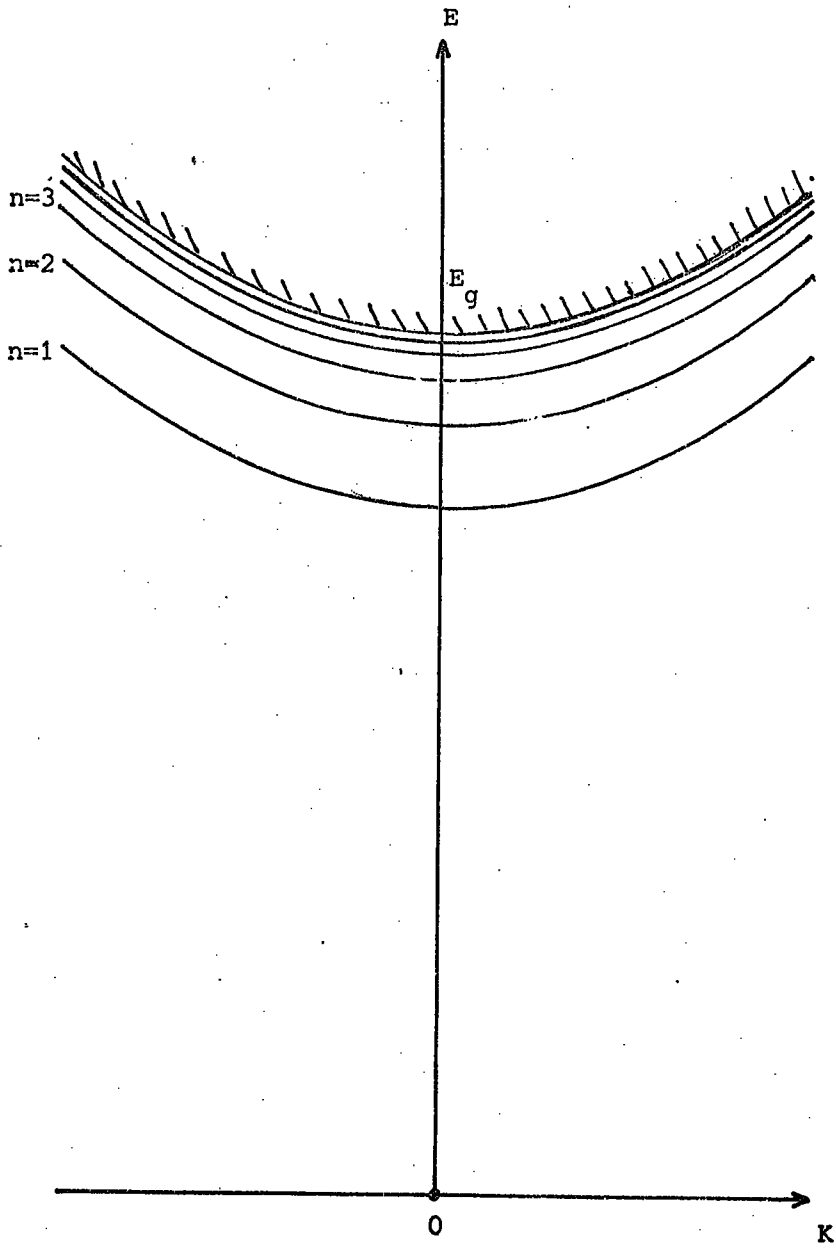


Fig. 2.3 Energy of exciton bands as a function of exciton momentum K .

Bound excitons are usually observed in the presence of ionised and neutral crystal defects. Bound exciton emission is characterised by even narrower spectral lines at lower photon energies than free excitons. The theory of bound excitons was developed extensively by Thomas and Hopfield (1962) with reference to CdS. Four exciton complexes are postulated. These are excitons bound to (i) neutral donors, (ii) ionised donors, (iii) neutral acceptors, and (iv) ionised acceptors. The ionisation energy E_i for the bound exciton is given by $E_i = E_{Bex} + E_b$ where E_{Bex} is the free exciton binding energy and E_b is the additional energy binding the free exciton to that centre (dissociation energy). The intensity of the bound exciton emission is strongly dependent on temperature.

(b) Pair Emission

Donor-acceptor pair emission was first suggested by Prener and Williams (1956). In this process an electron on a donor recombines with a hole on an acceptor. The coulomb interaction between donor and acceptor modifies the binding energy. The energy separating the paired donor and acceptor states is given by

$$E_p(r) = E_g - (E_a + E_d) + E_c \quad \text{where} \quad E_c = \frac{e^2}{\epsilon r} \quad (2.3.2)$$

where E_g is the band gap energy, E_d and E_a are the ionisation energies of the isolated donors and acceptors respectively, r is the donor-acceptor spacing, ϵ is the dielectric constant and e is the electronic charge. With donor-acceptor spacings greater than the effective Bohr radius, the transition is assisted by a tunneling process. Transitions between nearer pairs are more probable than transitions between distant pairs. At large separations (i.e. $> 40 \text{ \AA}$) the emission lines overlap

to form a broad spectral band. Since the life time of the pairs will vary with their separation, time resolved spectroscopy is an effective method for investigating the pair emission process. With this latter technique, the spectral distribution of a decaying pair band after flash excitation should shift to lower energies with time during the decay. When $E_a > E_d$ and the temperature is very low, carrier freeze-out will occur. At higher temperatures the pair emission process will be replaced by the recombination of free electrons with bound holes as the donors are ionised. The energy of the emitted photon will be given

$$E_{h\nu} = E_g - (E_a - E_k) \quad \dots \quad \dots \quad (2.3.3)$$

where E_k is the kinetic energy of the free electron.

2.3.3 Edge Emission in Zinc Selenide

The first detailed studies of edge emission in cubic ZnSe crystals were carried out by Reynolds et al (1961) and Halsted and Aven (1965). Iida (1968) also studied edge emission in zinc selenide and calculated the donor and the acceptor binding energies to be 0.026 and 0.1 eV from time resolved measurements. Dean and Merz (1969) examined the photoluminescence emission from cubic zinc selenide at 4.2 K. They observed intense sharp lines on the high energy side of the spectrum. They attributed the line at 2.802 eV to the free exciton, the I_2 doublet at 2.799 and 2.795 eV to excitons bound to neutral donors and the I_1 line at 2.793 to excitons bound to neutral acceptors. Dean and Merz also observed two series of the broader distant pair emission bands. The higher energy series had its zero-phonon member at 2.710 eV with three LO phonon replicas. The second series of bands had its zero-phonon member at about 2.692 eV with three LO-phonon replicas. The higher

energy series exhibited several characteristics of the pair recombination, however no fine structure was associated with the lower energy series. Merz et al (1972) investigated edge emission in cubic ZnSe doped with substitutional donors. They found excitons bound to neutral donors (I_2 lines) in the region of 2.78 to 2.80 eV, and excitons bound to ionised donors (I_3 lines) between 2.797 and 2.794 eV. The donors were identified using these lines. Merz et al, observed that, as the excitation power increased, the distant pairs became saturated and the peak of the pair band began to move to higher energies.

2.3.4 The Deep Centre Luminescence

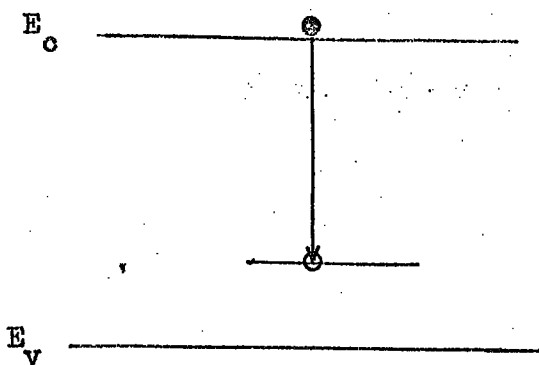
It is a well-known practice to add impurities to most phosphors to activate their luminescence. By adding different impurities to the II-VI compounds, light emission can be obtained over a wide range of wavelengths extending from the edge emission region to the infrared. Luminescent transitions involving impurities in phosphors can be divided into two categories, namely localised and non-localised.

Non-localised transitions are those in which conduction and valence band electrons of the phosphor make transitions to the luminescence centre itself. Two types of impurities can be incorporated in II-VI compounds to produce non-localised centres. Activators can be elements from group I (i.e. Cu, Ag, Au) substituted for the metal atoms. The co-activators can be elements from group III (i.e. Al, Ga, In) or elements from VII (i.e. Cl, Br, I) substituting metal and non-metal atoms respectively. ZnS was the first II-VI phosphor to be studied in great detail. There are three basic models for interpreting the non-localised luminescent transitions, namely the Schön-Klasens (Schön, 1941 and Klasens 1946), Lambe and Klick (1955) and Prener and Williams

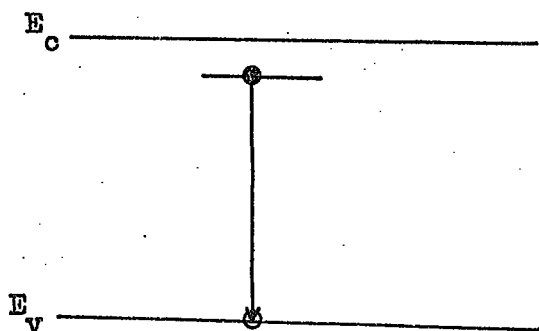
(1956) models, see Figure 2.4. According to the Schön-Klasens model, the luminescence is a result of radiative recombination of a free electron from the conduction band with a hole trapped at an acceptor level (Figure 2.4(a)). The model proposed by Lambe and Klick attributes the luminescence (see Figure 2.4.(b)) to the recombination of a free hole with an electron trapped at a donor level. The third model proposed by Prener and Williams describes the luminescence as the result of the recombination of electrons and holes trapped at localised centres in the same region of the lattice, that is pair emission.

Localised transitions are observed when a transition metal element e.g. manganese, or a rare-earth ion is introduced in II-VI compounds as an impurity. Then the emission and absorption processes take place entirely within the electronic configuration of the ion. The excited electron in the atomic shell of the ion does not interact with the free electrons or holes. However, the crystal field and the lattice vibrations of the host crystal may have a profound effect on the transition. The electronic absorption and emission processes can be better understood using the so-called configurational co-ordinate model. This model was first suggested by Seitz (1939) and improved by Williams (1953).

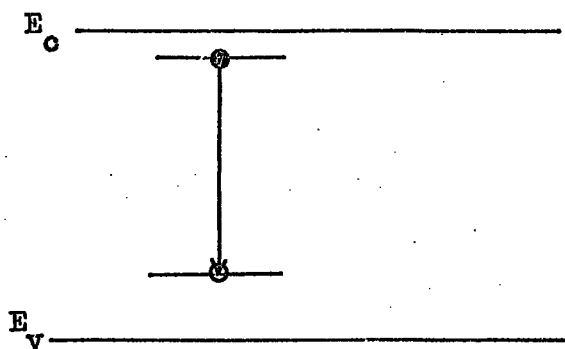
In this model, the impurity ion is thought of as surrounded with the neighbouring lattice ions which vibrate about it. The energy of the system, formed by the impurity ion interacting with these neighbouring ions, can be characterised by the distance r between the impurity and the nearest neighbour ions. This distance is called the configurational co-ordinate. The configurational co-ordinate diagram (see Figure 2.5) defines the potential energy of the system of the impurity ion and the lattice as a function of the co-ordinate r . The two curves represent the ground, E_{gr} , and the excited, E_{exc} , states of the impurity ion.



(a) - Schon - Klasens model



(b) - Lambe - Klick model



(c) - Prener - Williams model

Fig. 2.4 Schematic representation of three basic models for the radiative transition processes in II-VI compounds

The minimum energies in the ground and excited states occur at slightly different values of the configurational co-ordinate. According to the Frank-Condon principle, optical transitions take place in a much shorter time than the lattice takes to respond to changes in the charge distribution. Therefore optical transitions are represented by vertical lines on the configurational co-ordinate diagram. After the electron is raised from the ground state at A to the excited state at B, by absorbing a photon with an energy $h\nu_a$, the whole system gradually relaxes to thermal equilibrium at C. This means that a displacement of Δr in the configurational co-ordinate has occurred. The excited electron thus loses some of its energy which is dissipated by the emission of a number, N_1 , of localised phonons with energy $h\nu$. When the electron returns to the ground state by emitting a photon with energy $h\nu_e$, the lattice will again relax with the emission of N_0 localised phonons with energy $h\nu$. The emitted photon energy, $h\nu_e$ is less than the energy absorbed, $h\nu_a$, the excess being emitted as lattice phonons. The difference between the absorbed and the emitted energy is called the **Stoke's shift**.

At higher temperatures the lattice vibrations increase in amplitude. This gives rise to a larger range of values of configurational co-ordinates with a wider variation in energy. In this case the transitions in the configurational co-ordinate diagram occur from either side of the energy minimum point A. The energy distribution of electron within the luminescent centres is determined by Maxwell-Boltzmann statistics. One consequence of this is that the absorption and emission bands are Gaussian in shape. Since the energy of the system is quantised both the emission and absorption bands should consist of a number of discrete lines associated with the localised phonons. However, these discrete lines are broadened by the Stark effect and overlap so that a

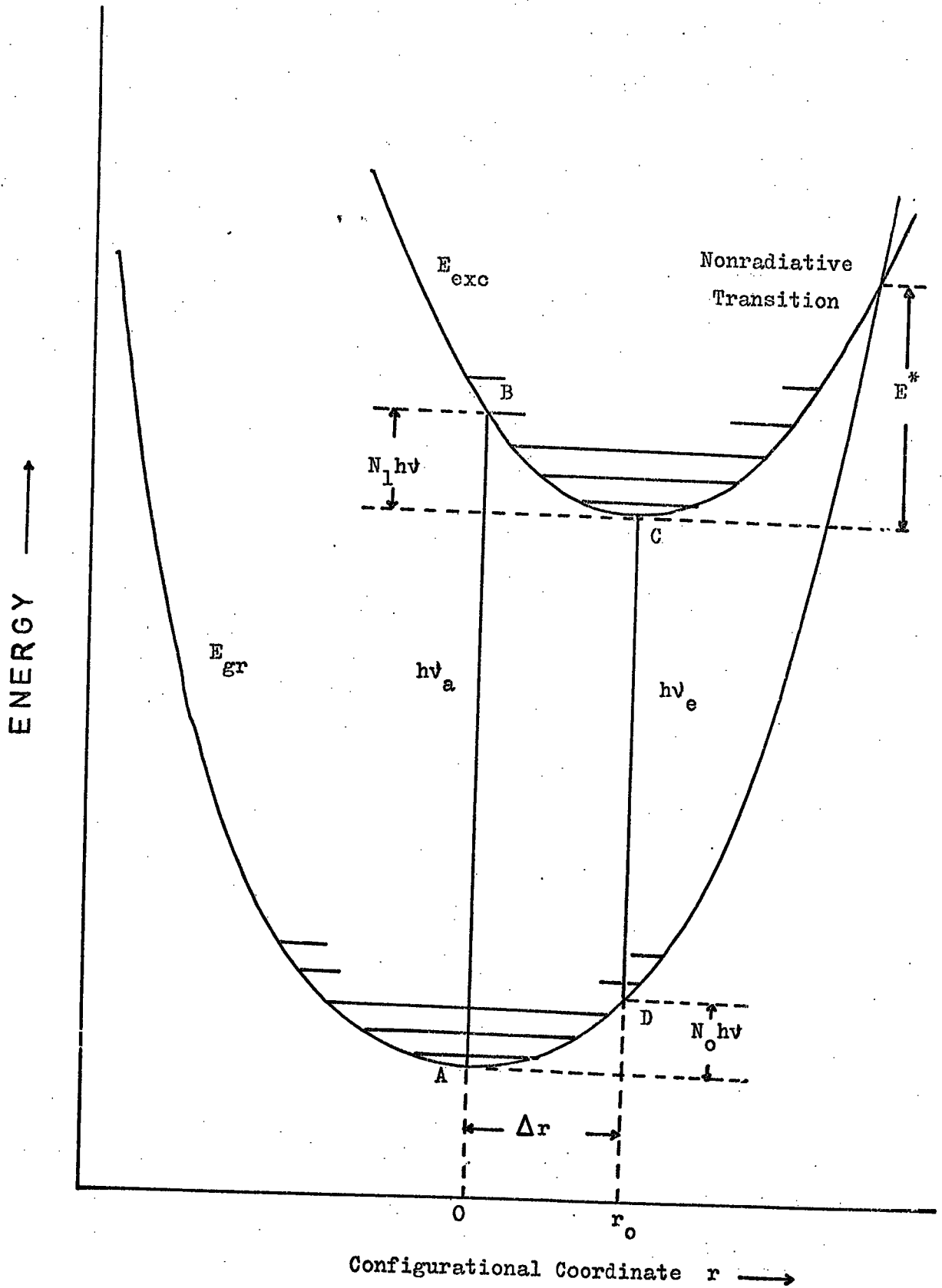


Fig. 2.5 A typical configurational coordinate diagram.

broad featureless band results. In many luminescent systems however several sharp lines can be detected at low temperatures. The resonant line in absorption and emission is known as the zero phonon line. It occurs when the excitation and emission take place between the minimum energy points (A and C) of the excited and ground states.

The width of the emission band at half height can be calculated using quantum mechanical considerations (see for example Klick and Shulman, 1957) as

$$W(T) = W(0) \left[\coth (h\nu/2kT) \right]^{\frac{1}{2}} \dots \dots (2.3.4)$$

where $W(T)$ is the width of the emission band at half-height measured at $T(K)$, and $h\nu$ is the phonon energy associated with the vibrational mode of the excited state. At low temperatures the half width is independent of temperature and the equation reduces to $W(T) \approx W(0)$. At high temperature however (i.e. $2 kT \gg h\nu$) $W(T)$ is proportional to $T^{\frac{1}{2}}$. Therefore, the phonon frequency can be found by measuring the change of half width as a function of temperature.

The configurational co-ordinate model is useful when the optical transitions are highly localised. For example, with rare earth atoms, such as erbium and thulium, the transitions take place in the partially filled 4f shell. Since this shell lies deep within the atom, lattice vibrations have little effect and the resulting emission bands are very narrow. However, the optical transition in the transition elements (i.e. cobalt, nickel, manganese) take place in the outermost 3d shell. Here phonon interaction is more important and consequently the observed emission bands are broader. Manganese as an activator had been studied in many phosphor systems. The Mn^{++} ion occupies a substitutional anion site in II-VI compounds and is well-known as being responsible for the

yellow-orange luminescence in zinc sulphide. The radiative transition is associated with a change in the spin of one of the five 3d electrons. The ground state of the free manganese ion is 6S , where five 3d electrons are aligned with their spins parallel. The excited state is split into five degenerate levels 4G , 4P , 4D , 4F and 4S because of spin-orbit interaction. The energy separation of the first excited state 4G from the ground state is 3.2 eV. The 4G state has five 3d electrons with one of the spins reversed. The 4S excited state, $3d^4S$, is some 7.2 eV above the ground state and is not involved in luminescence transitions. The crystal field has a profound effect in splitting these excited levels. Orgel (1955) has calculated the energy level diagram of the Mn^{++} ion in a cubic field relative to the 6S (6A_1) ground state, (see Figure 2.6). The observed emission results from transitions between the $4T_1$ (4G) excited state and the 6A_1 (6S) ground state. The transitions involved in excitation are ${}^6A_1 \rightarrow 4T_1$, ${}^6A_1 \rightarrow 4T_2$ and ${}^6A_1 \rightarrow 4A_1, 4E$. Although the excitation and emission spectra are easily explained for localised impurities such as Mn^{++} , it is difficult to determine the energetic position of the ground state of that ion with respect to the conduction and the valence band edges of the host lattice.

In general the luminescence efficiency of a phosphor decreases exponentially when the temperature is raised sufficiently. This is mainly caused by an increase in non-radiative recombination. The process is known as thermal quenching. The variation of the luminescence efficiency with temperature is given by

$$\eta = \eta_0 / \left[1 + C \exp (- E/kT) \right] \quad \dots \quad (2.3.5)$$

where C is a constant and E is an activation energy. With non-localised centres, where the luminescence is of the Schön-Klasens type, thermal

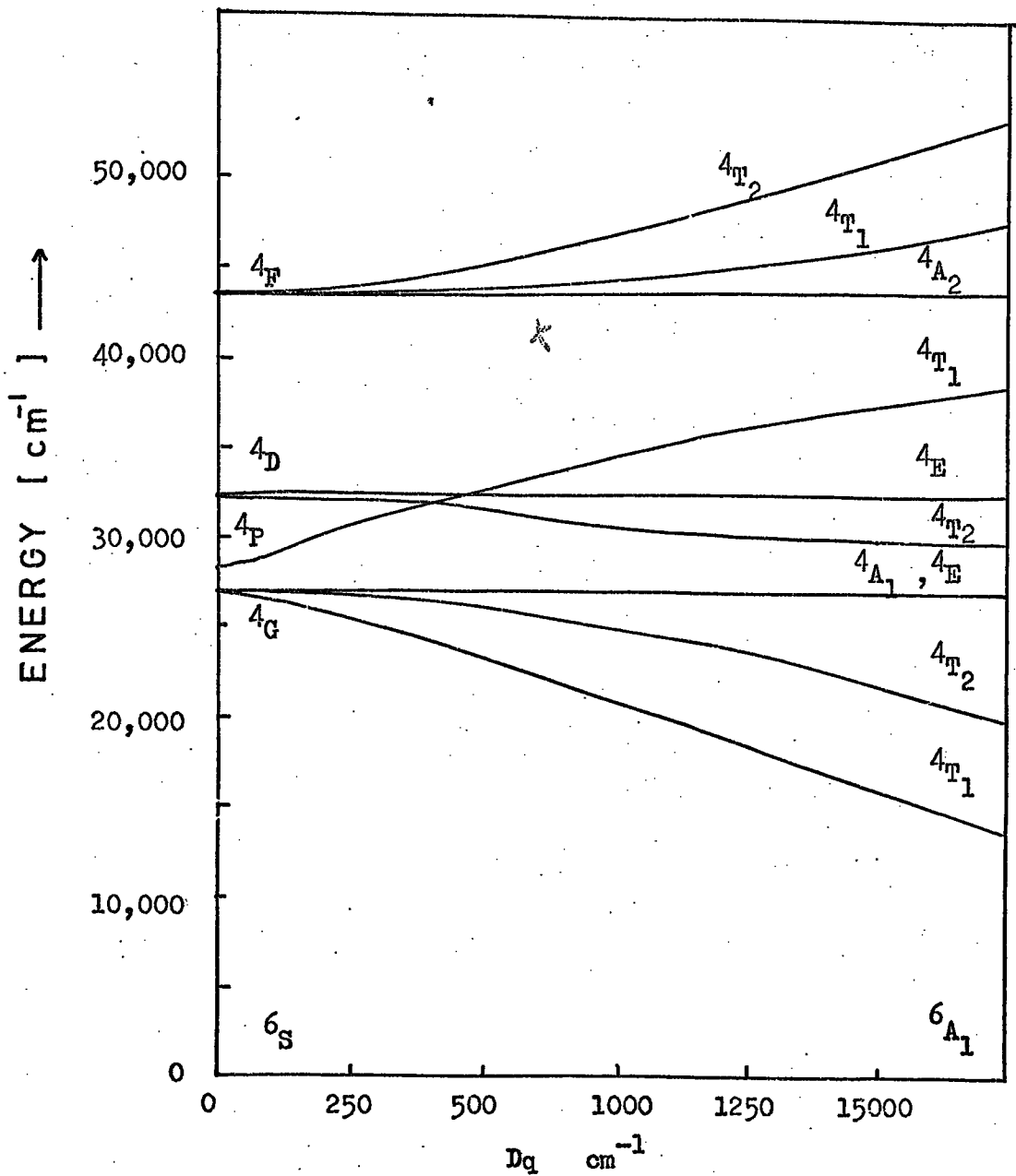


Fig. 2.6 Energy level diagram of the Mn²⁺ ion in a cubic field relative to the ⁶A₁ (⁶S) ground state as calculated by Orgel, 1955.

quenching will occur when the temperature is sufficiently high for electrons to be excited thermally from the valence band to the empty activator centre. Then excited electrons in the conduction band cannot make radiative transitions via this centre. The activation energy E is the energy required to excite an electron from the valence band to the luminescent centre. Similarly, if the radiative transition is of the Lambe-Klick type, the electron in the donor state may be excited thermally to the conduction band before it recombines with a free hole. In this case, E , in equation 2.3.5, represents the depth of luminescent (donor) centre below the conduction band. With localised transitions, the thermal quenching of luminescence efficiency is again described by equation 2.3.5. The models proposed by Mott (1940), and Dexter et al (1955) suggest that the ground state crosses the excited state at an energy E^* above the equilibrium position C , in the excited state (see Figure 2.5). As the temperature is raised the electron can reach this energy and return to the ground state non-radiatively.

2.3.5 Deep Centre Luminescence in ZnSe, ZnS and Zn(S,Se)

(a) Self and copper activated luminescence in ZnSe and ZnS

Most of the studies of deep centre luminescence in II-VI compounds have been made on ZnS. The self-activated emission from ZnS containing coactivator impurities such as Cl, I, Al, etc. all give similar broad emission bands in the blue region of the spectrum. Prener and Williams (1956) proposed a complex centre consisting of a doubly ionised zinc vacancy (acceptor) and an ionised impurity donor. Such a complex centre can be represented as $(V_{Zn} - Al_{Zn})^{\cdot\cdot}$ or $(V_{Zn} - Cl_s)^{\cdot\cdot}$ etc. Prener and Weil (1959) studied the emission from cubic ZnS at 300 K.

They found the peak of the self-activated emission band at 4620 \AA for Br and Cl impurities and at 4700 \AA for Al and Ga. In addition to the self-activated band, Gill and Rothschild (1960) and Van Gool (1961) have both reported a higher energy band with a peak at 3920 \AA for cubic ZnS doped with Cl, Br or Al. Rothschild (1963) suggested that this emission was of the Lambe-Klick type with an electron trapped at an isolated halogen or group III impurity donor. The luminescence from ZnS doped with group I activators has been of interest for a long time. For example, the presence of copper as an activator leads to a blue (4400 \AA), a green (5200 \AA) and a red (6970 \AA) emission. The green band is often attributed to a Prener-Williams transition between electrons at donor levels (coactivators) and holes localised at associated copper centres, whereas the blue band has been considered to result from a Schön-Klasens transition to the same copper level associated with the green band (Curie and Curie, 1960). This suggestion is supported by time resolved spectroscopy (Shionoya et al, 1966) and by luminescence decay measurements (Suzuki and Shionoya, 1971).

Some early work concerning the deep centre luminescence in ZnSe was reported by Leverenz (1950). Self-activated emission in ZnSe occurs at wavelengths between 6020 and 6450 \AA , whereas the wavelengths reported for the red (6360 \AA) and green (5300 \AA) emission bands associated with copper are fairly consistent (see for example Halsted et al, 1965). However, some complication arises in the assignment of the centres involved, because both the self-activated and the low energy copper band overlap in the red region of the spectrum (Jones and Woods, 1974).

(b) Manganese Emission in ZnSe and ZnS

Manganese, as a luminescence activator in zinc sulphide, has been studied most extensively. The luminescence emission from ZnS doped with

Mn^{++} consists of a broad band at 5860 \AA (McClure, 1963; Langer and Ibuki, 1965; Beserman and Balkanski, 1971), with a number of narrow emission lines superimposed on the high energy side of the band. The transition is from ${}^4T_1({}^4G) \longrightarrow {}^6A_1({}^6S)$. All the investigations saw similar fine structure in the absorption bands at low temperatures. McClure explained the fine structure in terms of crystal-field theory and spin-spin interaction of ion pairs, whereas Langer and Ibuki explained it in terms of electronic transitions coupled with lattice phonons. They took the zero phonon line to be at 5589 \AA . The absorption spectrum was assigned to transitions from the ground ${}^6A_1({}^6S)$ level to various excited crystal field states. McClure (1963) and Langer and Ibuki (1965) assigned the various excited states as follows:

$5350 \text{ \AA} - {}^4T_1({}^4G)$; $4980 \text{ \AA} - {}^4T_2({}^4G)$; $4650 \text{ \AA} - ({}^4A_1, {}^4E)({}^4G)$;
 $4300 \text{ \AA} - {}^4T_1({}^4P)$; $3900 \text{ \AA} - {}^4T_2({}^4D)$, and ${}^4E({}^4D)$.

Manganese activation in ZnSe has received relatively little attention partly because of the wide variation of the emission peak (i.e. $5940 \text{ \AA} - 6500 \text{ \AA}$) observed by many authors (see for example Leverenz, 1950, and Larach, 1953). Langer and Richter (1966) found a fine structure in the optical absorption spectrum of ZnSe containing manganese at 4.2 K. They found two absorption bands with maxima lying at 5300 \AA for ${}^6A_1 \longrightarrow {}^4T_1({}^4G)$ and 4995 \AA for ${}^6A_1 \longrightarrow {}^4T_2$, but the absorption due to the ${}^6A_1 \longrightarrow {}^4A_1, {}^4E$ transition coincided with the intrinsic fundamental absorption in ZnSe. The maximum of the emission band associated with the ${}^4T_1 \longrightarrow {}^6A_1$ transition was located at 5815 \AA , with the zero phonon emission line at 5547 \AA . The fact that the Mn^{++} emission and the self-activated emission lie in the same region of the spectrum (Jones and Woods, 1973; Allen et al, 1973) causes some confusion. Jones and Woods suggested that the self-activated luminescence excited

by photons with band gap energy in ZnSe swamped the characteristic Mn^{++} emission. The Mn^{2+} emission (at 5860 Å) was only obtained when the crystal was excited in a characteristic excitation band.

Allen (1964) using crystal field theory suggested that the ground state ${}^6A_1({}^6S)$ of Mn^{2+} in ZnS lies some tenths of one eV above the valence band. Braun et al (1972), using photocapacitance measurements placed the ground state of Mn^{2+} in ZnSe some 0.6 eV above the valence band. Later Özsan and Woods (1975) measured the short circuit photocurrent and argued that the ground state of Mn^{2+} in ZnSe lies about 0.3 eV above the valence band. Further experimental investigation will be necessary to resolve this matter.

(c) Luminescence in Mixed Crystals

It is possible to vary the energy of luminescence by alloying phosphors. It has been shown by Bundel et al (1961), and Lehman (1966) that binary compounds between Zn and Cd on the one hand and S, Se and Te on the other, can be alloyed conveniently to form ternary compounds, i.e. (Zn, Cd) S and Zn(S,Se). Later Ozawa and Hersch (1973) studied the self-activated luminescence in single crystals of cubic Zn(S,Se):I. The results obtained by these authors have shown that the blue S.A. emission band of ZnS is replaced by a green band as the sulphur is replaced by selenium. This then changes gradually to orange as the selenium content is further increased. Morehead (1963) investigated the luminescence in Zn(S,Se):Cu,Cl phosphors, and he concluded that the luminescence emission in Zn(S,Se):Cu,Cl phosphors could be explained with a modified Schön-Klasens model. He suggested that the blue and green recombination centres could be represented as two of the three possible states of a single, doubly ionisable centre. Lehman (1966) observed that the blue (2.79 eV) and green (2.35 eV) emission bands of

copper-activated ZnS are replaced with new bands at about 2.6 eV and 2.23 eV when less than 1% of the sulphur in ZnS is replaced with selenium. Further gradual increase in the concentration of selenium was found to cause only a comparatively slow shift of both bands towards longer wavelengths until, in ZnSe:Cu, Cl, they were found to occur at about 1.95 eV (red) and 2.34 eV (green) respectively.

2.4 ELECTROLUMINESCENCE

2.4.1 Introduction

The historical background and various mechanisms of exciting EL have been previously reviewed by many authors, i.e. Henisch (1962), Ivey (1963), Fisher (1966), Morehead (1967), Aven (1967) and Berg and Dean (1972). In the following sections the properties of Schottky barriers and possible mechanisms leading to electroluminescence in ZnS and ZnSe will be discussed.

2.4.2 Mechanisms of Electroluminescence in II-VI Compounds

In general there are two types of mechanism by which electroluminescence can be obtained in solids, namely (1) injection, and (2) high field (avalanche) luminescence.

With process (1) the injection of minority carriers across a potential barrier is followed by their radiative recombination with majority carriers in the active region of the device, either directly or via a luminescent centre.

With process (2) the majority carriers are accelerated in a high electric field to energies sufficiently large to excite the filled luminescent centres, or ionise the lattice to generate electron hole pairs, by impact. Radiative recombination may then occur as the excited

carriers return to the luminescent centres.

Injection electroluminescence may be obtained under forward bias conditions, at a p-n junction (Figure 2.7a) or metal semiconductor (Figure 2.7b) contacts, while avalanche electroluminescence appears when p-n junctions or metal semiconductor contacts (Figure 2.7c) are reverse biased. Electroluminescence can also result from the tunneling processes (field emission) at forward and reverse biased junctions or metal semiconductor contacts.

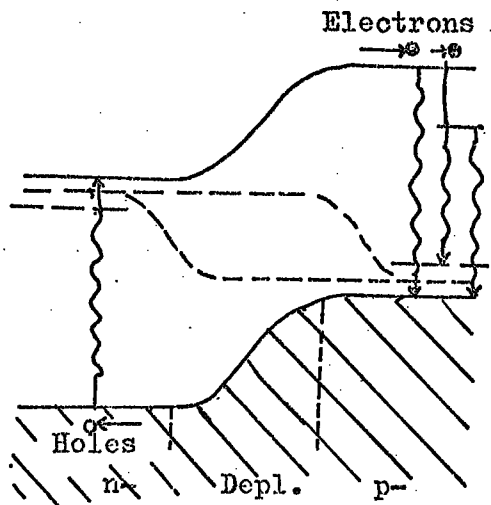
Radiative and the non-radiative recombinations will always compete. The quantum efficiency of an electroluminescent device is described as the ratio of radiative recombinations (or number of photons) to the number of injected carriers.

With injection electroluminescence, the energy of the emitted light is limited by the band gap of the material. However, with the impact ionisation process, majority carriers can become "hot" and the photon energy of the emission accompanying radiative recombination may exceed the energy of the band gap. Acceleration of carriers to energies sufficient to cause impact ionisation, requires high fields, i.e. at the order of 10^5 V cm^{-1} or greater. Now a necessary prerequisite for radiative recombination in most electroluminescent devices is the injection of minority carriers into the active region of the device where the recombination will take place. Since the impact generated electrons and holes, in reverse biased p-n junctions or reverse biased metal semiconductor contacts, are both extracted from, rather than injected into, the active region, the quantum efficiency is expected to be low. The quantum efficiency can be expressed as the ratio of transit time, t , of the impact generated carriers across the width, W , of the high field region to the recombination lifetime, τ , (see for example Morehead 1967).

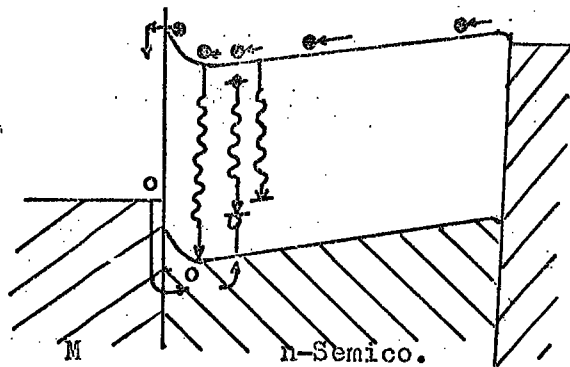
$$t/\tau = (W^2 / \mu V \tau) \dots \dots (2.4.1)$$

where V is the applied field and μ is the carrier mobility.

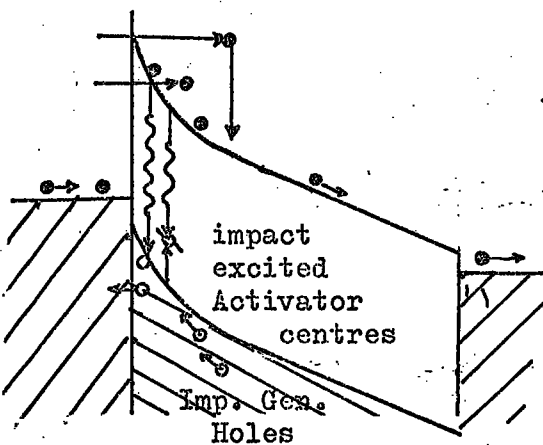
With unipolar II-VI compounds, which are of particular interest, electroluminescence can be obtained in metal semiconductor (M-S) or metal-insulator-semiconductor (M-I-S) devices. (The latter will be described in detail in the next section). With such devices a high field is produced within the semiconductor. The electroluminescence resulting from an M-S contact with an inversion layer has been described by Fisher (1964, 1966). In a reverse-biased M-S contact, electrons are injected from the metal, through or over the potential barrier into the semiconductor where they are accelerated and the lattice or luminescent centres are excited by impact. The excited carriers then recombine radiatively, directly or via luminescent centres. Under forward bias with dissimilar metal contacts as shown in Figure 2.7b, holes will be injected from the contact with the high work function and radiative recombination will take place near the anode. Electroluminescence can also be achieved by tunnel injection through a thin insulating film. For example, a thin insulating film of a wide band gap material can be placed between the metal and n-type semiconductor to produce a M-I-S device. Under reverse bias (see Figure 2.7d) the Fermi level in the metal is pinned to a level within or slightly below the conduction band edge of the semiconductor. The electrons tunnel from the metal through the thin insulating film to the semiconductor. They are then accelerated by the high field and excite the luminescent centres or ionise the lattice to generate electron-hole pairs by impact. Radiative recombination occurs at the cathode where impact generated holes accumulate close to the insulating film. Under forward bias conditions (see Figure 2.7e) the Fermi level in the metal is pinned downwards to a level within, or



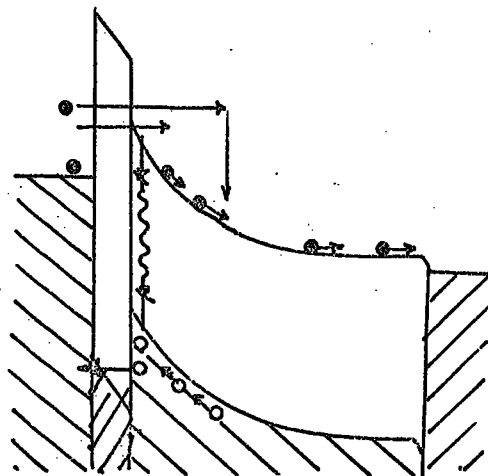
(a) - Forward biased
p-n junction



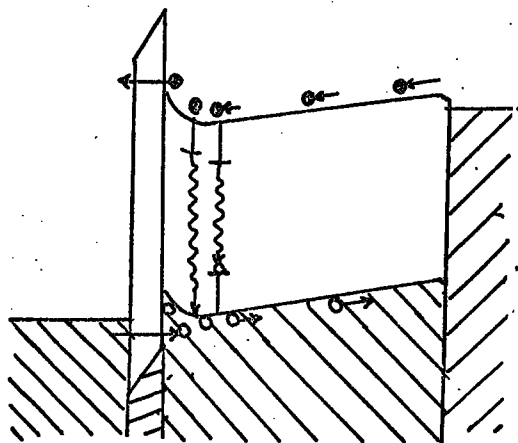
(b) Forward - biased
M-S contact



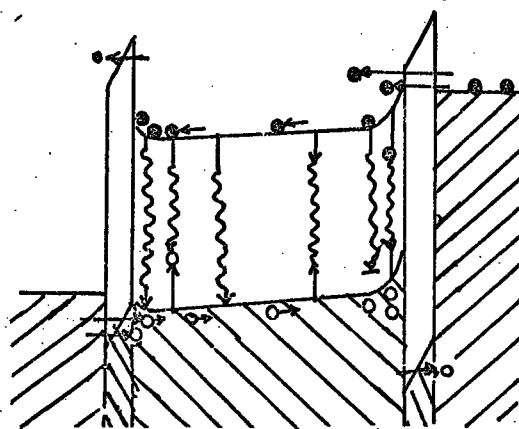
(c)- Reverse-biased
M-S contact



(d)- Reverse-biased
M-I-S contact



(e)- Forward-biased
M-I-S contact



(f)- Forward-biased
M-I-S-I-M contact

FIG. 2.7 Schematic representation of energy states of possible structures and contacts showing the mechanisms for the electroluminescence

only slightly above, the valence band edge of the semiconductor. The holes may tunnel through the insulating film to the valence band of the semiconductor and recombine radiatively at the anode with the electrons, injected from the metal with the low work function. In this case the extraction of electrons is impeded by the insulating film at the anode. Since the extraction of one of the carriers involved with electroluminescence in an M-I-S contact is inhibited, the efficiency of light generation at an M-I-S contact should be greater than at an M-S contact. Further improvement would result if the extraction of both minority and majority carriers could be prevented. This might be achieved for example by interposing a thin layer of a very wide band gap insulator between each contact and the crystal, (Fischer, 1966), (see Figure 2.7f). The insulators in such a device, (M-I-S-I-M) should be chosen so that the one at the anode has a low barrier for holes from the valence band edge and a high barrier for electrons from the conduction band, with the opposite being true at the cathode barrier. However, it has proved difficult to find insulators, with the requisite properties.

Injection electroluminescence in II-VI compounds (see for example Aven, 1967, 1973) can also be realised with semiconductor-semiconductor heterojunctions.

The mechanism of direct-current electroluminescence must also account for the observed current-voltage-luminance characteristics. In a perfect minority carrier injected light emitting device, with 100% quantum efficiency, the luminance is expected to be proportional to the square of the current because of the two-stage (bimolecular) recombination process.

The high-field electroluminescence can result from impact excitation or tunneling in the barrier region. In this case the current is

proportional to $\mathcal{E}^2 \exp(-\text{constant}/\mathcal{E})$, where \mathcal{E} is the field. If the barrier is formed at the cathode by the ionisation of donors under the applied field, the high-field region concentrates in the vicinity of the cathode and tunneling is predominant. The field is then proportional to $V^{1/2}$. However, if the cathode barrier is due to the depletion of donor centres in the phosphor surface, then the field is proportional to applied voltage V . The luminance is proportional to the number of excited luminescent centres. The probability of carriers achieving sufficiently large energies to excite the luminescent centres follows the same exponential dependence on voltage. Therefore the luminescent-voltage characteristics will obey a similar law.

Direct excitation of localised centres (e.g. Mn) by tunneling would still be involved with similar exponential current-voltage characteristics. However, since ionisation would not occur in this process, recombination is monomolecular. Therefore, linear luminance-current characteristics should be observed.

2.4.3 The Schottky Barrier

Schottky barriers are usually formed by evaporating a metal film on to the surface of a single crystal semiconductor. The basic theory, and the early history of metal-semiconductor contacts, has been summarised by Henish (1957). More recently the properties and applications of Schottky barriers have been reviewed by Atalla (1966) and Rhoderick (1969, 1974).

(I) Metal-semiconductor (M-S) system

When a metal and an n-type semiconductor are brought together electrons are transferred from one to the other. The direction of the transfer depends upon the work function of the metal, ϕ_m , and on the

electron affinity of the semiconductor X_s . When $\phi_m > X_s$ electrons pass from the semiconductor to the metal and the Fermi levels in the two materials are forced into coincidence (see Figure 2.8). An electric field, due to the contact potential difference is then set up and exists largely within the semiconductor. It opposes further flow of electrons from the semiconductor to the metal and allows equilibrium to be established. Now the potential energy of an electron at rest, at the bottom of the conduction band, in the interior of the semiconductor differs from the potential energy of such an electron at rest at the surface by an amount $q(\phi_m - X_s)$, which is known as the surface potential, V_B . The negative electric charge at the surface of the metal is balanced by the positive charge of the uncompensated donor ions in the barrier region of the semiconductor. Since the donor concentrations in semiconductors are much less than the concentration of electrons in metals, the balancing positive charges and accompanying electric field must extend to an appreciable depth in the semiconductor. As a result the net population of free electrons in the semiconductor near the surface is reduced from its bulk equilibrium value. The conduction and the valence band edges are shifted upwards with respect to Fermi level. The surface region in the semiconductor is referred to as a 'depletion' region.

When $\phi_m < X_s$ for an n-type semiconductor, electrons will flow from the metal to the semiconductor to establish equilibrium. Here the metal acquires a positive charge and the semiconductor a negative one and the semiconductor bands bend downwards at the surface. Now the electron concentration is greater than the original free electron concentration and a so-called accumulation layer is formed.

(a) Schottky barrier formation

An ideal Schottky barrier in an n-type semiconductor is formed

when a blocking metal electrode (with $\phi_m > X_s$) makes intimate contact with it. To make a Schottky diode, an ohmic contact with $\phi_m < X_s$ is also applied to the semiconductor to allow current transport through the semiconductor. The important point here is that the ohmic contact should not present any potential barriers to the electrons in the conduction band. Thus the only barrier that electrons experience will be the barrier in the depletion region, i.e. the Schottky barrier.

(b) Depletion region

Assuming that the charge density in the depletion region is due to ionised donor atoms only, it is possible to find some parameters of the space charge, depletion region, see Figure 2.8(a). One can use the abrupt approximation that ρ (charge density) $\approx qN_D$ for $x < w$, and $\rho \approx 0$, $dV/dx \approx 0$ for $x > w$. The solution of Poisson's equation leads to the depletion layer width, W ,

$$W = \left\{ \left(\frac{2\epsilon_s}{qN_D} \right) (V_{BO} - V - V_2) \right\}^{1/2} \dots \quad (2.4.2)$$

where ϵ_s is the permittivity of the semiconductor, V_{BO} is the diffusion potential which represents the zero-bias value of the surface potential, and N_D is the uncompensated donor concentration. $V_2 = kT/q$ is a contribution from the mobile carriers at the edge of the depletion region and V is applied bias. The field in the depletion region is given by

$$\left| \mathcal{E}(x) \right| = qN_D/\epsilon_s (W - x) = \left| \mathcal{E} \right|_{\max} - (qN_D/\epsilon_s) x \dots \quad (2.4.3a)$$

where

$$\left| \mathcal{E} \right|_{\max} = (qN_D/\epsilon_s) W \dots \dots \quad (2.4.3b)$$

$\left| \mathcal{E} \right|_{\max}$ is the maximum electric field which occurs at $x = 0$, and the potential function is given as

$$V(x) = (qN_D/\epsilon_s)(Wx - \frac{1}{2}x^2) - \phi_{Bn} \quad \dots \quad (2.4.4)$$

where ϕ_{Bn} is the value of the barrier height at $x = 0$.

The space charge density, Q_{sc} , and the depletion layer capacitance C per unit area of the contact are

$$Q_{sc} = qN_D W = \left[2q\epsilon_s N_D (V_{BO} - V - V_2) \right]^{\frac{1}{2}} \text{ coul/cm}^2 \quad \dots \quad (2.4.5)$$

$$C = \frac{\partial Q_{sc}}{\partial V} = \left[(q\epsilon_s N_D) / 2 (V_{BO} - V - V_2) \right]^{\frac{1}{2}} = \epsilon_s / W \text{ farad/cm}^2 \quad (2.4.6)$$

Thus the relationship between C^{-2} and V is linear when N_D is constant throughout the depletion region, and the slope of such a plot reveals the uncompensated donor density N_D since

$$- d(1/C^2) / dV = 2 / (q\epsilon_s N_D) \quad \text{or} \quad N_D = (2/q\epsilon_s) \{ -dV/d(1/C^2) \} \quad (2.4.7)$$

(c) Schottky barrier (image force) lowering

Another force experienced by electrons in a metal-semiconductor contact is the image force. When an electron in the semiconductor is at a distance x from the metal, a positive charge will be induced on the metal surface. The attractive, image force between this induced charge and the electron is

$$F = - q^2 / \left[4\pi (2x)^2 \epsilon_s \right] \dots \quad \dots \quad \dots \quad (2.4.8a)$$

and the work done by an electron in being transferred from infinity to the point x , is given by

$$U(x) = \int_{\infty}^x F dx = q^2 / (16\pi\epsilon_s x) \quad \dots \quad (2.4.8b)$$

which represents the potential energy of an electron at a distance x from the metal surface. When an external field \mathcal{E} is applied the total

potential energy, $U_T(x)$, is given by the sum

$$U_T(x) = q^2 / (16\pi\epsilon_s x) + q\mathcal{E}x \quad (\text{eV}) \quad \dots \quad (2.4.9)$$

The extent of the barrier lowering, $\Delta\phi$, and the location of this lowering x_m , see Figure 2.8a, are given by the condition $[U(x)]/dx = 0$ (see for example Sze et al, 1964) which leads to

$$x_m = \left(q/16\pi\epsilon_s |\mathcal{E}| \right)^{1/2} \quad (\text{cm}) \quad \dots \quad \dots \quad (2.4.10a)$$

and

$$\Delta\phi_{Bn} = \left[\frac{q^3 N_D (V_{BO} - V - kT/q)}{8\pi^2 \epsilon_o^3 \epsilon_d^2 \epsilon_s} \right]^{1/4} = \left[\frac{q |\mathcal{E}|_{\max}}{4\pi \epsilon_o \epsilon_d} \right]^{1/2} \quad \dots \quad (2.4.10b)$$

$\epsilon_s = \epsilon_d$

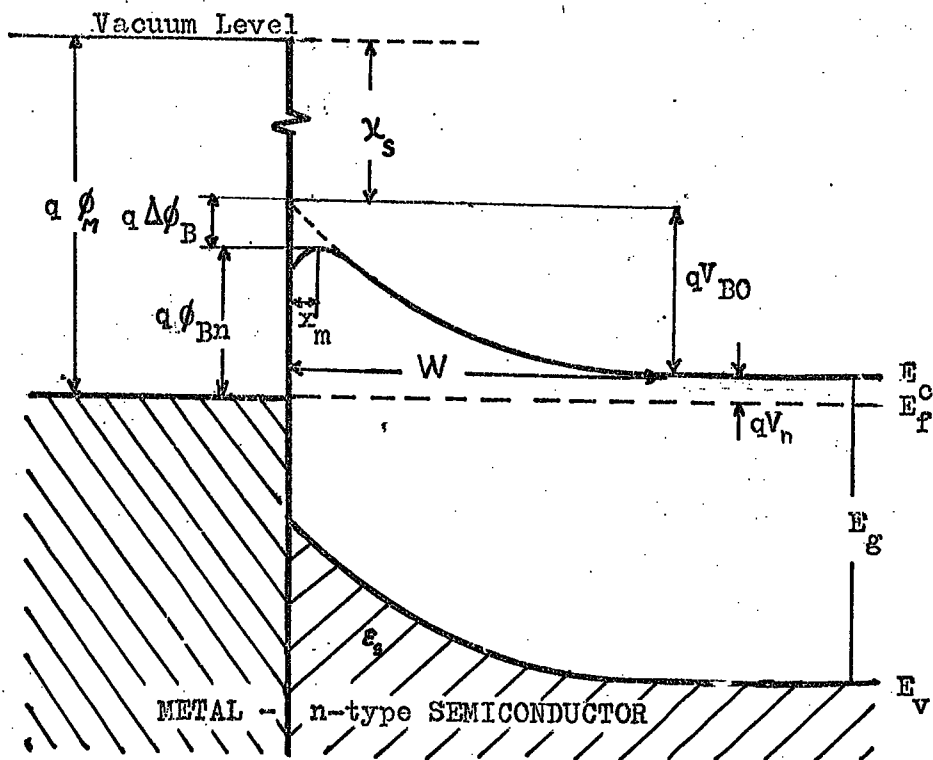
where ϵ_o is the permittivity of free space, ϵ_s the static dielectric constant, ϵ_d the image force dielectric constant and $|\mathcal{E}|_{\max}$ is the electric field of the metal-semiconductor interface.

(d) Barrier Height

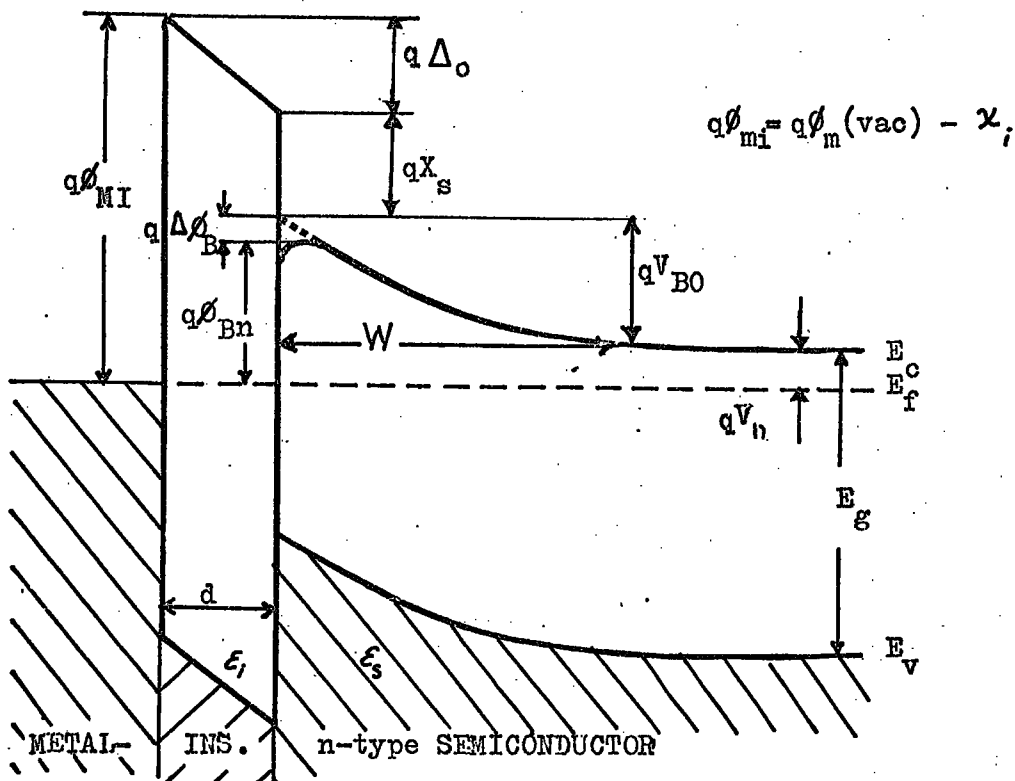
The barrier height can in principle be determined by capacitance measurements. When a small a.c. signal is superimposed on a d.c. bias, charges of opposite sign are induced in the metal and the semiconductor and the relation between C, the capacitance, and V, the d.c. bias, is given by equation 2.4.6. When c^{-2} is plotted as a function of V the barrier height ϕ_{Bn} can be determined from the intercept on the voltage axis since

$$\phi_{Bn} = V_i + V_n + kT/q - \Delta\phi_{Bn} \quad (\text{eV}) \quad \dots \quad (2.4.11)$$

where V_n is the depth of the Fermi level below the conduction band, V_i is the measured voltage intercept and in this case $V_i = V_{BO}'$



(a) - (M - S) Contact at zero applied bias



(b) - (M-I-S) Structure at zero applied bias

FIG. 2. 8 Band diagrams for (M-S) and (M-I-S) contacts. ϕ_M = Metal work function, $\Delta\phi_B$ = Image force lowering, V_{BO} = Diff. potential in Sem. V_d = Depth of Fermi level below the conduction band, ϕ_B = Barrier height, Δ_0 = Potential across interfacial-layer, χ_s = Semicon. electron affinity ϵ_i, ϵ_s = Semiconductor and interfacial-layer permittivity respectively.

kT/q is the contribution from the mobile carriers in the reverse layer (Goodman, 1963), and $\Delta\phi_{Bn}$ is the Schottky barrier lowering. The depth of the Fermi level from conduction band is obtained from

$$qV_n = (E_C - E_f) = kT \ln(N_C / N_d) \quad (\text{eV}) \dots \dots (2.4.12)$$

Here N_C is the effective density of states in the conduction band and is given by

$$N_C = 2 \left[2\pi m_{de} kT/h^2 \right]^{3/2} M_C \quad \dots \quad \dots \quad \dots (2.4.13)$$

m_{de} is the density of state effective mass for electrons, h Plank's constant, and M_C the number of equivalent minima in the conduction band. With II-VI compounds $M_C = 1$. Using the electron effective mass $m_e^* = 0.17 m_e$ (Marple, 1964), an effective density of states N_C of $3.38 T^{1.5} \times 10^{14} \text{ cm}^{-3}$ was calculated for ZnSe.

(II) Metal-Insulator-Semiconductor (M-I-S) System

M-I-S devices are formed when the metal is evaporated on to a semiconductor surface which is already carrying an insulating layer. This contact was first analysed by Goodman (1963). More recently the theory has been modified by Cowley (1966) and Card and Rhoderick (1971). The potential energy diagram of this system under zero bias condition is shown in Figure 2.8b. Δ_0 is the voltage drop across the insulator, which has a thickness d . Using Gauss' law to relate the space charge density Q_{sc} in the semiconductor to the voltage drop across the insulator. Assuming there is no surface states,

$$\Delta_0 = (d/\epsilon_1) \left[2e \epsilon_s N_D (V_{BO} - V_2) \right]^{1/2} \quad \dots \quad (2.4.14)$$

where ϵ_1 is the permittivity of interfacial layer.

From the energy relation in Figure 2.8b ,

$$\phi_{MS} = V_{BO} + \Delta_O = \phi_{MI} - (V_n + X_s) \quad \dots \quad (2.4.15)$$

Defining

$$V_1 = 2e \epsilon_s N_D (d^2/\epsilon_i^2) \dots \dots \dots (2.4.16)$$

Equation 2.4.14 can be simplified to

$$\Delta_O = V_1^{1/2} (V_{BO} - V_2)^{1/2} \dots \dots \dots (2.4.17)$$

From equations 2.4.15 and 2.4.16 the diffusion potential V_{BO} can be written as

$$V_{BO} = \phi_{MS} + V_1/2 - V_1^{1/2} (\phi_{MS} + V_1/4 - V_2)^{1/2} \quad (2.4.18)$$

When a reverse bias V is applied to the junction, V_B and Δ differ from their values at zero bias. The equations 2.4.15 and 2.4.17 become

$$\phi_{MS} + V = V_B + \Delta \quad \dots \quad \dots \quad (2.4.19)$$

$$\Delta = V_1^{1/2} (V_B - V_2)^{1/2} \quad \dots \quad \dots \quad (2.4.20)$$

By eliminating Δ between these two equations one obtains

$$\phi_{MS} + V = V_B + V_1^{1/2} (V_B - V_2)^{1/2} \dots \dots \dots (2.4.21)$$

and the space charge Q_{SC} in the semiconductor is then given by

$$Q_{SC} = \left[2e \epsilon_s N_D (V_B - V_2) \right]^{1/2} \dots \dots \dots (2.4.22)$$

So that the capacitance of the junction becomes

$$C = \delta Q_{SC} / \delta V = (2e \epsilon_s N_D)^{1/2} \left\{ \delta [(V_B - V)^{1/2}] / \delta V \right\} \dots \quad (2.4.23)$$

Solving equation 2.4.21 for $(V_B - V_2)^{1/2}$ and using this value in equation 2.4.23 gives ,

$$C = (e \epsilon_s N_D / 2)^{1/2} (\phi_{MS} + V + V_1/4 - V_2)^{-1/2} \dots \quad (2.4.24)$$

Squaring and inverting, leads to the relation

$$1/C^2 = (2/e \epsilon_s N_D) (\phi_{MS} + V + V_1/4 - V_2) \dots \quad (2.4.25)$$

The magnitude of the intercept of the straight line plot of C^{-2} against V should therefore be

$$V_1 = \phi_{MS} + V_1/4 - V_2 \dots \dots \dots \quad (2.4.26)$$

Which from equations 2.4.15 and 2.4.17 with the value of ϕ_{MS} substituted in equation 2.4.26 leads to the following expression,

$$V_1 = V_{BO} - V_2 + V_1/4 + (V_1 V_{BO})^{1/2} \dots \dots \quad (2.4.27)$$

Cowley considered the case where the charge Q_s stored in the insulating layer varies with the voltage maintained across it. Then Gauss' law gives

$$\Delta_o = V_1^{1/2} (V_B - V_2)^{1/2} + (d/\epsilon_1) Q_s(0) \dots \quad (2.4.28)$$

where $Q_s(0)$ is given as

$$Q_s(0) = -eD_s (E_F - \phi_o) = eD_s (E_g - V_{BO} - \phi_o - \phi_n) \quad (2.4.29)$$

and D_s is the density of surface states. Similarly ,

$$\Delta = V_1^{1/2} (V_{BO} - V_2)^{1/2} + (d/\epsilon_1) Q_s(V) \dots \quad (2.4.30)$$

So that

$$\Delta - \Delta_o = V_1^{1/2} \left[(V_B - V_2)^{1/2} - (V_{BO} - V_2)^{1/2} \right] + (d/\epsilon_1) \Delta Q_s \quad (2.4.31)$$

and the charge in the surface state charge is

$$\Delta Q_s = -e N_s (\Delta - \Delta_o) \dots \dots \dots (2.4.32)$$

which leads to the following relation between C^{-2} and V , the applied bias

$$1/C^2 = \left(2/e \epsilon_s N_D \right) \left\{ \left(V_1^{1/2} (V_{BO} - V_2)^{1/2} / (1 + \alpha) \right) + \left(V_1 / 4(1 + \alpha)^2 \right) + V_{BO} + V - V_2 \right\} (2.4.33)$$

Here $\alpha = e D_s d / \epsilon_i$.

This equation implies that the slope would not change in the presence of an insulating layer.

Now the intercept on the voltage axis is :

$$V_i = V_{BO} + \left[V_1^{1/2} (V_{BO} - V_2)^{1/2} / (1 + \alpha) \right] + \left[V_1 / 4(1 + \alpha)^2 \right] - V_2 \dots (2.4.34)$$

However if the assumption is made that $\partial Q_s / \partial V = 0$, $Q_s(0)$ and $Q_s(V)$ in equations 2.4.28 and 2.4.29 will be equal, then :

$$\Delta - \Delta_o = V_1^{1/2} (V_B - V_2)^{1/2} - (V_{BO} - V_2)^{1/2} \dots \dots (2.4.35)$$

The intercept on the voltage axis is then given by the expression

$$V_i = V_{BO} + V_1^{1/2} (V_{BO} - V_2)^{1/2} + (V_1/4) - V_2 \dots \dots (2.4.36)$$

2.4.4 Current Transport Processes in Schottky Barriers

Current transport processes in Schottky barriers have been studied by many workers. The most recent review has been given by Rhoderick (1974). The conduction mechanism was first described by Wagner (1931) and Schottky and Spenke (1939). Their theory of current transport in Schottky diodes was based mainly on diffusion, and the current was limited by diffusion and drift in the depletion region. The current-voltage relation by

Spence (1958) was expressed as

$$J = J_s \left[\exp (qV/kT) - 1 \right] \dots \dots \dots (2.4.37a)$$

with the saturation current J_s given by

$$J_s = qN_D \mu \frac{|\mathcal{E}|_{\max}}{q} \left[\exp (-q\phi_{Bn}/kT) - 1 \right] \dots \dots \dots (2.4.37b)$$

where μ is the electron mobility, $|\mathcal{E}|_{\max}$ is the maximum electric field strength (see equation 2.4.3) in the barrier and ϕ_{Bn} is the barrier height. In this theory it was assumed that only those electrons in the semiconductor immediately adjacent to the metal were in thermal equilibrium with the electrons in the metal.

Bethe (1942) proposed the so-called diode theory which assumed that the current is limited by the thermionic emission process. The current-voltage relation obtained by Bethe was

$$J = J_s \left[\exp (qV / kT) - 1 \right] \dots \dots \dots (2.4.38a)$$

where

$$J_s = A^*T^2 \exp (-q\phi_{Bn} / kT) \dots \dots \dots (2.4.38b)$$

with

$$A^* = (4\pi m^* q k^2) / h^3 \text{ (Richardson constant)} \dots \dots \dots (2.4.38c)$$

The difference between the two theories is most clearly resolved in terms of the behaviour of the quasi-Fermi level for electrons (Rhoderick, 1970).

In the diffusion theory, the quasi-Fermi level for electrons is assumed to coincide with the Fermi level in the metal only in the vicinity of the interface. However the diode (thermionic emission) theory assumes that the quasi-Fermi level for electrons remains horizontal throughout the depletion region.

Crowell and Sze (1966), combined the diffusion and thermionic emission theories by considering the two mechanisms to be in series. Their model introduced the recombination velocity v_r at the top of the barrier. According to Crowell and Sze, equation 2.4.37 can be modified,

$$J = J_s \left[\exp \left(\frac{qV}{kT} \right) - 1 \right] \dots \dots (2.4.39a)$$

where

$$J_s = qN_c v_r / (1 + v_r / v_d) \exp \left(-q\phi_{Bn} / kT \right) \dots (2.4.39b)$$

where v_d is the drift velocity. This equation takes into account both diffusion and drift in the depletion region. Crowell and Sze also considered the effects of optical phonon scattering at the top of the barrier and of the quantum mechanical reflection of those electrons which have sufficient energy to surmount the barrier. In consequence they simply modified the Richardson constant A^* by writing,

$$A^{**} = (f_p f_Q A^*) / [1 + f_p f_Q (v_r / v_d)] \dots (2.4.40)$$

where f_p is the probability of electron emission over the barrier without interacting with an optical phonon, and f_Q is the average transmission coefficient. Crowell and Sze found that at room temperature in the range of values of electric field from 10^4 to about 10^5 V cm^{-1} , the current transport mechanism in most of the Schottky barrier diodes prepared on Ge, Si and GaAs was limited by the thermionic emission of the majority carriers.

Rhoderick (1972, 1974) showed that thermionic theory applies if $v_d \gg v_r$ in equation 2.4.39. This was shown to be equivalent to

$$\mu \mathcal{E}_{\max} \gg \bar{v} / 4, \quad q \mathcal{E}_{\max} \gg m^* \bar{v} / 4\tau \quad \text{or} \quad \lambda q \mathcal{E}_{\max} \gg 2kT / \pi \dots (2.4.41a)$$

where

$$\mu = q\tau/m^* \quad \text{and} \quad \bar{v} = (8kT/\pi m^*)^{1/2} \quad \dots \quad \dots \quad (2.4.41b)$$

and where λ is the mean free path of electrons in the semiconductor, τ is their mean free time.

In practice the voltage dependent image force lowering, $\Delta\phi$ (see equation 2.4.10b) may lead to departures from ideal behaviour, and it is used to write the experimental forward current-voltage characteristics as

$$J = J_s [\exp (qV/nkT) - 1] \quad \dots \quad \dots \quad \dots \quad (2.4.42)$$

where

$$n = (q/kT) [d(\ln J) / dV]^{-1} \quad \dots \quad \dots \quad \dots \quad (2.4.43)$$

and J_s is the saturation current. For ideal diode behaviour the value of n is expected to be unity. Sze et al (1964) showed with Si and GaAs diodes that the effect of image force lowering on the forward bias characteristics was negligible when $N_D < 10^{17} \text{ cm}^{-3}$, and $n \approx 1.02$. The value of n is greater than unity in the forward direction when there is an insulating layer between metal and semiconductor. According to Card and Rhoderick (1971) the value of n is affected by the presence of the interface states and is given by

$$n = 1 + \left\{ (d/\epsilon_i) (\epsilon_s/W + qD_{sb}) / (1 + (d/\epsilon_i) qD_{sa}) \right\} \dots \quad (2.4.44)$$

where D_{sa} is the density of interface states which are in equilibrium with the metal, and D_{sb} the density of states which are in equilibrium with the semiconductor, ϵ_i is the permittivity of the insulating film, and d its thickness, and ϵ_s is the permittivity of the semiconductor and W the thickness of the depletion region.

According to both the diode (thermionic) and diffusion theories the reverse current should saturate at J_s (see for example equation 2.4.38b). However there are often departures from this ideal behaviour, and saturation may not be observed. One of the possible reasons is that the barrier height, ϕ_{Bn} depends on the maximum electric field strength, $|\mathcal{E}|_{max}$ in the barrier, since $|\mathcal{E}|_{max}$ increases with the application of reverse bias the barrier height decreases accordingly. In this event the current would be expected to increase as $\exp(\Delta\phi_{Bn}/kT)$, where $\Delta\phi_{Bn}$ here is the barrier lowering. More recently Arizurai and Hirose (1969) and Andrews and Lepselter (1970) have described the reverse current-voltage characteristics of nearly ideal Si Schottky diodes in terms of image force lowering.

It may also be possible for electrons with energies below the top of the barrier to penetrate the potential barrier by quantum mechanical tunneling. The Field (F) and Thermal Field (TF) theories have been developed by Padovani and Stratton (1966) and Crowell and Rideout (1969). It was postulated that field emission occurred only in degenerate semiconductors because of the very small effective masses involved. At low temperatures the forward current was found to arise from electrons with energies close to the Fermi energy in the degenerate semiconductor, (Field emission). However, when the temperature is higher the electrons are excited to higher energies and the tunneling increases because the electrons experience thinner and lower barriers, (Thermionic-field (TF) emission).

2.4.5 Experimental determination of the barrier height in Schottky diodes

(a) Photoelectric Measurement

It is well known that the photoelectric measurement is the most

accurate and the most direct method of determining the barrier height (Crowell et al, 1962). When a metal-semiconductor junction is illuminated with monochromatic light either from the front or back through the bulk of semiconductors, a photocurrent may be generated. The light can excite electrons from the metal if $h\nu \geq q\phi_{Bn}$, and can generate electron-hole pairs in the semiconductor within one diffusion length of the contact when $h\nu \geq E_g$. Electrons emitted from the metal can surmount the barrier and are then accelerated in the high field ($> 10^5 \text{ V cm}^{-1}$) of the depletion layer and contribute to the short circuit photo-current. The photo-current per absorbed photon, R , as a function of the photon energy, $h\nu$, is described by Fowler (1931) theory which can be approximated for direct gap semiconductors as, $R \sim (h\nu - h\nu_0)^2$, which can be applied to M-S contact as ,

$$(R)^{\frac{1}{2}} \sim (h\nu - q\phi_{Bn}) \quad \text{for} \quad q\phi_{Bn} \leq h\nu < E_g \quad \dots \quad \dots \quad (2.4.45a)$$

and

$$(R)^{\frac{1}{2}} \sim (h\nu - E_g) \quad \text{for} \quad h\nu \geq E_g \quad \dots \quad \dots \quad \dots \quad (2.4.45b)$$

Therefore when the square root of the photoresponse, $(R)^{\frac{1}{2}}$, per absorbed photon is plotted against the photon energy, the intercepts of this straight line regions give the values of the barrier height and the band gap. Grimmeis (1974) pointed out the importance of the deep levels in the semiconductor in contributing to the photocurrent in M-S contacts.

(b) Capacitance-Voltage Measurements

The barrier height can also be determined by capacitance-voltage (C-V) measurements. When a small ($< 25 \text{ mV}$) a.c. voltage is superimposed on the d.c. voltage, charges of one sign are induced on the metal surface and the charges of opposite sign in the semiconductor. The relation

between C and V is given by equation 2.4.6. The built-in voltage, V_{Bo} , can be determined from the intercept, V_i , on the voltage axis of the straight plot of C^{-2} against V. The barrier height, ϕ_{Bn} , is given by 2.4.11.

With M-I-S diodes, a plot of C^{-2} vs. V again leads to a straight line (Goodman, 1963 and Cowley, 1966), (equation 2.4.33). However the intercept on the voltage axis now is given by equations 2.4.34 and 2.4.36, where V_{Bo} is determined by photoelectric measurements if V_n is known. The value of the barrier height, ϕ_{MS} , can again be expressed by equation 2.4.26.

(c) Current-Voltage Measurements

The barrier height in M-S contacts can also be determined from forward bias I-V measurements. The forward characteristics are represented by equation 2.4.42. The value obtained by extrapolating the current density to zero voltage gives the saturation current, J_s . The barrier height can then be obtained from the following equation ,

$$\phi_{Bn} = (kT/q) \ln (A^{**} T^2 / J_s) \quad \dots \quad \dots \quad (2.4.46)$$

2.5 DIRECT CURRENT ELECTROLUMINESCENCE IN THE SINGLE CRYSTALS OF ZnS, Zn(S,Se) AND ZnSe

(a) Electroluminescence in ZnS

Some of the first work on d.c. EL in single crystals of ZnS was reported by Piper and Williams (1952). They used crystals doped with copper. The emission originated at cathode. The light output increased exponentially with voltage and linearly with current. A mechanism of impact excitation of activator centres by hot electrons was proposed. Smith (1955) studied dc EL in single crystals of ZnS which did not

contain intentionally added impurities, and observed a broad emission band extending from 3400 (band edge) to 6000 Å. He favoured a mechanism involving the injection of holes and electrons. The first claim to have prepared a p-n junction device on single crystals of ZnS came from Narita (1960). According to him copper was evaporated and diffused into ZnS to form a p-type layer. The same method was later used with ZnS:Cl by Georgebiani and Steblin (1967). With these devices emission was apparent in the forward direction with applied biases of about 2 V. Indradev and Garlick (1967) examined the electroluminescence of ZnSe:Cu single crystals. They attributed the low voltage d.c. electroluminescence to copper precipitates at stacking faults, which behaved as reservoirs of holes. Biter et al (1969) studied electroluminescence in single crystals of ZnS:Cu which had been heated in molten zinc. They observed the blue self-activated and green emission bands of undoped and copper doped samples respectively. The light emission at low applied voltages (1.6 V) was attributed to the existence of n^+n junctions where the energy of the emitted photons was believed to be provided by hot electrons. The bright spots at the cathode which appeared at higher voltages of about 15 V were believed to result from impact ionisation in Schottky barriers, as will be described later. Özsan and Woods (1974) observed d.c. electroluminescence in single crystals of ZnS:I which had been heat treated in a molten alloy of zinc and aluminium. They observed self-activated emission in the blue region of the spectrum with a maximum intensity at 2.58 eV. They obtained a luminance of 90 ft-Lambert for a power dissipation of 600 mW at 20 V.

(b) Electroluminescence in mixed crystals

D.C. electroluminescence in II-VI solid solution systems such as Zn(Se,Te), has generally been investigated from the point of view of

obtaining efficient injection devices. Electroluminescent p-n junction diodes have in fact been prepared from the $\text{ZnSe}_x\text{Te}_{1-x}$ system, Aven (1965), by diffusing Al into as-grown p-type crystals.

Electroluminescence in powdered phosphors of Zn(S,Se) has been studied by some authors (see for example Larach and Scradler, 1959; Asano and Nakao, 1964 and Goldman et al, 1968), but electroluminescence in single crystals of solid solutions of Zn(S,Se) has not been fully investigated. However, Özsan and Woods (1975) described a green electroluminescence in crystals of $\text{ZnS}_{0.6}\text{Se}_{0.4}$ which had been heat treated in molten zinc and aluminium. With reverse biased Schottky diodes they achieved a luminance of 200 ft. Lamberts at an applied voltage of 11 V, corresponding to a power efficiency of $1 \times 10^{-3}\%$. At room temperature the light was emitted in a broad band centred at 2.27 eV. This shifted to 2.34 eV at 85 K. This work will be described in detail later in this thesis.

(c) Electroluminescence in ZnSe

Electroluminescence in single crystals of ZnSe has been studied by Fischer (1964, 1966). He used metal-semiconductor contacts on undoped n-type ZnSe crystals. Light was produced when the device was operated in reverse bias. He explained the observed electroluminescence in terms of impact ionization. The spectral distribution for the avalanche electroluminescence extended to the absorption edge. Fischer observed injection electroluminescence under forward bias conditions (see Figure 2b) using contacting metals with work functions higher than 4.8 eV (i.e. Pt or Ir). The resultant injection electroluminescence spectrum was contained in a broad band ($1,000 \text{ \AA}$) at 1.96 eV. The light emission was found to originate from the anode and was initiated with a potential as low as 1.35 V. Fischer also studied injection and avalanche electroluminescence in n-type ZnSe crystals in the presence of thin insulating

layers under the metal contacts, (see Figure 2. d,e). Aven and Cusano (1964) investigated the $\text{Cu}_2\text{Se-ZnSe}$ heterojunction. Light emission was observed at 1.4 V in forward bias. The emission spectra at 77 K consisted of several bands peaking at 1.96, 2.07, 2.36 and 2.68 eV. At 77 K brightness levels of 1,000 ft. Lambert were measured with ZnSe:Cl crystals. Park et al' (1972) observed a yellow-orange electroluminescence using various Schottky barrier devices on n-ZnSe:Al . The emission at 300 K was found to peak at 2.10 eV, and could be resolved into two bands at 2.21 and 1.95 eV at 4.2 K. External quantum efficiencies of 0.1% and brightness levels of 200 ft. Lambert were obtained at an input power of 100 mW at 300 K. Allen et al (1972) prepared Schottky barriers on n-type ZnSe:Al crystals containing either Mn or Cu, or both, to provide luminescent centres. The EL and PL emission spectra of the Cu doped samples both showed peaks at 1.91 eV. However, the reverse bias EL in the Mn doped samples was located at 2.10 eV and 300 K and 2.12 eV at 118 K. Later Livingstone et al (1972) described the light emission in forward biased ZnSe:Al diodes with Mn or Cu dopants. They found the forward bias EL peaking at 1.90 eV for Cu doped, at 2.0 eV for Mn doped and 2.675 eV for undoped samples. The threshold for light emission was at 1.3 V. Turvey and Allen (1973) observed a broad emission band extending from 0.4 to 2.65 eV when Schottky barriers of n-type ZnSe , without deliberately added impurities, were driven in reverse bias. They suggested that radiative transitions could occur between different points in the Brillouin zone and indeed demonstrated a correlation with the shape of the conduction band of ZnSe . Ryall and Allen (1973) have also observed exciton emission in the forward bias EL of ZnSe:Al Schottky diodes which were free of other intentionally added luminescence centres. Özsan and Woods (1975) have confirmed the observations of Allen et al (1972) and Park et al (1972),

and have shown that the EL reported by Park et al is the self activated luminescence, which coincidentally in ZnSe lies very near the same wavelength as the characteristic emission of manganese. This topic will be discussed later in this thesis. Recently the first claim to have observed injection EL in a phosphorus-ion-implanted ZnSe p-n junction diode came from Park and Shin (1974). EL appeared under forward bias. The emission peaked at 1.96 eV and had a quantum efficiency of 0.01% at 300 K.

CHAPTER 3

CRYSTAL GROWTH

3.1 INTRODUCTION

II-VI compounds are formed from the elements of groups II and VI of the periodic table. The opto-electronically important compounds are those which form subgroups of zinc and cadmium chalcogenides, namely ZnO, ZnS, ZnSe, ZnTe and CdO, CdS, CdSe, CdTe. Single crystals of zinc selenide, zinc sulphoselenide and zinc sulphide, with particular emphasis on zinc selenide, have been grown and studied during the course of this research. Some of the well-known crystallographic properties of the zinc chalcogenides, together with the purification and crystal growth techniques used in the present work, will be described in the following sections.

3.2 CRYSTAL STRUCTURE AND BONDING IN II-VI COMPOUNDS

In the II-VI compounds the valence electrons are provided by the atoms of the constituent elements, the electrons can either be transferred or shared between the atoms. In the former case, completely filled subshells (i.e. $\text{Zn}^{++}\text{Se}^{--}$) lead to an ionic bonding, whereas in the latter case (i.e. $\text{Zn}^{--}\text{Se}^{++}$) each atom possesses four electrons on average and the bond is covalent. For comparison, the bonding in compounds formed from elements of groups I and VII of the periodic table (i.e. NaCl, KCl) is strongly ionic. The well-known elemental semiconductors in group IV (i.e. Si, Ge) or III-V compounds (i.e. GaAs) show strong covalent bonding. The degree of ionicity decreases with the decrease in electronegativity difference between the elements. (i.e. 2.2 for KCl, 0.9 for ZnSe, 0.5 for GaAs and zero for Si). Thus the shift from ionic to covalent bonding is gradual.

The II-VI compounds are therefore expected to show a bonding which is neither ionic nor covalent but somewhere in between. Pauling (1960) compared the nearest neighbour separations, which were computed from the covalent and ionic radii of the atoms concerned, with the values obtained experimentally from the lattice parameter. This shows that most of the II-VI compounds do in fact possess covalent bonding. However, the ionic influence is evident since a decrease in the atomic weight in II-VI compounds leads to reduced mobilities, high melting temperatures and increased bandgap energies. The lattice parameters of the zinc chalcogenides obtained from recent experimental studies are given in Table 3.1

As with the elements of group IV, II-VI compounds also form tetrahedral bonds. Tetrahedral bonding and covalency are the results of highly directional sp^3 orbitals (directed towards the corners of a tetrahedron) formed by shared electrons. This arrangement produces two crystallographic structures in II-VI compounds, i.e. zinc blende (or cubic) and wurtzite (or hexagonal). Both zinc selenide and zinc sulphide have stable cubic and hexagonal structures, depending on the growth conditions. However, the zinc blende structure is the more stable phase of zinc selenide. In this structure each of the constituent atoms lies on a face-centred cubic sub-lattice with the two sub-lattices being displaced relative to one another by one quarter of the body diagonal of the cube.

3.3 CRYSTAL GROWTH

Methods of crystal growth and the crystallographic properties of the II-VI compounds have been reviewed by Lorenz (1967), Roth (1967) and Ray (1969). The most important requirement in crystal growth is the preparation of structurally and chemically pure crystals, which

COMPOUND	MELTING POINT TEMPERATURES (°C).	CRYSTAL STRUCTURE	LATTICE PARAMETER	
			a(Å)	c(Å)
ZnO		Wurtzite	3.2426	5.190 (5)
ZnS	1830 (1)	Wurtzite	3.820	6.260 (6)
		Zinc Blende	5.4093	(7)
ZnSe	1515 (2)(3)	Wurtzite	4.003	6.540 (8)
		Zinc Blende	5.6687	(9)
ZnTe	1295 (2)(4)	Wurtzite	4.270	6.990 (10)
		Zinc Blende	6.1037	(11)

(1) Addamiano.A, and P.A.Dell (1957)
(2) Narita.K.,H.Watanabe And M.Wada (1970)
(3) Aigrain.P. and M.Balkanski (1961)
(4) Lorenz.M.R. (1967)
(5) Heiland.M. and H.Mollwo (1959)
(6) Fuller.M.L. (1929)
(7) Skinner,B.J and P.B.Barton (1960)
(8) Chan,F.L. and Y.S.Park.(1964)
(9) Larach,S.,R.E.Shrader and C.F.Stocker (1957)
(10) Chistyakov,I.D and E.Krucheanu,(1961)

TABLE 3.1, Lattice parameters and melting points for zinc chalcogenides.

necessitates some knowledge of their thermodynamic properties. Crystals of II-VI compounds are usually grown in one of three ways: from the liquid phase, from the vapour phase or by chemical transport. Most of the II-VI compounds, especially the zinc chalcogenides, require vapour or chemical transport methods because of their high melting points (see Table 3.1) which lead to difficulties with the use of silica and the high vapour pressures at the melting temperatures. However, in spite of these difficulties, single crystals of zinc sulphide, zinc selenide and zinc telluride have been grown from melt in centimetre dimensions by Fischer (1958, 1959). High purity zinc oxide has been produced by oxidation of high purity evaporated zinc by Heiland and Mollwo (1959). Single crystals of II-VI compounds have been grown most frequently from the vapour phase and by chemical transport methods. The vapour growth method was first devised by Reynolds and Czyzak (1950) and modified later by Green et al (1958) and Piper and Polish (1961). They grew large single crystals of ZnS, ZnSe, ZnTe, CdS and CdTe. Samelson (1961) and Hartmann (1962) have shown with zinc sulphide single crystals that the formation of one preferred structure (either solely sphalerite or wurtzite) can be achieved by further refinement of the crystal growth conditions.

Single crystals of zinc selenide have been grown from the vapour phase by Burr and Woods (1971) using the technique originally employed by Clark and Woods (1968) to grow crystals of cadmium sulphide.

The chemical transport method was first applied to II-VI compounds by Nitsche (1960), who produced single crystals of zinc selenide and sulphide with millimetre dimensions. This technique has the advantage that the crystals grow at relatively low temperatures. However, it has the disadvantage that the transporting agent is incorporated as an impurity.

The crystals studied in this work were grown in this laboratory. The furnace arrangements and the methods of growth are discussed in the following sections.

3.3.1 PREPARATION AND PURIFICATION OF THE STARTING MATERIAL

B.D.H. Ltd. 'Optran' grade zinc selenide or zinc sulphide powder was used to produce most of the crystals used in this work. However, some of the starting material was produced from direct combination of the elements in this laboratory using 5N zinc, selenium or sulphur which were obtained from Metal Research Ltd. The system employed for the preparation of the starting material from the elements is illustrated in Figure.3.1(a). A three zone furnace was used to heat the elements in a silica tube in a stream of high purity argon. The first and second zones were used to contain the elements, and the crystals grew in the third zone. The temperatures over the three zones were varied and controlled automatically with the help of Pt-Pt/Rh thermocouples. The non-metallic and the metallic vapours from the first and second zones were mixed and passed to the third zone where supersaturation occurred at the cooler part of the zone. The excess metallic or non-metallic elements also sublimed in the gradient, towards the end of the third zone, to be deposited as a residue. Some non-volatile impurities were also expected to be extracted during this sublimation process. In fact there is always some degree of purification in the growth process where sublimation takes place, because of the one-step distillation process. B.D.H. 'Optran' grade zinc selenide powder was purified in a similar way by subliming it in a stream of argon. A typical flow run system for this purification operation is shown in Figure 3.1(b). A single zone furnace was used for this purpose. The

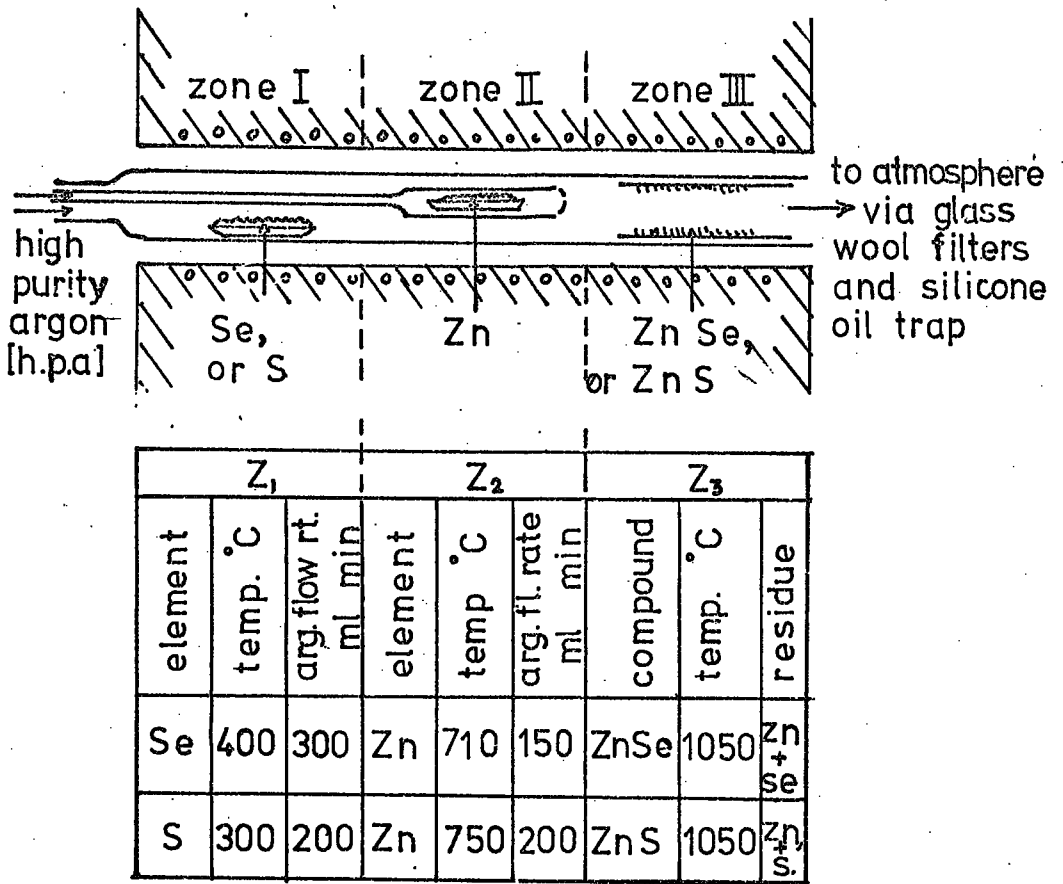


FIG.3.1.[a] System for direct combination from elements

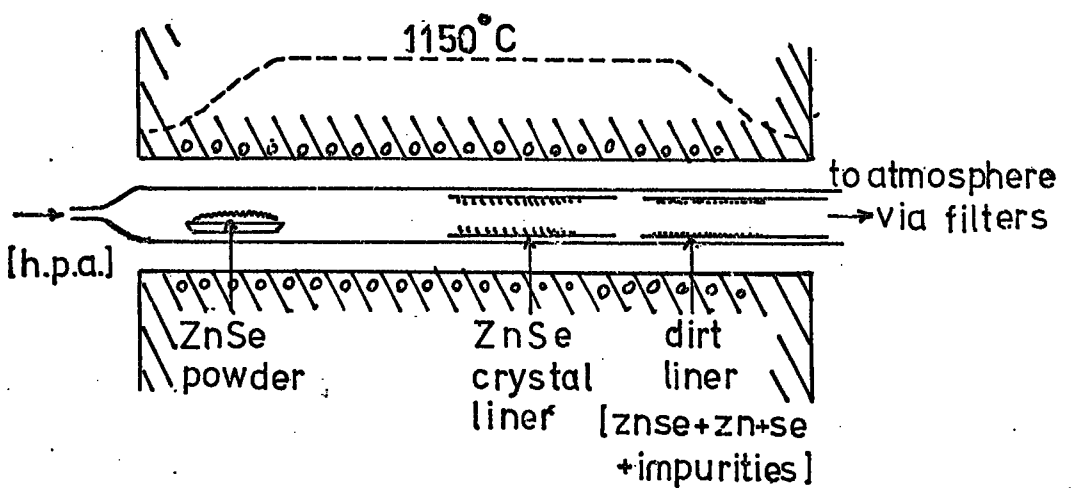


FIG.3.1.[b] The argon flow crystal growth system

powder was placed in a silica tube, in a stream of high purity argon, and heated to 600°C for ten hours to remove all non-volatile impurities. The temperature was then raised to 1150°C for about ten days. In this period of time the powder was sublimed towards the cool end of the tube. The large faces of platelet crystals of zinc selenide produced by this method were several mm^2 in area.

The B.D.H. zinc sulphide powder was purified in a different way and the argon flow was not used. The silica tube containing the powder was sealed at one end and continuously evacuated from the other. The tube was placed in a temperature gradient with the charge at 1150°C . The ZnS was then sublimed towards the cool end of the tube.

3.3.2 VAPOUR GROWTH

Large single crystals of zinc selenide were grown in this laboratory using the vapour phase technique described by Burr and Woods (1971). The growth system is illustrated in Figure 3.2(a). The platelet crystals that were obtained from the flow run process were crushed and used as the charge in a silica capsule. The growth capsule was in communication with a tail, via a narrow orifice which contained either zinc or selenium. The capsule and the tail were evacuated and flushed, and baked in high purity argon and then re-evacuated down to 3×10^{-6} torr and sealed. The tube was placed in a vertical furnace with the charge at 1150°C and the tail at 310°C when using selenium, or 570°C when using zinc. The growing crystal interface was usually at 1020°C . The partial pressure of zinc or selenium provided by the tail was necessary to control the pressure of one of the components to provide a minimum total pressure, P_{min} , and to achieve a near stoichiometric composition of the vapour in the

growth region of the capsule. The capsule was pulled upwards through a temperature gradient at a rate of 1.5 cm a day. The zinc selenide was sublimed from the bottom to the top in a period of fifteen days. The temperature of the capsule was reduced to room temperature slowly over 80 hours. Typical single crystal boules were one centimetre in diameter and several centimetres long, (see part a in Figure 3.3)

With this method, it was also possible to dope the zinc selenide crystals with certain impurities. For example, samples doped with indium or aluminium were obtained by adding these elements directly to the charge. Chlorine was introduced by adding zinc chloride, while copper was introduced as the metal or as the selenide. When crystals containing manganese were required, anhydrous manganese chloride was added to the tail, or introduced as the metal, or as the selenide to the charge. In this way crystals containing up to 2,000 ppm of manganese could be produced.

Single crystals of solid solutions of zinc selenide and zinc sulphide, i.e. zinc sulphoselenide, $Zn(S:Se)$, could also be grown successfully using this method. High purity powders of zinc selenide and zinc sulphide were crushed and ground together in the required proportions, to achieve an intimate mixture of the two. The mixed powder was used as the charge in the growth capsule, which was flushed with high purity argon, evacuated and sealed at a pressure of 2×10^{-6} torr and placed in a vertical furnace. The charge was pre-annealed for three days to allow sintering to occur and was then held at $1165^{\circ}C$ for most of the growth process. The tail, which contained zinc, was maintained at temperatures which would allow the P_{min} condition to be attained at the growth tip of the capsule. This temperature, and that of the growth tip therefore, depended upon the composition of the crystal being grown, (Cutter et al 1976). The capsule was then

pulled upwards at a rate of 1.5 cm a day for 15 days. In this way cylindrical boules of solid solution crystals were produced several cms long and 1 cm in diameter.

This method of growing single crystals of solid solutions of $\text{ZnS}_x\text{Se}_{1-x}$ was only successful for compositions up to 60 molar per cent of sulphur. High concentrations of sulphur led to multiple nucleation and non-uniform boules.

It was very difficult to grow single crystals of zinc sulphide using the same technique because the temperatures were essentially too low.

3.3.3 HIGH TEMPERATURE GROWTH

A few attempts were made to grow the crystals of interest at high temperatures using an argon atmosphere. A silica tube, of 5 mm diameter and 15 cm long, was used to contain the purified charge material. The tube was sealed at one end and made narrower at the other end. It was then placed in a horizontal furnace kept at 1300°C and an atmosphere of high purity argon was maintained inside it. The tube was pulled through a temperature gradient at a rate of about 2 cm a day. Sublimation took place at about $1200 - 1250^\circ\text{C}$ and the crystals grew at the narrow end (which was blocked by the growing crystal).

3.3.4 CHEMICAL TRANSPORT

The chemical transport system of crystal growth used in this work was based on the method described by Nitsche (1960). Iodine was used as the transporting agent. The system which is illustrated in 3.2(b) consisted of two furnaces, a main (single zone) and a mini (two zones) one. The mini furnace was inserted into the main one.

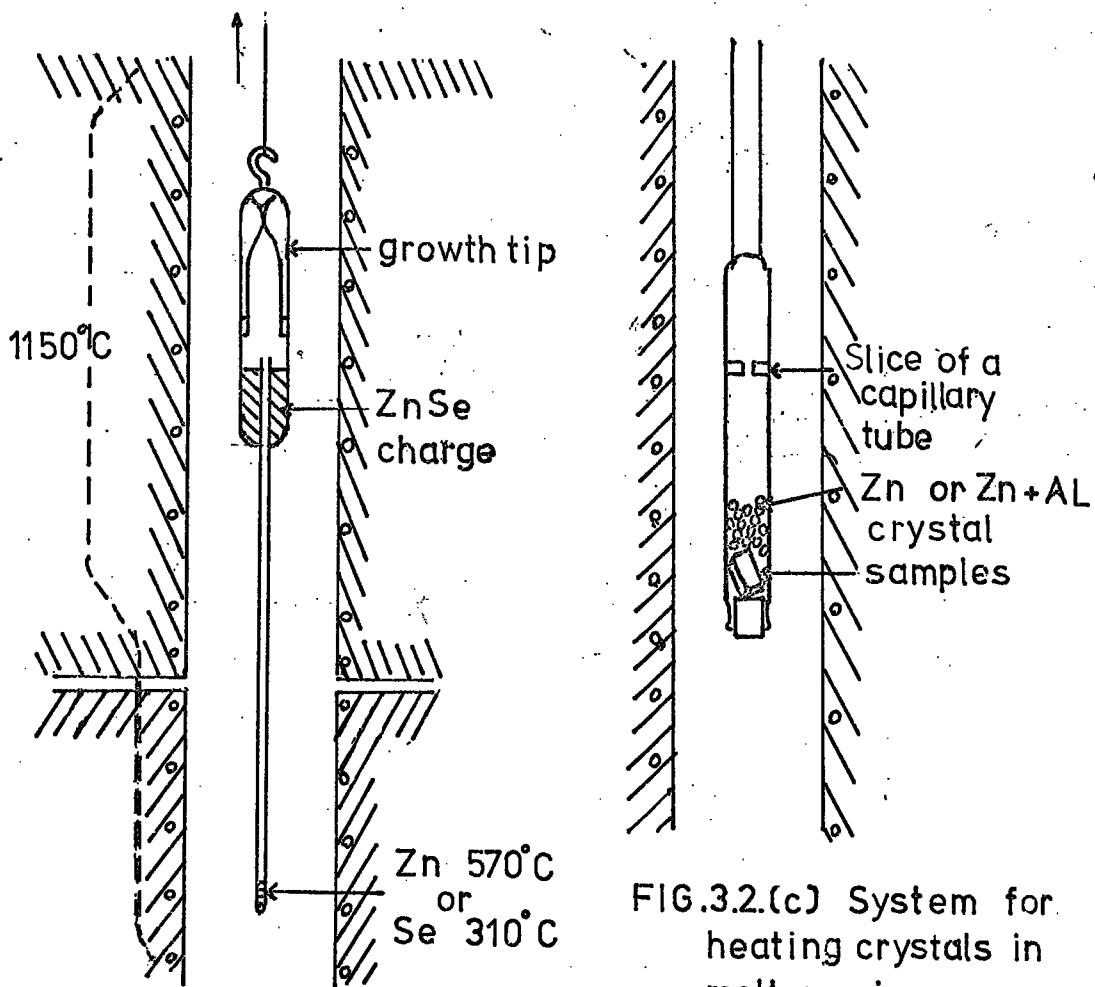


FIG.3.2.(c) System for heating crystals in molten zinc.

FIG. 3.2.(a) The growth system for vapor phase transport.

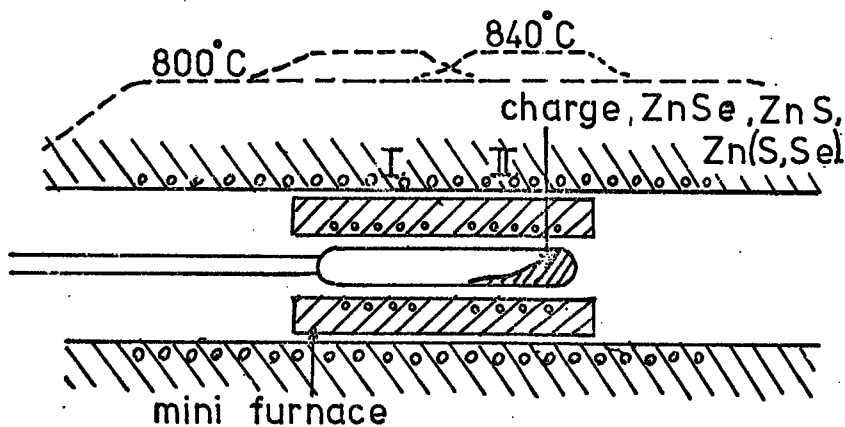


FIG. 3.2.(b) Chemical transport crystal growth system

The temperature of the main furnace and the temperatures of the two ends of the mini furnace were automatically controlled using Pt-Pt/Rh thermocouples. A silica tube of 6 mm inner diameter and about 10 cm long was used to contain 4 gm of purified charge material, with 2 milligrams of iodine for every cubic centimetre of the volume of the tube. The tube was flushed with high purity argon several times, then sealed at 10^{-4} torr and placed in a mini furnace. Next, the main furnace was heated to 800°C and maintained constant at that temperature throughout the growth period. Then the temperature of the mini furnace was adjusted until the growth tip of the capsule was at 900°C and the charge end at 800°C . With such a temperature profile it was possible to sinter the charge and clean the growth tip from stray powdered material, which was transported back to the charge within 24 hours. After this period, the temperature gradient over the mini furnace was reversed to achieve a temperature profile from 800° to 840°C between the growth and charge ends of the capsule. The capsule was held in this temperature gradient for about 12 days. At the end of this period single crystals of about 5-6 mm in diameter and one cm in length were found to have grown at the cool end (cleaning end) of the capsule.

Using this method, crystals of zinc selenide, zinc sulphide and zinc sulpho-selenide ($\text{ZnS}_x\text{Se}_{1-x}$) with all compositions were grown successfully.

3.4 HEAT TREATMENT FOR EXTRACTION OR INTRODUCTION OF 'IMPURITIES'

Most of the as-grown crystals of zinc selenide, zinc sulpho-selenide or zinc sulphide had high resistivities of the order of 10^{12} - 10^{14} ohm cm, although some of the zinc selenide crystals with

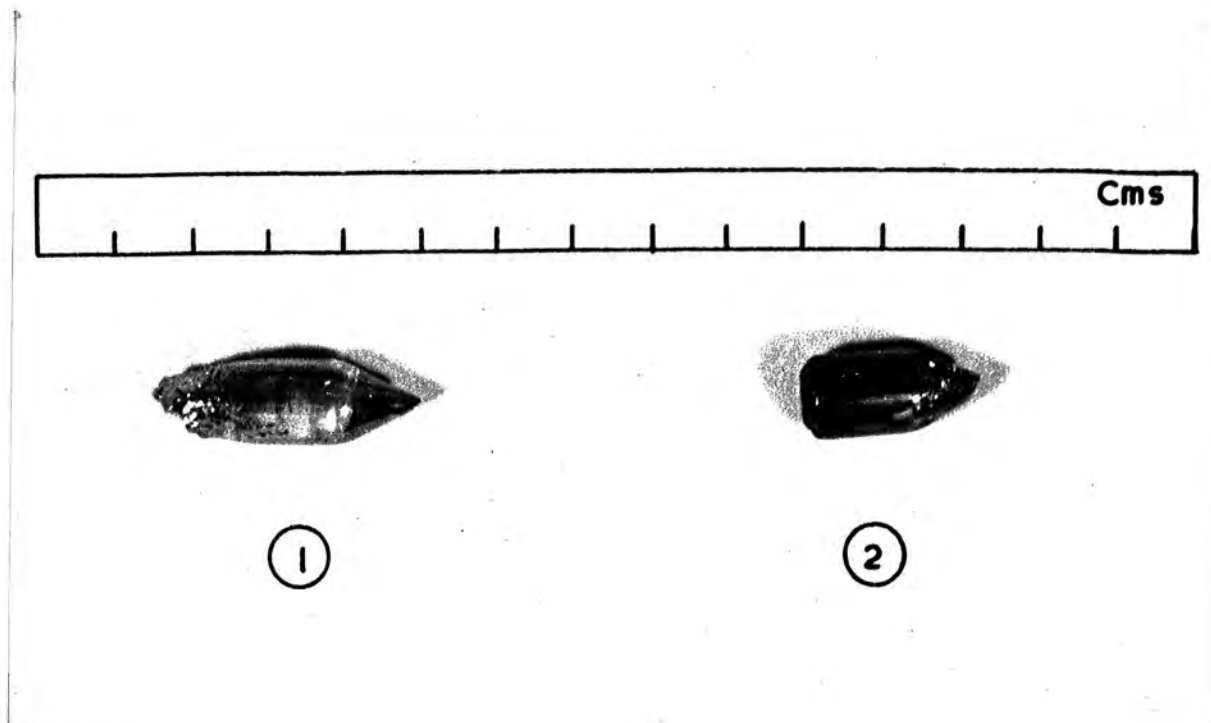
suitable donor impurities (i.e. those doped with Cl, Ga, etc.) sometimes had resistivities in the range $10^6 - 10^8$ ohm cm. To reduce the resistivities to the range 1-100 ohm cm it was necessary to heat the crystals in liquid zinc. Aven and Woodbury (1962) have shown that acceptor impurities such as copper and silver can be removed from zinc selenide using this process. To carry out the heat treatment of the crystal samples, a silica tube of 6 mm inner diameter and 15 cm long was used. See Figure 3.2(c). The tube was sealed at one end using a capillary silica rod and then left in aqua regia solution for several hours after which it was washed with distilled water. Finally it was rinsed with methanol and baked at 150°C for one day. The crystal slices with dimensions of $10 \times 6 \times 1 \text{ cm}^3$ were cut from a boule using a diamond wheel, polished with 1200 grade carborundum and etched in a solution of 1% bromine in methanol to eliminate the surface damage caused by mechanical polishing procedures. The slices were placed at the sealed end of the tube together with 5N zinc metal from Metals Research Ltd. If required, other metals such as aluminium could be added to the zinc. A slice from a capillary tube was sealed close to the other end of the tube (see diagram 3.2(c)) to facilitate the removal and separation of the slices from the melt after treatment. The tube was evacuated and flushed with high purity argon several times and sealed at a pressure of 4×10^{-6} torr. It was then suspended in a vertical furnace which was kept at temperatures of $850^\circ - 1000^\circ\text{C}$ for about 250 hours. On completion of the heating the tube was removed from the furnace and inverted. The molten zinc ran to the bottom of the capsule while the crystals were held on the ledge formed by the slice of the capillary tube.

3.5 X-RAY POWDER ANALYSIS

The x-ray powder photography method was used to investigate the structure and composition of the crystals which were grown using different methods. Most of the samples studied were those which had already been heated in zinc using the procedure described in Section 3.4. The main purpose was to determine the structure and the lattice parameters of those crystals used in this work.

To obtain samples suitable for x-ray powder photography, the crystals were crushed and ground to a fine powder of about 250 mesh size, which was stuck on to a cylindrical glass fibre of 0.2 mm diameter using flexible collodion as a binder. The fibre was then mounted at the centre of the Debye-Scherrer camera. The camera was loaded asymmetrically with the "Kodirex" x-ray film from Kodak Ltd. and mounted on the fast arm of a Philips "Smoothed D.C. X-ray Diffraction Generator" type PW 1009/30. An x-ray diffraction tube containing a copper target was used as an x-ray source. This was filtered with a nickel filter to isolate the copper K_{α} Lines (doublet $K_{\alpha 1} = 1.5405$ and $K_{\alpha 2} = 1.54434$). The tube itself was operated at 40 kv, 20 mA. The specimens were exposed to this radiation for 6 - 10 hours. X-rays were diffracted from the planes according to Bragg's Law. The film showed sharp lines at low and high θ (Bragg angle) values (see part (b) in Figure 3.3). The θ values were measured using a film measuring rule obtained from "Rigaku Denki Ltd."

The films were indexed using $\sin^2 \theta$ values (see for example Cullity 1967) to find the structure of the crystals examined. The lattice parameters were obtained by an extrapolation method (extrap. to $\theta = 90^{\circ}$) using the Nelson-Riley function (1945). This function takes into account the errors which might arise from



(a) Zinc selenide boules



ZnSe



ZnS_{0.6}Se_{0.4}



ZnS

(b) X-ray powder photographs

Fig. 3.3: Pictures showing:

- (a) ZnSe boules grown by vapour transport method
- (b) X-ray powder photographs recorded on some Zn(S,Se) mixed crystals grown by iodine transport method.

- (a) absorption of x-ray beams in the specimen
- (b) miscentring of the specimen, and
- (c) inaccurate determination of the camera constants.

3.6 RESULTS

Crystals of zinc selenide and zinc sulphoselenide were successfully grown from vapour using the techniques described by Burr and Woods (1971) and Cutter et al (1976). All the boules were transparent. The body colour of zinc selenide boules, with no intentionally added impurities, was usually greenish-yellow and that of boules which were doped with impurities (i.e. with Al, Cl, Ga, Cu and Mn) was usually yellowish-orange. However, $\text{ZnS}_{0.6}\text{Se}_{0.4}$ mixed crystals were colourless.

Crystals of zinc sulphoselenide, $\text{ZnS}_x\text{Se}_{1-x}$ were grown successfully over the whole range of compositions using the iodine transport method described by Nitsche (1960). These mixed crystals were also transparent. Zinc selenide grown by this method was usually orange in body colour. The body colour changed gradually to green as the sulphur content was increased, and then gradually faded away when the sulphur content exceeded 70 molar percent. Zinc sulphide of course is colourless.

The crystals grown in this laboratory were quite pure chemically. Spectro-chemical analysis of these crystals, using solid course mass spectroscopy by the Harwell laboratories, revealed that one of the major impurities was silicon at about 4 ppm. The concentration of copper was less than 0.1 ppm.

Heating the crystals of zinc selenide, either in molten zinc or zinc plus aluminium, reduced the electrical resistivity to 1-10 ohm cm.

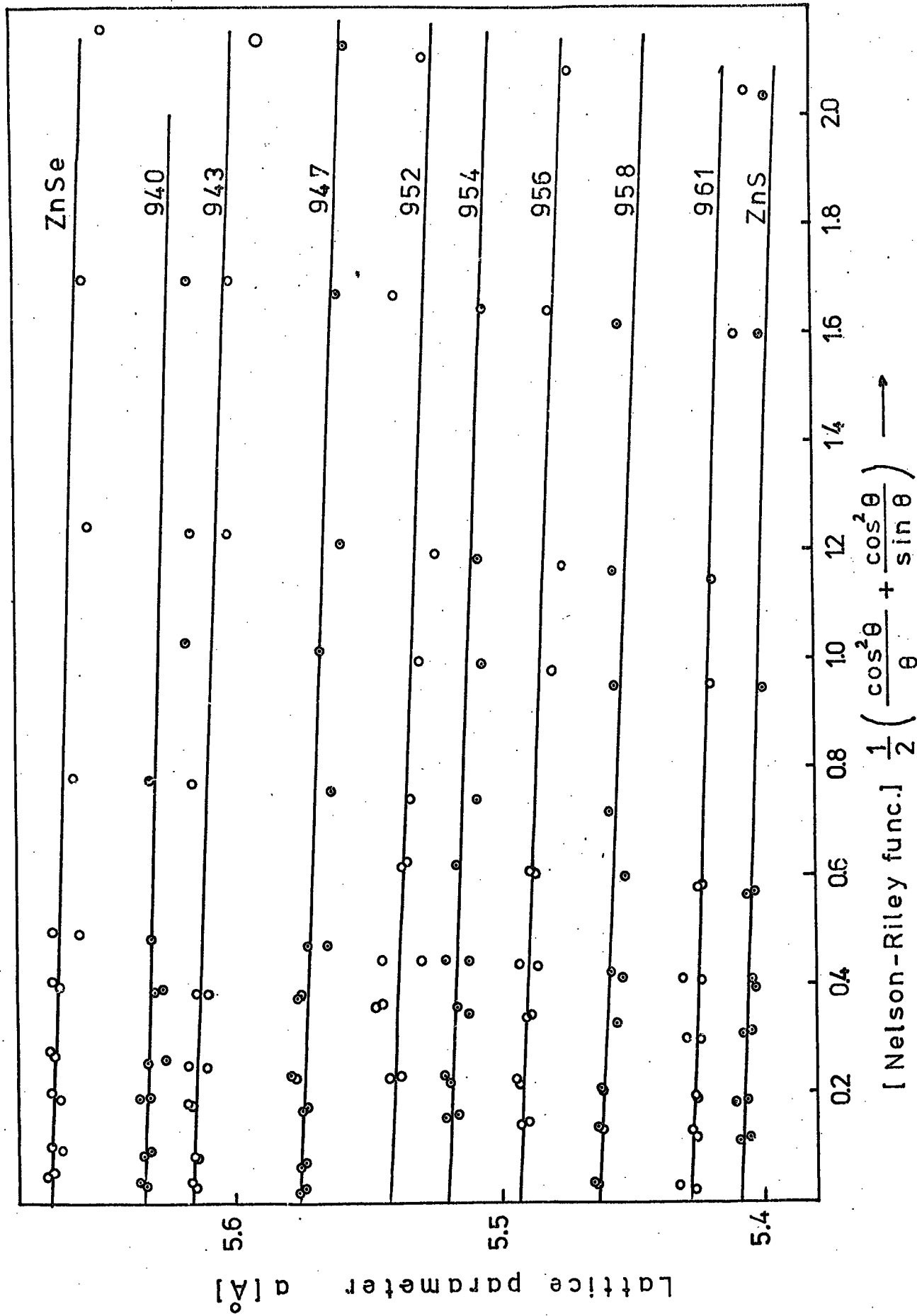


FIG:3.4. The determination of lattice parameter for ZnS_xSe_{1-x} crystals.

However, it was necessary to heat zinc sulphide crystals in zinc plus aluminium to bring their resistivity down to $10^2 - 10^3$ ohm cm. After this heat treatment the body colour of zinc selenide had usually changed to brilliant yellow. However, no change was found in the body colour of zinc sulphide and it remained colourless.

The results obtained from x-ray powder photography showed that all the crystals studied were cubic (sphalerite) in structure. The lattice parameters of cubic zinc selenide and zinc sulphide were measured to be about $a_0 = 5.668 \pm 0.002$ and $a_0 = 5.408 \pm 0.002$ respectively. These values are comparable with the A.S.T.M. values of a_0 for ZnSe and ZnS which are $a_0 = 5.667$, $a_0 = 5.4060$ respectively. Some of the measured values of the lattice parameters for the crystals grown by different methods are given in Table 3.2.

The lattice parameters of the mixed crystals of cubic zinc sulphoselenide were also measured using the same x-ray powder method. A plot of the calculated lattice parameters against the Nelson-Riley function is given in Figure 3.4. Assuming that Vegard's Law holds for the solid solution, (Hartmann 1960), i.e. that the lattice parameter varies linearly with composition, it is possible to estimate the molar composition of the mixed crystals. In fact the x-ray powder analysis indicated that the molar composition of a mixed crystal was very close to that of the starting charges. Electron microprobe analysis performed in the Geology Department, University of Durham, together with examination in transmission in the electron microscope by Russell (1974), revealed that the mixed crystals were all homogeneous. Cutter et al (1976) found that the crystals grown by vapour transport technique, described in Section 3.3.2, had their free growth faces within a few degrees of the $(\bar{1}, \bar{1}, \bar{1})$ non-metal face of the cubic crystal.

COMPOUND	CRYSTAL NUMBER	GROWTH TECHNIQUE	GROWTH TEMPERATURE (°C)	LATTICE PARAMETER a(A) 40.002 (measured using x-ray powder tech.)	MOLE % of ZnS in ZnSe (cal. Vegard's law)
ZnSe	HT 1	Vapour (argon)	1250	5.670	
ZnSe	172	Vapour	1020	5.669	
ZnSe	246	Vapour	1020	5.670	
ZnSe	900	Iodine transport	800	5.668	
ZnS	R 3	Iodine transport	800	5.408	
ZnS Se _x 1-x (comp. in weight)					
ZnS _{0.1} Se _{0.9}	940	Iodine transport	800	5.633	13.5
ZnS _{0.2} Se _{0.8}	943	"	800	5.616	20.2
ZnS _{0.3} Se _{0.7}	947	"	800	5.576	35.6
ZnS _{0.4} Se _{0.6}	952	"	800	5.542	48.7
ZnS _{0.5} Se _{0.5}	954	"	800	5.520	57.2
ZnS _{0.6} Se _{0.4}	956	"	800	5.493	67.4
ZnS _{0.7} Se _{0.3}	958	"	800	5.463	79.1
ZnS _{0.8} Se _{0.2}	961	"	800	5.428	92.5
ZnS _{0.5} Se _{0.5}	241	Vapour	1140	5.512	60.3
ZnS _{0.5} Se _{0.5}	HT 2	Vapour (argon)	1250	5.544	50.0

TABLE 3.2. THE LATTICE PARAMETERS AND MOLAR COMPOSITION FOR ZnSe, ZnS, AND ZnS_xSe_{1-x} SINGLE CRYSTALS.

The most apparent crystallographic defects in most of the boules produced by the vapour transport technique were twins. However, the quality of the crystals obtained by the iodine transport technique was greatly superior. Recently Cutter et al (1976), using a transmission electron microscope, showed that as-grown zinc selenide boules were purely cubic and of high crystallographic quality, with few dislocations between grain boundaries. However, investigation of minute areas of mixed crystals of $\text{ZnS}_{0.6}\text{Se}_{0.4}$ (grown by the vapour transport technique) indicated the presence of a small hexagonal component, together with intrinsic stacking faults and a higher density of even thinner twins. They concluded that these owe their origin basically to post-growth stress.

3.7 DISCUSSION

The crystal structure of zinc selenide and zinc sulphide depends on the crystal growth conditions. Fitzgerald et al (1966) showed that zinc selenide crystals grown in a stream of argon at 1000°C were hexagonal. They also showed that mixed cubic-hexagonal zinc selenide could grow at temperatures of 900°C - 950°C . Cubic crystals of zinc selenide were grown by Burr and Woods (1971) at 1100°C . Later Cutter and Woods (1975) suggested that the cubic modification was stable for zinc selenide at temperatures above 1000°C and below 800°C , and that mixed cubic-hexagonal crystals are to be expected between these temperatures. Allen and Creshaw (1912) showed that zinc sulphide had an unstable transition temperature at about 1020°C , at which both cubic and hexagonal zinc sulphide tended to grow. They also showed that the reaction cubic to hexagonal was reversible. This was also shown later by Green et al (1958). In this process the crystals

of zinc sulphide had to be cooled from the inversion temperature (i.e. 1020°C) to room temperature in a period of 30-60 minutes. Then the crystals were solely hexagonal. In order to convert a mixed crystal structure completely to cubic, the crystals were heated to $800^{\circ} - 1000^{\circ}\text{C}$ for a period of 72 hours. They also predicted a second transition back to the cubic structure at temperatures near 1240°C . Samelson (1961) showed that crystals of zinc sulphide, grown from vapour at temperatures in the range $1170 - 1330^{\circ}\text{C}$, had structures which changed from pure hexagonal to a highly disordered mixture of cubic and hexagonal and of cubic. He also showed (Samelson 1962), using zinc sulphide crystals grown by chemical transport, that their structure was solely cubic when the growth temperature lay between 760° and 970°C , and became mixed cubic-hexagonal or hexagonal when the crystals were grown at temperatures above 970°C .

X-ray powder photography was the only technique used here to study the structure of the crystals grown in the laboratory. It showed that all the crystals were cubic (sphalerite) in structure. These results support the suggestions made by Cutter and Woods (1975). However, Cutter et al (1975), using the transmission electron microscope, showed that the mixed crystals of $\text{ZnS}_{0.6}\text{Se}_{0.4}$, as-grown from vapour, contained a small amount of hexagonal components of almost the same composition. This is probably because the crystal growth temperature (i.e. 1145°C) was very close to the phase transition temperature at which faulted cubic crystals containing a small quantity of hexagonal component tend to grow.

The crystals of $\text{ZnS}_x\text{Se}_{1-x}$, grown using the iodine transport technique were expected to be solely cubic because the growth temperature (i.e. 800°C) was far below the phase transition temperature

for both zinc selenide and zinc sulphide. Stacking faults have frequently been observed in ZnS by previous workers. (See for example Roth pp. 145-153). Although Cutter et al found the zinc selenide grown here to be of high crystallographic quality, stacking faults were observed in $\text{ZnS}_x\text{Se}_{1-x}$ crystals and increased in density as the sulphur composition was increased.

Heating crystals in molten zinc (or zinc plus aluminium) was an essential part of the preparation of the electroluminescent devices used in this work. The process was usually conducted at temperatures of about 850 - 1000°C. X-ray powder analysis of crystals showed that the crystal structure remained cubic after such treatment. Any twins usually remained, although dislocation etch pits (observed on as-grown crystals of zinc selenide by Gezci and Woods 1972) were observed to decrease in density after such heat treatment. Pashinkin et al (1960), showed that the faulted and mixed (cubic-hexagonal) crystals of zinc selenide could be transformed to the cubic phase by annealing them at 900°C. This has also been reported previously for zinc sulphide crystals by Green et al (1958). Thus the heat treatment used in this work presumably helped to anneal out structural imperfections, as well as reducing the resistivity.

CHAPTER 4

EXPERIMENTAL PROCEDURE

4.1 INTRODUCTION

The light emitting devices studied in this work were prepared from single crystals of n-type ZnSe, Zn(S:Se) and ZnS. Almost all of the light emitting devices were of the Schottky barrier type prepared on low resistivity materials. Both the electrical and the optical characteristics of these devices are described in the following sections.

4.2 DEVICE PRODUCTION

To produce light emitting devices the crystals were subjected to heat treatment in molten zinc as described in Chapter 3.4. Such heat treatment was essential in order to reduce the resistivity and allow the passage of sufficient current to excite the luminescence. The low resistivity materials were then cut into small dice with typical dimensions of $0.2 \times 0.2 \times 0.1 \text{ cm}^3$ using a diamond wheel. The dice were polished mechanically with 1200 grade carborundum powder and then with 1 micron diamond paste until flat parallel surfaces were obtained.

4.2.1 SURFACE TREATMENT

In order to remove the surface damage caused by the mechanical polishing procedure the dice were etched in a 1% solution of bromine in methanol. The dice were immersed in the solution which was continuously stirred for three minutes, and then slowly diluted by the addition of methanol. The dilution was continued for a further two minutes until the concentration of bromine became negligible. Following the etching process, the dice were washed in CS_2 to dissolve any possible

compounds of selenium or sulphur with bromine (i.e. Br_2Se_2 or Br_4Se_2) which would otherwise form on the surface. Etched crystals were stored either in absolute alcohol or chloroform.

4.2.2 OHMIC CONTACTS

Ohmic contacts to the crystals of zinc selenide, zinc sulpho-selenide and zinc sulphide were provided by pure indium metal wire which was obtained from Johnson Matthey Chemicals Ltd. The indium wire was either vacuum evaporated or pressed on to the chemically etched surface of a crystal. To obtain an ohmic contact on zinc selenide for example it was necessary to heat the dice for five minutes at about 250°C in an atmosphere of argon. The temperature was raised to the required temperature rather slowly, i.e. within 15 minutes, and a similar period of time was used to cool the dice to room temperature. The temperature required for the satisfactory formation of an ohmic contact on zinc sulpho-selenide was between 280 and 380°C , depending on the composition. The process of ohmic contact formation on zinc selenide using indium has been described by Blount et al (1966), in terms of the penetration of a chemical impurity layer on the surface of the semiconductor, followed at high temperatures by the indiffusion of indium. However, Kaufman and Dowbar (1974) using indium on zinc sulpho-selenide, zinc selenide and zinc sulphide crystals, described ohmic contact formation as a liquid epitaxial process.

The ohmic behaviour of the various contacts was checked by alloying indium on to the opposite faces of the dice. Satisfactory ohmic contacts were made on zinc selenide and zinc sulpho-selenide with compositions up to 80% sulphur. With higher sulphur compositions, and with zinc sulphide, it was difficult, if not impossible, to form ohmic contacts. Virtually no difference was observed in the ohmic behaviour

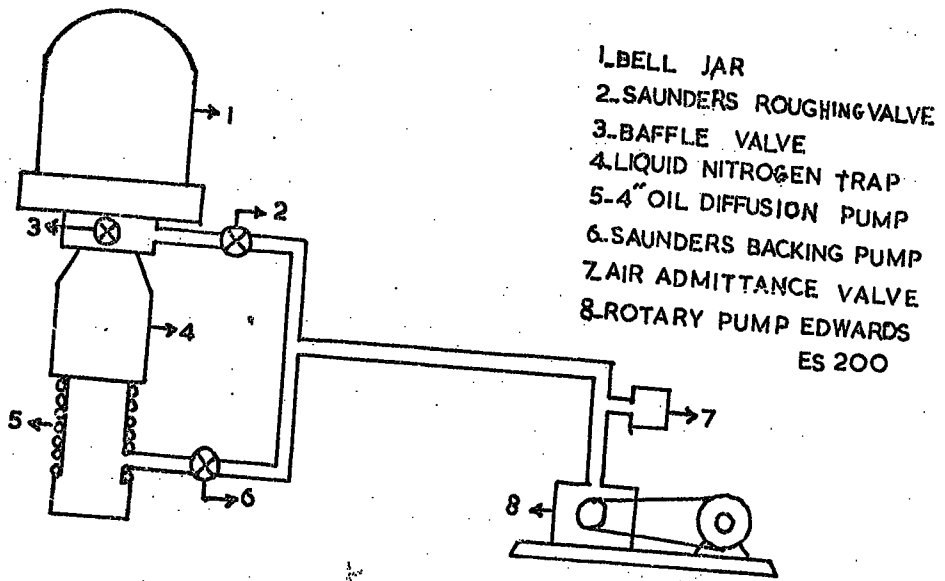
of the contacts formed on surfaces which have been chemically cleaned or cleaved.

4.2.3 SCHOTTKY BARRIER FORMATION

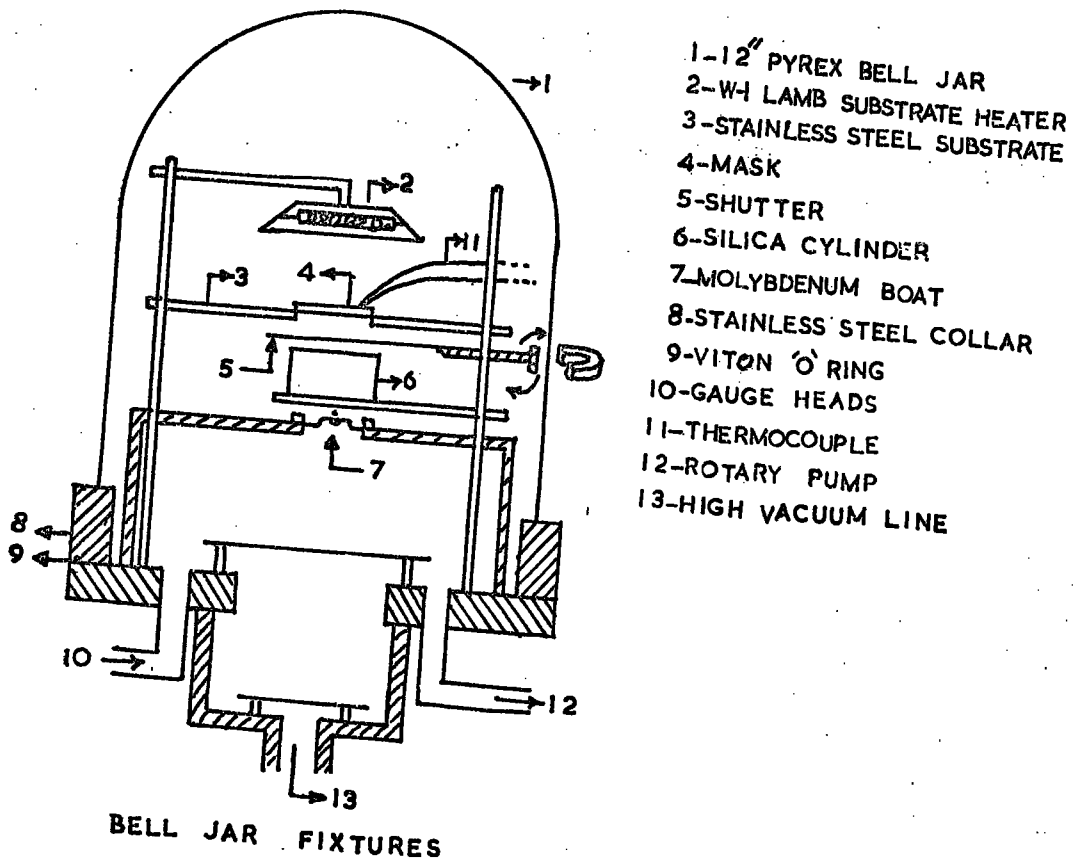
The Schottky barriers were prepared by vacuum deposition of the rectifying contacts. The rectifying contact was formed on the face of a dice opposite that to which the indium contact had been applied. Pure gold, obtained from Johnson Matthey Chemicals, was used almost exclusively to provide the rectifying contact. The face to receive the thin gold film layer was again put through the full process of surface treatment, including the mechanical polishing procedure, after alloying the indium contact on to the opposite face. During the whole of this process the indium contact was covered with a protective layer of "locomite" which the chemical etchants did not affect. The thin protective layer was peeled off easily later on. If the dice were stored in chloroform, the locomite was removed first, because it dissolves in chloroform. Ultimately, gold films, 10^{-2} cm² in area, were deposited on the freshly cleaned surfaces. In a few samples, gold layers were deposited on to faces which had been freshly cleaved in air.

4.2.4 VACUUM SYSTEM AND METAL FILM DEPOSITION

The schematic diagram of the vacuum system used is shown in Figure 4.1. All parts were obtained from Edwards High Vacuum Ltd. The system was built around a 4" oil diffusion pump which was sufficient to handle the outgassing of the source (this facility was initially provided to enable an electron gun to be used at high powers). Edward's 70 series units were employed to measure the pressure in the work chamber, i.e. a Pirani 11 gauge for pressures below 10^{-3} torr, and



SCHMATIC DIAGRAM OF PUMPS AND VALVES OF EVAPORATOR



BELL JAR FIXTURES

FIG.4.1 SCHMATIC DIAGRAM OF EVAPORATOR AND BELL JAR FIXTURES

a 1G5 ionisation gauge for pressures below 10^{-3} torr. With liquid nitrogen in the cold trap and silicone fluid 705 in the diffusion pump, the lowest pressure attained in the chamber was 1×10^{-6} torr. The pressure was maintained below 6.0×10^{-6} torr during most of the depositions.

The vacuum chamber used to deposit thin metal film layers on the single crystal dice is illustrated diagrammatically in Figure 4.1. The dice were placed on top of the copper masks over small holes, through which the thin metal films would be deposited. The copper masks were mounted on an 8 mm thick stainless steel disc, which was placed 8 mm above the source. Resistively heated molybdenum boats containing small pieces of gold metal were used as sources. The source was supplied by an L.T. transformer enabling 30 amps at 30 volts to be drawn if required. Substrate heating was provided by the focussed light from a 750 watt tungsten halogen lamp internal to the system. The temperature of the substrate (copper masks) was controlled by a Eurotherm "phase angle" controller in conjunction with a NiCr/NiAl thermocouple in contact with the copper masks. A silica cylinder, 5 cm in diameter, was located in the volume between the source and the copper masks and a magnetic shutter was situated just below the substrates.

Before insertion in the vacuum system both the copper masks and the pure gold metal were cleaned in chromic acid and washed with absolute alcohol. The initial step, before any metallic evaporation was proceeded with, was to outgas the chamber. For this, the work chamber was evacuated down to 1.0×10^{-6} torr and power was applied to an empty molybdenum boat while the substrate holder was heated to 200°C using the tungsten halogen lamp heater. When this outgassing procedure was completed the work chamber was let down to air for a short

period, during which time the dice were quickly mounted on the copper masks, and the small gold pieces were placed in the molybdenum boat. The work chamber was then re-evacuated to 1.0×10^{-6} torr when the gold evaporation was carried out. Initially the shutter was kept closed so that the substrate would not be exposed to metallic vapours until a steady evaporation rate had been attained, and minor outgassing was completed. The substrate was kept at 60°C throughout the evaporation, and the pressure was usually less than 6.0×10^{-6} torr during most of the depositions. A rough guide to the thickness of a gold layer was achieved by weighing the source before and after the evaporation. The estimated film thicknesses were usually around a few thousand Angstroms. The light emitting devices produced were not encapsulated.

4.3 ELECTRICAL MEASUREMENTS

Most of the light emitting devices produced here were Schottky barrier devices on n-type material. The electrical properties of these devices have been studied in conjunction with the light emission.

4.3.1 CURRENT-VOLTAGE CHARACTERISTICS AS A FUNCTION OF EMITTED LIGHT (LUMINANCE) OF THE DIODES

The diodes were mounted on the copper finger of a metal cryostat. The cryostat formed an open sided copper enclosure with a silica window facing the diode at one end, and the vacuum inlet at the other (Fig. 4.2). All electrical connections were made via a 6-way glass-to-metal seal at the bottom of the cryostat. A soft copper wire was used to make a probe contact to the Schottky barrier. It also served to hold the sample vertically on the copper block. A copper-constantan thermocouple placed very close to the diode made contact with the copper block. The pressure inside the cryostat was reduced to 10^{-1} torr with a rotary pump. The

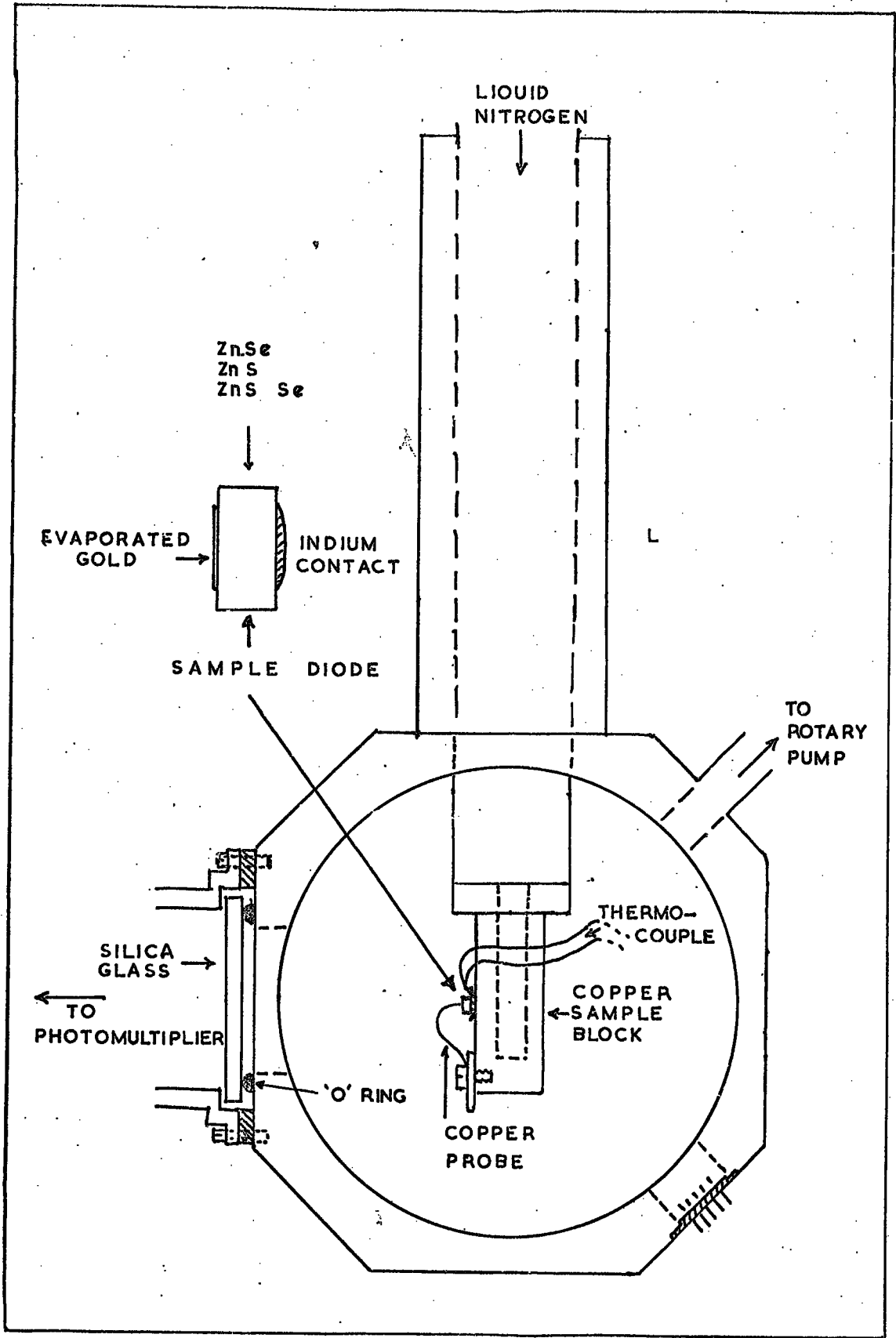


FIG.4.2 CRYOSTAT USED FOR ELECTRICAL AND OPTICAL MEASUREMENTS ON SAMPLE DIODES

sample block was directly cooled by liquid nitrogen contained in a German-silver cylinder above it, and it was possible to obtain temperatures down to 85 K.

Current voltage characteristics were measured in the dark. A Philips microvoltmeter type PM 2440 or E.I.L. vibron electrometer type 33B were used to measure applied biases smaller than one volt. For higher applied voltages a digital multimeter type DMM2 and an Avometer were used.

The luminance of the diodes was measured directly with an SEI photometer which gave the brightness in foot-lamberts. In general the intensity of emitted light covering the whole emission spectrum was measured using an EMI photomultiplier type 9781R which had an extended 85 cathode. The output of the photomultiplier was calibrated against that of the photometer.

4.3.2 CAPACITANCE - VOLTAGE MEASUREMENTS

The differential capacitance (C) of the Schottky diodes was measured as a function of applied bias (V). The C-G-V plotter used was designed and built in this laboratory by P.G. Martin. It operated accurately in the frequency range of 10 Hz to 300 kHz. An external oscillator provided the signal voltage 25 mV (p-p) applied to the device. The instrument included a low frequency sweep generator capable of biasing the device under test over the range -20 to +20 volts. Most of the C-V plots were taken with biases between 3 volts (reverse) -0- .2 volts (forward). The voltage limitation in the forward direction was due to the high conductance of the device. A "Bryans" X-Y Autoplotter, model 21005, was connected to the output of the C-G-V plotter to obtain an automatic record.

The C-V measurements were made on diodes mounted in the cryostat. The pressure was reduced to 10^{-1} torr and most of the C-V plots were made in the dark at a frequency of 200 kHz. With a few samples C-V plots were also made at low temperatures.

4.4 OPTICAL MEASUREMENTS

Extensive optical studies were made on most of the devices. Although the emphasis was on electroluminescence, photoluminescence emission and excitation spectra, in conjunction with the spectral distribution of the photoresponse, were also studied to contribute to the understanding of the actual mechanism concerned with electroluminescence. In the following sections the experimental techniques and the apparatus used will be described.

4.4.1 APPARATUS

Two kinds of apparatus were used for the luminescence measurements. Most measurements were carried out using a Barr and Stroud double monochromator type VL.2 fitted with Spectrosil 'A' quality prisms. This system was used to determine the emission spectra of both the electroluminescence and photoluminescence, and provide a monochromatic light source for luminescence excitation and photoresponse measurements. An E.M.I. photomultiplier type 9558, with a trialkali S-20 photocathode, was used for most of the emission and excitation measurements. The output from the photomultiplier was amplified by taking the signal from the 10 k.ohm load resistor to the input terminal of a Brookdeal lock-in amplifier type 401 and a Philips valve voltmeter type PM 2440. The valve voltmeter was used to ensure that the photomultiplier was not over exposed during the mirror alignment procedure. The reference

signal to the lock-in amplifier was obtained from light falling on to a photodiode which was fed from the internal 9 volt supply of the amplifier. Both the light incident on the entrance slit of the monochromator and the light falling on the photodiode were chopped with a multibladed chopper which was driven by a synchronous motor via a flexible drive. This motor allowed a chopping frequency of 200 cps to be obtained with the help of a 40 bladed chopper.

The cryostat used for luminescence measurements was identical to that used in electrical measurements, except that the sample block was built to rotate about its vertical axis. Copper plates holding various filters provided a vacuum-tight seal at the side, enabling photoluminescence and excitation spectra measurements to be made. 80 K was the lowest attainable temperature with this cryostat. A copper-constantan thermocouple, placed very near the sample, was used to measure the temperature.

The second system used for optical measurements was an Optika CF 4NI grating spectrometer. It was possible to make optical measurements down to 18 K with this system, which employed an Oxford Cryogenics cryostat. The cryostat had a helium capacity of 1.5 litres and the copper sample block was directly cooled. The diodes were held in contact with the sample block with springy copper wire and the gold contact faced the detection system. The pressure inside the cryostat was maintained below 10^{-4} torr, and a gold-iron/chromel thermocouple was used to measure the temperature of the sample block. The automatic recording spectrometer was provided with an E.M.I. photomultiplier type 9781R with an extended S-5 photocathode.

4.4.2 EMISSION SPECTRA

Figure 4.3 shows the arrangement used to measure the electroluminescence and the photoluminescence of the sample diodes. Most of the diodes were operated from a constant current D.C. power supply. However, in some cases the diodes were operated under pulsed conditions using a Solartron pulse generator type GO 1101. In the latter case the optical chopper was removed and the reference signal was obtained from the pulse generator. With most devices both forward and reverse bias electroluminescence (FEL, REL) was measured at room and liquid nitrogen temperatures.

Photoluminescence was excited by 3650 Å ultra violet (UV) radiation from a 250 watt compact source mercury lamp. The UV line was isolated with a Chance glass OX.1 filter. Some of the emission spectra were obtained using excitation of lower photon energy, in which case a 250 watt, 24 volt quartz-halogen projector lamp with suitable interference filters provided the required excitation. Infra red radiation was removed by using a Chance glass HA.3 heat absorbing filter in conjunction with a 7 mm path length of a 10% solution of copper sulphate.

The emission spectra were corrected for two factors, namely spectral sensitivity of the photomultiplier and the dispersion produced by the spectrometer. The data used for these factors were supplied by the manufacturers.

In this work the intensity of the emission curve was plotted in terms of number of photons per unit energy interval, I_{hv} , and the abscissa were expressed in terms of photon energy in electron volts.

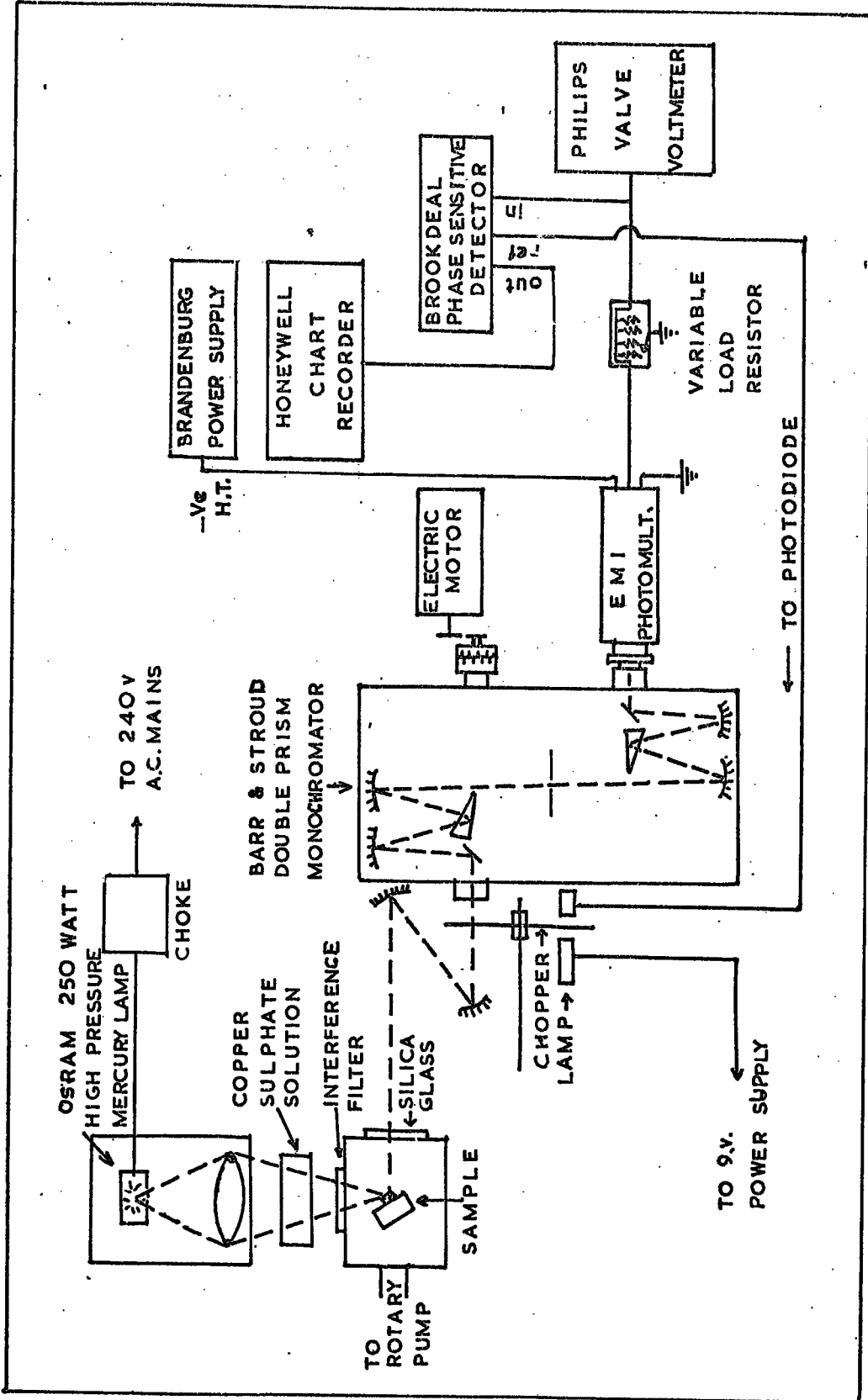


FIG 4.3 APPARATUS FOR MEASURING THE ELECTROLUMINESCENT AND PHOTOLUMINESCENT EMISSION SPECTRA

4.4.3 PHOTORESPONSE AND EXCITATION SPECTRA

For these measurements the apparatus used to obtain the emission spectra was re-arranged as shown in Figure 4.4. In this case, the cryostat was placed in front of the exit slit. The quartz halogen projector lamp was used in conjunction with the monochromator to obtain a monochromatic beam of light which fell on the face of the diode which had the gold contact. The short-circuit photocurrent was measured either with an EIL Vibron electrometer or with a Brookdeal lock-in amplifier type 401. In the latter event light was chopped at a frequency of 200 Hz.

To measure the excitation spectra, the luminescence emission was isolated from the excitation by using a Chance glass filter together with a graded interference filter, i.e. when observing an orange emission an OR.I chance filter was employed together with the graded interference filter, enabling a bandwidth of about 200 Å to be attained at 6000 Å. The normal procedure was such that when the emission was observed the interference filter was readjusted slightly to achieve the maximum signal. When observing the green and blue emissions in the zinc sulpho-selenide crystals, the combinations of filters allowed a bandwidth of about 200 Å to be attained at 5,300 and 4,900 Å.

The excitation and photoreponse spectra were corrected for the spectral distribution of the intensity of the monochromatic light source. This was measured using the same photomultiplier. Intensity in the excitation spectra is plotted in terms of $I_{h\nu}$, whereas the current in the photoreponse curves is proportional to $I_{h\nu}$ falling on to the junction. The abscissa are again expressed in terms of photon energy in electron volts.

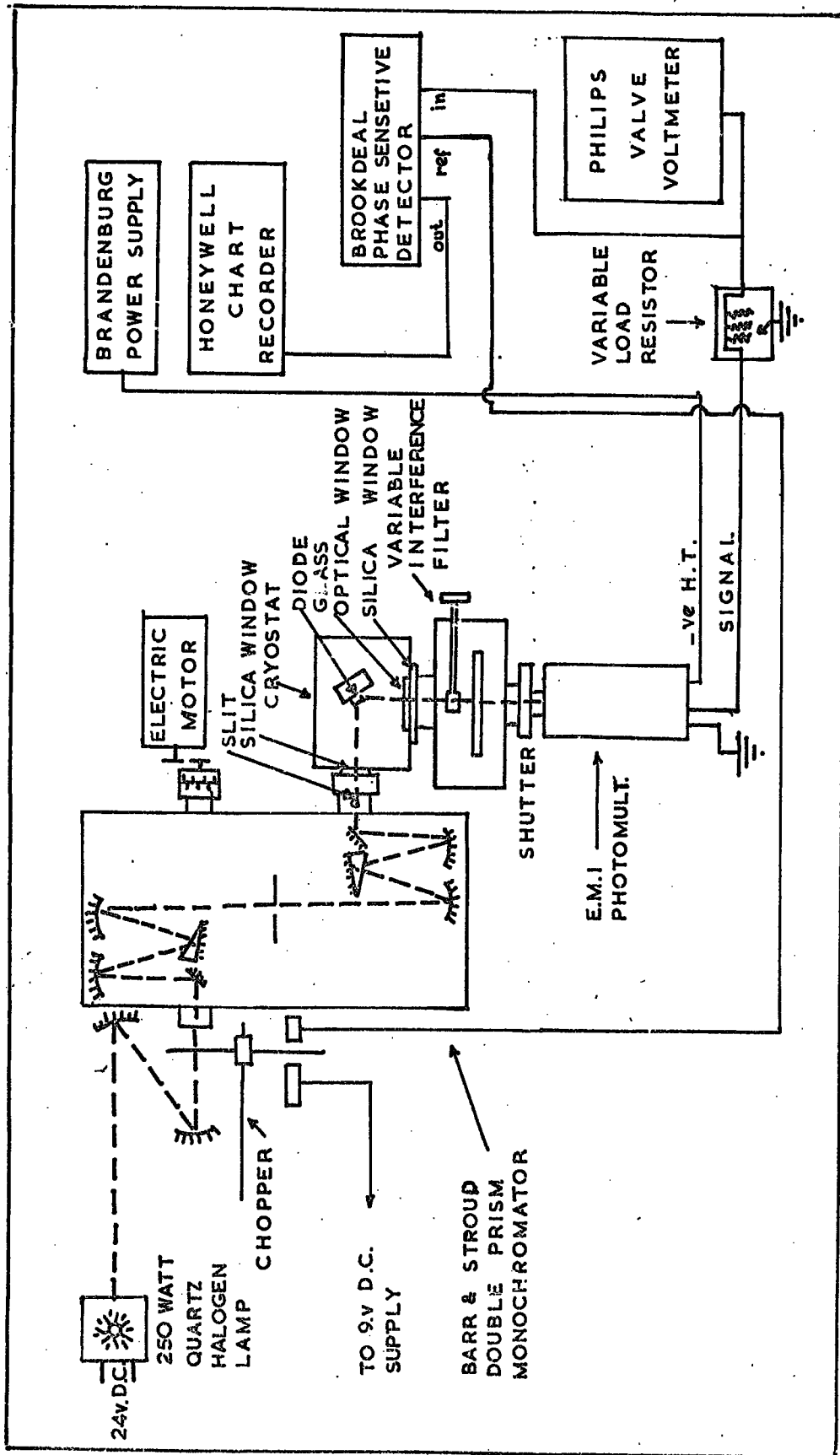


FIG 4.A. ARRANGEMENT FOR MEASURING THE PHOTO RESPONSE AND THE PHOTOLUMINESCENT EXCITATION SPECTRUM

4.5 THE POWER EFFICIENCY OF THE DIODES

To measure the power efficiency of the electroluminescent diodes (the ratio of light output to input power), it was necessary to express the light output in terms of watts and this was done roughly in two ways. First, the surface brightness of the diodes (in foot-lamberts) was measured directly using the SEI photometer. This brightness was converted into $\mu\text{W}/\text{mm}^2$ using the conversion, one foot-lambert = 1 lumen/sq. foot, 680 lumens = 1 watt. Secondly, with reference to intensity measurements, it was assumed that the light was emitted with a hemispherical polar diagram, with the photocathode at a known distance in front and along the axis of the diode.

By measuring the output of the photomultiplier and knowing the sensitivity of the photocathode which was provided by the manufacturers, the light output could be calculated in terms of lumens. To obtain the power efficiency, the light output in watts was divided by the input power of the diode. The results from the two methods of measurements were of the same order of magnitude.

CHAPTER 5

ELECTRICAL PROPERTIES OF Au-ZnSe DIODES

5.1 INTRODUCTION

The electrical properties of Au-ZnSe diodes have been investigated fairly extensively. The devices were prepared on single crystals of ZnSe as described in Chapter 4.2.3. The spectral response of the short-circuit photocurrent has been measured and used to find barrier heights. These measurements also revealed the band gap of ZnSe. The uncompensated donor density was calculated from the capacitance-voltage (C-V) measurements. The results obtained from the photoresponse and capacitance-voltage measurements can be explained in terms of the presence of a semi-insulating film between the gold and ZnSe. Conductance-voltage (G-V) characteristics have also been studied for a few samples. The current-voltage (I-V) characteristics have been investigated in both forward and reverse directions. Long term ageing processes which affect the electrical characteristics of Au-ZnSe devices have also been investigated in an attempt to understand how to produce stable LEDs.

In order to facilitate the presentation of results, the Schottky barrier devices formed by deposition a gold electrode on ZnSe will be referred to as Au-ZnSe:X,Y,Z where X,Y,Z represent the dopant elements introduced either during the growth procedure (see Chapter 3.3) or during the subsequent heat treatment (see Chapter 3.4).

5.2 SURFACE PREPARATION

The treatment of the surface of the crystal (see Chapter 4.2.1) prior to the deposition of the gold films was found to have a considerable effect on the electrical properties of the devices produced. The surfaces

of ZnSe crystals were etched at room temperature with a solution of 1% bromine in methanol. This was followed with a rinse in CS₂ and then absolute alcohol. This etching procedure will be referred to as the standard etching procedure in the following sections.

The chemical composition of the thin semi-insulating layer which was found to have formed after such chemical etching, is not yet known. However the approximate chemical composition of the surface was investigated using ESCA (Electron Spectroscopy for Chemical Analysis). The results indicated that apart from Oxygen and Carbon, other elements such as Br, Cl and S were also present in the following ratios:-

$$\text{Se/Br} \approx 5 \quad \text{S/Br} \approx 2 \quad \text{Cl/S} \approx 1$$

Furthermore, examination in reflection in the transmission electron microscope revealed that the structure of this layer was amorphous. The insulating layer probably contains more than one oxide, one of which is almost certainly ZnO.

5.3 OHMIC CONTACTS

The techniques of growing and treating the ZnSe crystals to reduce their resistivity has been described in Sections 3.3 and 3.4. A brief summary of the growth parameters and heat treatment administered to the samples used in this work is recorded in Table 5.1. Ohmic contacts were formed by alloying indium metal. To test their ohmic behaviour symmetric indium contacts were formed on the opposite faces of the crystal chip. With satisfactory contacts the plot of log I against log V was found to be linear over nearly three orders of magnitude of both current and applied bias (see Fig. 5.1) for either polarity. Similar characteristics were also obtained when indium contacts were formed on surfaces produced by cleaving a crystal in air. The linearity

Crystal No.	Growth Conditions				Heat Treatment		
	Deliberately Added Impurities to Boule	Excess Pressure in Tail	Furnace Temperature (°C)	Tail Temperature (°C)	Molten Element	Temperature (°C)	Time (hrs)
172A	none	Se	1175	360	Zn	900 - 1000	240
172B	none	Se	1175	360	Zn + Al	900	150
139	In	Zn	1150	555	Zn	850	150
176	Ga	Zn	1160	555	Zn	750	14
931	I ₂ (iodine transport)		850		Zn	850	200
242	(Cl)	ZnCl ₂	1160	450	Zn	850	200
247	Al	Zn	1160	555	Zn	850	240
246	Mn, Zn	MnCl ₂	1160	560	Zn	850	200
165A	Cu	Zn	1150	555	Zn + Al	900	200
191	Mn, Cu	MnCl ₂ , Zn	1165	560	Zn + Al	950	200

Table 5.1: The growth and heat treatment conditions for the ZnSe crystals containing impurities.

of the ohmic behaviour was found to be maintained at 85 K, however small deviations were often observed at voltages below 10^{-3} V, at 85 K.

5.4 PHOTORESPONSE MEASUREMENTS

Almost all of the photoresponse measurements were made on freshly produced Au-ZnSe diodes. The technique used is described in Chapter 4.4.3. At first large area devices ($0.4 \times 0.4 \times 0.1 \text{ cm}^3$) were investigated and the junction was illuminated through a thin ($\sim 100 \text{ \AA}$) layer of gold or through the bulk of the ZnSe (i.e. front and back illumination respectively). No difference in the shape of the spectral photoresponse was observed except that the amplitude of the photocurrent was greater with front illumination. Second, the photoresponse of small area devices ($0.15 \times 0.15 \times 0.1 \text{ cm}^3$) was investigated. The observed spectral response was essentially the same as that from large area devices. However, the amplitude of the short circuit photocurrent increased when the edges of the gold contact were illuminated at the same time. Since the characteristic photoresponse was essentially the same in large or small area devices, almost all the subsequent measurements were made on small area devices with contact areas of 10^{-2} cm^2 . This also facilitated the evaluation of C-V measurements made on the same junctions. The quantity actually determined was short circuit photocurrent I_{sc} , which was measured as a function of photon energy in the range $1.3 < hv < 3.0 \text{ eV}$.

5.4.1 Photoresponse of Au-ZnSe Diodes

Two sample diodes were prepared from boule No.246 which contained grown-in manganese. The first was a bar of $0.15 \times 0.15 \times 0.5 \text{ cm}^3$, which was cut and chemically cleaned. Then thin slices were cleaved from both ends to which the ohmic indium contacts were applied. The

I_{SC} SHORT - CIRCUIT PHOTOCURRENT (ARBITRARY UNITS)

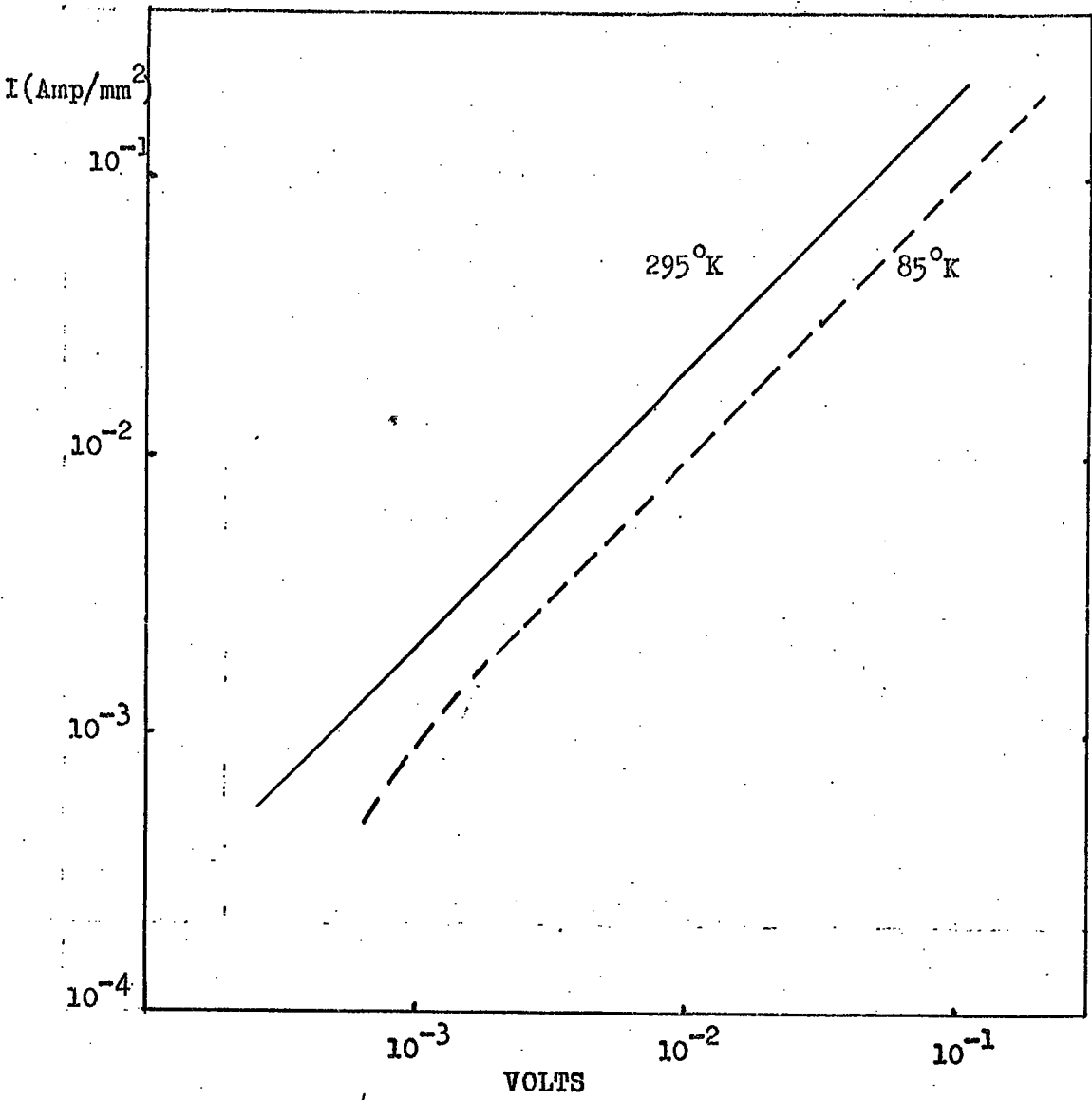


FIG.5.1 The I-V characteristics of symmetric indium (ohmic) contacts formed on ZnSe single crystals

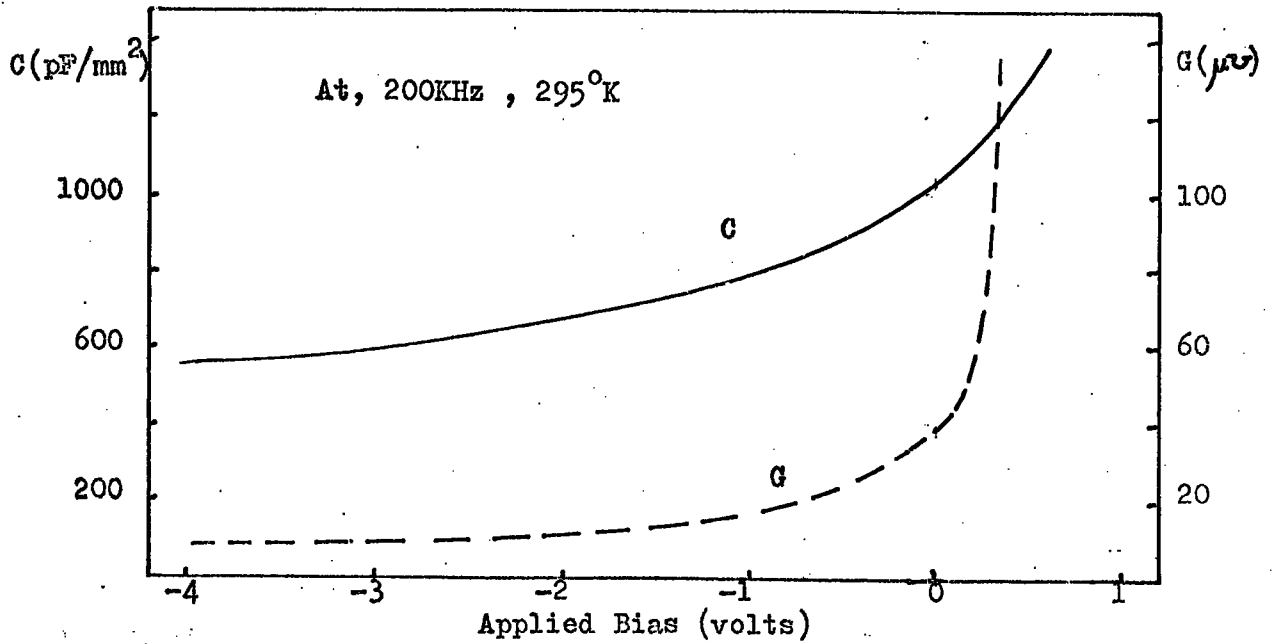


FIG.5.2 The C - V and G - V characteristics of Au - ZnSe diode formed on cleaved surface

bar was then cleaved into two through the middle and the two parts were transferred to the vacuum system for immediate deposition of the gold films. The orientation of the cleaved surface was found to be $\{1,1,0\}$ using x-ray back reflection technique. The diode thus formed on a surface produced by cleaving in air will be referred to as the "cleaved diode (246A)" in following sections. For comparison a second type of device was formed on a chip ($0.2 \times 0.2 \times 0.1 \text{ cm}^3$) cut from the same boule. The chip was cleaned with a standard chemical etching procedure in bromine in methanol and the Schottky barrier was formed on a chemically cleaned surface as described in Chapter 4.2.1.

Some typical curves of photoresponse as a function of photon energy for etched and cleaved diodes from boule 246 are shown in Fig.5.3. The photocurrent at the lower photon energies is associated with photoelectric emission from the gold into ZnSe, and the low energy threshold is a measure of the barrier height ϕ_{Bn} . The threshold is difficult to determine with any accuracy from plots such as those shown in Fig. 5.3(a) and 5.3(b). However when the square-root of the photocurrent was plotted against photon energy in the vicinity of the threshold, good straight lines were obtained for all junctions investigated (see the curves in Fig. 5.3(c)) and the barrier heights ϕ_{Bn} could then readily be determined from the intercepts. In this way the value of the barrier height formed by gold on cleaved ZnSe was found to be $\phi_{\text{Bn}} = 1.36 \pm 0.01 \text{ eV}$ at 295 K. This value increased slightly to $1.41 \pm 0.01 \text{ eV}$ at 85 K. The value of the barrier height on chemically cleaned surfaces was found to be around $1.59 - 1.65 \pm 0.01 \text{ eV}$ at 295 K and this is often increased to $1.68 \pm 0.01 \text{ eV}$ at 85 K.

The large increase in the photocurrent when the photon energies exceeded the band gap of ZnSe, was due to the creation of electron-hole

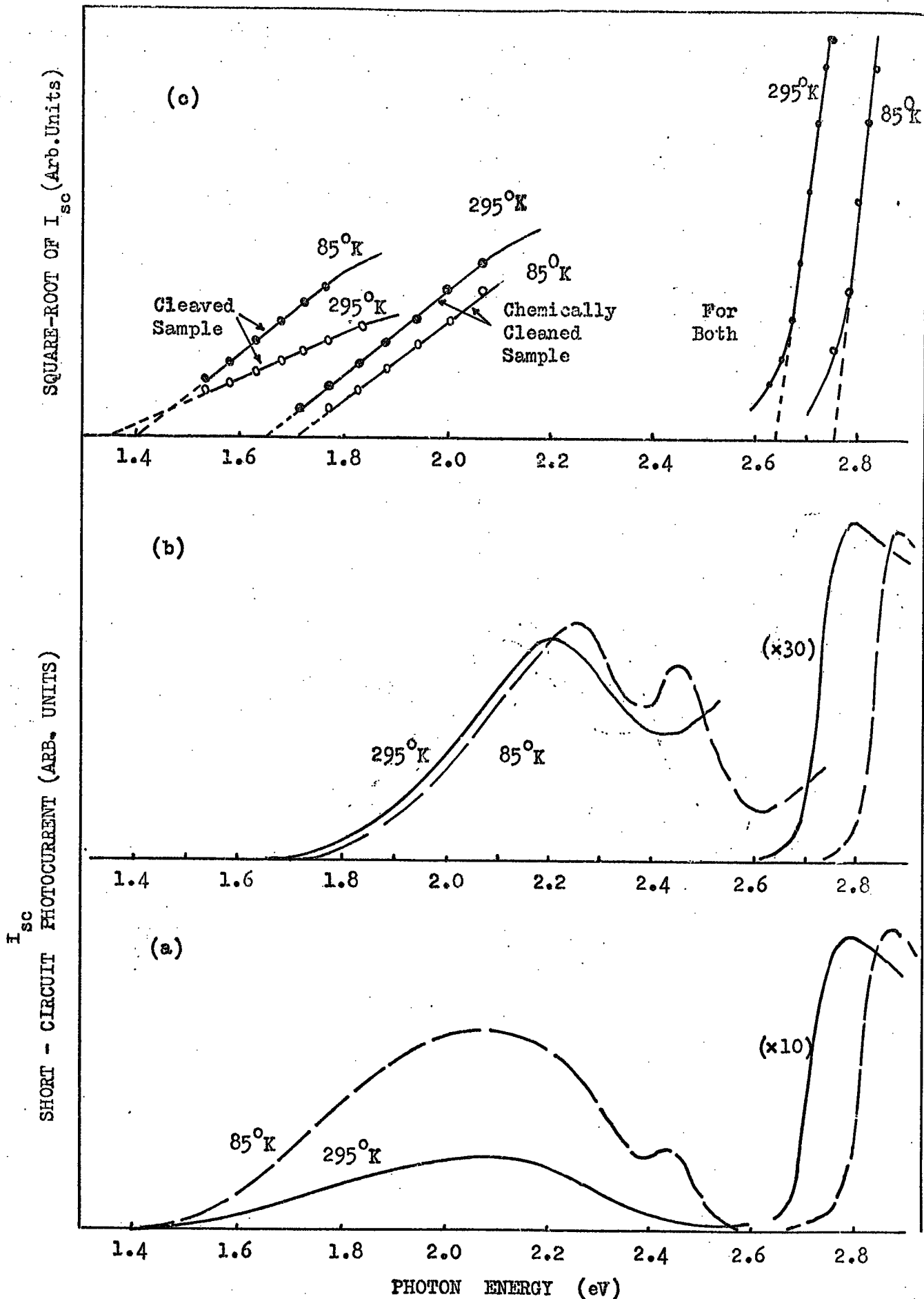


FIG.5.3 The photoresponse characteristics of Au - ZnSe:Mn,Cl,Zn diode (a)- prepared on cleaved surface, (b)- prepared on chemically cleaned surface and (c)- Square-root of the photoresponse measurements

pairs within one diffusion length of the contact. Again a plot of the square-root of the photocurrent gave a good straight line which could be extrapolated to give the value of the band gap. The value of the band gap of ZnSe was found to be $E_g = 2.64 \pm 0.01$ eV at 295 K and $E_g = 2.75 \pm 0.01$ eV at 85 K. The values for the band gap of ZnSe were essentially the same whether or not Au-ZnSe diodes were formed on cleaved or chemically cleaned surfaces.

Measurements of short circuit photocurrent were also made on samples containing no intentionally added impurities and on samples containing donors (i.e. In, Al, I or Cl) or acceptors (i.e. Cu). The results obtained at 295 and 85 K are illustrated in Figs. 5.4 and 5.5. All of the diodes examined were prepared on chemically cleaned surfaces. The plots of the square-root of the short circuit current against photon energy were similar to those illustrated in Fig. 5.3(c). The band gap energies for all these samples were found to be essentially the same as that of the manganese doped samples. The barrier height at 295 K was found to be around $\phi_{Bn} \approx 1.63 \pm 0.01$ eV for samples doped with donors while the copper doped sample gave a value of $\phi_{Bn} \approx 1.45$ eV. The value of the barrier height increased slightly at 85 K to about 1.68 eV for samples doped with donors and to 1.5 eV for the sample doped with copper.

One notable feature of most of the photoresponse curves was that they showed a minimum at photon energies just equal to or less than the band gap of ZnSe. This minimum coincided with a maximum in the luminescence excitation spectra and will be described in detail in Chapter 6.

An interesting feature of the spectral response of the short circuit photocurrent of the Au-ZnSe:Mn,Cl,Zn diode can be seen in the curves measured at 85 K (Fig. 5.3). This is the small second maximum centred at 2.45 eV. Such a maximum was not observed in any of our diodes which did not contain manganese. Measurement of the excitation

I_{sc} SHORT - CIRCUIT PHOTOCURRENT (ARBITRARY UNITS)

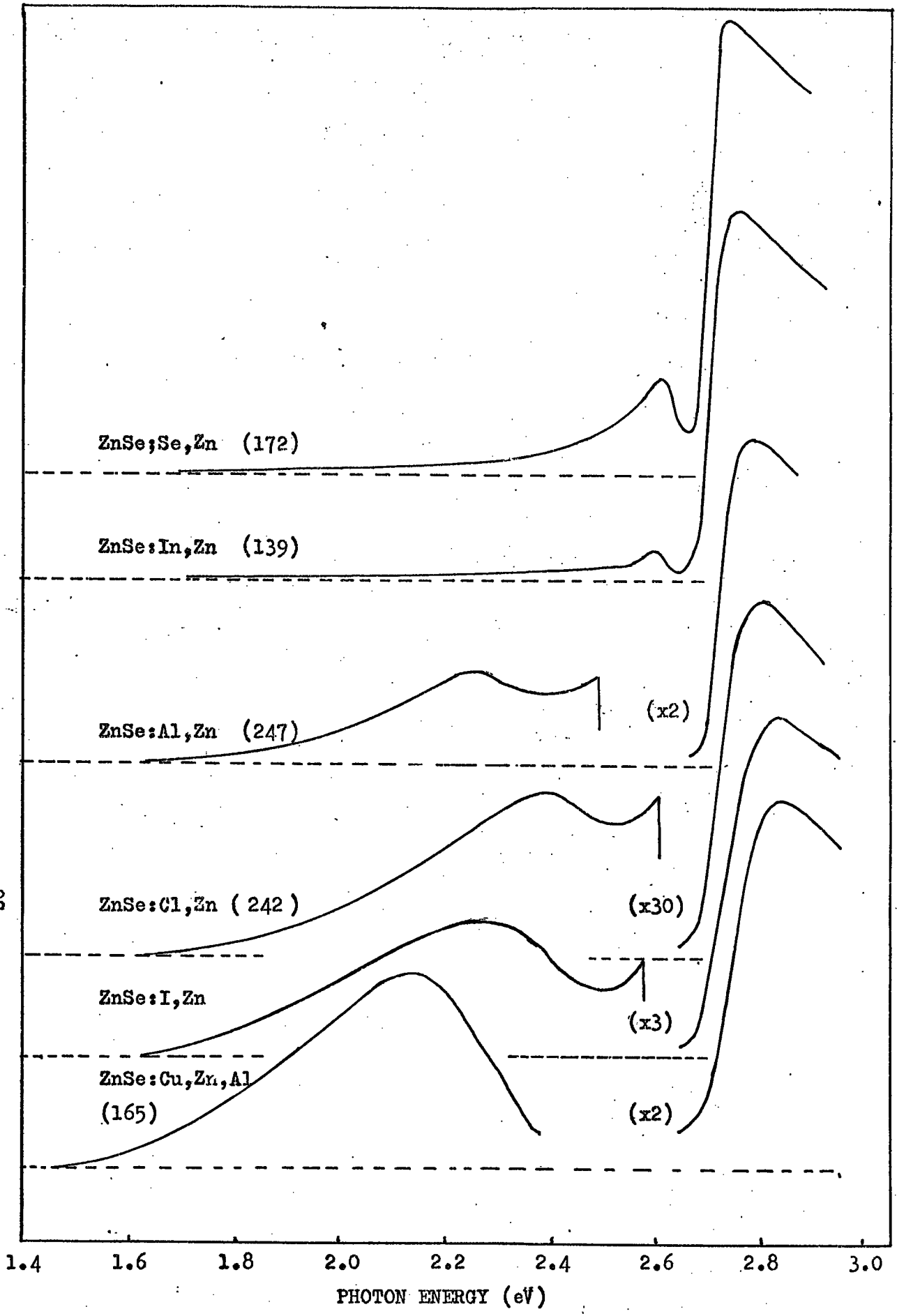


FIG. 5.4 Photoresponse characteristics of Au-ZnSe diodes at 295°K

spectrum of photoluminescence (Chapter 7) showed that 2.45 eV is the energy separation between the ground state and the second excited state of Mn^{++} in ZnSe. It would appear therefore that irradiation of the barrier region with light with sufficient energy to raise the valence electrons in Mn^{++} ion to the second excited state, leads to auto-ionisation and the appearance of a maximum in the spectral response of the photocurrent.

5.5 CAPACITANCE - VOLTAGE MEASUREMENTS

5.5.1 Introduction

The C-V characteristics of the Au-ZnSe diodes were measured as described in Chapter 4.3.2. A typical C-V plot measured at 200 KHz for a diode prepared on the cleaved surface of a manganese doped crystal is illustrated in Fig. 5.2. The bias range was typically from 3 V in the reverse to 0.5 V in the forward direction. The plots of C^{-2} against V were found to be linear for all junctions examined. Linearity of the plots was often found to prevail up to a bias of 8 volts in the reverse direction. The C-V characteristics of Au-ZnSe diodes doped with various impurities such as In, Al, Ga, Cl, I (donors) and Cu (acceptor) were investigated and typical C^{-2} -V plots are shown in Fig. 5.6. The uncompensated donor concentration was found from the slope of such plots using equation 2.4.7 and N_d was found to lie in the range from 10^{16} to $3 \times 10^{17} \text{ cm}^{-3}$ at 295 K. The intercept V_1 of the straight line on the voltage axis gave an average value of 2.0 eV for diodes constructed on chemically cleaned surfaces. However, the value of V_1 was found to be 1.39 eV when the gold had been deposited on surfaces cleaved in air. (see for example line (9), Fig. 5.6). At 85 K the values of N_d were found to have decreased slightly for all diodes examined. In contrast

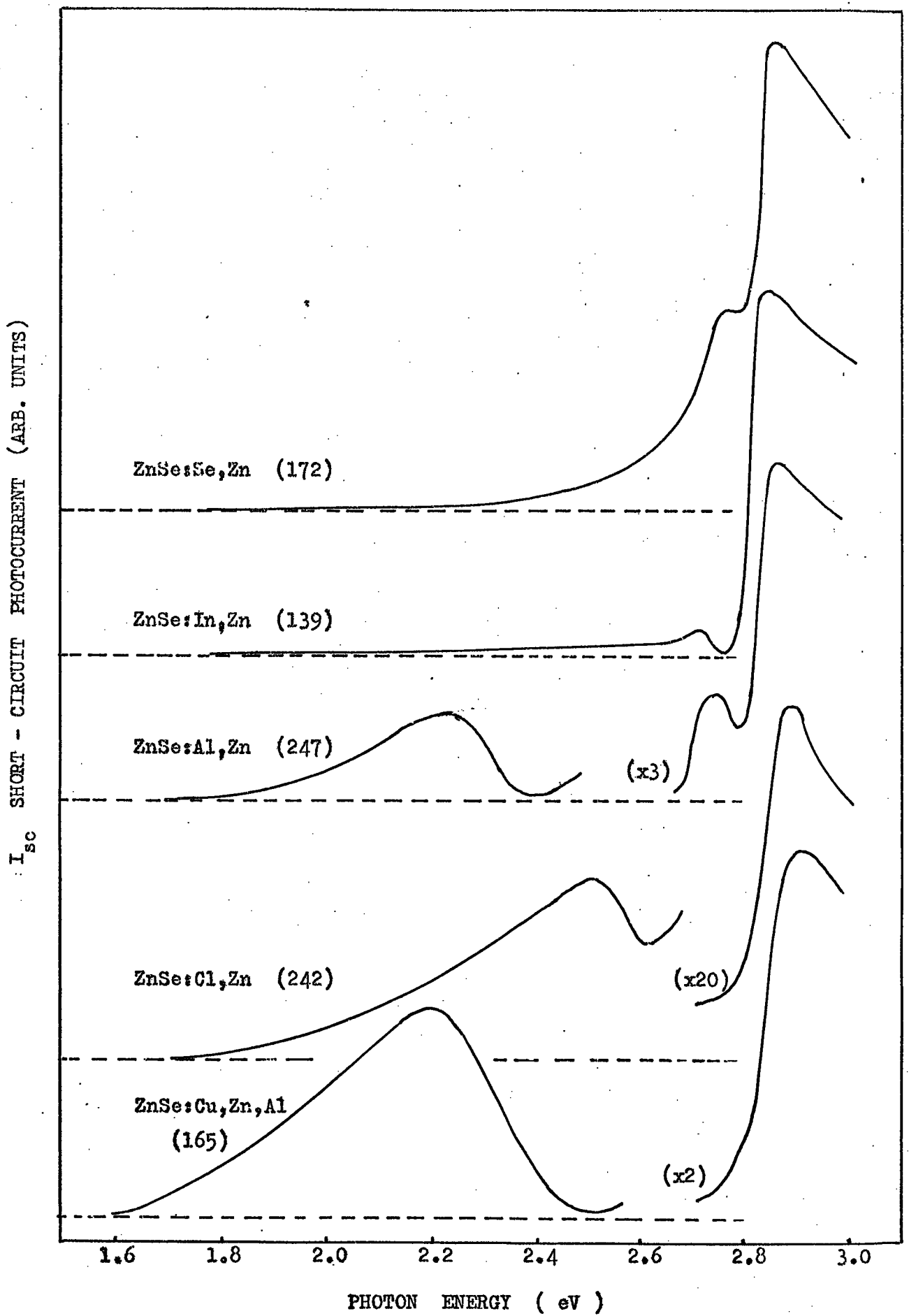


FIG. 5.5 Photoresponse characteristics of Au-ZnSe diodes at 85°K.

the V_i values had increased slightly to an average value of 2.2 eV for diodes prepared on chemically cleaned surfaces, (see for example Fig.5.6).

A typical C^{-2} -V variation for an Au-ZnSe diode prepared on a chemically cleaned surface of ZnSe containing no intentionally added impurities, (diode No.172A) is illustrated by line (1) Figs. 5.6(a) and (b). The uncompensated donor concentration was $N_d = 1.41 \times 10^{16} \text{ cm}^{-3}$ at 295 K and $N_d = 1.06 \times 10^{16} \text{ cm}^{-3}$ at 85 K. The voltage intercepts were 2.1 at 295 K and 2.28 eV at 85 K. The value of N_d of $1.4 \times 10^{16} \text{ cm}^{-3}$ was the highest concentration of native donors observed in a sample to which foreign impurity donors had not been added. The donor content could be easily raised (after growth) to levels of the order of 10^{17} cm^{-3} by diffusion of donors (i.e. Al) during the heat treatment in molten zinc. Of course, doping ZnSe with Al by diffusion is not necessary if sufficient donors are introduced during the growth.

5.5.2 C-V measurements on Au-ZnSe diodes doped with donors

The C-V characteristics of Au-ZnSe diodes prepared on ZnSe crystals doped with various donors (i.e. In, Al, Ga, I, Cl) have also been studied and some of the C^{-2} -V plots are shown in Fig. 5.6.

ZnSe crystals doped with In, and Ga at concentrations of about 1000 ppm formed precipitates when they were heat treated in molten Zn for about 200 hrs. at 850°C . (See for example Jones, 1973).

However, at low doping levels of about 100 ppm, precipitation after heat treatment in molten zinc did not occur. The indium doped ZnSe crystal No.139 is one example of this. Alternatively, when the dopant concentration was of the order of 1000 ppm (see for example Ga doped ZnSe crystal No.176) the precipitation caused by heating in molten zinc could be avoided by using low temperatures, i.e. $600 - 750^\circ\text{C}$, for shorter times (i.e. 15 hours). Following this procedure In or Ga doped

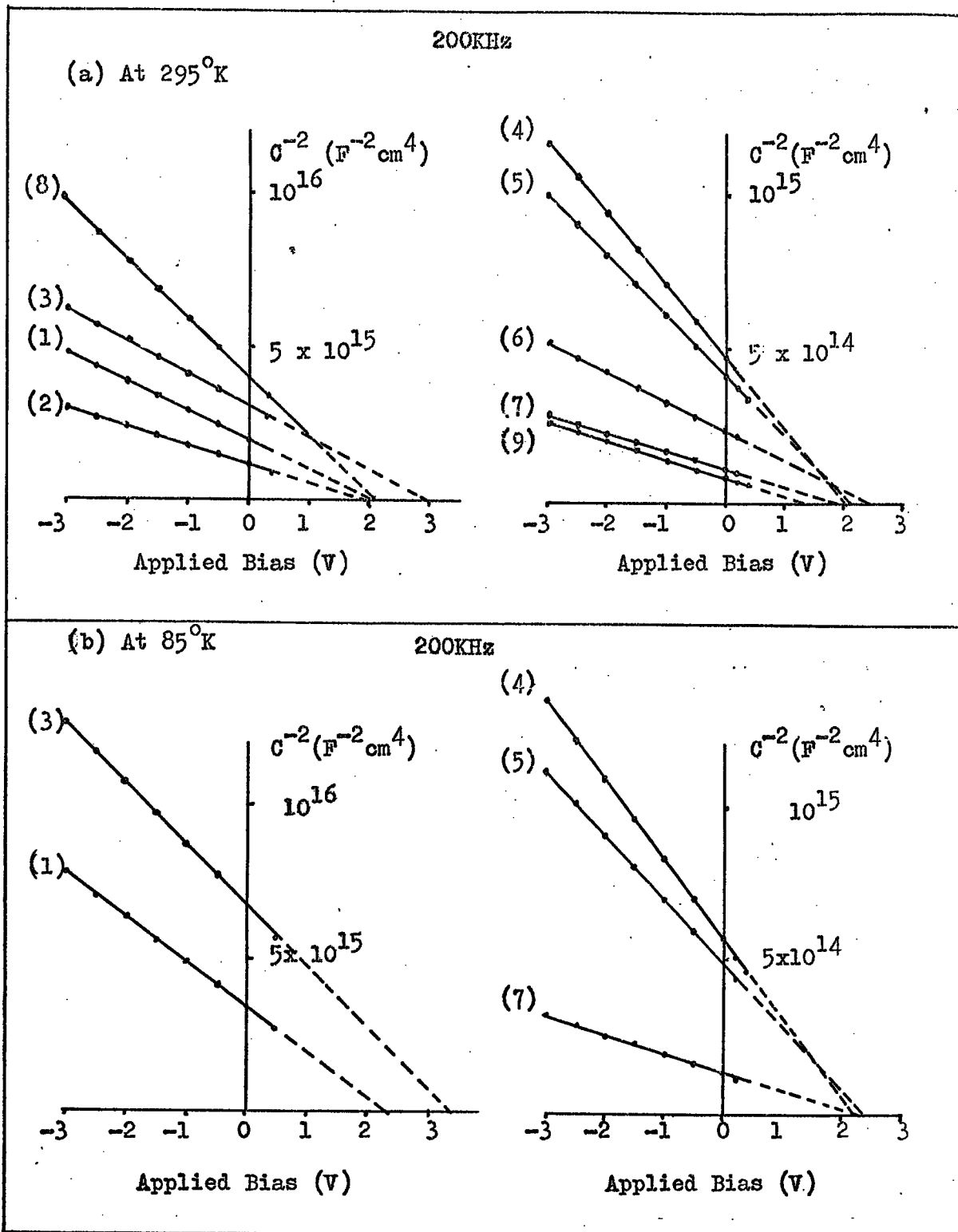


FIG. 5.6 C^{-2} vs V plots for freshly produced Au-ZnSe formed on chemically cleaned surfaces of ZnSe doped with (1)-Se,Zn (172) (2)-Se,Zn Al(172), (3)-Ga,Zn(176), (4)-In,Zn(139), (5)-Al,Zn(247), (6)-I,Zn(931), (7)-Cl,Zn(242), (8)-Cu,Zn,Al(165a) and for Au-ZnSe diode prepared on cleaved surface of ZnSe doped with (9)Mn,Cl,Zn(246)

ZnSe crystals with resistivities of the order of 10 - 100 ohms cm were obtained.

Au-ZnSe diodes doped with substitutional In or Ga were prepared on crystals treated as just described. The C^{-2} -V plots for these diodes, prepared on chemically cleaned surfaces, were found to be linear. (See Fig. 5.6). From the slopes, the donor concentrations proved to be of the order 6×10^{16} and $1.6 \times 10^{16} \text{ cm}^{-3}$ for In and Ga doped samples respectively. The voltage intercept of the C^{-2} -V plot for the In-doped sample was 0.2 eV but with the Ga-doped sample No.176 it was much higher.

$$(V_i = 3.2 \text{ eV}).$$

Iodine was introduced into ZnSe during the iodine transport method of growing the crystals. The C^{-2} -V plot for a diode containing iodine is also illustrated in Fig. 5.6. The donor concentration found from the constant slope of this plot was $N_d = 1.6 \times 10^{17} \text{ cm}^{-3}$ with a value of $V_i = 2.36 \text{ eV}$. Aluminium and chlorine were introduced during the growth of ZnSe crystals (No.247 and 242) and the C^{-2} -V plots from the corresponding Au-ZnSe diodes (see 5,7 in Fig. 5.6) gave donor densities of 8.5×10^{16} and $2.8 \times 10^{17} \text{ cm}^{-3}$ for Al and Cl doped samples respectively. The voltage intercepts V_i were 2.06 and 1.9 eV.

The donor densities and voltage intercepts obtained from C^{-2} -V plots shown in Fig. 5.6 are tabulated in Table 5.2.

5.5.3 C-V Results on Au-ZnSe Diodes containing Donors and Acceptors

With acceptor doped ZnSe crystals (i.e. with Cu) containing no foreign donors, the resistivity could not be decreased below about 10^4 ohm cm by heat treatment in molten zinc. Therefore copper was either introduced into ZnSe with compensating impurity donors, during the growth process, or the crystals containing copper were subsequently heated in a molten mixture of zinc and aluminium. The sample was cut from

crystal No. 165A containing grown-in copper and was then heat treated in a molten mixture of Zn and Al, (for details see Table 5.1). The corresponding $C^{-2}-V$ plot is shown as line (8) in Fig.5.6. The uncompensated donor concentration was found to be $N_d = 1.0 \times 10^{16} \text{ cm}^{-3}$, with a value of $V_i = 1.9 \text{ eV}$.

In another crystal (boule No.191) copper was also introduced into ZnSe together with Mn and Cl and then heat treated in the molten mixture of Zn and Al as described in Table 5.1. The $C^{-2}-V$ plot also gave a straight line with an uncompensated donor concentration of $N_d = 1.63 \times 10^{17} \text{ cm}^{-3}$ and a voltage intercept of $V_i = 2.1 \text{ eV}$.

5.5.4 C-V Variation with Temperature

A few attempts were made to observe the effect on the C-V characteristics of changing the temperature. In this investigation, the first diode (No.172) was formed on a chemically cleaned surface of an undoped material (Au-ZnSe:Se,Zn) and the second one was formed on a cleaved surface of a sample doped with chlorine and manganese (Au-ZnSe:Mn,Cl,Zn). The $C^{-2}-V$ plots were found to be linear over the whole range of temperature from 85 - 295 K. Values of uncompensated donor concentration N_d and voltage intercept V_i were determined as a function of temperature for both diodes and these are illustrated in Fig. 5.7 and Fig. 5.8 for chemically cleaned and cleaved surfaces respectively. In both series the donor concentration decreased slightly as the temperature was reduced. However, the variations of V_i with temperature were different for both types of diode. The value of V_i which was 2.0 eV at 295 K for chemically cleaned surfaces increased steadily with decreasing temperature, reached a maximum of 2.4 eV at 180 K, and then decreased rapidly to a value of 2.1 eV at 85 K. (See Fig. 5.7). With cleaved samples, however, the value of V_i increased almost linearly with

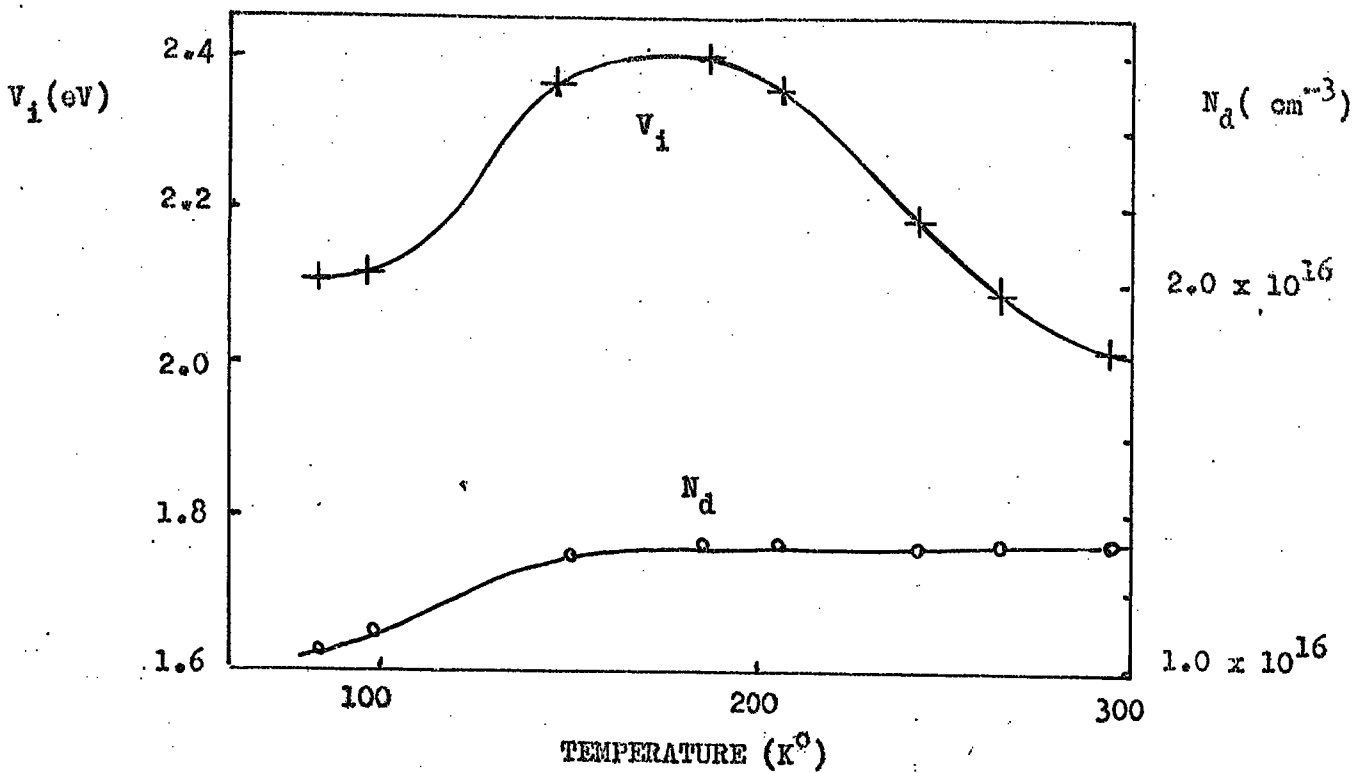


FIG.5.7 The temperature variation of N_d and V_i obtained on Au-ZnSe:Se,Zn diode (no 172) prepared on chemically cleaned surface, using C-V plots.

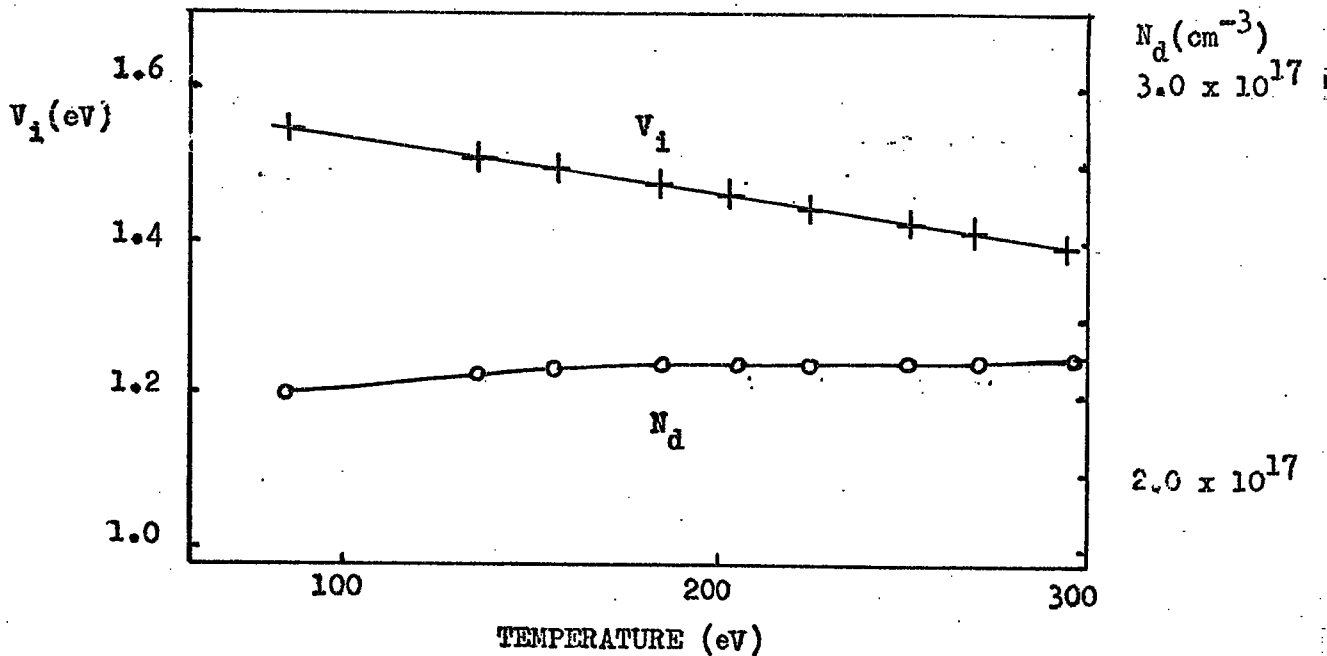


FIG.5.8 The temperature variation of N_d and V_i obtained on Au-ZnSe:Mn,Cl,Zn diode (246 A) prepared on a cleaved surface, using C-V plots.

decreasing temperature from 1.39 eV at 295 K to 1.54 eV at 85 K. Using equation 2.4.11, the barrier height was calculated to be $\phi_{\text{Bn}} = 1.39$ eV and $\phi_{\text{Bn}} = 1.47$ eV at 295 and 85 K respectively. The increase of ϕ_{Bn} with temperature, at a rate of 4×10^{-4} eV/K is to be compared with the increase of band gap with temperature of 6.6×10^{-4} eV/K, determined from free exciton measurements (see Chapter 6). The anomalies observed with chemically etched surfaces are believed to be associated with changes in the properties of the interfacial layer which remains after chemical etching procedure.

The decrease in the uncompensated donor concentration at 85 K was observed in all diodes studied here and is attributed to incomplete donor ionisation. A knowledge of the concentration of ionised donors can be used to determine the ionisation energy of the dominant donor level E_d . The ionised donor concentration N_d^+ is given by the expression: (see for example Sze, 1969)

$$N_d^+ = N_d \{1 + 2 \exp (E_f - E_d)/kT\}^{-1} \quad 5.1$$

Here E_f and E_d are the energetic depths of the Fermi and donor levels below the conduction band. At high temperatures (i.e. 300 K) all the donors are thought to be ionised and therefore the number of uncompensated carriers at 295 K is taken to be N_d . The position of the Fermi level can be calculated using equation 2.4.12. The uncompensated donor concentrations, at 85 and 295 K for diodes containing different donor impurities are recorded in Table 5.2. Using equations 2.4.12 and 5.1, the ionisation energies for Cl, Ga, In and Al donors were calculated to be 25, 25.3, 28.9 and 29.3 ± 1 meV respectively. The ionisation energy of the native donors in the undoped sample (No.172A) was found to be 39 meV using the same method.

Crystal No.	931	247	242	139	176	172B	172A	Cleaved 246
Dopants	I, Zn	Al, Zn	Cl, Zn	In, Zn	Ga, Zn	Se, Zn+Al	Se, Zn	Mn, Cl, Zn
1								
Uncompensated donor concentration N_d ($\times 10^{16} \text{ cm}^{-3}$)	300 K 85 K	8.44 7.5	28.2 26.1	6.75 5.95	1.65 0.104	2.56	1.41 1.28	22.9 22.5
Fermi level	300 K 85 K	79 9	47 0.11	84 11	120 40	110 22	120 22	51 136
E_F (meV)								
Donor level	85 K	29.3	25	28.9	25.3		39	28
E_d (meV)								
Photorethreshold ϕ_{Bn} (ph) (meV)	300 K 85 K	1.63 1.68	159 1.68	1.63 1.68			1.63 1.68	1.36 1.41
Voltage intercept in C ⁻² - V plots V_i (eV)	300 K 85 K	2.36 2.4	1.9 2.2	2.0 2.22	3.15 3.2	1.9	2.1 2.28	1.39 1.54
Diffusion potential V_{BO} (eV)	300 K 85 K	1.53 1.67	1.54 1.68	1.546 1.67			1.51 1.66	1.31 1.41
Depletion width w (Å)	300 K 85 K	957 1485	735 798	1504 1666			3252 3580	750 794
Maximum electric field strength at the surface $ \epsilon _{MAX}$ 10^5 V cm^{-1}	300 K 85 K	3.13 2.21	4.12 4.14	2.02 1.97			0.912 0.911	3.41 3.48
Image force lowering $\Delta\phi$ (meV)	300 K 85 K	71 59.1	80.7 80.9	56.5 55.8			37.9 37.9	73.5 74.2

Table 5.2: Some of the parameters of Au-ZnSe diodes obtained from C-V plots and short circuit photocurrent measurements.

5.5.5 Surface Leakage and C-V Characteristics

Other chemical etchants such as (1) $\text{HNO}_3 + \text{HCl}$, (2) H_2O_2 (100 volume) + an equal part of HCl and (3) $\text{K}_2\text{Cr}_2\text{O}_7$ in H_2SO_4 were also used as surface treatments prior to gold deposition. The C-V plots obtained on Au-ZnSe diodes cleaned with such etchants were all found to be linear. The donor concentrations found from the slopes were slightly larger than the corresponding values obtained using standard etching procedures. However, the voltage intercepts of the $C^{-2} - V$ plot were around 3.0 - 3.5 eV. Similar behaviour was observed if the dice were stored in chloroform, at room temperature, for several days, after being etched prior to gold film deposition. In contrast, the barrier heights of these diodes determined from phototreshold measurements, were by no means so large being around 1.64 eV at 295 K. With a few diodes the surface was cleaned by argon ion bombardment in an attempt to eliminate the semi-insulating layer. However, the results were not successful and the $C^{-2} - V$ plots still showed large values of V_i .

With one or two chemically etched diodes thin slices were cleaved from each of the four faces orthogonal to the contacts. The procedure led to a slight increase in the slope of the $C^{-2} - V$ plot but there was no change in the voltage intercept. A typical example illustrating this is shown in lines (1) and (2) in Fig. 5.21 for the Au-ZnSe:Mn,Cl,Zn diode. The calculated value of N_d decreased from 1.7×10^{17} to $1.46 \times 10^{17} \text{ cm}^{-3}$ after the cleavage of the orthogonal faces, whereas the value of v_i remained unchanged at about 2.0 eV.

5.6 THE FREQUENCY DEPENDENCE OF C-G-V PLOTS AND SURFACE STATES

5.6.1 Frequency Dependence of C-G-V Characteristics

The C-V characteristics of the various diodes were measured at several frequencies in the range of 800 Hz to 300 kHz in the dark.

The slopes of $C^{-2} - V$ plots were found not to change over the frequency range from 150-300 kHz. However, the slope of a plot was often observed to decrease at lower frequencies. The maximum discrepancy was observed at about 10 kHz for diodes constructed on chemically cleaned surfaces. It was thought that the greatest change would occur in the situation where the surface states responded to the a.c. signal frequency. This discrepancy might then be accounted for if some of the parameters concerning the surface states were known. Valuable information about interface states can be obtained by measuring the equivalent conductance G_p of what is in effect an M-I-S (metal-insulator-semiconductor) capacitor which arises solely from the steady state loss due to the capture and emission of carriers by interface states. Studies of the frequency dependence of capacitance using the conductance technique have been developed and used extensively for the Si-SiO₂ interface (see for example Nicollian and Goetzberger, 1967). The method relies on the fact that the time constant of the interface states will give rise to a conductance $G_s = C_s/t$, as the distribution of charge at the interface lags behind the measuring signal. Here C_s is the capacitance associated with the interface states. The equivalent circuit of an MIS capacitor, assuming a single trap model, can be represented as

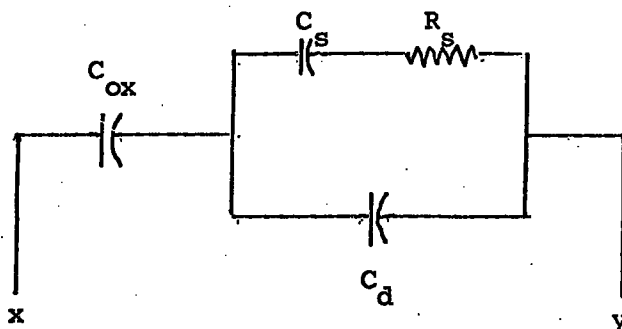


Diagram 5.1

where C_{ox} and C_d are the oxide and the depletion layer capacitances respectively and R_s is the resistance representing the loss mechanism due to interface states. The measured capacitance C_m , across the

terminals of X and Y of this equivalent circuit is then

$$1/C_m = 1/C_{ox} + 1/C_p \quad 5.2$$

where C_p is the capacitance in the parallel branch of the equivalent circuit. Following a change in the applied voltage, the surface states will reach equilibrium with the semiconductor exponentially with the characteristic time $t = R_s C_s$. The capacitance and the conductance of the parallel branch in diagram 5.1 can be written as:

$$C_p = C_d + \frac{C_s}{1 + w^2 t^2} \quad 5.3$$

$$\frac{G_p}{w} = \frac{C_s w t}{1 + w^2 t^2} \quad 5.4$$

The above equations can be extended to include the effect of C_{ox} so that comparison can be made directly with the experimental data, i.e. with the measured conductance G_m and measure capacitance C_m across the terminals X and Y of the equivalent circuit in Fig. 5.9. Then equations 5.3 and 5.4 become:

$$C_p = \frac{C_{ox} (G_m^2 + w^2 C_m^2) [w^2 C_m (C_{ox} - C_m) - G_m^2]}{w^2 C_{ox}^2 G_m^2 + [w^2 C_m (C_{ox} - C_m) - G_m^2]^2} \quad 5.5$$

and

$$\frac{G_p}{w} = \frac{w C_{ox}^2 G_m (G_m^2 + w^2 C_m^2)}{w^2 C_{ox} G_m^2 + [w^2 C_m (C_{ox} - C_m) - G_m^2]^2} \quad 5.6$$

Equation 5.3 depends on both C_d and C_s , while equation 5.4 depends only on the surface state branch of the equivalent circuit. A plot of G_p/w against w goes through a maximum which occurs when

$$wt = 1 \quad 5.7$$

The maximum is related to C_s in the following way

$$\left[\frac{G_p}{w} \right]_{\max} = \frac{C_s}{2} \quad 5.8$$

which is related in turn to the surface state density D_s since

$$D_s = \frac{C_s}{eA} \quad 5.9$$

Here e is the electron charge and A is the area of the device.

5.6.2 G-V Measurements

G-V characteristics have been measured using the G-C-V plotter described in Chapter 4.3.2. Measurements were made in the dark, in the range of frequencies from 1 - 300 kHz. A typical G-V plot at 200 kHz is illustrated in Fig. 5.2. In all Au-ZnSe diodes examined, the conductance was found to increase quite steeply at applied voltages greater than 0.5 volts in the forward direction. This large conductance lay outside the range of the C-G-V plotter used here. The capacitance could not therefore be measured at forward bias voltages greater than 0.5 V (i.e. under accumulation conditions). In perfect MIS diodes the measured capacitance is expected to saturate in accumulation conditions at the value of the oxide capacitance C_{ox} . Such a saturation was not detected in the ZnSe diodes studied here. An attempt was made therefore to investigate the variation of G_p/w with w by ignoring the contribution of C_{ox} ; that is the measured capacitance G_m was assumed to be equal to G_p in equation 5.3.

The G_p/w versus w characteristics plotted as a function of applied bias for a diode containing diffused-in aluminium (No.247) are shown in Fig.5.9. This diode was formed on a chemically etched surface and thin slices were cleaved from each of the four faces orthogonal to the contacts. Cleaving the orthogonal faces often caused a small decrease in the measured conductance. The G_p/w versus w plots were broad curves with maxima occurring at about 100 kHz regardless of bias. When a diode formed on a cleaved surface (diode No.246A) was investigated, the G_p/w versus w plots led to much narrower curves (see

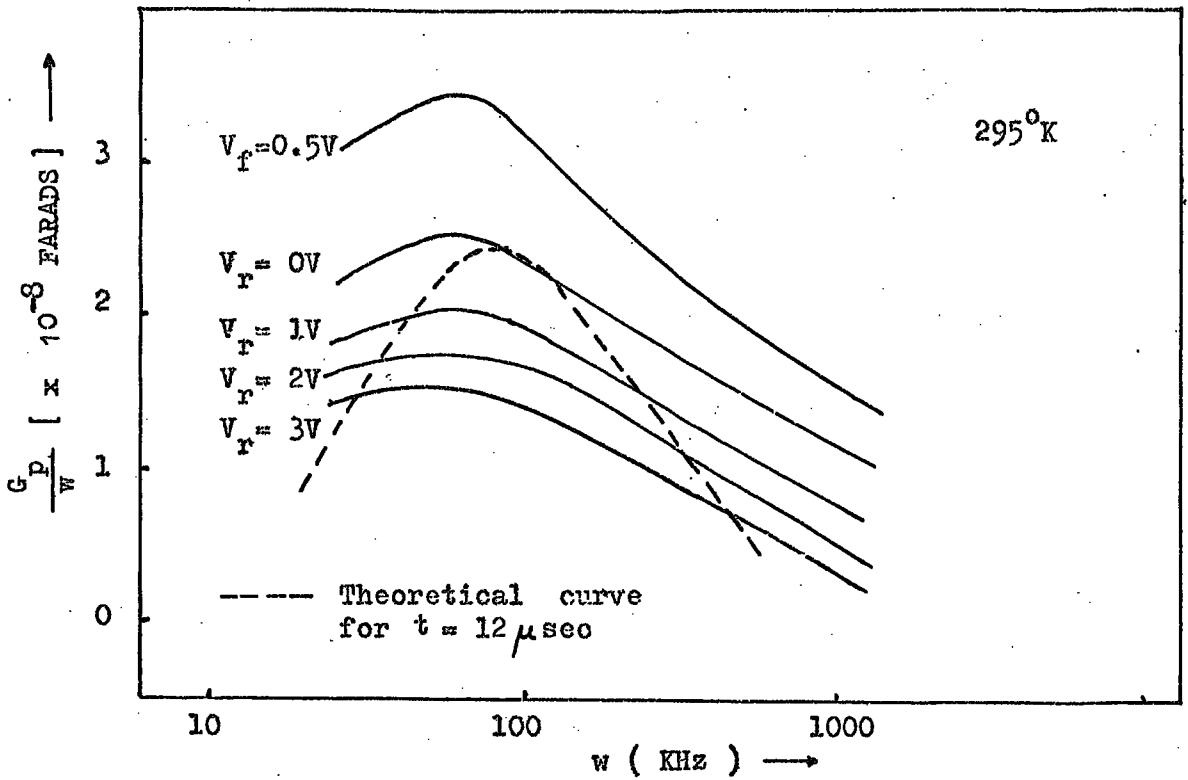


FIG.5.9 G_p/w against w plot for Au-ZnSe:Al,Zn (247) diode prepared on chemically cleaned surface

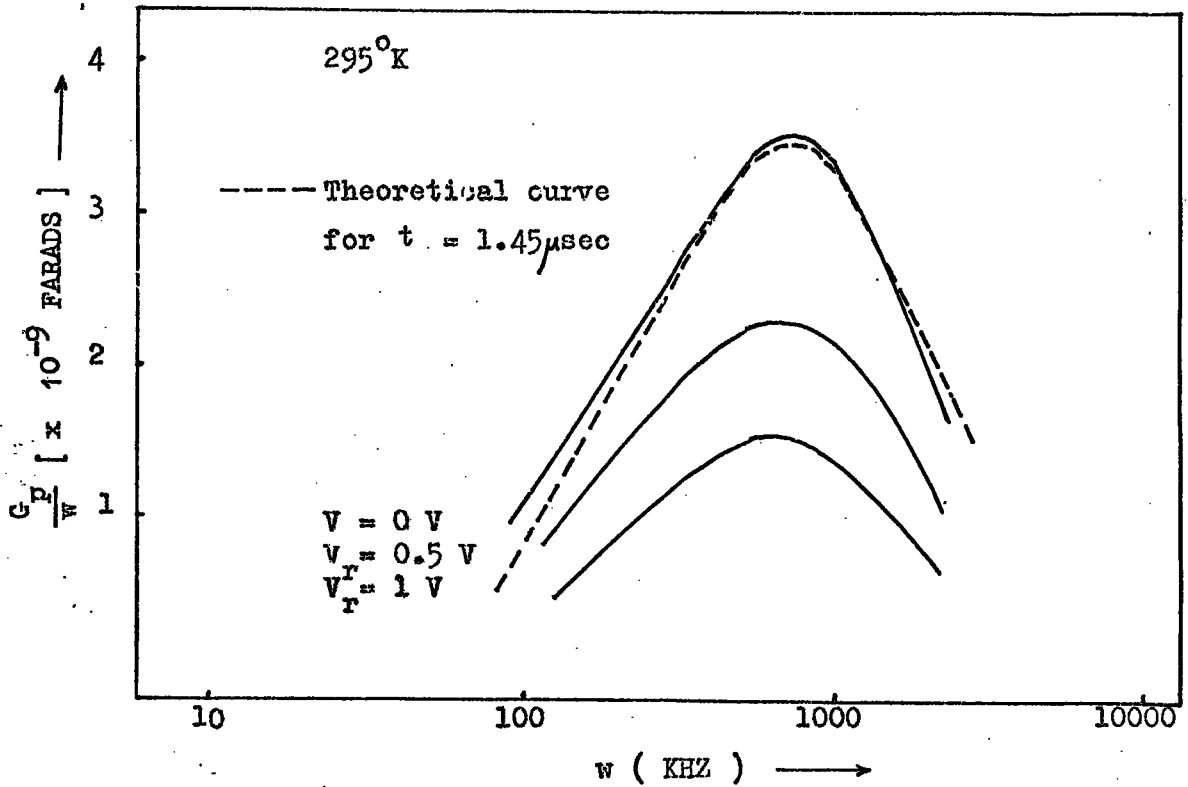


FIG.5.10 G_p/w against w plot for Au-ZnSe:Kn,Cl,Zn (246A) diode prepared on acleaved surface

Fig. 5.10). The values of $(G_p/w)_{\max}$ at $V = 0$ were 3.5×10^{-10} and 3.7×10^{-11} F for chemically cleaned and cleaved diodes respectively. Substituting these values in equation 5.7, time constants of 12 and 1.4 μsec were obtained for the interface states on chemically cleaned and cleaved surfaces respectively. Again, using the above values of $(G_p/w)_{\max}$ in equations 5.8 and 5.9, the densities of the surface states were calculated to be about 4×10^{11} states/eV/cm² for chemically cleaned and 5×10^{10} states/eV/cm² for cleaved (see Fig. 5.10) surfaces, at zero applied voltage.

An attempt was also made to include the effect of oxide capacitance C_{ox} so as to be able to make use of equation 5.6. For this an estimated value of $C_{\text{ox}} = 3 \times 10^{-7}$ F/cm² (see Sec. 5.7.4) was used with the sample for which the G_p/w versus w plots are shown in Fig. 5.9. At some frequencies (i.e. 10 kHz, 200 kHz) the values of G_p/w calculated using 5.6 were found to be bigger than the measured value by a factor of 2. It follows therefore that the density of surface states calculated using equation 5.4 (where the effect of C_{ox} was ignored) can be in error for a factor of 2.

The effects of the surface states on the C^{-2} - V plots at high frequencies are negligible. This is because $C_d \approx C_p$ when $\omega t \gg 1$ (see equation 5.3). However the discrepancies in the C^{-2} - V plots at lower frequencies which arise from ignoring the surface states can be calculated. When an oxide layer is present and $C_{\text{ox}} \approx C_p$, then the contribution from C_{ox} should also be considered. First the contribution from C_{ox} is allowed for, and C_p is calculated from the measured capacitance C_m . Once the plots of G_p/w versus ω have been made and C_s and t determined from the magnitude and location of the maxima, the second term on the right hand side of equation 5.3 can be calculated for each value of the bias at which the conductance measurements were made. The true value of C_d can then be extracted from equation 5.3. The application of this procedure is best illustrated with some results for sample diode 242. Using uncorrected capacitances measured at 10 kHz led to a value of N_d of 6.7×10^{17} and a voltage intercept

of V_i of 2.5 V. When the correction procedure was applied, the new values of capacitance led to a straight line $C^{-2} - V$ plot with a value of N_d of $5.48 \times 10^{17} \text{ cm}^{-3}$ and a voltage intercept of 1.61 V. The value of N_d after correcting the $C^{-2} - V$ plots at 10 kHz was almost identical with the value of N_d of $5.40 \times 10^{17} \text{ cm}^{-3}$ obtained using uncorrected capacitances at 200 kHz. Therefore the error in the value of N_d using uncorrected capacitances measured at 10 kHz was around 25%.

5.7 DEVICE PARAMETERS

5.7.1 Introduction

Some of the device parameters such as the Fermi level E_f , Schottky barrier lowering, $\Delta\phi_B$, the depletion layer width W , the electric field $|E|$ and the diffusion potential V_{BO} in the bulk of ZnSe could be calculated from the photoresponse and C-V measurements. It was also possible to find the thickness and the capacitance of the interfacial semi-insulating layer (ZnO) between the gold and ZnSe. These calculations were based on the assumption that the barrier height between the gold and the zinc selenide is given by the photothreshold $\phi_{Bn}(\text{ph})$ obtained directly from the short-circuit photocurrent measurements.

5.7.2 The Diffusion Potential V_{BO}

The diffusion potential V_{BO} can be obtained directly from the photothreshold values of the barrier height $\phi_{Bn}(\text{ph})$. The value of $\phi_{Bn}(\text{ph})$ is related to V_{BO} by $\phi_{Bn} = V_{BO} + E_F$ represents the depth of the Fermi level below the conduction band in the bulk of the semiconductor. The Fermi level can be calculated using equations 2.4.12 and donor concentrations determined from the slopes of $C^{-2} - V$ plots. For many of the diodes studied here the value of the Fermi level E_F lay in the range 40-120 meV at 295 K (see Table 5.2). Values of V_{BO} obtained by subtracting the values of E_F from the observed photoresponse thresholds are listed in Table 5.2.

5.7.3 The Depletion Layer Width, W

The width W of the depletion layer in the semiconductor is given by equation 2.4.2 and can be calculated if the diffusion potential V_{BO} and the uncompensated donor concentration N_d are known. Using $\epsilon_s = 9.1 \epsilon_0$ for ZnSe, and the data given in Table 5.2, the depletion layer width W for most of the Au-ZnSe diodes could be calculated. According to equation 2.4.2 the depletion layer decreases when the diode is biased in the forward direction and increases when the diode is biased in the reverse direction. The typical values of W for Cl doped samples, for example, were found to be about 750 \AA at zero applied bias, but the width could be as high as 3250 \AA if the donor concentration was around 10^{16} cm^{-3} (diode 172 A). The depletion widths were found to increase slightly at 85 K (see Table 5.2).

5.7.4 Maximum Electric Field, \mathcal{E}_{max} , and the Image Force

Lowering $\Delta\phi$, at the Interface

The maximum electric field strength $|\mathcal{E}|_{max}$ in the depletion region of the semiconductor is given by equation 2.4.3(b). Therefore if N_d and W are known $|\mathcal{E}|_{max}$ can be calculated. Using the data given in Table 5.2, the value of the $|\mathcal{E}|_{max}$ at zero applied bias was found to be greater than 10^5 V/cm^2 . For example the value of $|\mathcal{E}|_{max}$ at $V=0$, was calculated to be approximately $4 \times 10^5 \text{ V/cm}^2$ for the Cl doped samples (diode No.242), and the lowest value of 10^5 V/cm^2 was found in the diodes with no intentionally added impurities (i.e. for diode No.172). See Table 5.2.

The image force lowering $\Delta\phi_B$ of the barrier height is described by equation 2.4.10(b). Assuming that the image force dielectric constant and the static dielectric constant of ZnSe are equal (i.e. $\epsilon_d = \epsilon_s = 9.1$), the value of $\Delta\phi_B$ can be calculated if $|\mathcal{E}|_{max}$ is known.

Substituting the calculated values for $|\mathcal{E}|_{\max}$ into equation 2.4.10(b) the values of $\Delta\phi_B$ for most of the diodes were found to lie in the range of 38 - 81 meV at zero applied bias (see Table 5.2). Again the higher values were found in samples containing high donor concentrations.

5.7.5 Interfacial Layer Thickness, d

Values of the above mentioned parameters such as $W, |\mathcal{E}|_{\max}, \Delta\phi_B$, can also be found from C-V measurements using equation 2.4.6, by finding W from the measured capacitance. However, this procedure was not followed because the C-V plots deviated from ideal behaviour when an interfacial layer was present. However, the thickness of the interfacial layer can be calculated at zero applied bias using equations 2.4.34 or 2.4.36 if $V_{BO}, V_i, N_d, D_s, N_c$ are known. For example if the following calculated parameters:

ϵ_s	= 9.1 ϵ_o (Berlincourt et al, 1963)		
T^o	= 295 K	N_d	= $8.44 \times 10^{16} \text{ cm}^{-3}$
$\phi_{Bn}(\text{ph})$	= 1.63 eV	N_c	= $1.7 \times 10^{18} \text{ cm}^{-3}$
V_i	= 2.06 eV	D_s	= $3.6 \times 10^{11} \text{ states/eV/cm}^2$
E_F	= 0.08 eV	$\epsilon_i(\text{ZnO})$	= $8.5 \epsilon_o$ (Dietz et al 1961)
$V_2(\text{kT/q})$	= 0.0259 eV	ϵ_o	= $8.85 \times 10^{-14} \text{ F/cm}$

for a chemically etched diode (No.247) Au-ZnSe:Al, Zn are substituted in equation 2.4.34, the interfacial layer thickness d is found to be about 240 \AA . On the other hand, if one assumes that there are no surface states, or $\delta Q_{ss}/\delta V = 0$, one can then use equation 2.4.27 or 2.4.36. With this assumption the above parameters lead to a thickness of around 200 \AA .

When the gold was deposited on to a cleaved surface, particularly with diode (No.246A) Au-ZnSe:Mn, Cl, Zn the following parameters were obtained at 295 K.

$$\begin{array}{ll}
 \phi_{\text{Bn}} (\text{ph}) = 1.36 \text{ eV} & N_{\text{d}} = 2.43 \times 10^{17} \text{ cm}^{-3} \\
 V_{\text{i}} = 1.39 \text{ eV} & N_{\text{c}} = 1.7 \times 10^{18} \text{ cm}^{-3} \\
 E_{\text{F}} = 0.051 \text{ eV} & D_{\text{ss}} = 4.6 \times 10^{10} \text{ states/eV/cm}^2 \\
 V_2 (kT/q) = 0.0259 \text{ eV} & \epsilon_{\text{i}} (\text{ZnO}) = 8.5 \epsilon_0
 \end{array}$$

Substituting these values in equation 2.4.34 gives an interfacial layer thickness of $d = 27 \text{ \AA}$. However, if once again one accepts that there are virtually no surface states and used the equation 2.4.27 or 2.4.36 a value of about $d = 15 \text{ \AA}$ is found for the thickness of the interfacial layer.

An approximate estimate of the thickness of the interfacial layer can also be obtained from the C-V measurements in a different way. According to equations 5.2 and 5.3, C_{OX} can be calculated from the measured capacitance C_{m} when C_{d} and C_{s} are known. The value for the depletion layer capacitance C_{d} can be calculated separately using equation 2.4.6 if V_{BO} and N_{d} are known. On the other hand C_{s} can be calculated by the conductance method. To illustrate the calculation the Au-ZnSe:Al, Zn diode (No.247) mentioned above had the following parameters:

$$\begin{array}{ll}
 C_{\text{m}} (\text{measured}) & = 4.95 \times 10^{-8} \text{ F/cm}^2 \text{ (at 200 kHz)} \\
 \epsilon_{\text{ox}} (\text{ZnO}) & = 8.5 \epsilon_0 \\
 C_{\text{d}} (\text{calculated}) & = 5.97 \times 10^{-8} \text{ F/cm}^2 \\
 C_{\text{s}} /_{v=0} \text{ (from Fig.5.9)} & = 5.26 \times 10^{-8} \text{ F/cm}^2
 \end{array}$$

Substituting these values into equations 5.3 and 5.2, the oxide capacitance was found to be $C_{\text{OX}} = 2.8 \times 10^{-7} \text{ F/cm}^2$, and assuming that the insulating layer would form a parallel plate capacitor, i.e. $C_{\text{OX}} = \epsilon_{\text{OX}}/d$, the interfacial layer thickness was found to be $d = 260 \text{ \AA}$. Finally if one treats the insulating layer as having a series resistance, r , it is possible to derive the following relation (Goodman, 1963):

$$V_i = V_{BO} + \frac{2w^2 r^2}{d(1/c^2)/dv} \quad 5.10$$

Using the results contained in the $C^{-2} - V$ plot for diode No.247, in Fig. 5.6, the value r for the oxide resistance was found to be of the order of $10^5 - 10^6$ ohm.

5.8 CURRENT VOLTAGE (I-V) CHARACTERISTICS

5.8.1 Introduction

The experimental current-voltage characteristics of a rectifying M-S contact are usually described by equation 2.4.42, and the saturation current J_s depends on what kind of transport process is taking place in the particular M-S contact. A condition for thermionic emission over the barrier to occur was given by equation 2.4.41. The maximum electric field strength was typically $|\mathcal{E}|_{\max} = 4 \times 10^5$ V/cm², the value of the average velocity \bar{v} of electrons in ZnSe, using $m^* = 0.17 m$ (Marple, 1964) is calculated to be $1.5 \times T^{0.5} \times 10^6$ cm sec⁻¹ from equation 2.4.41(b). Using the value of $\mu_e = 530$ cm² V⁻¹ sec at 300 K (Woodbury and Aven, 1962), the ratio of $(\mu_e |\mathcal{E}|_{\max}) / (\bar{v}/4)$ is found to be about 30. Thus the condition for thermionic emission to occur (equation 2.4.41) is satisfied.

The I-V characteristics were investigated in Au-ZnSe diodes formed on chemically cleaned or cleaved surfaces of ZnSe. The technique used to measure I-V characteristics was described in Chapter 4.3.1, and in the following sections a brief discussion of forward and reverse I-V characteristics is given.

5.8.2 Forward-Bias I-V Characteristics

Typical forward I-V characteristics for a freshly prepared

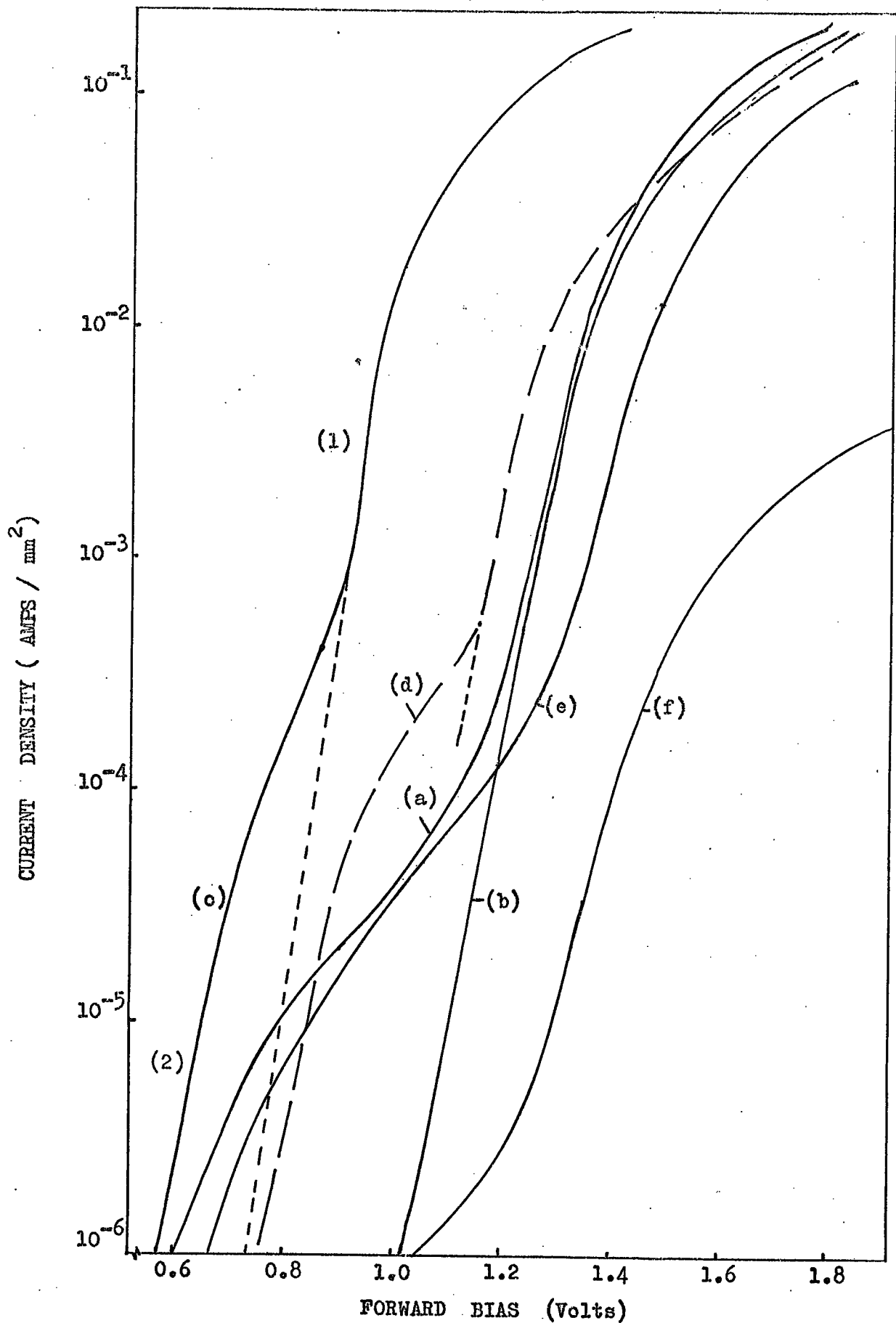


Fig.5.11 The forward I-V characteristics of Au- ZnSe diodes doped with (a)Mn,Cl,Zn,as produced, (b)Mn,Cl,Zn (246,after sides were cleaved) (c)MnClZn (246,Cleaved), (d) (c at 85°K), (e) Al,Zn (247), (f)Se,Zn(172)

Au-ZnSe:Mn,Cl,Zn diode, formed on a chemically cleaned surface, can be seen in curve (a) Fig. 5.11. However, when thin slices were cleaved from each of the four faces of the diode orthogonal to the contacts, a new characteristic was obtained, see curve (b) Fig. 5.11. It was concluded that the high currents originally observed in curve (a) with applied voltages less than 1 V were attributable to the shunting effects of the semi-insulating layer left by the etching process on the orthogonal faces of the dice. When the shunting layers were removed the forward I-V characteristics became exponential with voltage for current densities in the range $10^{-8} - 10^{-2}$ amps/mm² with a diode perfection factor "n-value" of 1.26.

Assuming that the density of interface states was sufficiently small so as not to influence the potential distribution in the junction, the n-value described by 2.4.44 becomes:

$$n = 1 + \frac{de}{W\epsilon_1} \quad 5.11$$

The value of the depletion width W was determined to be 890 Å using photoresponse measurement. From the value of n=1.26, the thickness of the insulating layer was calculated from the forward I-V characteristics to be approximately 215 Å.

At the highest current densities the curves appeared to saturate. This was entirely due to the fact that the current was then limited by the series differential resistance of the device.

Curve (c) Fig. 5.11, was obtained from an Au-ZnSe:Mn,Cl,Al diode (No. 246A) where the gold was deposited on a cleaved surface. It also showed the presence of leakage currents, with applied biases below 0.8 V, part 2 in curve (c) Fig. 5.11. When the forward voltage exceeded 0.9 V an exponential region was observed over nearly two decades of current with an n-value of 1.06, part 1 curve (c) Fig. 5.11. The

depletion layer of this diode was 750 Å thick, while the interfacial layer was about 35 Å wide. The n-value corresponding to part 2 of curve (c) Fig. 5.11 was 1.38.

Similar behaviour in the forward bias I-V characteristics was also observed for Au-ZnSe:Al,Zn diode (No.247) shown in curve (e) Fig. 5.11 and for Au-ZnSe:Se,Zn diode No.172A in curve (f) Fig. 5.11.

The maximum electric field $|\mathcal{E}|_{\max}$ decreases under the application of forward bias. Therefore the validity of equation 2.4.41 has to be checked over the range of bias voltages for which the current stays exponential. From Fig.5.11, the maximum current density up to which the forward I-V characteristics for all the diodes studied here remained exponential was around 10^{-2} Amps/mm². This corresponds for example to a forward voltage of 1 and 1.3 V for the diodes illustrated by curves (c) and (b) in Fig. 5.11, and the calculated values of $|\mathcal{E}|_{\max}$ at these biases were 1.6×10^5 and 1.3×10^5 V/cm² respectively. These values in turn both led to a calculated ratio of $(\mu_e |\mathcal{E}|_{\max}) / (\bar{v}/4)$ of around 12. The evaluation of curves (e) and (f) Fig. 5.11 gave similar results. The conclusion is, therefore, that the condition for thermionic emission over the barrier (i.e. equation 2.4.41) was satisfied for the forward I-V characteristics of most of the Au-ZnSe diodes studied here.

The experimental current-voltage characteristics for an M-S contact obeying thermionic emission theory is described by equation 2.4.38(a) with the saturation current given by equation 2.4.38(b). The diffusion potential V_{BO} and thus the barrier height ϕ_{Bn} can now be found from the saturation current. The Richardson constant A^* can be calculated for ZnSe if one uses the value of $m^* = 0.17 m$ (Marple, 1964).

The saturation current from part (1) of curve (c) Fig. 5.11, that is the cleaved sample, was found by extrapolation to be $J_s = 3 \times 10^{-16}$ amp/cm², from which the diffusion potential V_{BO} was

calculated to be 1.29 eV. The barrier height was then found by adding the Fermi energy to V_{BO} , which gave a value of $\phi_{Bn} = 1.34$ eV. In contrast, if one considers part (2) of curve (c) Fig. 5.11, the saturation current of 10^{-11} A/cm², which is dominated by leakage currents, reveals a value of V_{BO} of 1.04 eV which is much too small of course.

With the chemically cleaned sample which gave the current-voltage characteristic shown in curve (b) Fig. 5.11, the saturation current was of the order of $J_s = 4 \times 10^{-18}$ amp/cm² and the resultant diffusion potential was calculated to be $V_{BO} = 1.41$ eV ($\approx \phi_{Bn}$). Similar values for V_{BO} were found for diodes No.247 and 172 from the curves (e) and (f) Fig. 5.11.

At 85 K the forward I-V characteristics were shifted parallel to themselves towards high voltages. A typical example is illustrated by curve (d) Fig.5.11. The barrier height of 1.41 eV, observed from phototreshold measurements, would require a thermionic saturation current much smaller than the observed saturation current of 8×10^{-18} amps/cm² which is obviously attributable to leakage at least at 85 K.

5.8.3 The Reverse Current-Voltage Characteristics

The reverse current-voltage characteristics, for a cleaved diode (246A) for which the forward I-V characteristics are shown in Fig.(c) Fig.5.11, is illustrated in curve (a) Fig. 5.12. The reverse I-V characteristics were substantially exponential for current densities in the range $10^{-5} - 10^{-2}$ amp/mm². No saturation was observed and indeed an avalanche effect developed when the bias exceeded 15 V. The maximum electric field $|\mathcal{E}|_{max}$ increases with the application of the reverse bias. For example, the value of $|\mathcal{E}|_{max}$ was calculated to be about 1.2×10^6 V/cm² at $V_R = 15$ V for this sample. The reverse bias

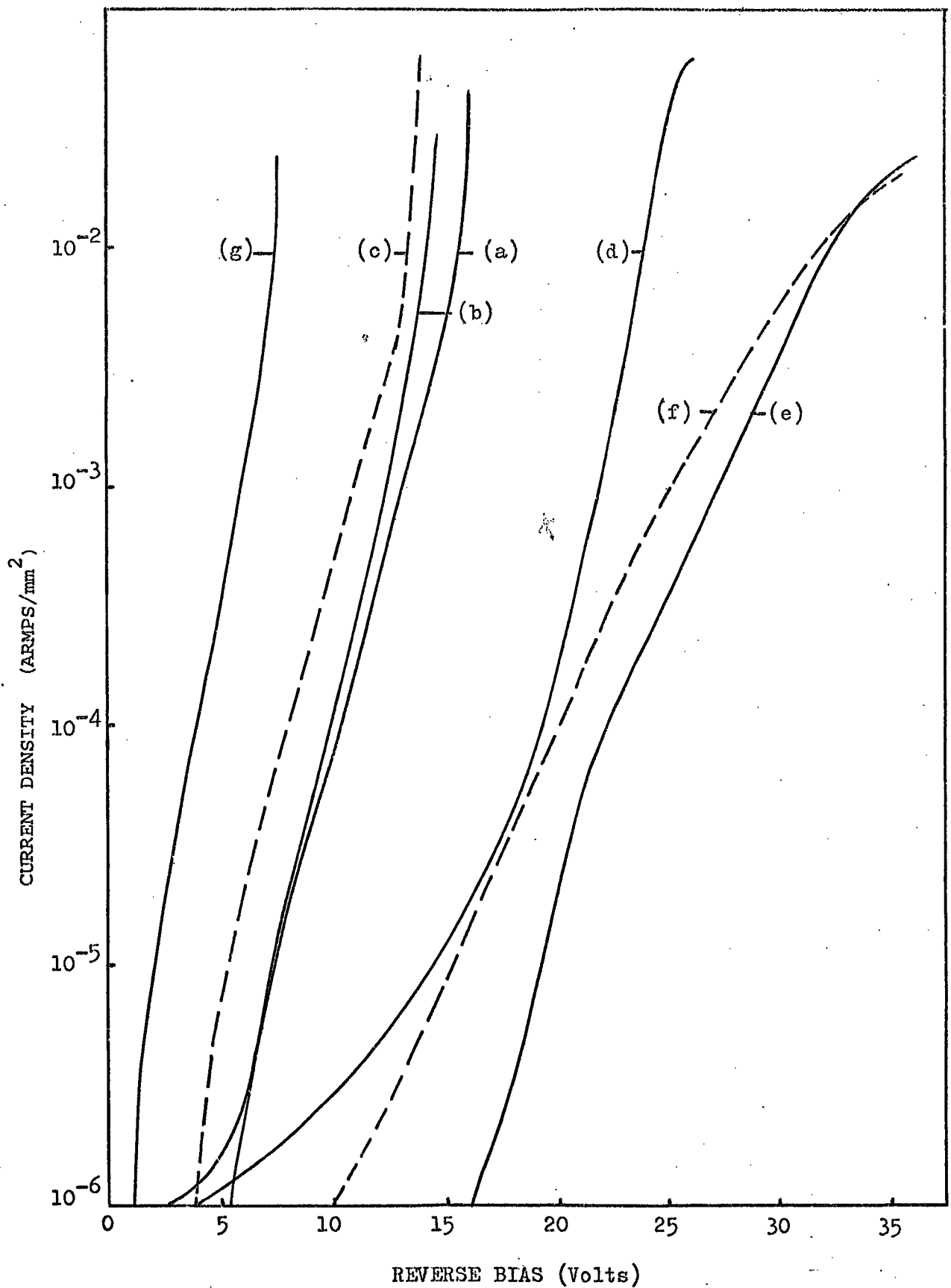


FIG.5.12 Reverse current voltage characteristics of various Au-ZnSe diodes. (a) Au-ZnSe:Mn,Cl,Zn prepared on cleaved surface(no 246A) and prepared on chemically cleaned surface (b). (c) Cleaved diode 246A at 85°K. (d) Au-ZnSe:Al,Zn , (e) Au-ZnSe:Se,Zn , (f) Au-ZnSe:Se,Zn at 85°K and (g) Au-ZnSe:Cu,Mn,Cl,Zn+Al all prepared on chemically cleaned surfaces.

I-V characteristic for an Au-ZnSe:Mn,Cl,Zn diode prepared on a chemically cleaned surface is illustrated in curve (b) Fig.5.12. The I-V characteristic was again exponential. The current at any particular applied bias was slightly greater than that in diodes prepared on cleaved surfaces. However, the avalanching effect at higher bias was less pronounced. Again no saturation was observed.

The reverse I-V characteristics for Au-ZnSe:Al,Zn (No.247) and Au-ZnSe:Se,Zn (172) diodes are illustrated in curves (d) and (e) of Fig.5.12. In these diodes the reverse voltage required to obtain a current density of 10^{-2} amp/mm² was higher. Again there was no sign of saturation at high current densities. The small deviation from exponential behaviour at high currents was found to be due to Joule heating. When short voltage pulses were used this effect was not observed.

The reverse I-V characteristics were also investigated at 85 K. In general the I-V characteristic retained the same basic slope but the current at a given voltage increased. A typical example is illustrated for diode 246A in curve (c) Fig.5.12. The reverse I-V characteristics at 85 K obeyed an exponential law over four decades of current. The avalanche effects were also quite apparent at high current densities at 85 K.

The reverse I-V characteristics have also been investigated for Cu doped samples and will be described in later chapters. However, an interesting feature of the reverse I-V characteristics of diode No.191 which contained copper and manganese, is illustrated by curve (g) Fig.5.12. The reverse current of this diode reached a value of 2×10^{-2} amp/mm² with a very low applied bias of 7.5 V. The current followed an exponential variation over four decades and avalanching occurred at the highest current densities. The low values of the

photothreshold in Cu doped samples (i.e. $\phi_{Bn} \approx 1.45$ eV) may explain these observed reverse I-V characteristics. The voltage intercept from the C^{-2} - V plot was $V_i = 2.1$ eV, and N_d was $1.63 \times 10^{17} \text{ cm}^{-3}$ indicating the presence of an interfacial layer with a thickness of $d \approx 205 \text{ \AA}$, which was of the same order as that for many diodes studied here. The only effect of the copper was apparently to decrease the barrier height in Au-ZnSe diodes, which is rather difficult to understand.

To summarise, the reverse I-V characteristics in Au-ZnSe diodes were largely exponential and avalanching only occurred in those devices which had a donor content of the order of $2 \times 10^{17} \text{ cm}^{-3}$. The maximum electric field $|\mathcal{E}|_{\text{max}}$ was around $1.2 \times 10^6 \text{ V/cm}^2$ at an applied reverse bias of $V_R = 15$ V for diodes containing added foreign donors (e.g. diode 246A) as against $4 \times 10^5 \text{ V/cm}^2$ for an undoped diode at $V_R = 30$ V. It also follows that the thermionic emission theory would be expected to hold in reverse bias as well. However, the observed value for the saturation current was around $3 \times 10^{-8} \text{ amp/cm}^2$, from which the barrier height would be 0.8 eV, using equation 2.4.38(b). This value is small compared with the values of 1.41 eV obtained from the forward I-V characteristics. Under reverse bias the width of the barrier increases, but at the level of the Fermi energy becomes narrower, thus enhancing the possibility of electron tunnelling. On the other hand, the Schottky barrier lowering, $\Delta\phi_B$, increases at reverse biases. For example the value of $\Delta\phi_B$ was calculated to be 0.15 V for the cleaved diode (246 A) at an applied bias of $V_R = 15$ V.

5.9 AGEING AND THE ELECTRICAL PROPERTIES OF Au-ZnSe DIODES

Au-ZnSe diodes prepared on chemically cleaned surfaces of ZnSe had stable current-voltage characteristics when biased in the forward direction. However, the reverse current-voltage characteristics

of these diodes were often found to be unstable while making point by point measurements. What happened was that an increasing reverse voltage was required to maintain a constant current. C^{-2} -V plots obtained after biasing the diodes in the reverse direction showed a slight decrease in the values of N_d and V_i . Remeasurement of the forward I-V characteristics showed that the leakage currents had increased considerably after ageing. The exponential form of the forward I-V characteristics was found not to change, but the slope, or "n-value", was often found to increase. The magnitude of the short circuit photocurrent was also found to have decreased. Ageing effects of this type were found to be reduced to a minimum when a standard chemical cleaning procedure was followed (see Chapter 4.2.1). However, ageing effects were pronounced and variable when alternative etching procedures were used. Since a standard etching procedure gave reproducible results, this etchant was used in all samples examined, and since Au-ZnSe:Mn,Cl,Zn diodes were found to be promising light emitting devices, the ageing of these diodes was studied in some detail. All ageing experiments described below were made in a rough vacuum (i.e. at the pressure of 10^{-3} torr). Ageing in EL output will be discussed in Chapter 7.

5.9.1 Long Term Ageing in Au-ZnSe:Mn,Cl,Zn Prepared on Cleaved Surfaces of ZnSe

Here the ageing of a cleaved diode (246A) was studied. This diode was constructed on a {1,1,0} cleaved surface as described in Section 5.4.1. The barrier height was found to be 1.36 eV from the short circuit photo-current measurements (see Fig.5.3).

(a) Forward Current Voltage Characteristics

The forward current-voltage characteristic of this freshly produced diode was exponential over four decades of current (see Fig.5.13).



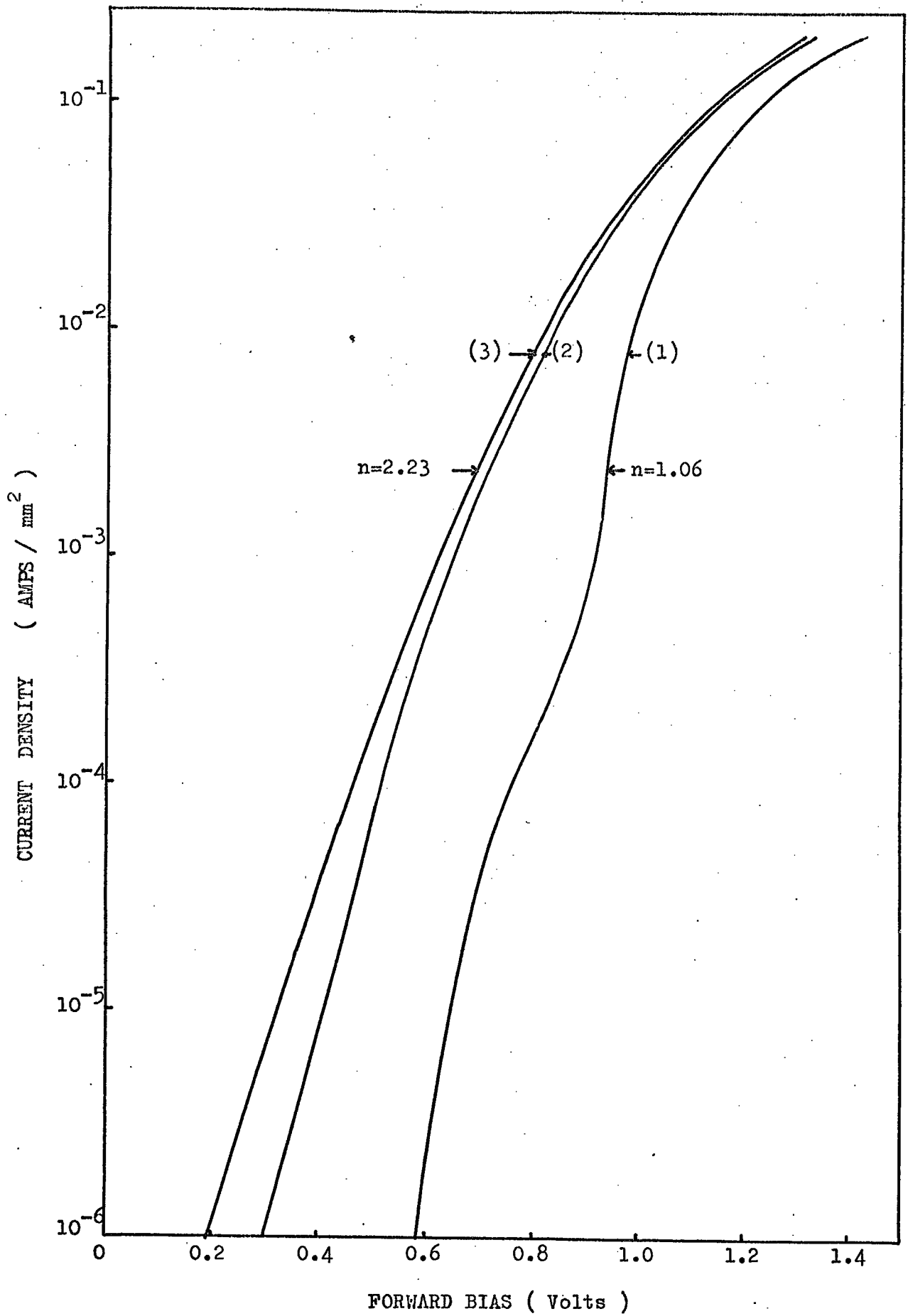


FIG.5.13 Ageing on forward current-voltage characteristics for Au-ZnSe: Mn,Cl,Zn diode (no 246A) prepared on cleaved surface.

From the saturation current of about 3×10^{-16} amp/cm² the diffusion potential was calculated to be $V_{BO} = 1.28$ eV. When a reverse bias of $V_R = 16$ V was applied for a few hours, no immediate change in the forward current-voltage was apparent except for an increase in the leakage current at applied voltages below 0.8 V. However, after the diode had been operated in reverse bias at a d.c. current density of $I_R = 1.5$ A/cm² continuously for 350 hours, the forward current density at voltages below 0.8 V had increased by almost two orders of magnitude (see Fig.5.13). The n-value of the diode increased to 1.9 and the saturation current to a value of about 10^{-7} amp/cm², corresponding to a barrier height of around 0.8 eV. Further continuous operation up to a total of 1000 hrs. at a constant current of $I_R = 1.5$ A/cm² increased the forward current density at lower voltages slightly, but the variation was still basically exponential. After 1000 hours, the forward characteristics gave an 'n' value of 2.23 which the saturation current had increased further to 10^{-6} amp/cm², for which the calculated barrier height was about 0.7 eV.

(b) Ageing and reverse bias characteristics

The reverse bias current-voltage characteristics, measured just after fabrication, varied exponentially over four decades of current (see curve (1), Fig.5.14). At voltages higher than 16 V an avalanche effect was observed. Continuous operation of the diode at a constant reverse current of 1.5 A/cm² for 350 hours changed the reverse current-voltage characteristics slightly, see curve 2 Fig.5.14. This change leads to an increase in a reverse current density at voltages below 14 V but the voltage required to obtain a current density of 2 amp/cm² was increased slightly from 16 to 16.5 volts. After 1000 hours operation at constant current, the reverse characteristics, curve (c) Fig. 5.14, had shifted slightly to higher voltages with respect to curve (b). The avalanche effect which set in at a current density of about 1 amp/cm²

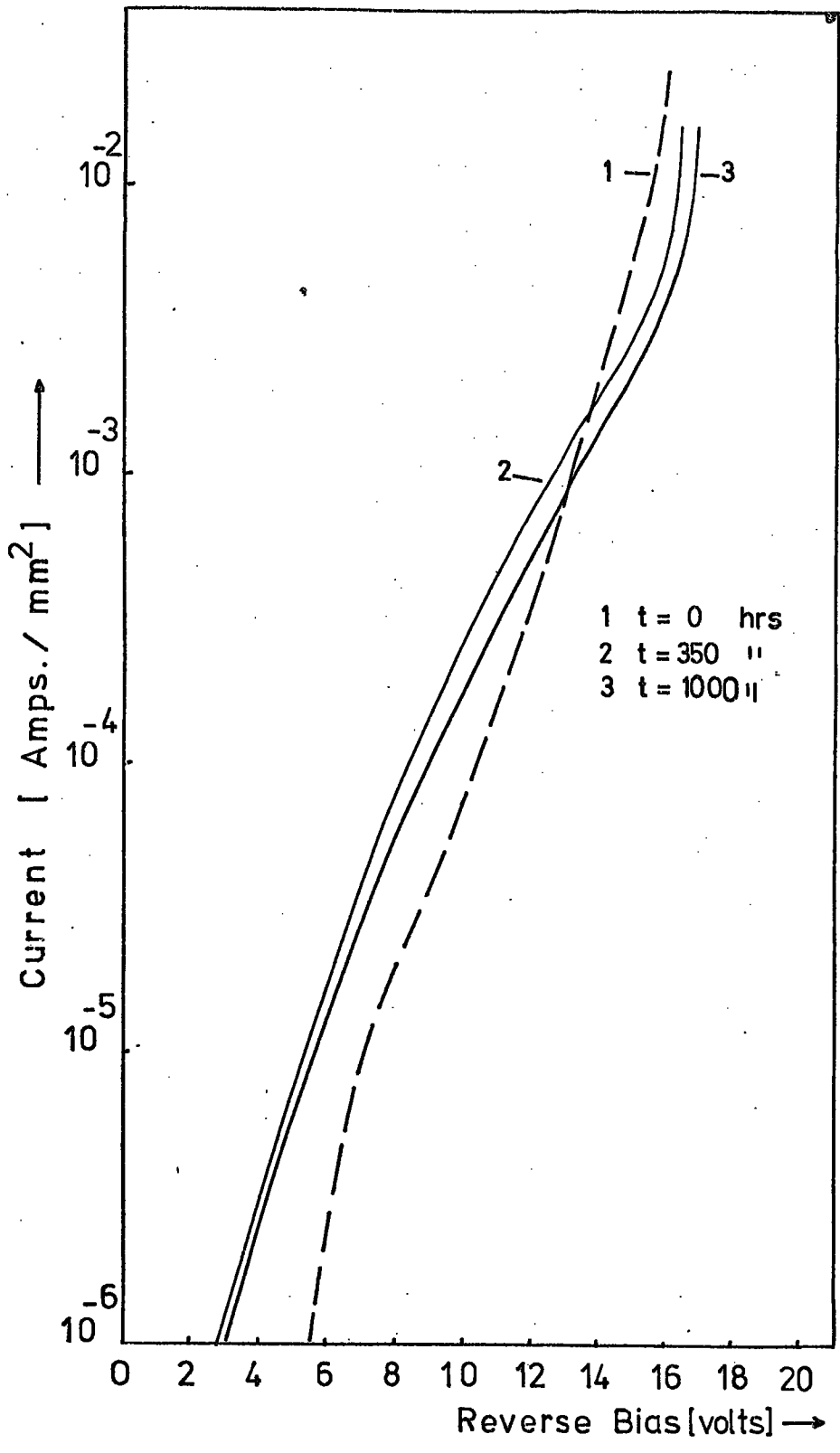


FIG.5.14. Ageing effects on Reverse Current—Voltage Characteristics for Au-ZnSe:Mn Diode prepared on cleaved sample.

became more pronounced after 350 and 1000 hours of continuous operation. In this period the operating voltage rose to 16.8 V.

(c) Ageing and C-V characteristics

The C-V characteristics were also examined at intervals during the continuous operation. The initial C^{-2} -V plot was linear, giving an uncompensated donor concentration of $2.3 \times 10^{17} \text{ cm}^{-3}$, and an intercept voltage V_i of 1.39 eV. (see curve 1 Fig.5.15). Initially the diode was operated in the reverse direction with voltages up to $V_R = 16.4 \text{ V}$ while the current-voltage characteristic was measured. Even this procedure was found to change the C^{-2} -V plot (see curve 2, Fig. 5.15). The shape of curve (2) suggests that the donor concentration N_d had decreased to a value of $1.97 \times 10^{17} \text{ cm}^{-3}$. The intercept voltage was $V_i = 1.37 \text{ eV}$. After this C-V measurements were made at intervals during the continuous operation at a constant current of 1.5 amps/cm^2 . The C^{-2} -V plots remained linear up to 1000 hrs of constant operation. However, the slopes of the plots increased during this time. Apparent donor concentrations calculated from these slopes are tabulated in Table 5.3, together with the values of the voltage intercept V_i . The donor concentration was found to drop to $1.64 \times 10^{17} \text{ cm}^{-3}$ at the end of 1000 hour period of constant operation. However, the intercept value V_i remained almost constant at about 1.40 eV during this time. The thickness of the insulating layer was calculated to be around 28 \AA when the device was produced, and evidently increased to 40 \AA after 1000 hours operation.

5.9.2 Long Term Ageing of Au-ZnSe Diodes Prepared on Chemically Cleaned Surfaces

The gold layer which had been deposited on a cleaved $\{1,1,0\}$ surface was removed and the surface was mechanically polished and

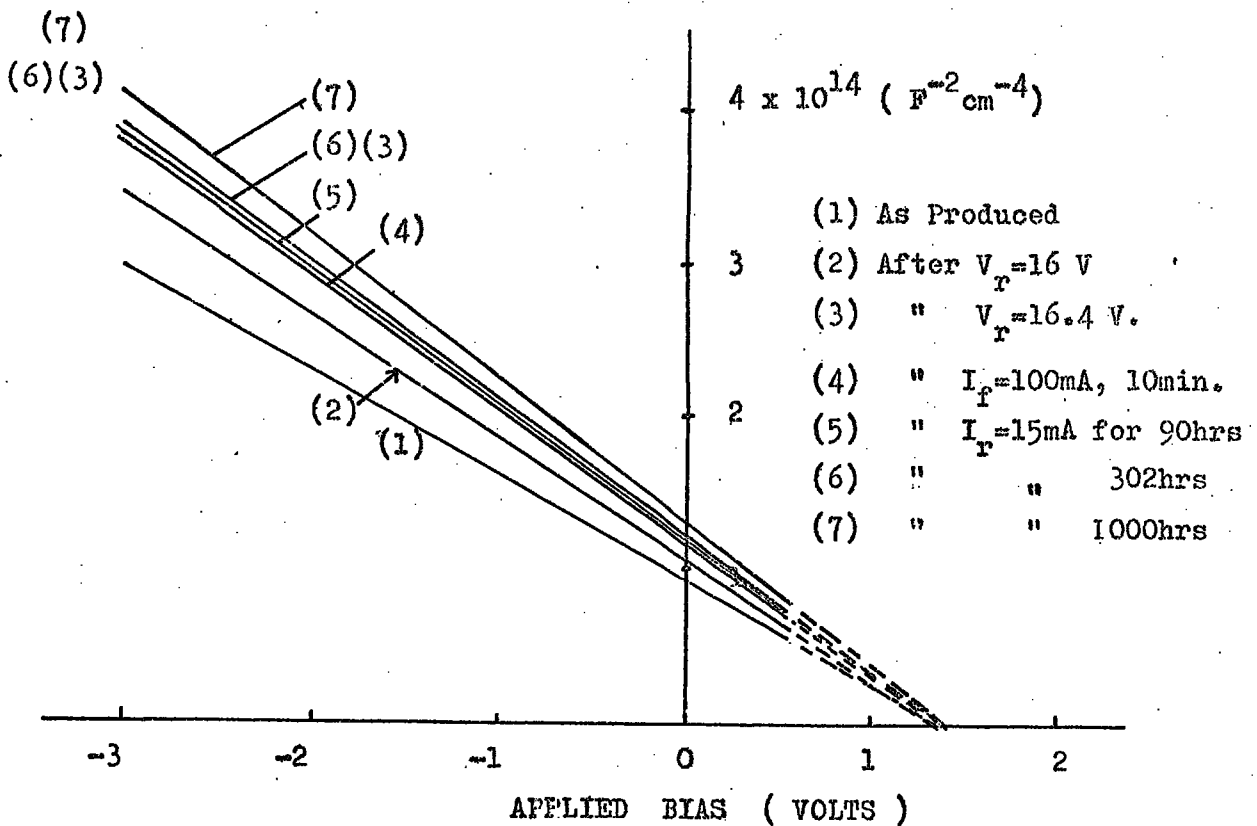


FIG.5.15 Aging effects on $C^{-2} - V$ plots for Au-ZnSe:MnClZn diode prepared on cleaved surface.

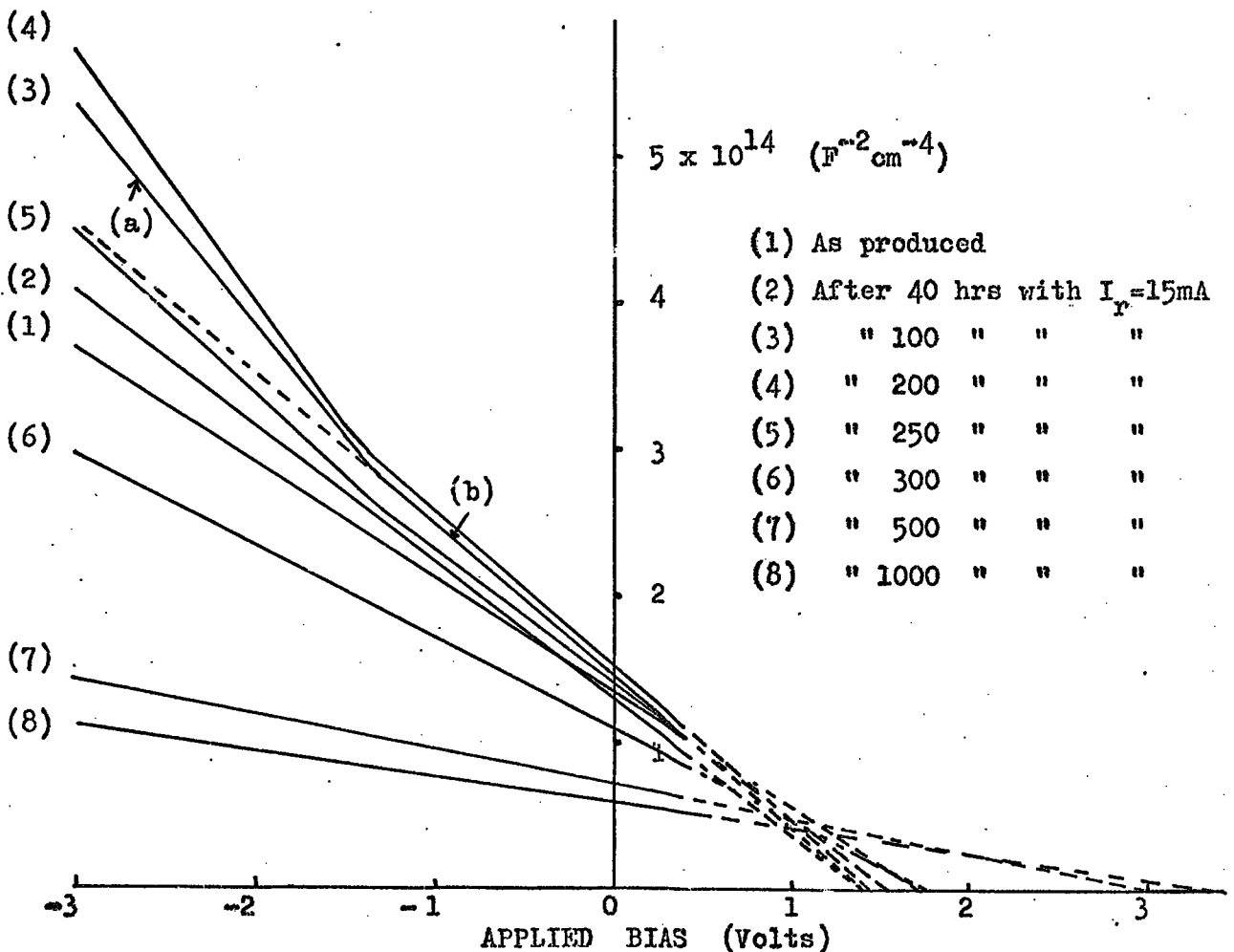


FIG.5.16 Aging effects on $C^{-2} - V$ plots for Au-ZnSe:Mn,Cl,Zn diode prepared on chemically cleaned surface.

chemically etched as described in Chapter 4, then the gold was deposited. Photoresponse measurements on this freshly produced diode (see Fig.5.3) revealed a barrier height of 1.62 eV.

(a) Ageing and forward I-V characteristics

Again the forward current-voltage characteristic was measured just after production' (see curve (a), Fig.5.17). The current was found to vary exponentially with voltage over nearly three orders of magnitude of current. This diode had an n value of 1.21 and a saturation current of 3×10^{-11} amp/cm². The diffusion potential was 1.0 eV. This diode was also subjected to continuous operation in the reverse direction with a current density of 1.5 amp/cm². After 200 hours, the current voltage characteristic in the forward direction was found to have shifted to lower voltages, i.e. the current density at applied voltages lower than 0.8 V had increased by almost two orders of magnitude. See curve (b), Fig.5.17. The n-value and the saturation current were found to increase steadily as the constant current operation proceeded, see Fig.5.17. After 1000 hours of operation in reverse bias, the forward characteristics gave an n-value of 1.58 and saturation current of 2×10^{-6} amp/cm. The diffusion potential corresponding to this value of saturation current was 0.71 eV.

(b) Effect of ageing on reverse I-V characteristics

The reverse bias current-voltage characteristic measured on a freshly produced diode is illustrated in curve (i), Fig.5.18. The current varied exponentially over nearly four orders of magnitude of current. No saturation was observed. The avalanche effect was less pronounced in comparison with that in cleaved diodes (see curve (a), Fig.5.12). The diode was then subjected to constant current operation in reverse direction at 1.5 amp/cm². The voltage required to maintain this constant current increased steadily with time, from 14.5 to 21.5 V

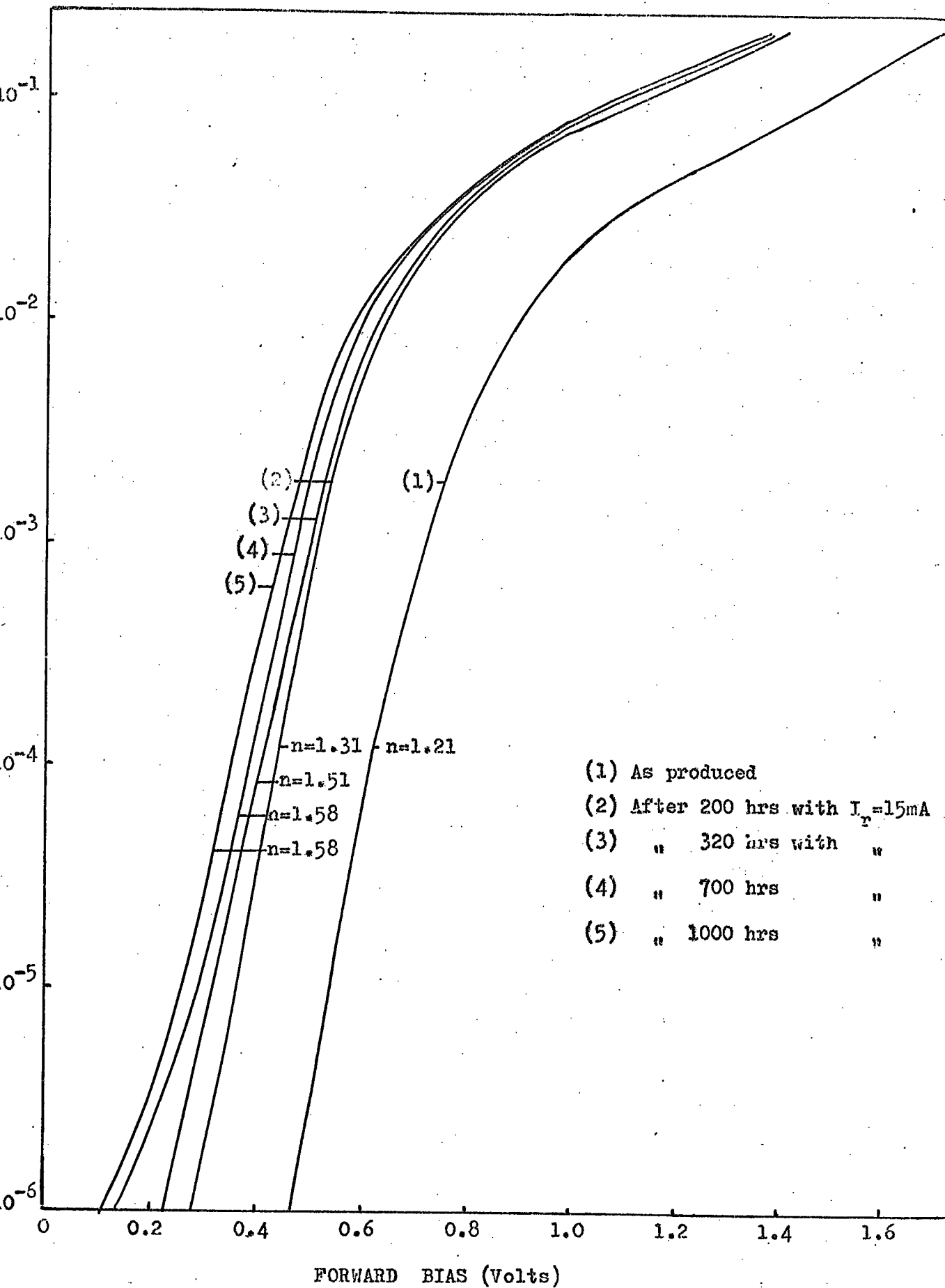


FIG.5.17 Ageing on forward current voltage characteristics for Au-ZnSe:Mn,Cl,Zn diode prepared on chemically cleaned surface.

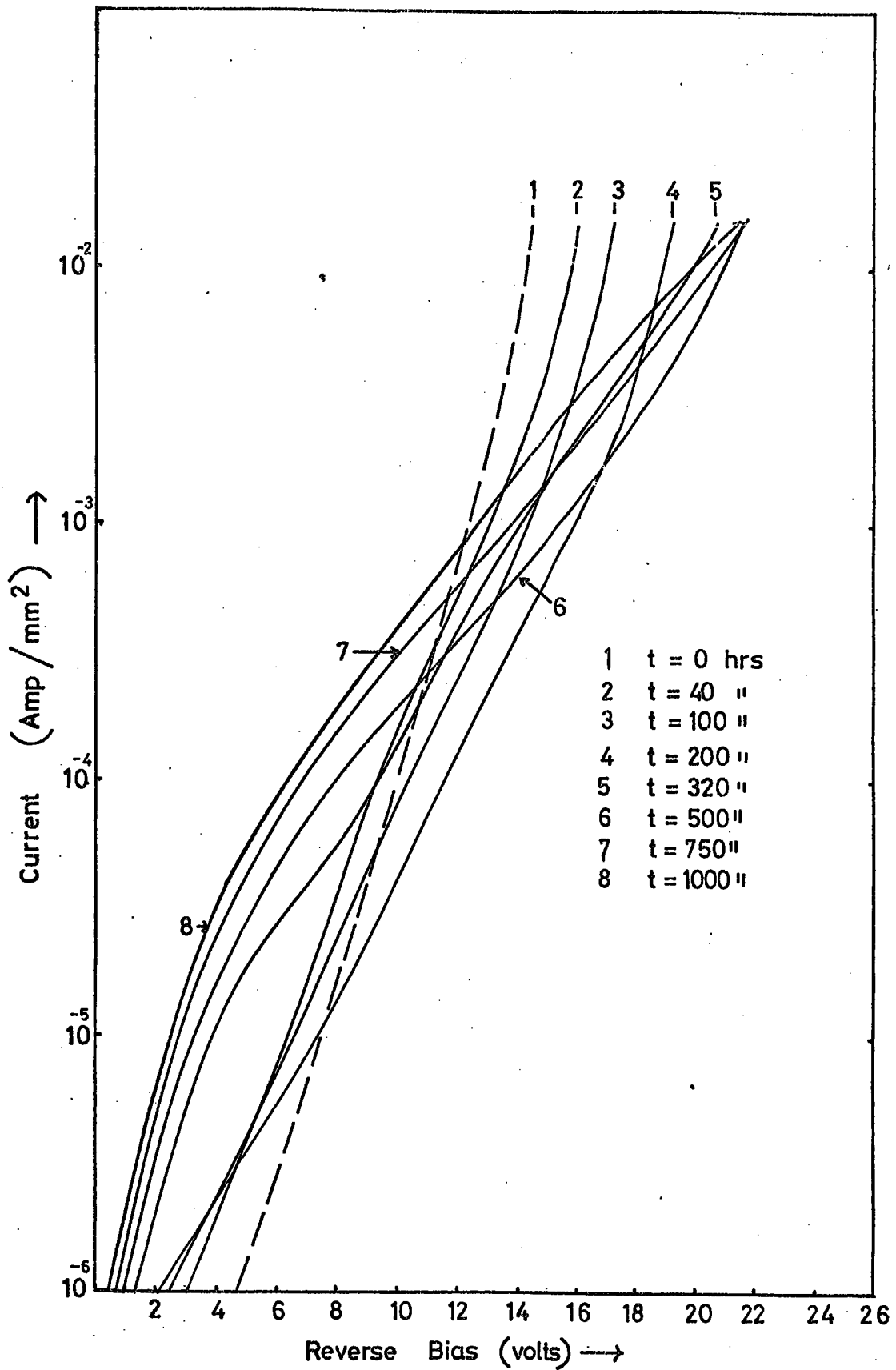


FIG.5.18. Ageing effects on Reverse Current - Voltage Characteristics for Au-ZnSe:Mn diode prepared on chemically cleaned sample.

in 500 hours. Thereafter it appeared to saturate at 21.6 V for the next 1000 hours. However, the shape of the I-V characteristics changed considerably. The diode current was observed to decrease with applied voltages above 10 V, for the first 200 hours, see Fig.5.18 but the leakage current at biases below 10 volts was found to increase steadily with time. After 200 hours the leakage currents at low voltages became more dominant and the diode current at fixed bias increased steadily with time (see curves 5,6,7,8, Fig.5.18). The small avalanching effects at high currents seemed to disappear after about 200 hours operation.

(c) Effect of ageing on C-V characteristics

The C-V characteristics were also examined during this ageing procedure. The C^{-2} -V plots were found to be linear when the device was first produced (see Fig.5.16) with an initial donor concentration of $N_d = 1.93 \times 10^{17} \text{ cm}^{-3}$ and voltage intercept of 1.7 eV.

During constant current operation, the C-V characteristics were measured from time to time. After 40 hours of such operation, the C^{-2} -V plot was still linear, see line 2, Fig.5.16, but its slope had increased slightly giving a value of $N_d = 1.66 \times 10^{17} \text{ cm}^{-3}$. The voltage intercept was now 1.4 eV, which was almost the same value as that obtained for a cleaved surface (1.39 eV). After 100 hours, the C^2 -V plots were found to consist of two linear sections shown as (a) and (b) in curve (3), Fig.5.16. The donor concentration calculated from the slope of section (a) of curve 3 was $9.9 \times 10^{16} \text{ cm}^{-3}$, whereas that calculated from section (b) was $1.56 \times 10^{17} \text{ cm}^{-3}$. The extrapolated intercepts of these two sections were 0.5 and 1.42 eV respectively. However, it was soon realised that if the diode were biased so as to pass a large forward current of 20 amp/cm^2 for 10 minutes, then the C^{-2} -V plot became linear with a slope similar to that of section (b) over the whole voltage range of Fig.5.16 Further operation in reverse bias reduced the slope of the C^{-2} -V

	N_d ($\times 10^{17} \text{ cm}^{-3}$)	E_F (meV)	V_i (eV) (C-V)	d (calculated) \AA	C_o (pF/mm ²)
as produced	2.29	5.1	1.39	28.6	
after $V_r = 16.4\text{V}$	1.97	5.5	1.37	26.2	
at $t = 0$	1.86	5.6	1.42	42.3	903
after 17 hrs.	1.80	5.7	1.40	37.8	900
after 90 hrs.	1.78	5.75	1.40	37.5	905
after 302 hrs.	1.74	5.81	1.40	38.2	897
after 560 hrs.	1.65	5.95	1.40	39.7	880
after 680 hrs.	1.64	5.96	1.40	39.8	878
after 1000 hrs.	1.64	5.96	1.40	39.8	878

Table 5.3: Some parameters obtained from the ageing of cleaved diode (from Figure 5.15)

	N_d ($\times 10^{17} \text{ cm}^{-3}$)	E_F (meV)	V_i (eV)	d (calculated)
$t = 0$ hrs.	1.93	5.7	1.7	40
$t = 40$ hrs.	1.66	6.1	1.4	
$t = 100$ hrs.	1.56	6.27	1.42	
$t = 200$ hrs.	1.5	6.37	1.39	
$t = 250$ hrs.	1.7	6.04	1.54	
$t = 300$ hrs.	2.76	5.1	1.76	
$t = 500$ hrs.	6.6	2.5	3	48
$t = 1000$ hrs.	7.6	2.0	3.4	166

Table 5.4: Some parameters obtained from the ageing of diode prepared on chemically cleaned surface (see Figure 5.16)

curves (increasing N_d) and the voltage intercept gradually increased up to 3.5 V at the end of 1000 hours operation. The appropriate values of V_i and N_d are tabulated in Table 5.4.

Photoresponse measurements were only made initially when the device was freshly produced revealing a photothreshold of 1.62 eV. According to the $C^{-2} - V$ plots the value of V_i which was initially 1.7 eV decreased at first to 1.39 and then increased again to 3.4 V. The thickness of the interfacial layer was calculated to be about 40 Å when the device was produced. However, assuming that an unchanged photothreshold would be obtained after 1000 hours, the interfacial layer would then have increased in thickness to 166 Å.

5.9.3 Ageing a Chemically Cleaned Diode with thin slices cleaved from the sides

Finally an attempt was made to investigate the contribution to the ageing effects of the orthogonal faces. The forward-current-voltage characteristics in curves (1) and (2), Fig.5.19 were measured before and after the cleaving. The effects of cleaving off the orthogonal faces on C-V plots are illustrated in Fig.5.21. After a reverse bias had been applied to the diode, the forward current-voltage characteristics showed a progressive shift to smaller voltages, i.e. the leakage currents increased by about two orders of magnitude, and the n-value increased from 1.26 to 3.07 within 174 hours. The observed saturation current of $J_s = 4 \times 10^{-18}$ amp/cm (from curve 2, Fig.5.19) increased to about 7×10^{-5} amp/cm² at the end of a period of 1000 hours of constant current operation.

The effects of ageing on the reverse I-V characteristics of this diode are shown in Fig.5.20. The exponential behaviour of the characteristics was maintained and the I-V curves shifted parallel to themselves

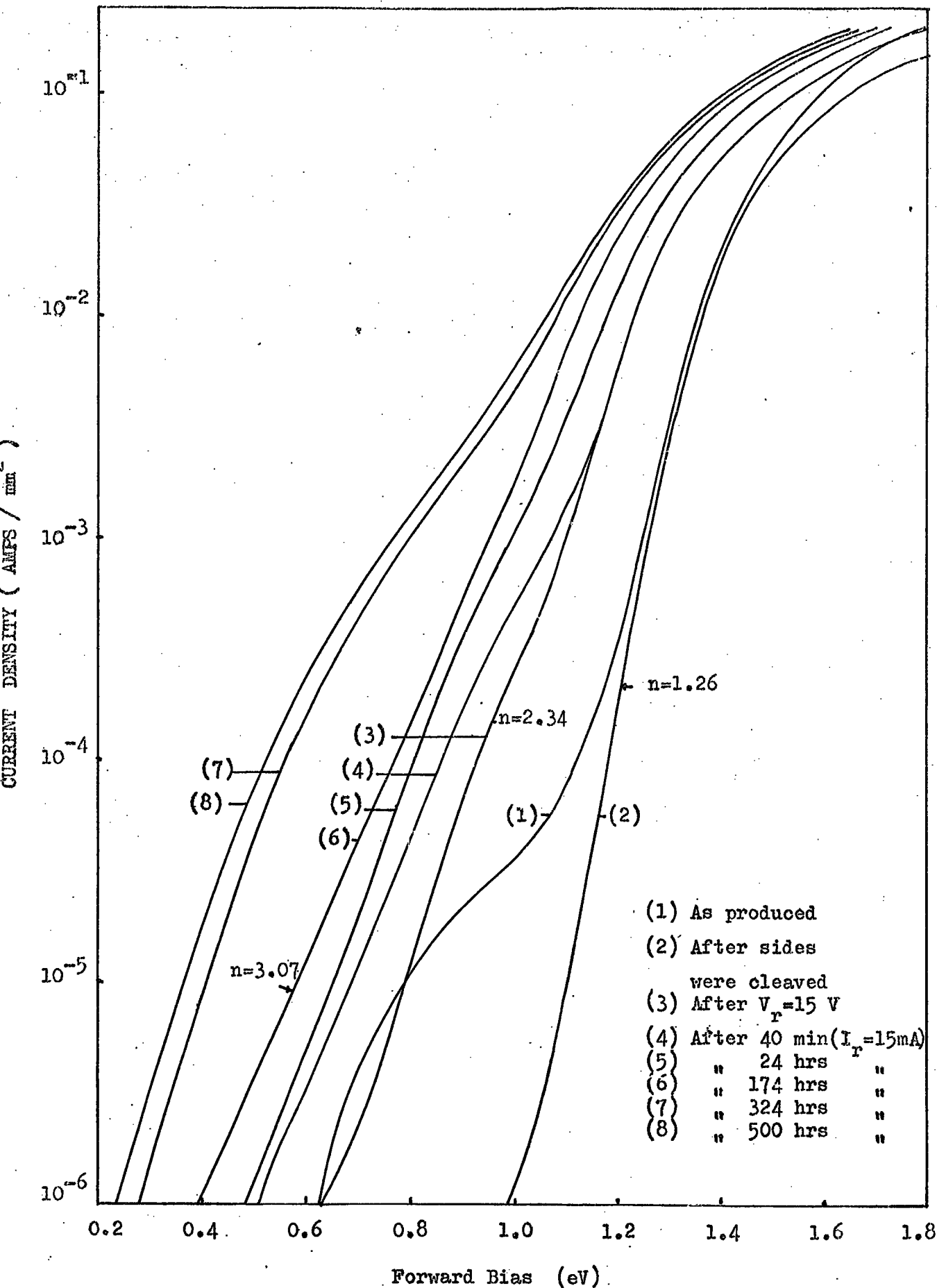


FIG.5.19 Ageing effects on Forward current - voltage characteristics for Au-ZnSe:Mn,Cl,Zn prepared on chemically cleaned surface and thin slices were cleaved from each of the four faces of the diode orthogonal to the contacts

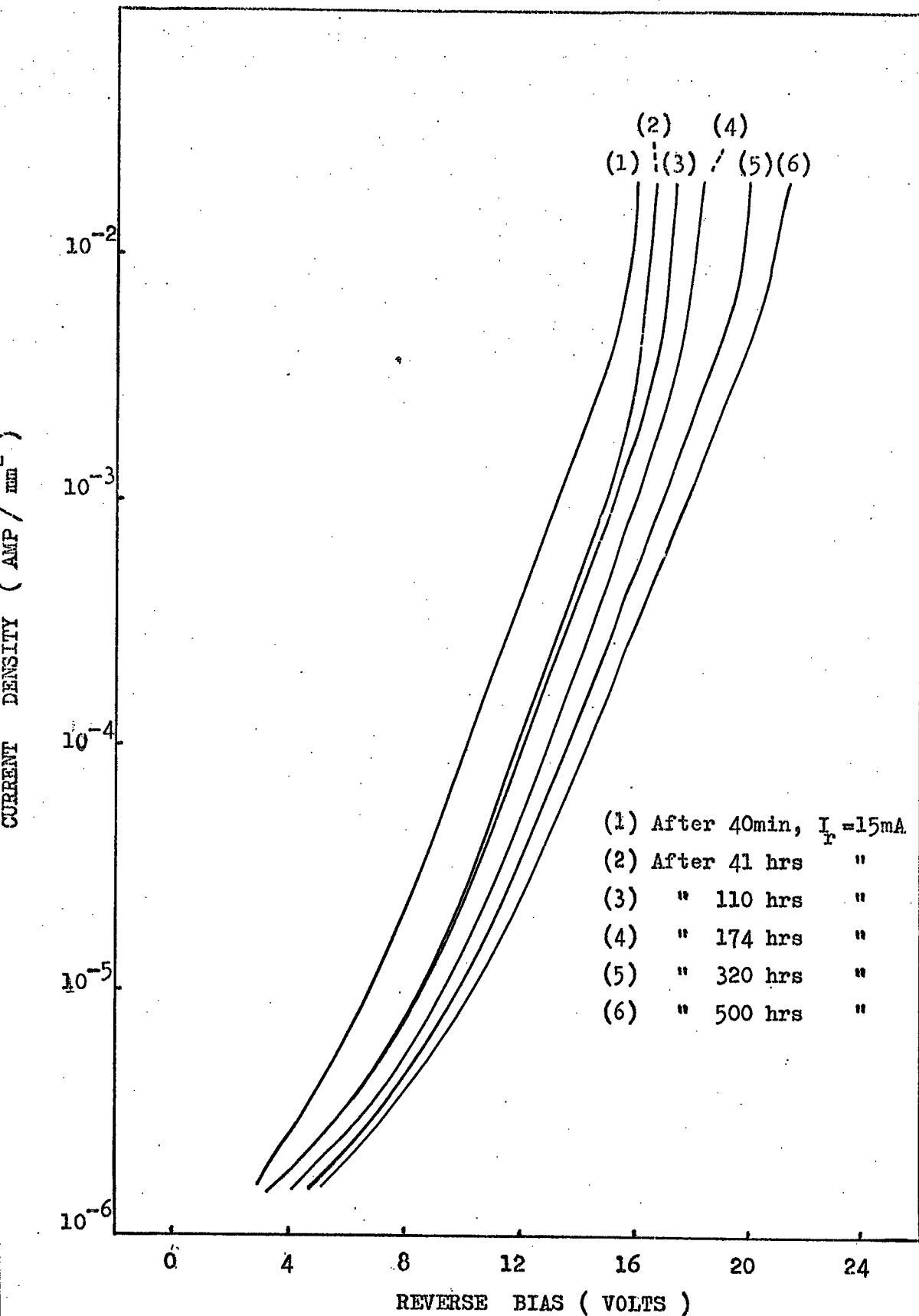


FIG.5.20 Aging effects on reverse voltage-current characteristics for Au-ZnSe:Mn,Cl,Zn diode prepared onchemically cleaned surface and thin slices were cleaved from each of the four faces of the diode orthogonal to the contacts.

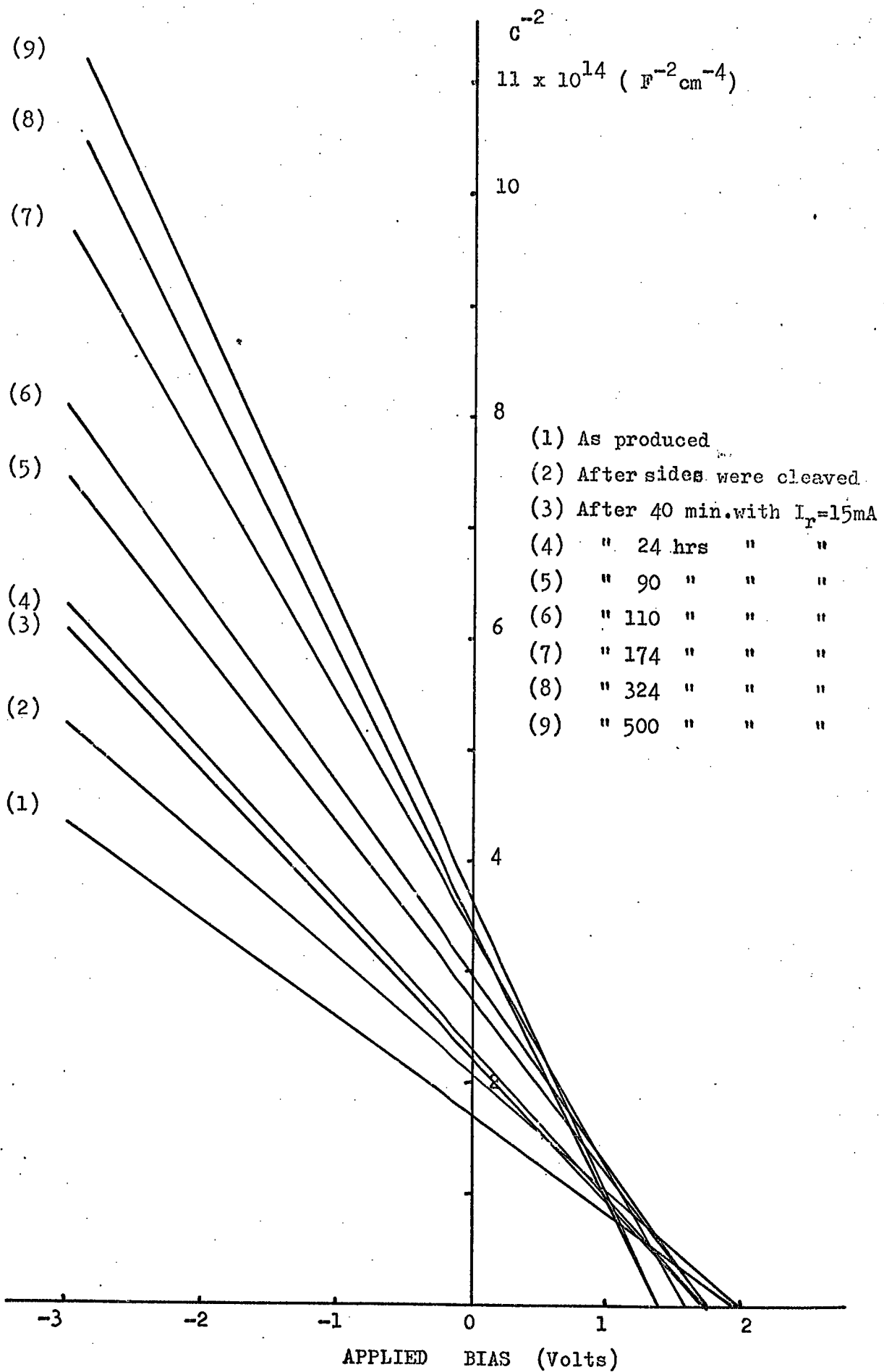


FIG.5.21 Ageing effects on $C^{-2}-V$ plots for Au-ZnSe:MnCl₂Zn diode prepared on chemically cleaned surface and thin slices were cleaved from each of the four surfaces of the diode orthogonal to the contacts.

		$N_c (10^{17} \text{ cm}^{-3})$	$V_i (\text{eV}) (C-V)$
as produced	(1)	1.76	1.99
after sides were cleaved	(2)	1.46	1.98
after 40 mn	(3)	1.22	1.72
after t = 41 hrs.	(4)	1.17	1.78
after t = 90 hrs.	(5)	0.98	1.78
after t = 110 hrs.	(6)	0.89	1.70
after t = 174 hrs.	(7)	0.72	1.60
after t = 300 hrs.	(8)	0.64	1.39
after t = 500 hrs.	(9)	0.55	1.39

Table 5.5: Some of the parameters obtained during ageing from the $C^{-2} - V$ plots shown in Figure 5.21.

towards higher voltages. No cross over of the I-V characteristics was observed in contrast with the behaviour of the chemically cleaned sample shown in Fig.5.18. This suggests that the increasing leakage currents observed in the reverse I-V characteristics in Fig.5.17, are attributable to leakage currents flowing along the side surfaces of the chip.

The C^{-2} -V plots all remained linear, the effect of cleaving the sides is demonstrated by lines 1 to 9 in Fig.5.21. During constant current operation in reverse bias, the slope of the C-V characteristics increased, i.e. the values of N_d decreased slowly from the original value of $1.76 \times 10^{17} \text{ cm}^{-3}$ to $5.5 \times 10^{16} \text{ cm}^{-3}$ after 500 hours ageing. The voltage intercept was also decreased steadily to 1.39 eV in this time. Some of the relevant parameters, i.e. the values of N_d and V_i obtained from the C^{-2} -V plots (Fig.5.21) are given in Table 5.5.

5.10 DISCUSSION

5.10.1 Ohmic Contacts

Alloying indium metal on to ZnSe has proved to form a satisfactory ohmic contact. In this process the chip was heated to 280°C in an argon atmosphere. A significant step towards a better understanding of the indium contact was made by Blount et al (1966). The requirement of relatively high temperatures to form an ohmic contact on ZnSe was also predicted by Bjerkeland and Holweck (1972). Later Kaufman and Dowbar (1974) showed that the formation of ohmic indium contacts on ZnSe was an alloying process, i.e. indium dissolves ZnSe, and the ZnSe then regrows epitaxially, heavily doped with indium. The possibility of the in-diffusion of indium and the creation of compensating Zn vacancies would seem to be negligible at temperatures below

400°C (Swank et al, 1969). Nonetheless, during the preparation of the Schottky barriers on ZnSe, the surface to receive the gold film was repolished and chemically etched or cleaved to remove any high resistivity layer which might have formed on this surface during the indium alloying procedure. Furthermore, the standard etching procedure gave more reproducible results.

5.10.2 Photoresponse Measurements

The photoresponse measurements were made to ascertain both the barrier height of the Au-ZnSe system and the value of the bandgap of ZnSe. The measurements were corrected for the spectral distribution of the source and the dispersion of the monochromator. The threshold of the short-circuit photocurrent at low photon energies was taken as a measure of the barrier height between the gold and ZnSe and this was found to be 1.36 ± 0.01 eV for cleaved and 1.64 ± 0.01 eV for chemically cleaned surfaces at 295 K.

The band gap of ZnSe was found to be 2.64 ± 0.01 eV at 295 K and 2.76 ± 0.01 eV at 85 K, which is essentially in agreement with the values of E_g found from absorption measurements in this laboratory by Gezci (1973). These values would appear to be 0.06 eV smaller than previously published results, i.e. 2.7 eV at 300 K (Aven et al, 1961) and 2.807 eV at 85 K estimated from the value of 2.809 eV at 80 K reported by Hite et al (1967). However, values of 2.69 eV at 295 K and 2.81 eV at 85 K were obtained in the present work from studies of the free exciton emission in forward bias electroluminescence (see Chapter 6). It would appear therefore that measurements of the photocurrent lead to values of the band gap which are some 0.06 eV too small.

Almost all the photoresponse curves, see for example Fig.5.4 and 5.5, contained a minimum at some energy just less than that of the bandgap. It will be demonstrated later (in Chapter 6) that the maximum

of the luminescence excitation spectra of self-activated emission coincides with this minimum in the photoresponse.

It would seem that the position of this minimum was determined by the bulk rather than the surface properties of ZnSe. It is concluded therefore that irradiation of the barrier with photons with this energy would raise electrons to the excited states of the self-activated luminescent centres, and since the life time of these excited states is fairly short (10 μ s), recombination would occur preferentially before any auto-ionisation took place, so that no significant contribution to photocurrent would be observed. However, with manganese doped diodes, the spectral distribution of the photocurrent at 85 K contained a small maximum at 2.45 eV which is attributed to a transition from the 6A_1 ground state of the Mn^{++} ion to the 4T_2 second excited state. The life time of this state is long enough (~ 1 ms) for auto-ionisation to occur, and with it a maximum in the spectral response of the short circuit photocurrent. The spectral response of the photocurrent of this manganese doped diode contained no peak appropriate to the first excited state of Mn^{++} (i.e. 2.31 eV). It follows therefore that electrons raised to the first excited state are not ionised to the conduction band, while electrons in the second excited states are. This implies that the ground state of Mn^{++} lies about 0.3 eV above the valence band. This should be compared with the phot capacitance studies of ZnSe:Mn by Braun et al, 1972. They suggested that the ground state of Mn^{++} in ZnSe may lie 0.6 eV above the valence band.

5.10.3 Capacitance-Conductance-Voltage Measurements

The voltage intercept V_1 in the plot of C^{-2} against V was larger than the photoelectric threshold for all diodes examined. For diodes cleaved in air prior to the formation of the gold contact

$V_i \approx \phi_{Bn}$ (C-V) was 1.39 eV and the difference was slight (ϕ_{Bn} (Ph) = 1.36 eV). However, with the etched diodes values of V_i as high as 3.5 eV were found depending on the surface treatment prior to the gold deposition, (with the standard etching process an average value of 2.0 eV was usually obtained). This has been interpreted as indicating the presence of interfacial layers under the gold, which can become as thick as 250 Å or more, depending on the chemical etching procedure used.

The uncompensated donor concentration N_d was found from the slopes of C^{-2} -V plots, and the values obtained were in good agreement with the donor concentrations obtained from measurements of the Hall coefficient made in this laboratory (Jones 1973). The values of N_d together with those of V_{BO} (obtained from short-circuit photocurrent measurements) were used as the basis from which to calculate most of the other device parameters, i.e. E_f , W , $\Delta\phi_B$, $|C|_{max}$.

The C-V curves were measured as a function of temperature to find the variation N_d with temperature. The decrease in the density of uncompensated donors at 85 K was due to the incomplete ionisation of donors at the lower temperatures, and using this fact the donor levels associated with substitutional Cl, Ga, In and Al were calculated to lie 25, 25.3, 28.9 and 29.5 ± 1 meV below the conduction band. These values are to be compared with the previously published results of 26.9, 27.9, 28.9 and 26.3 ± 0.6 meV for Cl, Ga, In and Al respectively, obtained from a study of bound exciton emission by Merz et al (1972).

Some G-V measurements were made on a few samples to find some of the parameters of the interfacial layer, i.e. D_s and t . The density of surface states was found to be 4×10^{11} and 5×10^{10} states/eV/cm² for chemically cleaned and cleaved surfaces respectively. These results are to be compared with the previously published data on other II-VI compounds, i.e. $D_s = 10^{11}$ states/eV/cm² for CdS obtained from the study

of surface photovoltaic measurements by Williams (1966) and $D_s = 2 - 5 \times 10^{11}$ states/eV/cm² for CdSe observed by Consigny and Madigan (1970).

5.10.4 The Current-Voltage Characteristics

The influence of the interfacial layer was also apparent in the I-V characteristics where it was responsible for leakage currents. With the forward I-V characteristics the leakage currents were found to be less pronounced in cleaved diodes. It has been conclusive demonstrated that the leakage current flows through the orthogonal surfaces, and can be eliminated when thin slices are cleaved from the faces orthogonal to the contacts. In general, therefore, the forward I-V characteristics on chemically cleaned surfaces can be regarded as composed of two currents in parallel, namely (1) the leakage current flowing through the surface and (2) the current flowing through the bulk of ZnSe and over the barrier into metal. The applied bias is shared by the interfacial layer and the depletion layer. At small applied biases the surface path will have a low resistivity in comparison with that of the depletion layer. Then the predominant current will flow through the surface regions limited by the series resistance of the insulating layer. When the voltage is increased however, the barrier height and the depletion width are reduced and the current will be dominated by the current passing over the barrier until it is limited by the series resistance of the bulk of the crystal itself. The exponential variation of the leakage current with voltage, accompanied by the spurious high saturation current, may suggest that the leakage current is also flowing over a potential barrier, which is smaller than that encountered by the electrons flowing through the ZnSe. When thin slices were cleaved from the faces orthogonal to the contacts the current flowing through

the surface was eliminated and the remaining current flowed through the bulk of ZnSe. This was found to vary exponentially with voltage over about 6 decades of current. When the diode was formed on a cleaved surface, the diode quality factor n was found to be close to unity ($n = 1.06$). The barrier height obtained from the saturation current $\phi_{Bn}(J_s) = 1.34$ eV is in good agreement with the value of $\phi_{Bn}(Ph) = 1.36$ eV obtained from the short circuit photocurrent measurements. With diodes formed on chemically cleaned surfaces the n -value was 1.26 or larger and the saturation current was greater ($J_s = 4 \times 10^{-18}$ A/cm²) than that (9×10^{-22} A/cm²) expected from a diode with a barrier height of 1.63 as obtained from short circuit photocurrent measurements. The observed electroluminescence in the forward direction (see next chapter) would support the suggestion that the high currents may be due to hole injection via this insulating layer.

The reverse current also varied exponentially with voltage over about four decades of current. The currents observed at small biases can also be attributed to leakage currents. The magnitude of the maximum electric field increases with the application of reverse bias, and the condition for the thermionic emission theory (equation 2.4.41) to apply was found to be satisfied. However, the measured saturation current was very large, i.e. of the order of 10^{-7} amp/cm², corresponding to a value of V_{BO} of about 0.8 eV, so that some other mechanism must have been operative. Allen et al (1972) have also studied the reverse I-V characteristics in Au-ZnSe diodes. They observed an exponential variation but they reported a saturation current of the order of 0.2 amp/cm² which is much higher than the values of saturation current found in our work. Relying on the fact that the current varied strongly with voltage and weakly with temperature, they concluded that the electrons were injected by tunnelling through the barrier rather than

by thermal activation over it. The magnitude of our observed saturation current, of the order of 10^{-6} - 10^{-7} amp/cm², would suggest that the electrons are injected into the ZnSe both by thermal activation over, and tunnelling through, the barrier.

The presence of a semi-insulating layer would be expected to decrease the effective barrier height with increasing reverse bias, as a result of the increasing voltage dropped across the insulating film. This might also be the reason why no saturation was observed in most diodes. Card and Rhoderick (1971) have shown using the Si-SiO₂ system that because of the reduction in barrier height, the reverse current of a diode with a fairly thick interfacial layer may actually be greater than that of a diode with a thin layer. This behaviour has also been observed here with diodes with thick interfacial layers ($d \approx 300 \text{ \AA}$).

5.10.5 Barrier Height

Barrier heights were determined directly from the photothresholds. The barrier height ϕ_{Bn} (ph) was 1.36 eV for an Au-ZnSe diode prepared on a cleaved {1,1,0} surface of ZnSe. The barrier height from the forward I-V characteristics was found to be about 1.34 eV which is in good agreement. The barrier height, however, was found to be 1.41 eV when measured from C-V plots. The value of 1.36 eV had also been obtained from photoelectric measurements on Au-ZnSe diodes prepared on cleaved surfaces in ultra-high vacuum (see for example Mead, 1966), and is to be contrasted with that of 1.4 eV which was obtained by Swank et al (1969) using I-V and C-V plots for an Au-ZnSe contact formed in an ultra high vacuum.

Mead (1965) measured the barrier heights formed by several metals on ZnSe and found that the barrier height varied with the work function of the metal, the measurements were repeated on ZnSe by

Swank et al (1969) who confirmed Mead's results, i.e. the barrier height is strongly influenced by the work function of the metal. All these results indicate that the density of the interface states in the vicinity of the Fermi level is small. A surface state density of the order of $D_s \approx 10^{11}$ states/eV/cm² as found in the present work is clearly in good agreement with the earlier work.

5.10.6 A Possible Model for the Au-ZnO-ZnSe System

The value of the photothreshold was found to be $\phi_{Bn}(\text{Ph}) = 1.63$ eV for etched diodes with interfacial surface layers which are thought to contain ZnO. Because of the low density of interface states, the barrier height in ZnSe diodes is expected to be strongly dependent on the work function of the material making contact with it. When the observed barrier height of 1.63 for the Au-ZnO-ZnSe system is compared with that of 1.36 eV for the Au-ZnSe system, one may suggest that the Fermi level at the surface of ZnSe in the Au-ZnO-ZnSe system would be located about 0.27 eV below that in the Au-ZnSe system and that there is virtually no direct communication between the Fermi levels of gold and ZnSe when the layer of ZnO is about 200 Å thick.

Although the properties of the interfacial layer of "zinc oxide" would probably not be the same as that of single crystal ZnO, it is necessary to assume that the layer does have these properties in order to make any progress. Swank (1967) investigated the surface properties of many II-VI compounds, including ZnO. Clean surfaces of ZnSe cleaved in ultra-high vacuum were also studied. He found the electron affinities of ZnO and ZnSe to be 4.57 and 4.09 eV respectively. This means that in an ideal ZnO-ZnSe n-n heterojunction, taking the vacuum level to be everywhere parallel to the band edges and continuous, the conduction band of ZnO would lie below that of ZnSe with a discontinuity

of $\Delta E_c \approx 0.48$ eV at their junction. Then, since the band gap of ZnO is 3.25 eV (Swank, 1967), while that of ZnSe is 2.7 eV (Aven et al, 1961), the valence band of ZnO would have to be placed below the valence band of ZnSe with a discontinuity of $\Delta E_v \approx 1.0$ eV. The barrier height of 1.63 eV observed here for our ZnO-ZnSe n-n heterojunction, would require work functions of 4.12 and 5.72 eV for ZnSe and ZnO respectively if one uses the value of 5.6 eV for the work function of gold (Swank, 1967). The potential energy diagram, see Fig.5.22 is suggested as a model for the Au-ZnO-ZnSe system. From this diagram it can be seen that the interfacial layer remains transparent to photoexcited electrons and the photo-threshold gives the height of the conduction band in ZnSe above the Fermi level at the interface. The high values of the voltage intercept V_i of 2.0 eV or greater obtained from C-V measurement, can be explained in terms of the series capacitance of the oxide. The low values of the barrier height obtained from the forward I-V characteristics, typically ϕ_{Bn} (I-V) ≈ 1.46 eV could be attributed to leakage currents and hole injection into ZnSe. The proposed model would lead to an inversion layer in the ZnSe with a plentiful supply of free holes just beneath the oxide layer.

5.10.7 Ageing Effects

All ageing experiments were carried out in a rough vacuum at a pressure of 10^{-3} torr. Long term operation of Au-ZnSe diodes at forward current densities of the order of 1 amp/cm^2 did not affect the electrical properties. However, once a reverse bias was applied the electrical characteristics were changed in an irreversible manner.

Ageing led to an increase in the leakage current and a decrease in the donor content. The decrease in the donor content was seen even after the application of a reverse bias for a short period of time

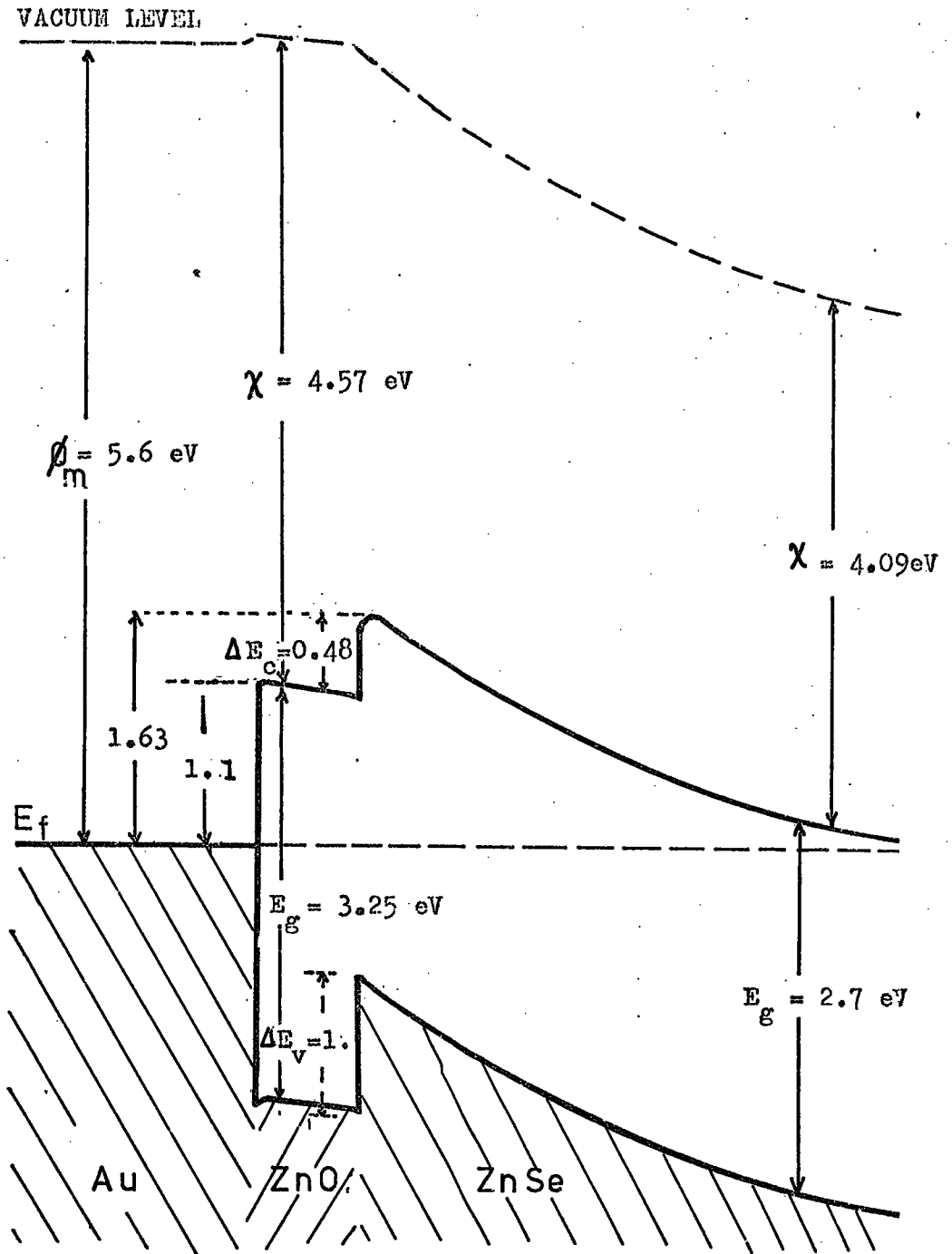


FIG.5.22 Proposed energy band diagram for Au - ZnO - ZnSe system

(5-15 minutes). This aspect of short term ageing was slight in samples containing impurity donors. For example, when a diode containing Cl (diode No.242) was biased at $V_R = 15$ V with $I_R = 2$ amp/cm² for five minutes, the donor content was seen to drop from 1.4×10^{17} to 1.2×10^{17} cm⁻³. However, if the diode contained both foreign acceptors and donors, i.e. Au-ZnSe:Cu,Mn,Cl,Al (diode No.191) the application of a reverse bias of $V_R = 7.5$ V with $I_R = 2$ amp/cm² for a few minutes decreased the donor content from 1.63×10^{17} to 1.05×10^{16} cm⁻³.

In the case of long term ageing (i.e. 1000 hrs), it appeared that any changes in the electrical properties would strongly depend on the type of surface treatment. For example, with a cleaved sample, the donor concentration fell from 3×10^{17} to 1.66×10^{17} cm⁻³ after 1000 hours operation. The voltage intercept ($V_i = 1.40$) on the $C^{-2} - V$ plot did not change. However, the voltage required to maintain a constant reverse current increased slightly from 16.1 to 16.9 V. With an etched diode however the changes in the electrical properties during ageing were much more obvious. The increase in the leakage current was much more pronounced than in the cleaved diode. The intercept in the $C^{-2} - V$ plot usually fell from 2.0 to 1.39 eV after several hundred hours of constant operation. The donor concentration, for example for the diode shown in Fig.5.21, decreased from 1.76×10^{17} to 5.5×10^{16} cm⁻³ after 500 hours of constant operation.

The processes which take place during ageing are by no means understood. The decrease in the donor content is probably due to ionic migration of ionised donors in the high electric field of the depletion layer. The process is more pronounced in etched diodes where the greater barrier heights lead to higher electric fields.

The increases in the forward and reverse leakage currents, which became more apparent during ageing, make it increasingly difficult

to determine device parameters after a few hundred hours of operation. This is aggravated by the fact that the photosensitivity of the diodes decreases as electron-hole recombination through interfacial states becomes more pronounced. Despite these effects, some measurements were possible which would suggest that the interfacial layers of cleaved diodes increased from about 28 to 40 Å in width after 1000 hours of operation.

The interpretation of the measurements made on etched diodes is much more difficult. However, although V_i decreased, the increase in the quality factor n and the increase in the bias (from 15 to 20 V) necessary to maintain constant reverse current suggest that the interfacial layer in etched diodes also increased in width during operation.

CHAPTER 6

ELECTROLUMINESCENCE IN ZnSe DOPED WITH SUBSTITUTIONAL DONORS

6.1 INTRODUCTION

The electroluminescence (EL) of Schottky diodes prepared on nominally pure ZnSe, and on ZnSe containing impurity donors (i.e. In, Al, Ga, Cl and I) is described in this chapter. The electrical properties of these diodes have already been discussed in detail in Chapter 5. Almost all diodes examined emitted EL when biased in the reverse direction. However to obtain detectable EL in forward bias it was necessary to have an interfacial film with thickness of 200 Å or more between the gold and ZnSe. The forward bias electroluminescence (FEL), reverse bias electroluminescence (REL), photoluminescence (PL) and luminescence excitation spectra have all been investigated for the same diode samples. In the diagrams in this chapter illustrating the emission and excitation spectra, the intensities are in arbitrary units. The surface brightnesses in REL and FEL were measured as functions of diode current and voltage, using chips of 0.15 x 0.15 x 0.1 cm³ in dimension. The thermal quenching of the luminescence was also studied in a few diodes operated at constant current.

6.2 EL AND PL OF SCHOTTKY DIODES PREPARED ON NOMINALLY PURE ZnSe

The FEL, PL and REL emission spectra of an undoped sample diode (No.172A) will be described first. Some of the measured parameters of this diode have already been recorded in Table 5.2.

6.2.1 Forward bias EL and PL

(a) Brightness/current-voltage characteristics

Forward B/I-V characteristics are illustrated in Figure 6.1. The current was found to vary exponentially with voltage for current

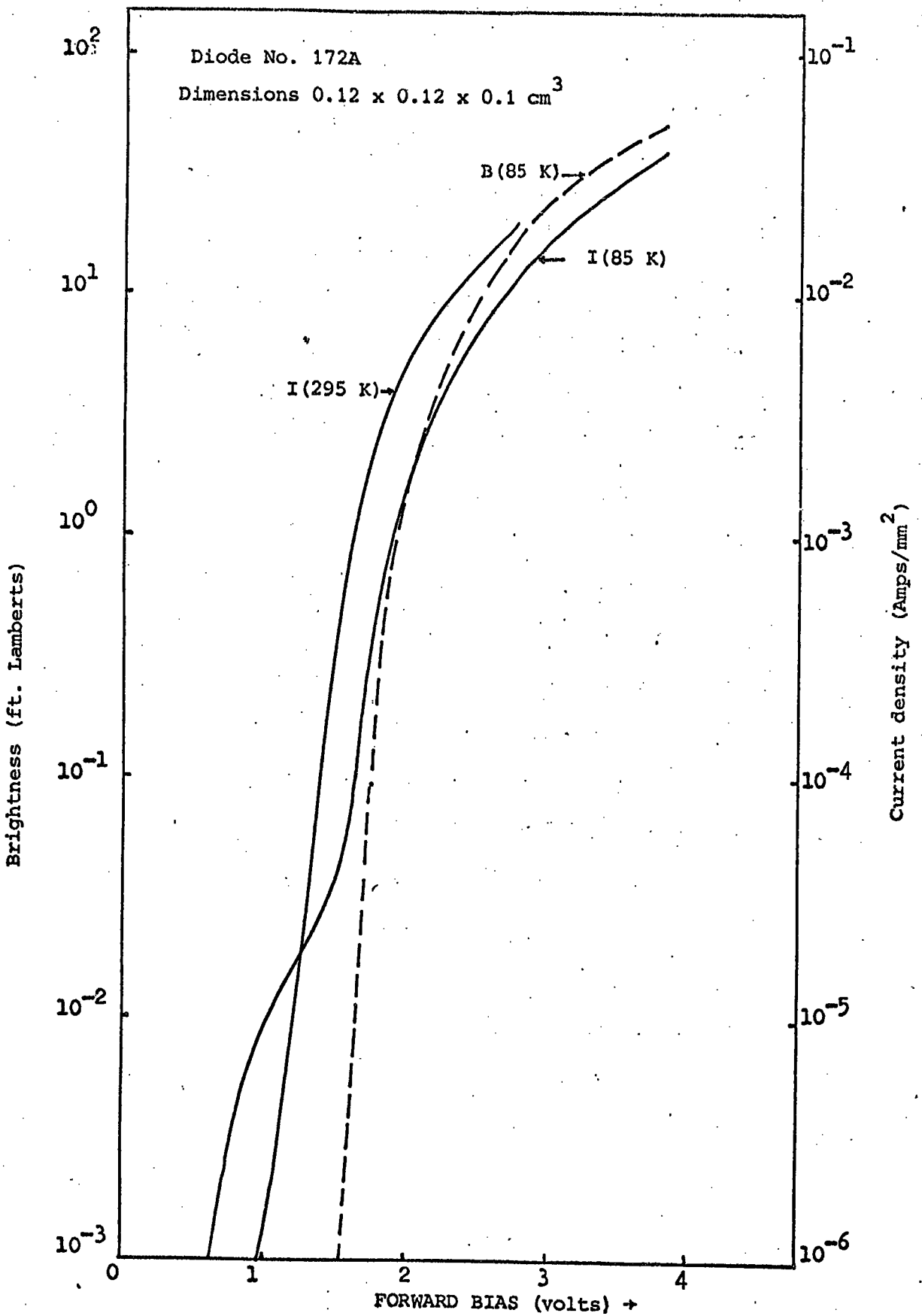


Fig. 6.1: Current/Brightness characteristics as a function of applied bias in Au-ZnSe:Se,Zn, diode No.172A.

densities up to $10^{-3} \text{ A mm}^{-2}$ at 295 and 85 K. The brightness also varied exponentially with applied bias over three orders of magnitude from 10^{-3} to 10^0 ft-L, at 85 K, but increased less rapidly at levels higher than 1 ft-L. The measurements showed that the brightness depended on the current as $B \propto i^n$ at 85 K, for brightnesses up to 10 ft-L, with $n = 1.7$. At higher current densities the value of n decreased. A brightness of 50 ft-L was achieved for the blue emission (see below) with an applied bias of 3 V and a diode current of $4 \times 10^{-2} \text{ A mm}^{-2}$. This corresponds to a power conversion efficiency of $5 \times 10^{-4} \%$.

(b) Spectral distribution

The spectral distributions of the FEL and PL in diode 172A are illustrated in Figure 6.2. The spectra can be divided into three regions associated with (i) Exciton emission, (ii) pair emission, (iii) Deep centre (self-activated) emission.

(i) Exciton emission

A full account of excitonic transitions, near the band gap of ZnSe has been given by Dean and Merz (1969) who studied PL. Exciton emission in forward biased ZnSe diodes has been observed previously by Ryall and Allen (1973).

Halsted and Aven (1965) have shown that in II-VI compounds the ratio of the dissociation energy E_{dis} , with which an exciton is bound to a neutral defect, to the ionization energy E_i of the defect is a constant. The dissociation energy of an exciton is taken to be the energy difference between the zero phonon line of the bound exciton and either the reflectivity or emission peak associated with the ground state of the free exciton from the $\Gamma_8 - \Gamma_6$ energy gap. With acceptor doped II-VI compounds Halsted and Aven's ratio is $E_{dis}/E_a = 0.1$, whereas for

donor doped II-VI compounds this ratio is $E_{\text{dis}}/E_{\text{d}} = 0.2$. E_{a} and E_{d} are the ionization energies of the acceptors and donors respectively. The ground state of the free exciton originating from the $\Gamma_8 - \Gamma_6$ energy gap was recently reported by Hite et al (1967) to occur at 2.799 eV (4430 Å) at 2.1 K. They used reflectivity measurements. Later Dean and Merz (1969) reported the free exciton emission in ZnSe at about 2.80 eV and 4.2 K.

In the present work exciton emission was detected only in FEL and not in PL. The implications of the absence of exciton emission in PL will be discussed later. At 20 K, the FEL emission spectra contained a relatively narrow band peaking at 2.785 eV (4450 Å), see Figure 6.2. This band also exhibited a shoulder at about 2.76 eV (4490 Å). It is suggested that these two bands originate from the decay of excitons bound to neutral, native acceptors. These two peaks would then correspond to the I_1 lines observed in PL emission by Dean and Merz (1967). The dissociation energies of the two bound excitons were calculated to be 12.4 and 35 meV respectively. These dissociation energies would imply that the exciton was bound to native acceptors with ionization energies of $E_{\text{a}} = 124 \pm 4$ and $E_{\text{a}} = 360 \pm 4$ meV.

The probability of the exciton recombination process involving LO-phonons was studied in the PL emission of CdS by Gross et al (1966). They showed that the variation of the half width of the LO-phonon assisted bands was linear with temperature with ΔE approximately equal to 2.9 kT, 1.8 kT and 1.2 kT for the 2, 1 and zero-LO phonon assisted exciton transitions respectively. In the present work the phonon assisted side bands were not observed because of the low emission intensity. As the temperature was raised from 20 to 380 K, the bound excitons dissociated from the acceptors and became free above about 130 K.

172 - ZnSe: Se,Zn.

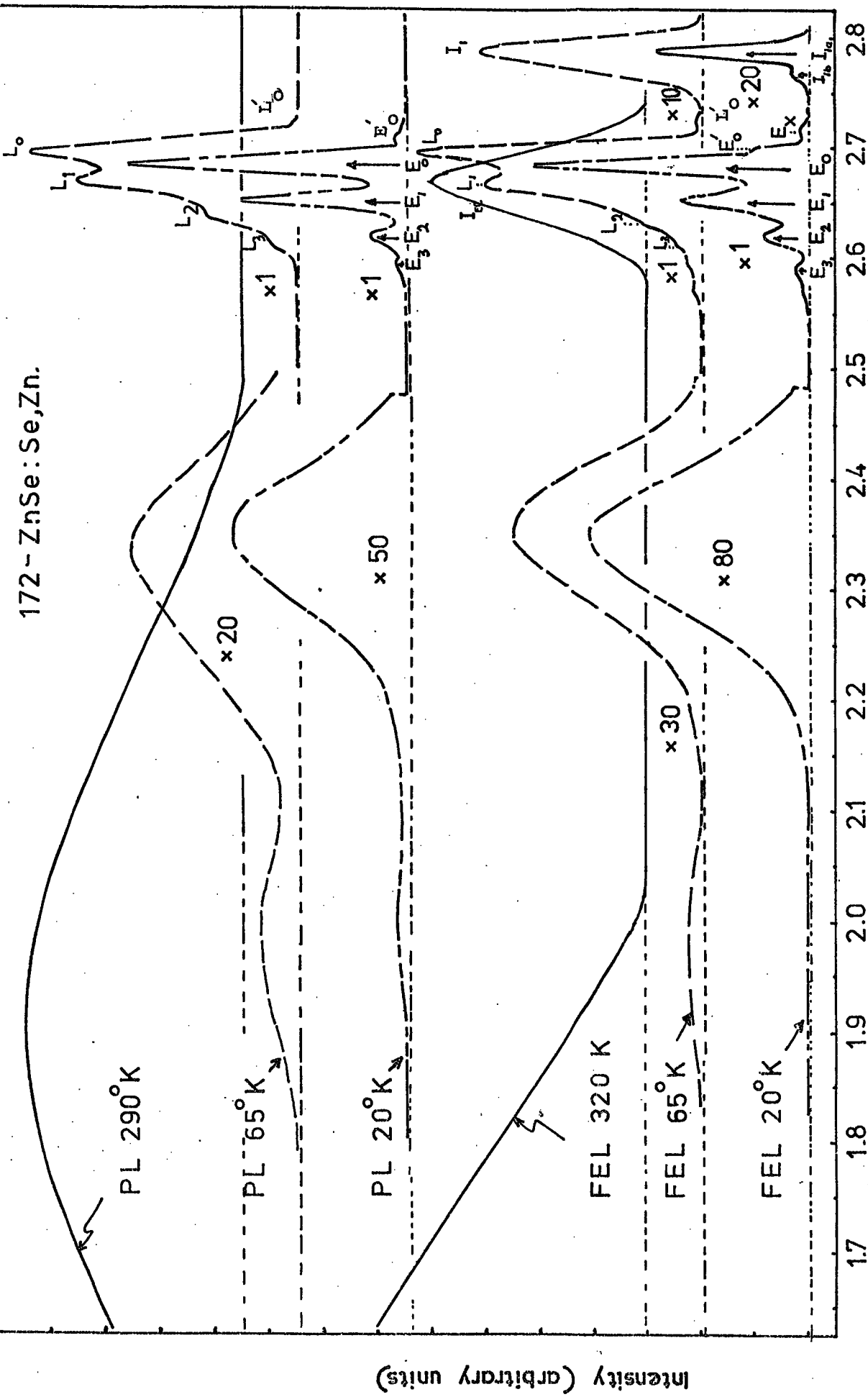


Fig. 6.2:

Forward Bias Electroluminescence and Photoluminescence in Au-ZnSe : Se,Zn

This can be seen from the plots of the measured exciton peak energy versus temperature in curve (a) Figure 6.3. The band gap energy of ZnSe can be obtained by adding the binding energy of the free exciton i.e. about 21 meV (Hite et al 1967) to the ground state energy. The variation of the energy of the ground state of the free exciton was almost linear with temperature from 150-380 K. From the variation the rate of change of the band gap was found to be about 6.6×10^{-4} eV/K. The variation of the width of the exciton band at half height with temperature was also linear (see curve (c) in Figure 6.4). The slope of this line showed that $\Delta E \simeq 1.3$ kT which is close to the theoretical value of $\Delta E \simeq 1.2$ kT predicted for the width of the zero-LO phonon assisted exciton emission line by Gross et al (1966). The variation of the intensity of the exciton emission with temperature is illustrated in curve (a) Figure 6.4. At room temperature the exciton emission was apparent in the form of small, bright blue spots originating around the edge of the gold contact.

(ii) Pair emission

The pair emission, at 85 K, in FEL and PL was found to be uniformly distributed over the whole volume of the chip. At 20 K both FEL and PL emission spectra were found to consist of a series of narrow bands (see Figure 6.2). These bands labelled as E_0 , E_1 , E_2 and E_3 shifted slightly, in FEL, to higher energies by about 1 meV when the diode current was increased from 4×10^{-2} to 1.5×10^{-1} A mm⁻². Such behaviour is typical of donor-acceptor pair emission which has been observed in PL studies by Iida (1968) and recently in this laboratory by Gezci and Woods (1975). The E series is therefore associated with the recombination of distant donor-acceptor pairs with the assistance of LO-phonons. The zero-phonon band (E_0) was found to occur at 2.683 eV (4620 Å). From the equal energy

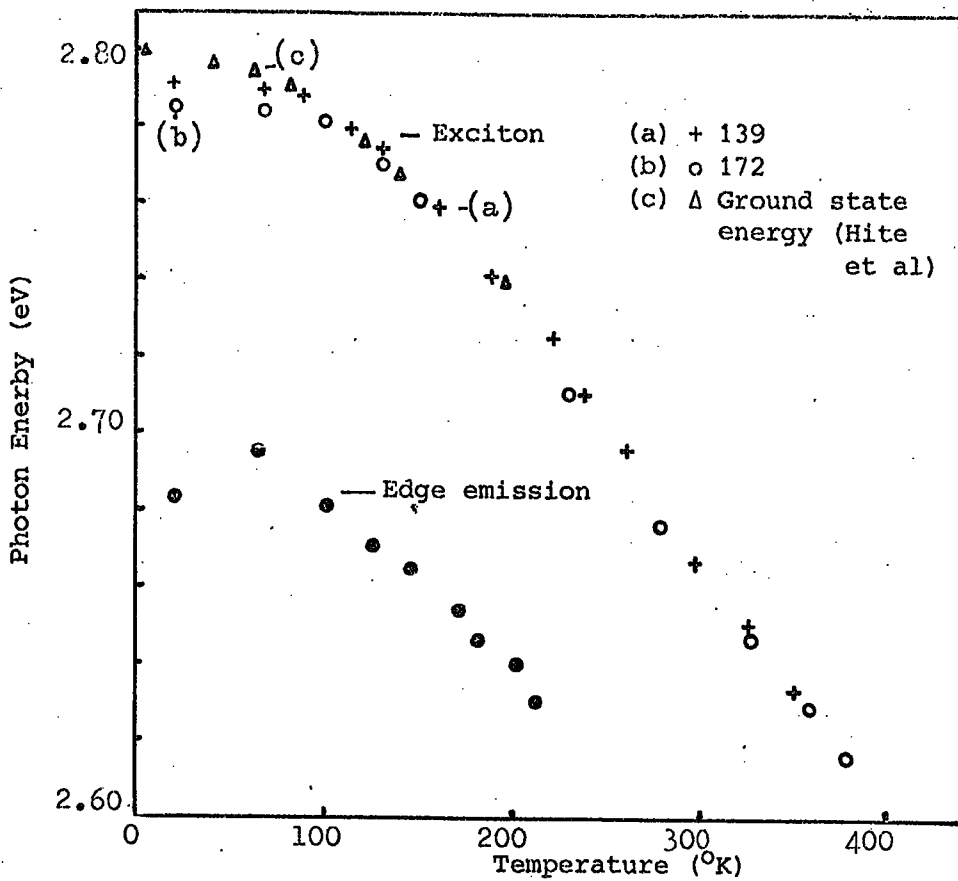


Fig. 6.3: Exciton and edge emission energy variation as a function of temperatures in Au-ZnSe:In,Zn and Au-ZnSe:SeZn

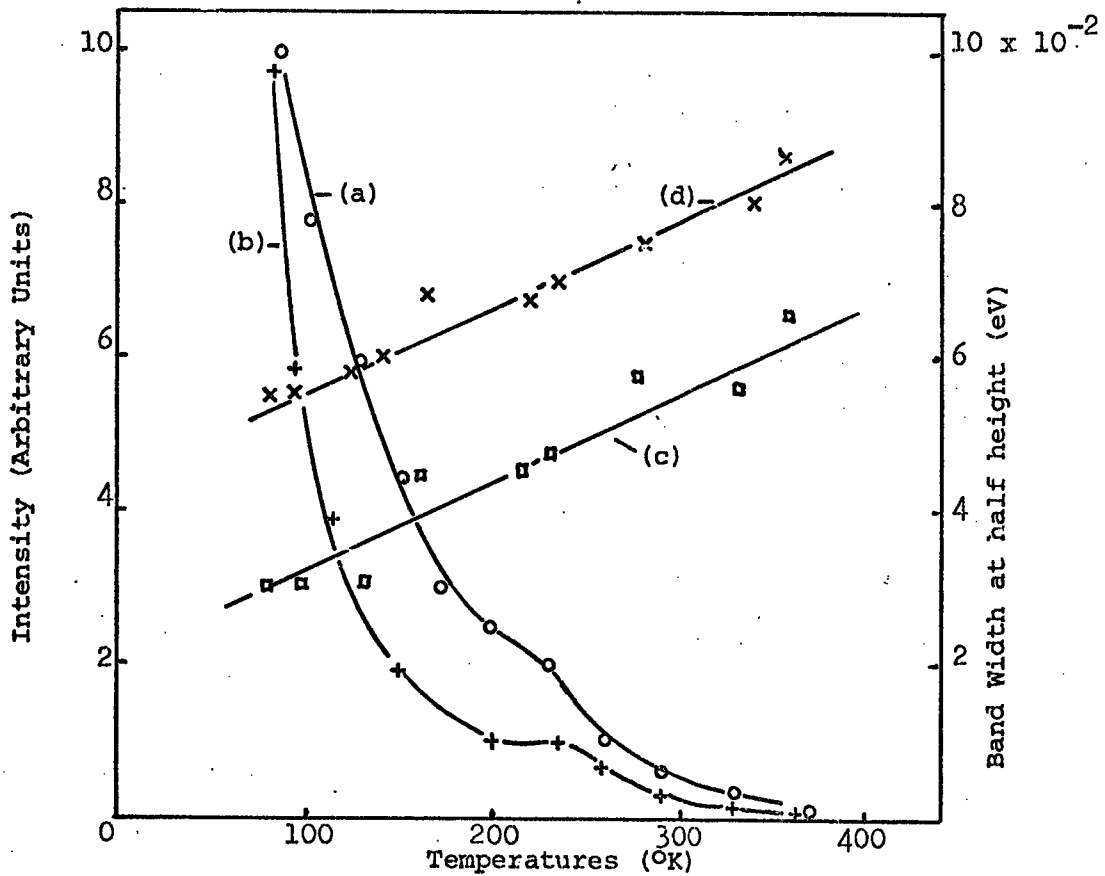


Fig. 6.4: Exciton peak intensity (a) in Au-ZnSe:SeZn, (b) in Au-ZnSe:In,Zn, and width at half height (c) in Au-ZnSe:Se,Zn, (d) in Au-ZnSe:In,Zn variation with temperature.

separations of the phonon assisted bands (see Figure 6.1), the LO-phonon energy was calculated to be 31.7 ± 0.3 meV. This value is in good agreement with the value of 31.9 meV determined by Dean and Merz (1969). A shoulder at E'_0 was also apparent on the high energy side of zero-phonon assisted band at 2.706 eV (4580 Å) in the FEL spectrum and has been attributed to a second donor-acceptor pair emission by Gezci and Woods (1975). The phonon assisted side bands of this second pair emission are probably superimposed on the E series and therefore are not detected. The energy separating the paired donor and acceptor states is given by equation 2.3.2. At 20 K, the band gap of ZnSe is estimated to be 2.818 eV. The energy of the zero-phonon band E_0 is 2.683 eV. Using the value of 14 meV for the coulombic attraction found in this laboratory by Gezci (1973), the sum of the donor and acceptor ionization energies was calculated to be 148 meV. At high temperatures the pair emission both in FEL and PL, shifts slightly to higher phonon energies (see Figure 6.2). For example the FEL emission spectra, at 65 K, exhibited a series of bands labelled as L (see Table 6.1) which were equally spaced in energy with a LO phonon energy of about 31 meV. The shift of the series to higher energies is often attributed to the ionization of the donors so that free electrons recombine with holes at the same acceptor level which is responsible for the lower energy pair emission. The value of the band gap energy of ZnSe at 65 K was estimated to be 2.812 eV, kT is 5.6 meV and the energy of the zero-phonon band (L_0) is 2.695 eV. Substituting these values in equation 2.3.3, the ionization energy of the native acceptor level involved, was calculated to be $E_a \approx 122 \pm 2$ meV which is in good agreement with the value of 124 ± 3 meV predicted from the measurement of the wavelength of the free exciton. Assuming the same acceptor level is responsible for the pair emission spectra

Line	Emitted Photon		Strength	Possible Assignment	Line	Emitted Photon		Strength	Possible Assignment
	Energy (eV)	Wavelength (Å)				Energy (eV)	Wavelength (Å)		
FEL SPECTRA									
20 K					65 K				
I _{1a}	2.785	4550	Strong	Exciton bound to Neutral acceptors	I _{1b}	2.783	4555	Strong	Exciton bound to neutral donors
I _{1b}	2.76	4490	Weak		L ₀	2.725	4550	Weak	Zero - LO phonon (free bound)
E _x	2.725	4550	Weak	?	L ₀	2.695	4600	Strong	Zero - LO phonon
E ₀	2.706	4580	Shoulder	Zero - LO phonon	L ₁	2.665	4652	Medium	1LO phonon
E ₀	2.683	4620	Strong	Zero - LO phonon	L ₂	2.634	4705	Shoulder	2LO phonon
E ₁	2.651	4675	Strong	1LO phonon	L ₃	2.594	4750	Shoulder	3LO phonon
E ₂	2.619	4732	Medium	2LO phonon	300 K				
E ₃	2.588	4790	Weak	3LO phonon	I _{EC}	2.671	4640	Strong	Free exciton
PL SPECTRA									
20 K					65 K				
E ₀	2.71	4.575	Weak	Zero - LO phonon	L ₀	2.725	4555	Weak	Zero LO phonon
E ₀	2.683	4620	Strong	Zero - LO phonon	L ₀	2.695	4600	Strong	Zero - LO phonon
E ₁	2.651	4676	Strong	1LO phonon	L ₁	2.667	4648	Medium	1LO phonon
E ₂	2.619	4732	Medium	2LO phonon	L ₂	2.634	4704	Shoulder	2LO phonon
E ₃	2.588	4790	Weak	3LO phonon	L ₃	2.594	4750	Shoulder	3LO phonon

Table 6.1: The position of the emission maxima of excitons and edge emission in FEL and PL of Au-ZnSe:Se,Zn, diode No.172A.

observed at 20 and 65 K, i.e. $E_a + E_d \simeq 148$ eV $E_a = 122$ meV, the donor ionization energy E_d is calculated to be 26 meV. Another small band (labelled as L'_0) was also observed at 2.715 eV (4550 Å) at 65 K which may have been due to the free to bound transition corresponding to the second possible pair line (E'_0) observed at 20 K. Following similar arguments the ionization energies of the acceptor and donor involved with this transition were found to be 93 ± 2 meV and 30 meV respectively.

The variation of the photon energy of the zero-phonon line with temperature, in FEL, is illustrated in curve (d) in Figure 6.3. At low temperatures the emission was due to donor-acceptor pair recombination. The maximum in this curve which occurs at about 60 - 80 K is associated with the ionization of the donor so that free to bound transitions occur at higher temperatures. At 20 K, the intensity of the pair emission was about 20 times greater than that of the exciton emission. However the pair emission was quenched more rapidly and could not be observed at temperatures above 200 K. The variation of the luminescence intensity of the pair emission in FEL and PL, was plotted in the form of $\log (I(0)/I(T) - 1)$ against $1/T$ (see Figure 6.5). The curve (a) for FEL exhibits two linear parts with slopes which correspond to acceptor ionization energies of $E_{a1} \simeq 120 \pm 2$ meV and $E_{a2} = 180 \pm 2$ meV respectively. However, curve (b) measured in PL contains only one line with an activation energy of ≈ 120 meV for the native acceptor level.

(iii) Deep centre emission

The FEL and PL emission spectra also contained a broad green band peaking at 2.36 eV (5250 Å) with an additional weak band at about 2.07 eV (6150 Å) at 20 K (see Figure 6.2). At 65 K, the two bands had shifted to slightly lower photon energies, i.e. 2.34 eV (5300 Å) and 1.98 eV (6250 Å) (see Table 6.3). As the temperature was raised further

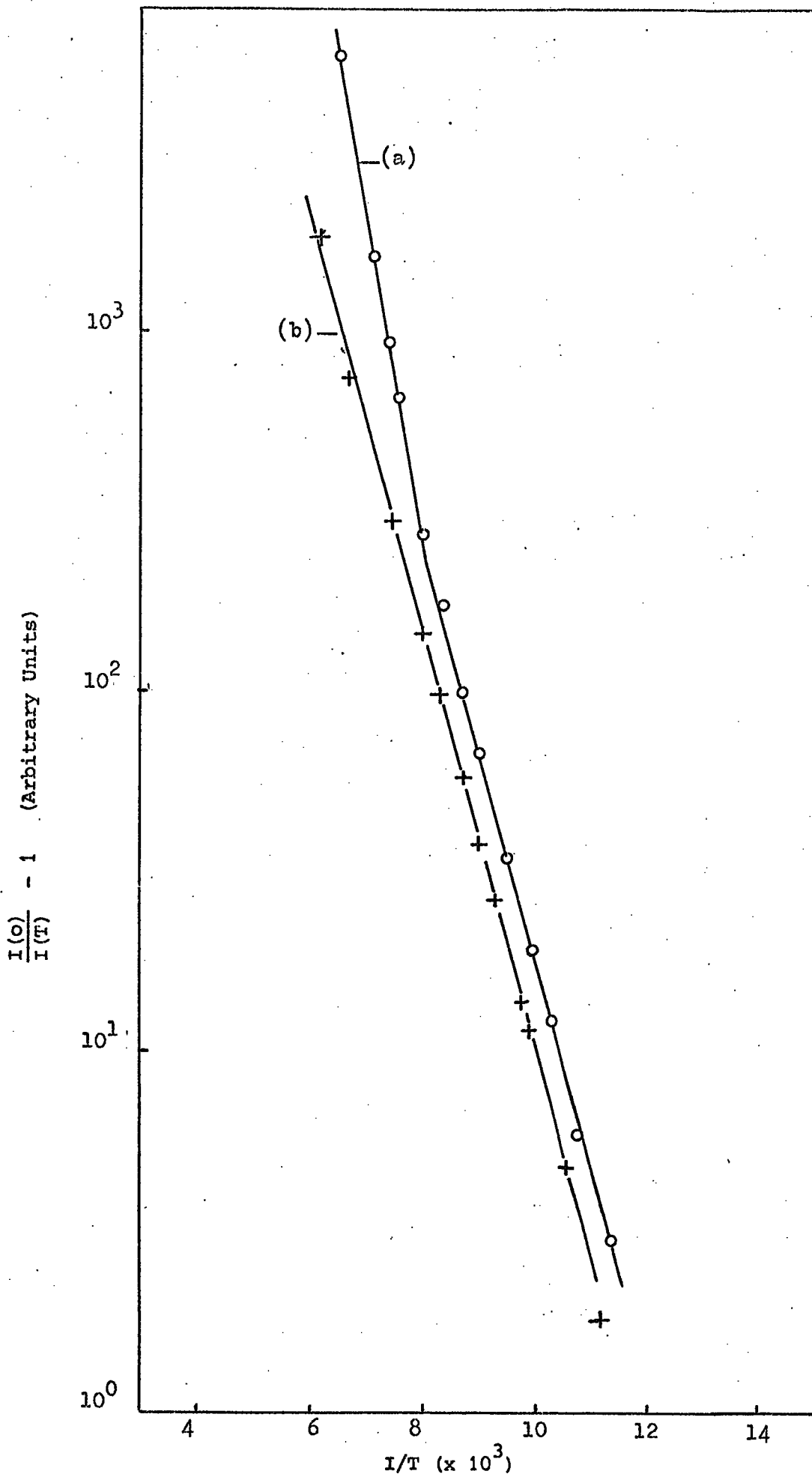


Fig. 6.5: Variation of the intensity of edge emission with temperature in (a) FEL, (b) PL, in Au-ZnSe:Se,Zn diode No.172.

to room temperature the two bands disappeared completely in FEL, leaving behind a broad band in the infrared with a long tail extending into the visible red region of the spectrum. However the PL emission at 295 K consisted of a single broad band at somewhat shorter wavelengths peaking at 1.93 eV (6400 Å). It was impossible to measure the temperature quenching characteristics of the green and orange bands because of their poor emission intensities.

The orange band in PL was observed to be excited at maximum efficiency with photon energies of about 2.78 eV (4460 Å) (see Figure 6.18).

6.2.2 Reverse bias EL

(a) Brightness/current-voltage characteristics

The reverse B/I-V characteristics of diode No.172A were measured at 295 and 85 K (see Figure 6.6): The current and brightness were found to vary exponentially with voltage in the range 20 - 30 V. The brightness-current relationship can best be described by the power law $B \propto i^n$, with $n = 1.07$ at 295 K and $n = 1.2$ at 85 K. Small deviations in the value of n can be attributed to leakage currents at low current levels and increasing joule heating at high current levels. The brightnesses of 20 and 40 ft-L at 295 and 85 K correspond to conversion power efficiencies of 3×10^{-5} and 6×10^{-5} %.

(b) Spectral distribution

The REL emission spectra were recorded at 20, 85 and 295 K (see Figure 6.7). The diode was operated at a current density of 2×10^{-2} A mm⁻². At 20 K, the spectrum contained two bands peaking at about 2.17 eV (5700 Å) and 2.38 eV (5200 Å). The tail to the high energy side of the emission cut off sharply at about 2.71 eV (4575 Å). This would mean that the electrons in the depletion layer are accelerated to energies

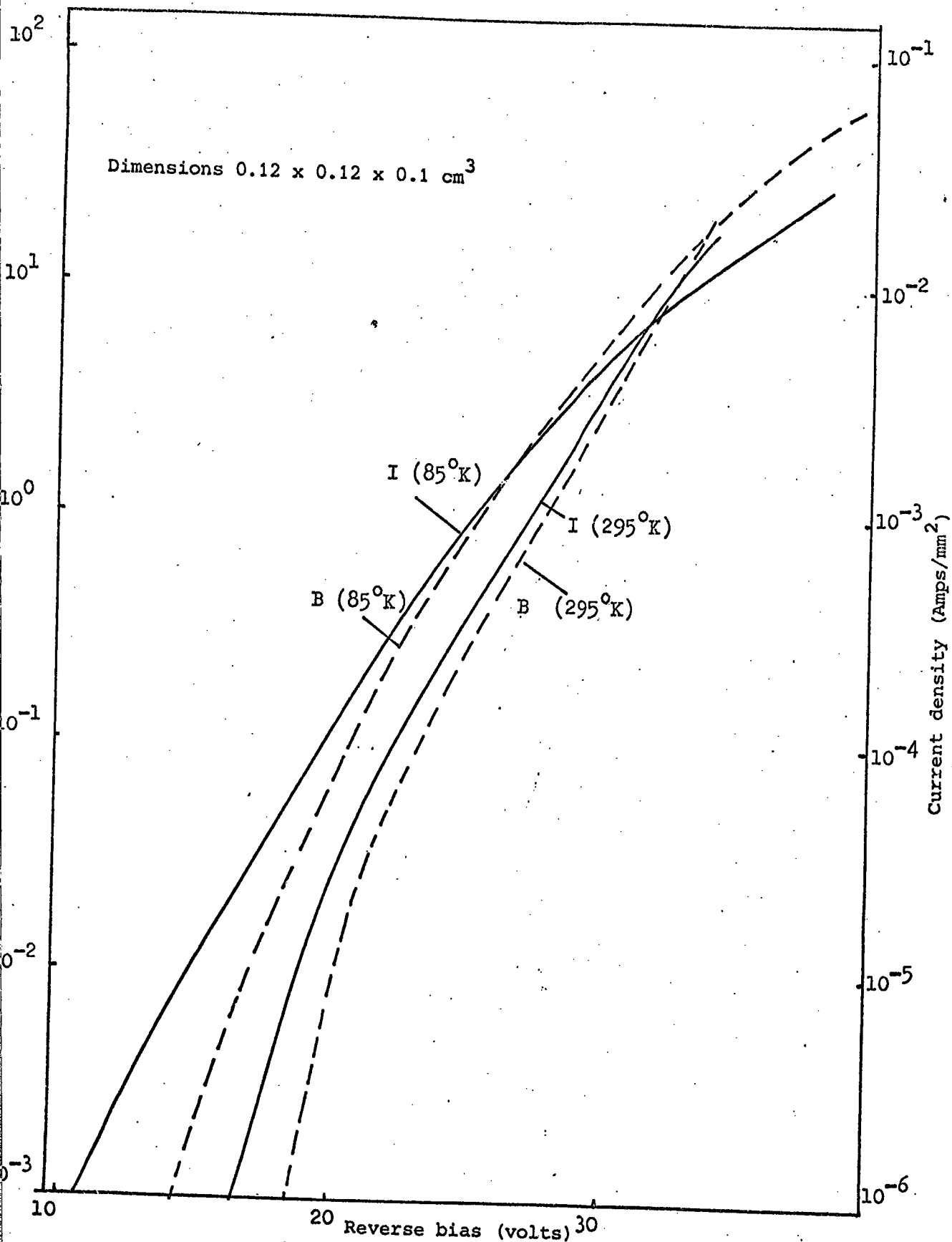


Fig. 6.6: Reverse current/brightness characteristics as a function of applied bias measured on Au-ZnSe:Se,Zn diode No.172A.

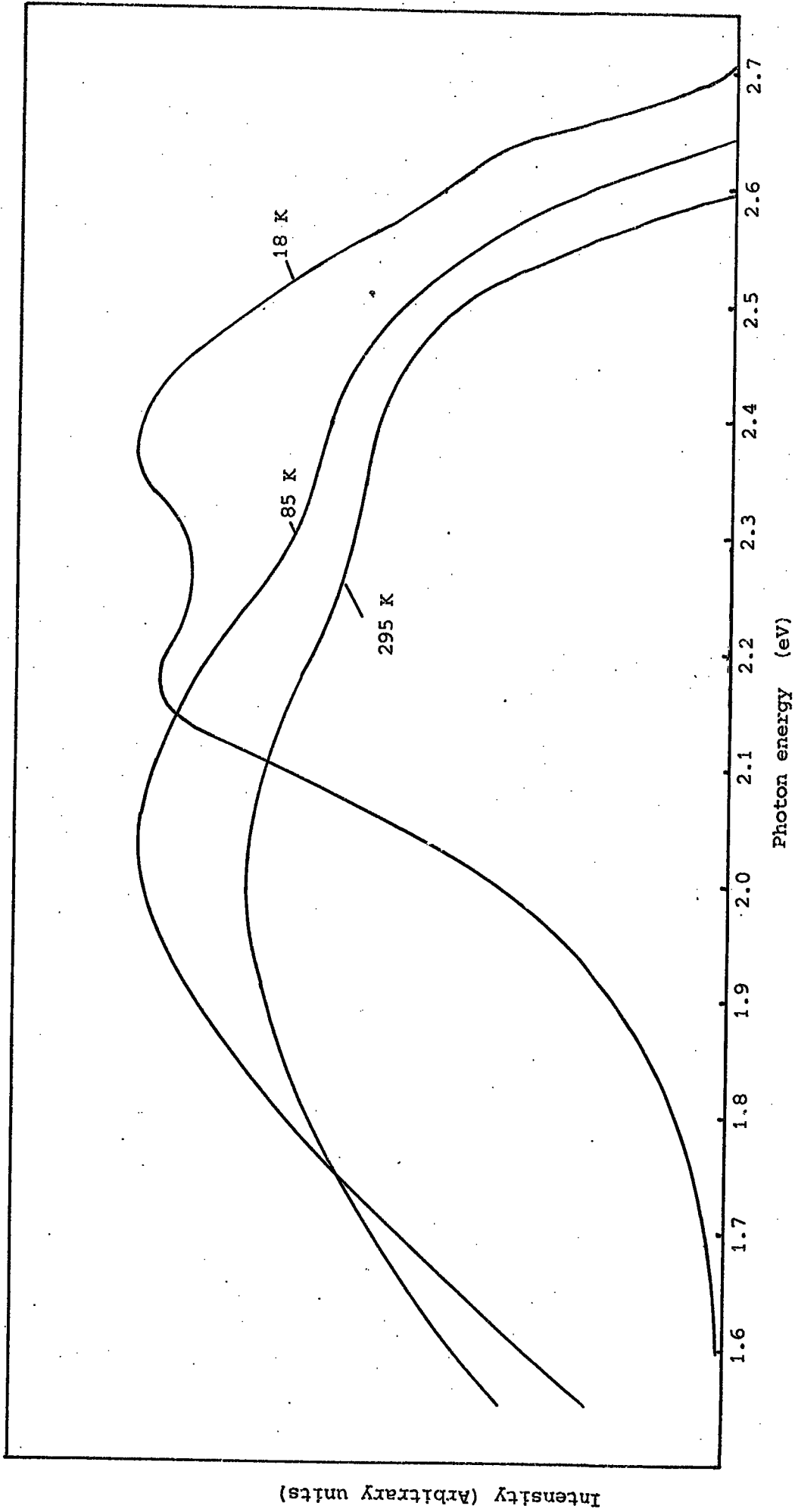


Fig. 6.7: Reverse bias electro luminescence in Au-ZnSe:Se,Zn, Diode No.172A.

equal to or greater than the band gap energy (~ 3 eV) and ionize the host lattice. Recombination of electrons and holes give rise to the shoulder in the blue region which is thought to be associated with pair emission. In fact bright blue spots were observed to have localized around the gold contact. However the high energy cut off at 2.71 eV suggests that no exciton emission was produced. At 85 K, the emission extends to longer wavelengths with a maximum at 1.98 eV (6250 Å) and a shoulder towards the blue. At 300 K the orange peak shifted slightly to 1.96 eV (6300 Å) but the emission was very similar to that at 85 K.

6.3 EL AND PL FROM A ZnSe DIODE DOPED WITH INDIUM DONORS

The FEL, PL and REL emission spectra of an indium doped diode (No.139) are reported in this section. The conditions of crystal growth and the details of the heat treatment given are summarized in Table 5.1. Some of the parameters of this device can be found in Table 5.2.

6.3.1 Forward bias electroluminescence (FEL) and photoluminescence (PL)

(a) Brightness/current-voltage characteristics

The forward B/I-V characteristics of this diode were found to be similar to that of the undoped diode No.172A. At 85 K, the current and brightness varied exponentially with voltage over three decades and the brightness-current relation followed a power law $B \propto i^n$ with $n = 1.73$. Brightness levels of 10 ft-L were achieved with an applied bias of 1 V and a current density of $3.5 \times 10^{-2} \text{ A mm}^{-2}$. This corresponds to a power conversion efficiency of $3.5 \times 10^{-4} \%$.

(b) FEL and PL emission spectra

FEL and PL emission spectra were recorded at 20, 65, and 295 K (see Figure 6.8). Again the emission spectra are described in detail in

three subdivisions, namely (i) exciton emission, (ii) pair emission, (iii) deep centre (self-activated) emission.

(i) Exciton emission

Again exciton emission was detected only in FEL and did not appear in PL. The FEL spectra were recorded at a diode current of $7 \times 10^{-2} \text{ A mm}^{-2}$. At 20 K, a single exciton emission band was observed at 2.79 eV (4440 Å). This is attributed to the decay of excitons bound to neutral donors. A dissociation energy of 5 meV was calculated for this line. Using Halsted and Aven's law (1965), a donor ionization energy of $E_d \approx 25 \text{ meV}$ was then derived. The variation of the peak energy of the bound exciton with temperature was studied from 20 - 350 K (see curve (b) in Figure 6.3). At 65 K the peak energy of the exciton was about 2.79 eV (4443 Å) and at about 80 K the energy difference between the ground state of the free exciton (see curve (a), Figure 6.4) and the bound exciton disappeared. This is attributed to the thermal dissociation from a bound to free exciton at 80 K. The width of the exciton band was slightly greater than that of the exciton in diode No.172A. From the variation of the band width with temperature (see line (d) in Figure 6.4), ΔE of a free exciton was found to vary as 1.3 kT . This is again in good agreement with the predicted theoretical variation 1.2 kT for the zero phonon exciton line. The variation of the intensity of the exciton emission with temperature is illustrated in curve (b), Figure 6.4. Again the exciton emission at 295 K was observed in the form of bright blue spots localized at the edges of the gold contact.

(ii) Pair emission

At 20 K, the pair emission in FEL and PL consisted of a series of equally spaced bands labelled as the F and N series in Figure 6.8.

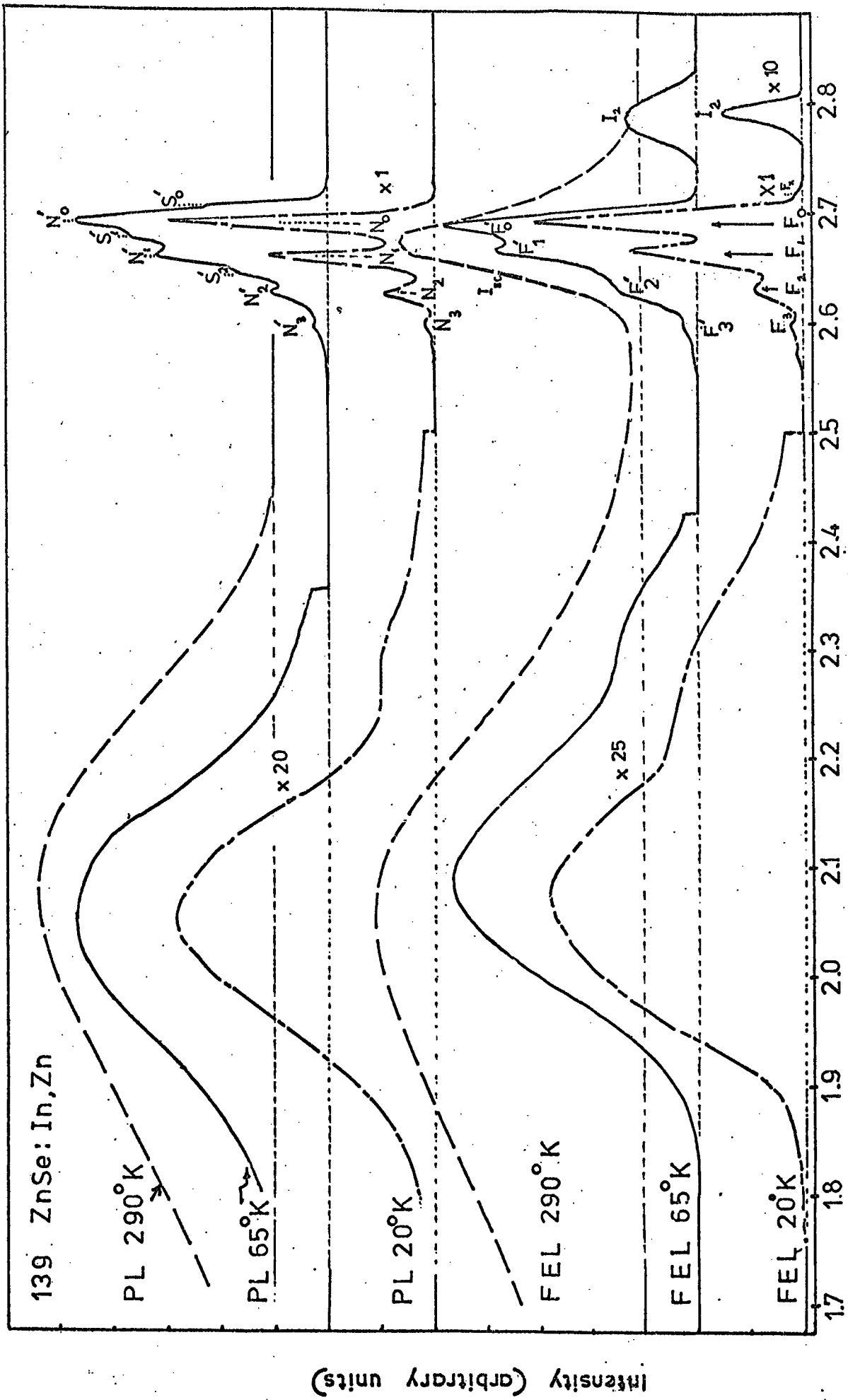


Fig. 6.8: Forward Bias Electroluminescence and Photoluminescence in Au-ZnSe: In Zn Diode

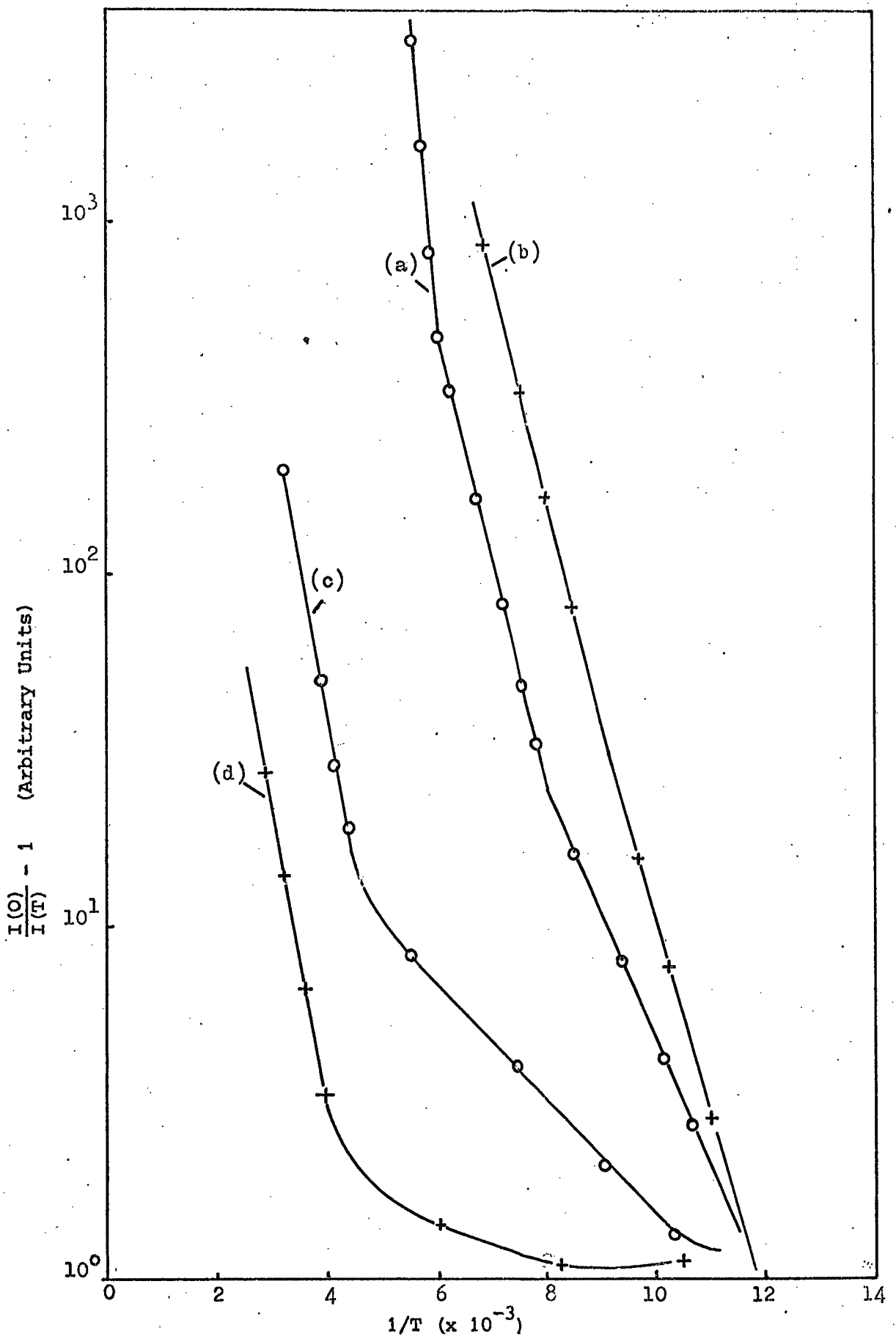


Fig. 6.9: The variation of the intensity of edge emission with temperature (a) in FEL, (b) in PL, and the variation of intensity of orange band (c) in FEL and (d) in PL using obtained in Au-ZnSe:InZn, diode No.139.

The bands are phonon assisted members of distant donor-acceptor pair recombination. The zero order component lay at 2.693 eV (4603 Å) in FEL and 2.690 eV (4608 Å) in PL, (see Table 6.2) indicating that the F series in FEL was slightly higher in energy (~ 1 meV) compared with the N series in PL. This is attributable to a higher density of excitation in FEL. As the device current was decreased this difference disappeared. From the equal energy separation between members of the F and N series, the LO phonon energies were calculated to be 31.7 meV and 30.7 meV. Using the energies of the zero order bands (F_0 , N_0) and 14 meV for the coulombic attraction and $E_g = 2.818$ eV, equation 2.3.2 gives the sum of the donor and acceptor ionization levels ($E_a + E_d$) as 139 ± 2 meV and 141 ± 2 meV for the two cases. At 65 K in FEL the energy of the F series decreased slightly (see Figure 6.8). The new series, F', apparently still corresponds to donor-acceptor emission. However two series of bands (labelled as N' and S') appeared in the PL emission spectra at 65 K. The S' series is thought to correspond to free to bound transitions to the same acceptor which is responsible for the bound-to-bound transitions of the N' series. Taking the energies of the zero-LO phonon components as 2.688 eV and 2.709 eV for N'_0 and S'_0 respectively (see Table 6.2) the ionization energies of the acceptor and donor levels were calculated to be $E_a \simeq 108 \pm 2$ and $E_d \simeq 30 \pm 2$ meV.

The thermal quenching of the edge emission was studied in the temperature range 85 - 180 K. The results are plotted in the form $\log \{ (I(0)/I(T)) - 1 \}$ against $1/T$ for FEL and PL emission (see curves (a) and (b) in Figure 6.9 respectively). Curve (a) for FEL contains three linear sections with slopes giving activation energies of 96 ± 2 meV ($T(K) < 110$ K), 125 ± 2 meV ($110 \text{ K} < T(K) < 160 \text{ K}$) and 360 ± 2 meV ($T(K) > 160 \text{ K}$). However, curve (b) contained only two linear

Line	Emitted Photon		Strength	Possible Assignment	Line	Emitted Photon		Strength	Possible Assignment
	Energy (eV)	Wavelength (Å)				Energy (eV)	Wavelength (Å)		
FEL SPECTRA									
20 K					65 K				
I ₂	2.791	4440	Medium	Exciton bound to neutral donor	I ₂	2.79	4443	Medium	Exciton bound to neutral donor
F _x	2.818	4560	Weak	?	F ₀	2.691	4606	Medium	Zero - LO phonon
F ₀	2.693	4603	Strong	Zero - LO phonon	F ₁	2.66	4660	Weak	1LO phonon
F ₁	2.661	4658	Strong	1LO phonon	F ₂	2.63	4715	Shoulder	2LO phonon
F ₂	2.629	4715	Medium	2LO phonon	F ₃	2.597	4773	Shoulder	3LO phonon
F ₃	2.596	4775	Weak	3LO phonon	I* _{EC} (295K)	2.675	4634	Strong	Free exciton
PL SPECTRA									
20 K					65 K				
N ₀	2.690	4608	2.690	Strong	S ₀	2.706	4575	Shoulder	Zero - LO phonon
N ₁	2.66	4661	2.66	Strong	N ₀	2.688	4612	Strong	Zero - LO phonon
N ₂	2.63	4717	2.63	Medium	S ₁	2.677	4630	Shoulder	1LO phonon
N ₃	2.596	4777	2.596	Medium	N ₁	2.658	4663	Medium	1LO phonon
					S ₂	2.646	4685	Shoulder	2LO phonon
					N ₂	2.628	4715	Weak	2LO phonon
					N ₃	2.597	4772	Weak	3LO phonon

Table 6.2: The position of the emission of exciton and edge emission in FEL and PL of Au-ZnSe:In,Zn, diode No.139.

parts with slopes of 108 ± 2 meV ($T(K) < 110$ K) and 126 ± 2 meV (110 K $< T(K) < 160$ K).

(iii) Deep centre emission

In addition to the exciton and edge emission, broad, orange and green bands were observed in both FEL and PL, (see Figure 6.8). At 20 K the broad orange band (see Table 6.3) was centred at 2.08 eV (5950 Å) FEL and at 2.05 eV (6050 Å) in PL. The green band appeared as a shoulder at about 2.34 eV (5300 Å) in both the FEL and PL at 20 K. The intensities of the orange and green bands were about 25 times less than that of the edge emission. At 295 K, the peak of the orange band shifted to lower energy, i.e. to 2.03 eV (6100 Å) in FEL and to higher energies 2.066 eV (6000 Å) in PL and became broader (see Table 6.3).

At 85 K, the orange luminescence was found to be efficiently excited by photons with energies near 2.75 eV (4500 Å), i.e. at energies just below the band gap (see Figure 6.17).

Thermal quenching of the orange band in FEL and PL (see Figure 6.9) suggests that the acceptor level involved had an energy of about 180 meV, in the case of FEL another level with ionization energy about 30 meV was also observed and attributed to a donor.

6.3.2 Reverse bias electroluminescence (REL)

(a) Brightness/current-voltage relations

Reverse B/I-V characteristics of the indium doped diode were measured at 85 and 295 K (see Figure 6.10). At 295 K, two exponential regions in the I-V and B-V characteristics were observed. At 85 K, avalanching occurred with applied biases greater than 16 V, but the I-V and B-V curves remained parallel. The brightness-current relation $B \propto i^n$ held with $n = 1.08$ at 295 and $n = 1.2$ at 85 K. As a brightness

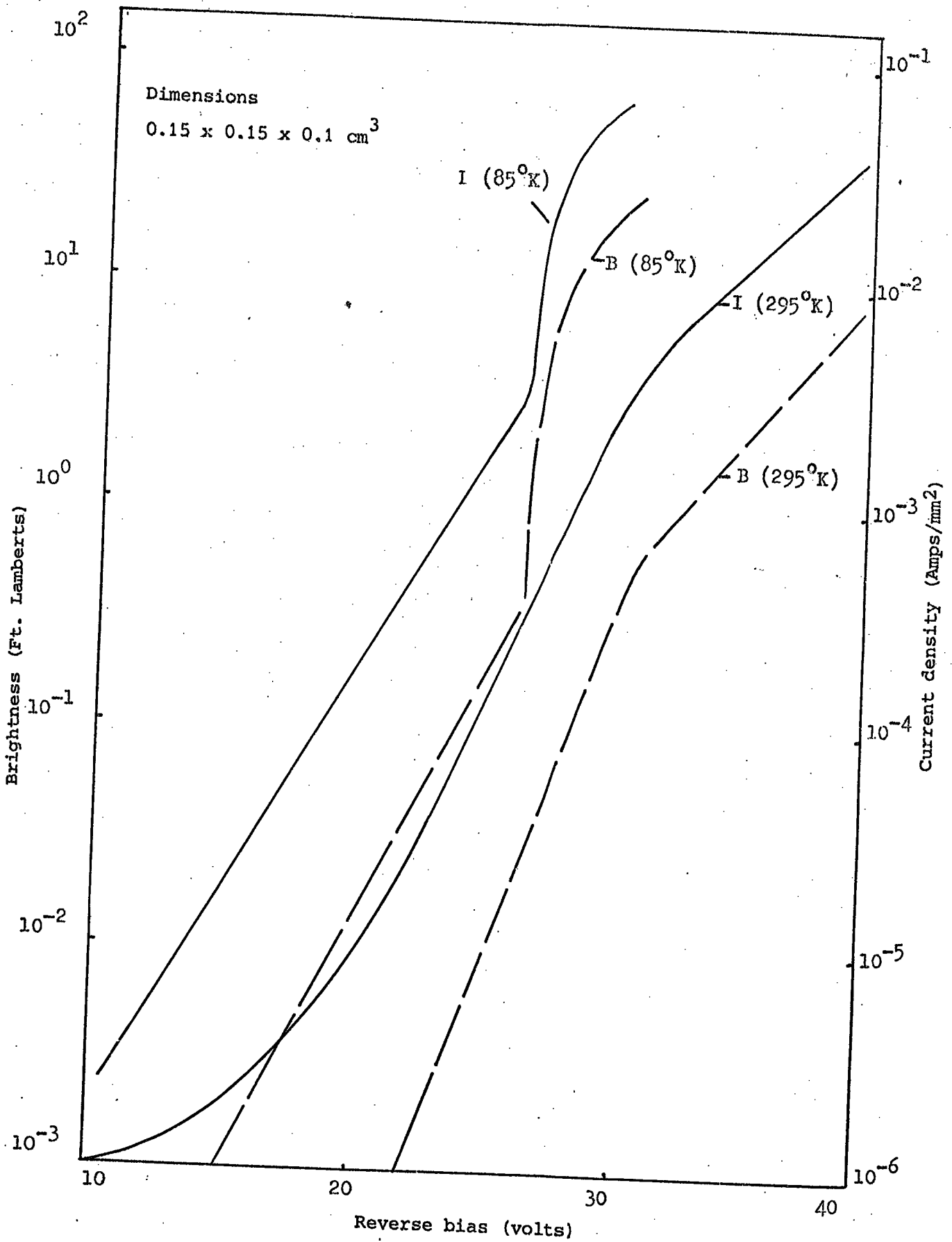


Fig. 6.10: Current/brightness characteristics as a function of applied bias in Au-ZnSe:In,Zn diode No.139.

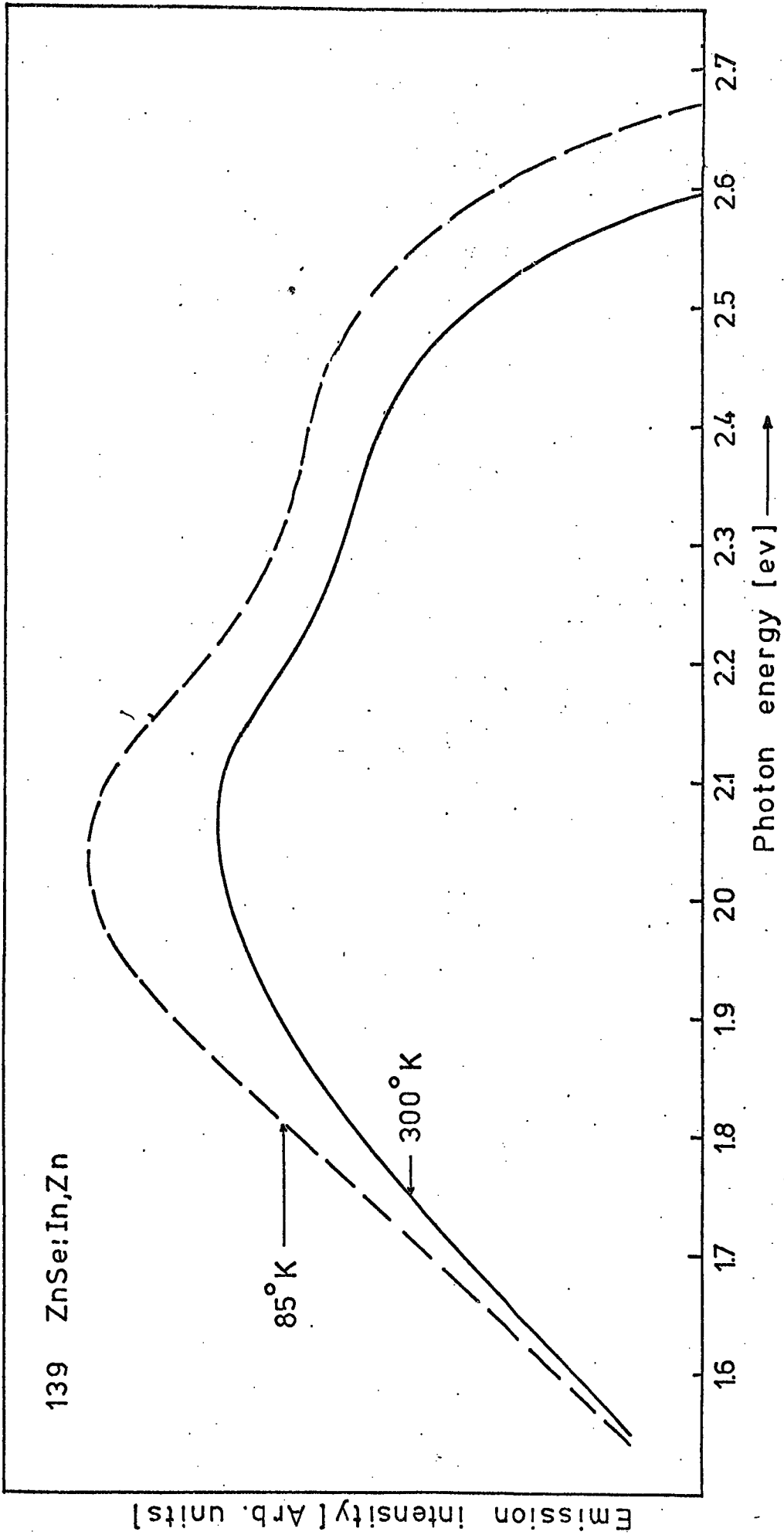


Fig. 6.11: Reverse bias electroluminescence in Au-ZnSe:In,Zn diode.

of 10 ft-L, the power conversion efficiency of this diode was calculated to be 6×10^{-6} at 295 K and 2×10^{-5} % at 85 K.

(b) Spectral distribution

The spectral distribution of the REL was measured at a diode current of $3 \times 10^{-2} \text{ A mm}^{-2}$ and is shown in Figure 6.11. The REL spectrum was very broad compared with that measured in FEL and PL (see Table 6.3). The main REL emission band peaked at 2.04 eV (6070 Å) at 85 and 2.06 eV (6000 Å) at 295 K. On the high energy side, the emission cut off fairly sharply at photon energies a little below the band gap.

6.4 EL AND PL IN ZnSe CONTAINING ALUMINIUM OR GALLIUM DONORS ONLY

As stated earlier in Chapter 3, aluminium (or gallium) could be introduced into ZnSe either during or after crystal growth. In the diode No.172B, aluminium was introduced by heating the ZnSe in molten zinc plus 10% Al. The second diode sample, No.246, was fabricated from a crystal containing grown-in aluminium. The gallium doped diode, No.176, contained grown-in gallium. The conditions for crystal growth and the heat treatment administered to these crystals prior to production of Schottky diodes are given in Table 5.1. With the gallium doped sample, the yellow, orange body colour of the as-grown crystal changed to darkish orange on the surface after the heating in molten zinc. This suggests a small degree of precipitation occurred as mentioned in Section 5.5.2. However when one of the sides was polished by removing a layer of about 100 μm the original yellow, orange body colour was restored. To form a diode the chip was chemically etched and an indium contact was applied to a polished face while gold was deposited on the opposite darkish orange face of the chip. Some of the parameters of the above mentioned diodes are listed in Table 5.2.

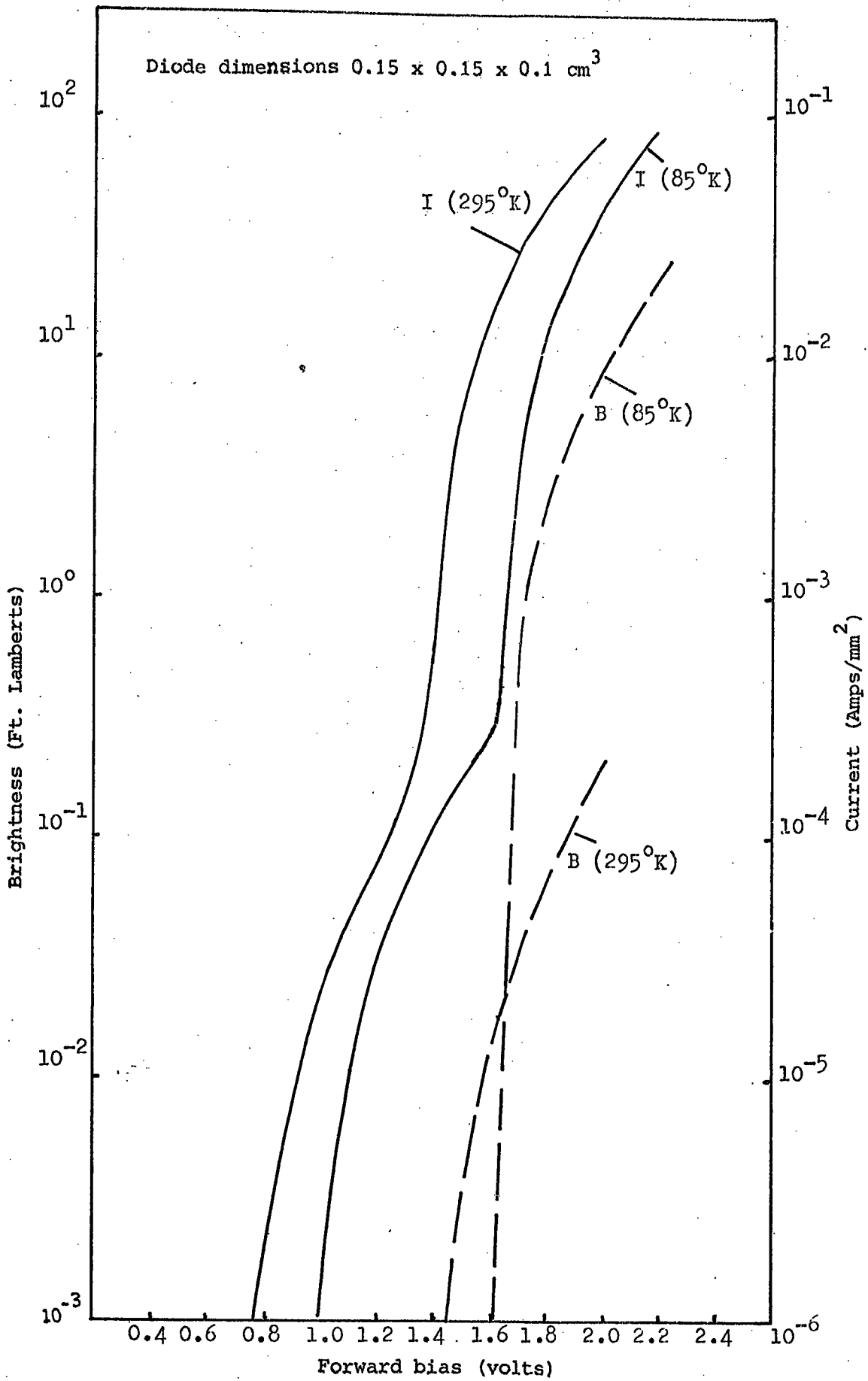


Fig. 6.12: Current/brightness characteristics as a function of applied bias in Au-ZnSe:Zn+Al, diode No.172B

6.4.1 Forward EL and PL

(a) Brightness/current-voltage characteristics

The forward B/I-V characteristics obtained from the aluminium doped diode (No.172B) are illustrated in Figure 6.12. The I-V characteristics were dominated by leakage currents at biases less than 1.3 V and 1.5 V at 85 K. At 295 K, the light emission was first observed at a voltage threshold of about 1.4 V. With current densities higher than $10^{-4} \text{ A mm}^{-2}$ the brightness obeyed the usual relation of $B \propto i^n$ with n equal to about 1.5. In Figure 6.12, the brightness level of about 0.2 ft-Lambert at 295 K would correspond to a conversion power efficiency of about $10^{-5} \%$. The brightness was found to increase two orders of magnitude on cooling to 85 K with a power efficiency approximately $1.3 \times 10^{-4} \%$. Similar I-V and B-V characteristics were also observed with the diode No.247. The light output of this device prepared on as-grown material was slightly better with an improved power efficiency.

The forward B/I-V characteristics of the gallium doped diode No.176 are illustrated in Figure 6.13. At 295 K, the current and brightness varied exponentially with voltage over three orders of magnitude of current and brightness respectively. At 85 K both the I-V and B-V characteristics shifted to higher voltages. This was partly due to the increased series resistance of the diode at low temperature. However when the applied bias was slightly increased beyond 22 V, the diode current increased rapidly from 10^{-2} to $2 \times 10^{-1} \text{ A mm}^{-2}$ while the voltage decreased to 18 V. Similar behaviour was repeated in the B-V characteristics. Again the brightness-current dependence obeyed a relation of the form $B \propto i^{1.5}$. The power conversion efficiency was about $1.7 \times 10^{-5} \%$ at a brightness level of 10 ft-L at 295 K.

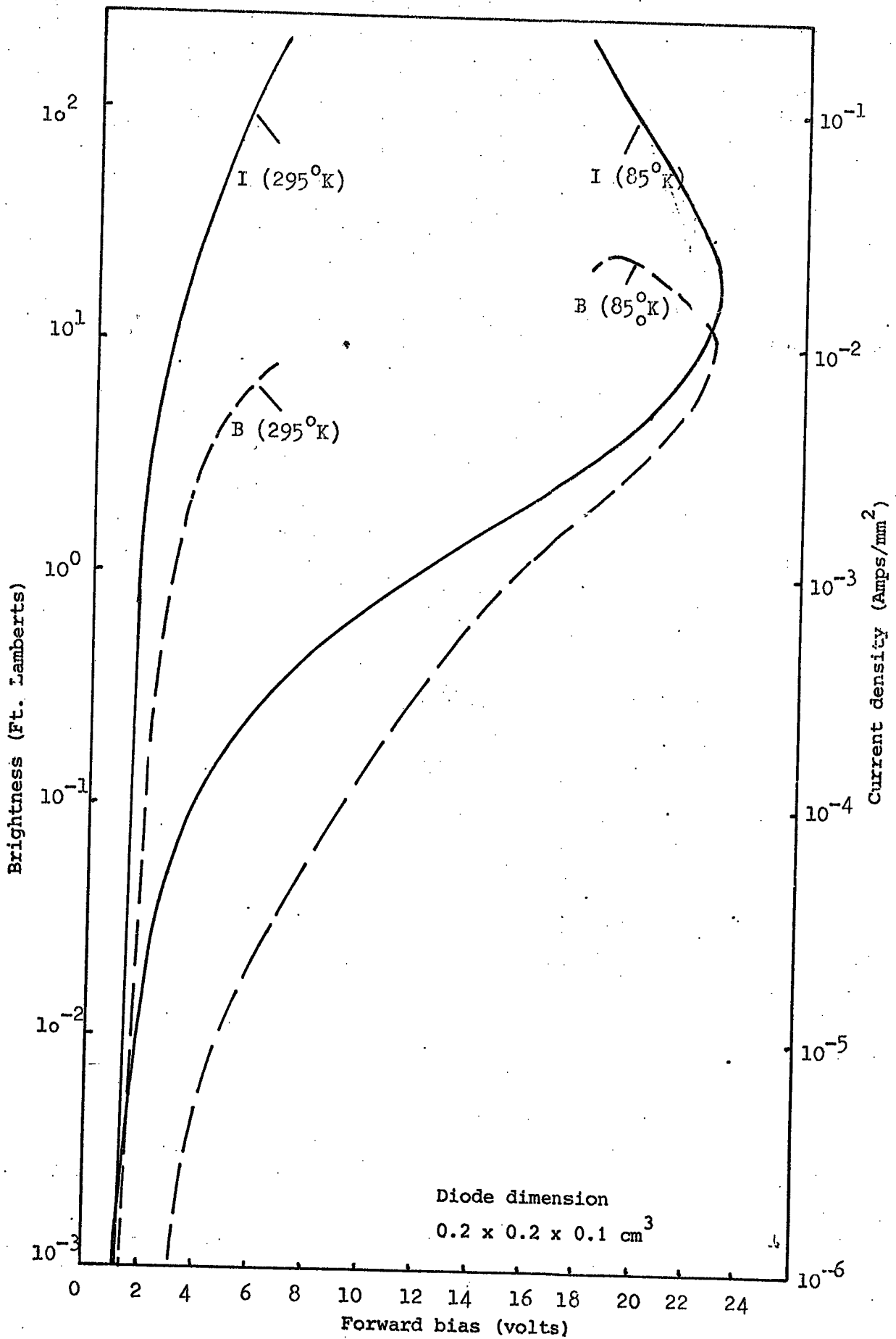


Fig. 6.13: Current/brightness - characteristics as a function of applied bias in Au-ZnSe:Ga,Zn, diode No.176

(b) Spectral distribution in FEL and PL

The spectral distribution of the FEL emission was measured at current densities of $4 \times 10^{-2} \text{ A mm}^{-2}$. The FEL and PL spectra measured on diodes No.172 B, 247 and 176 are shown in Figures 6.14, 6.15 and 6.16. The FEL and PL spectra of the aluminium doped samples contained edge and self-activated bands at 85 K. The intensity of the edge emission of Al-doped samples was much lower than that in undoped (No.172A) and indium doped (No.139) diodes and as a result no phonon replicas were resolved. The edge emission band was located at about 2.67 eV (4610 Å). In FEL, the broad band emission peaked at 2.23 eV (5550 Å) and 2.03 eV (6100 Å) in diode No.172B and at 2.21 eV (5600 Å) and 1.98 eV (6250 Å) in diode No.247. At 295 K, a broad orange band only was observed, at 2.06 eV (6000 Å) in diode No.172B, and at 1.98 eV (6250 Å) in diode No.247. The PL emission spectrum was similar to that in FEL at 85 K and 295 K (see Table 6.3), however the intensity of the green band in PL was slightly weaker. The spectral distribution of the FEL emission from the gallium doped sample consisted at 85 K, of a single broad band (see Figure 6.16 and Table 6.3) peaking at 2.15 eV (5750 Å) with a shoulder at about 2.0 eV (6200 Å) in the orange. At 295 K, the orange band was dominant. In PL emission only the orange band was observed (see Table 6.3).

The luminescence excitation spectra for the orange band of these diodes are shown in Figures 6.17 and 6.18. At 295 K, the orange band in diode No.172B was excited efficiently by photons with energies of 2.58 eV (4800 Å). However, the orange band was excited with high efficiency at the band gap and at photon energies of about 2.4 eV (5150 Å) and 2.45 eV (5050 Å) in diodes No.247 and 176 respectively (see Figures 6.17). At 85 K, the maximum excitation efficiency occurred at higher photon energies, for example at 2.72 eV (4550 Å) in diode No.172B and 2.61 eV (4750 Å) in diode No.176, (see Figure 6.18).

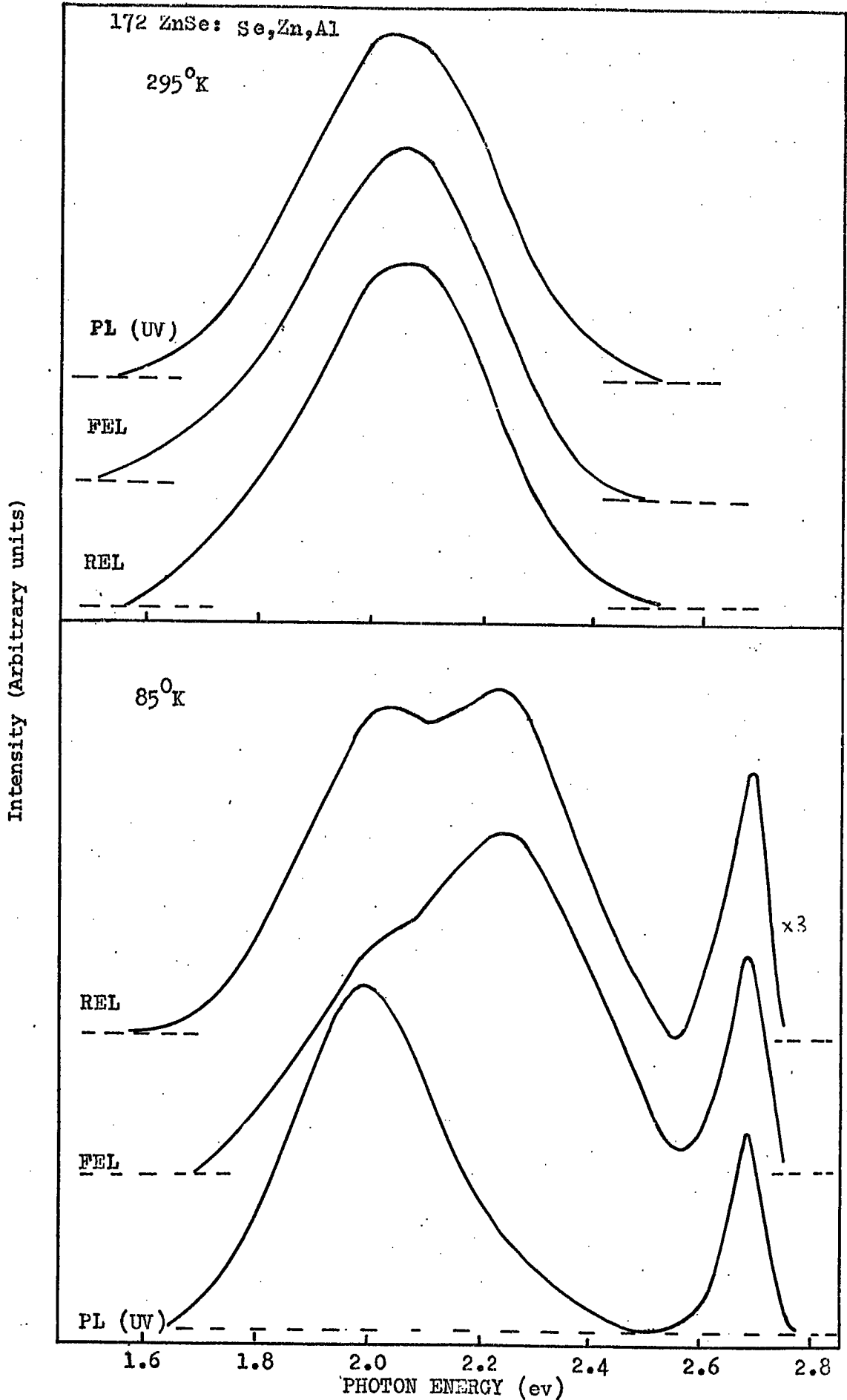


Fig.6.14 Reverse bias electroluminescence, Forward bias electroluminescence and Photoluminescence (excited by $Uv = 3650 \text{ \AA}$) spectra on Au-ZnSe: Se, Zn,Al. diode No.172B.

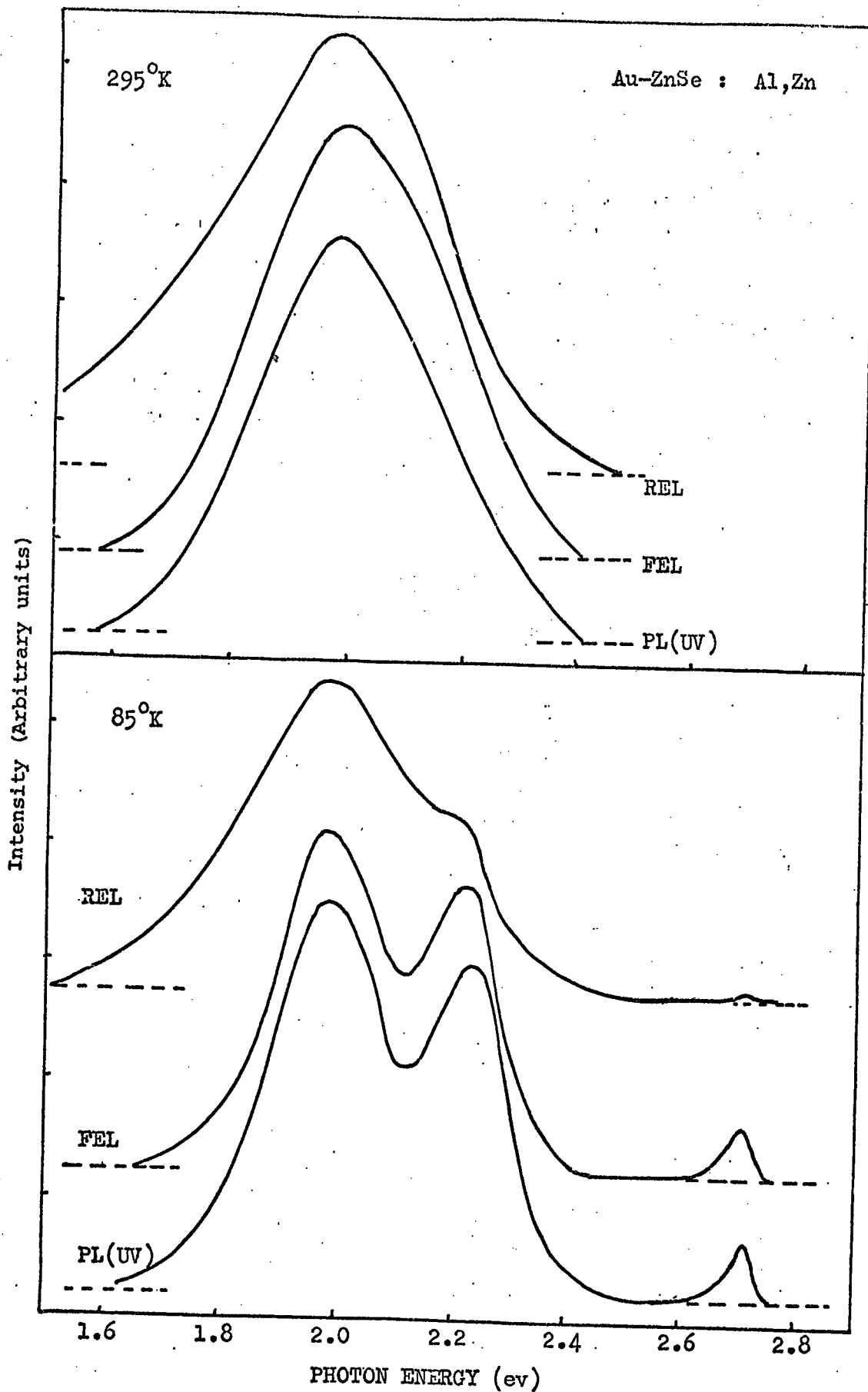


Fig.6.15: Reverse bias electroluminescence, Forward bias electroluminescence and Photoluminescence (excited by $UV = 3650 \text{ \AA}$) spectra on Au-ZnSe : Al, Zn diode No. 247 at 295° and 85°K .

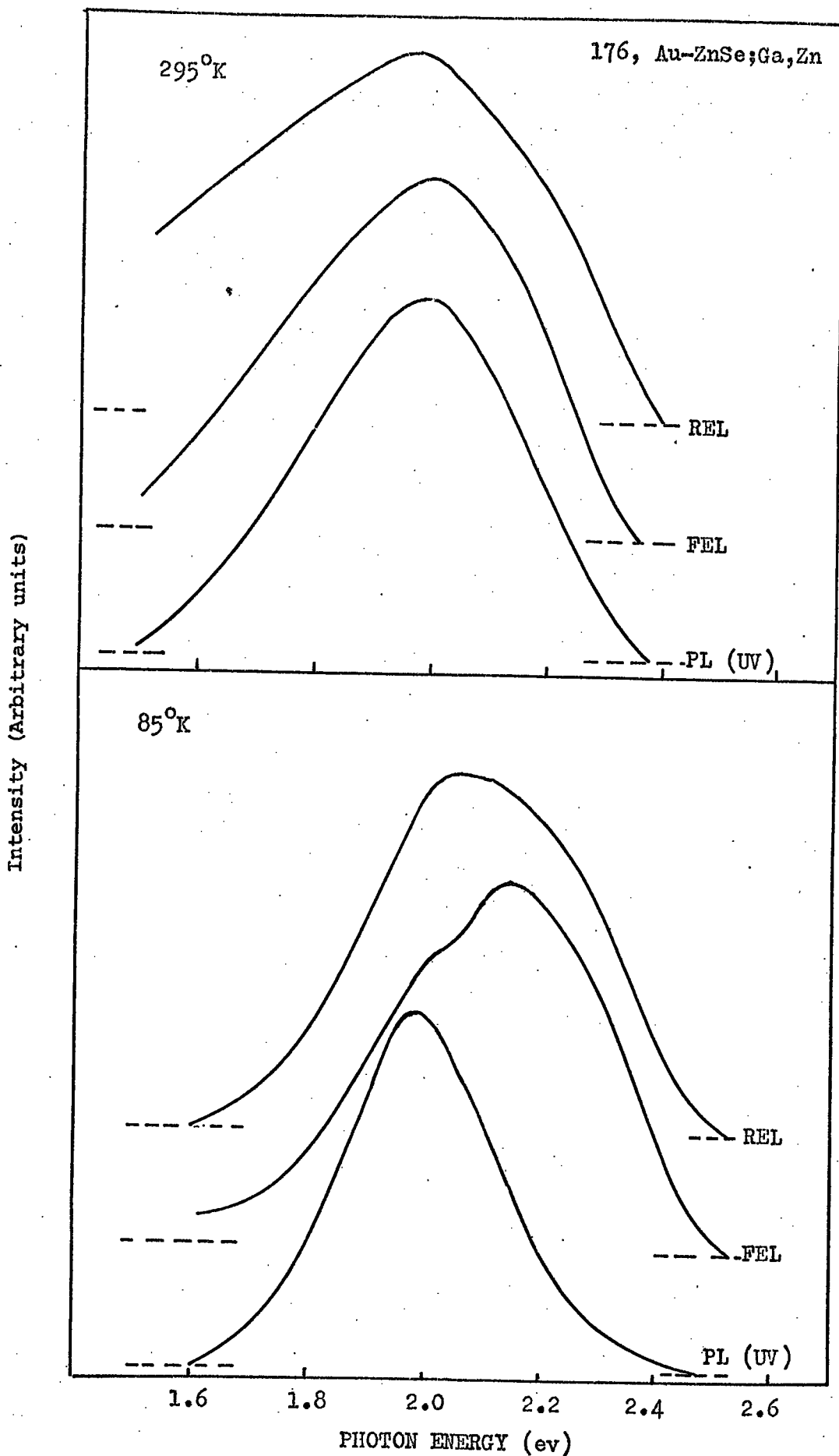


Fig. 6.16: Reverse bias electroluminescence, Forward bias electroluminescence and Photoluminescence (excited by UV = 3650 Å) spectra on Au - ZnSe:Ga, Zn diode.

6.4.2 Reverse bias EL

(a) Brightness/current-voltage characteristics

Reverse B/I-V characteristics measured on diode No.172B are shown in Figure 6.19 and are similar to those measured on diode No.247. The reverse B/I-V characteristics of the gallium doped diode (No.176) were similar to those of undoped diodes described earlier in this chapter. The brightness again followed the $B \propto i^n$ relation with n equal to about 1.2. A brightness level of 20 ft-L was achieved in diode No.172B with a power conversion efficiency of $5 \times 10^{-5} \%$. 80 ft-L was obtained in diode No.247 with a slightly improved efficiency of $10^{-4} \%$. The light output from the gallium doped sample was poor. A brightness of 2 ft-L was observed at a bias of 30 V and current density of $1.2 \times 10^{-2} \text{ A mm}^{-2}$ corresponding to a poor power efficiency of about $6 \times 10^{-6} \%$.

(b) Spectral distribution

The REL emission spectra of the above mentioned diodes were measured at a current density of $2 \times 10^{-2} \text{ A mm}^{-2}$. At 295 and 85 K, the REL emission spectrum of diode No.247 was the same as that measured in FEL and PL. Similar bands were also observed in the REL and PL emission spectra of diode No.172B (see Figures 6.14, 6.15 and Table 6.3). The REL emission from the gallium doped sample consisted of a broad yellow, orange band peaking at 2.08 eV (5950 Å) at 85 K (see Figure 6.16 and Table 6.3). This orange band became much broader at 295 K as the maximum shifted to lower energies at 1.96 eV (6300 Å).

6.5 EL AND PL IN ZnSe CONTAINING CHLORINE OR IODINE ONLY

As described earlier, chlorine or iodine was introduced into ZnSe during the crystal growth procedure (see Chapter 3). The crystal growth parameters and the heat treatment conditions of crystals No.242 containing

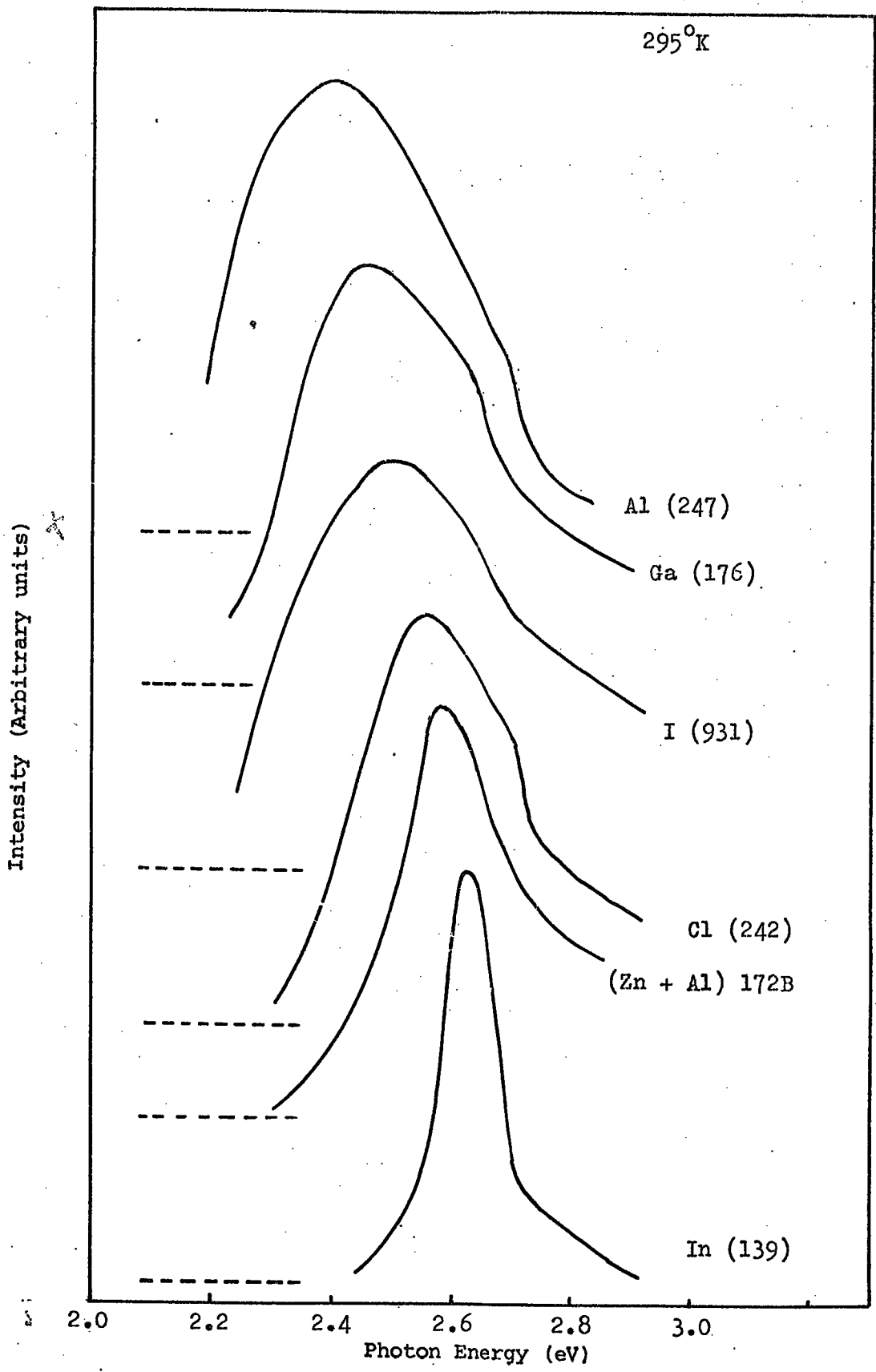


Fig. 6.17: Luminescence excitation spectra (295 K) for the orange band observed in PL in Au-ZnSe diodes.

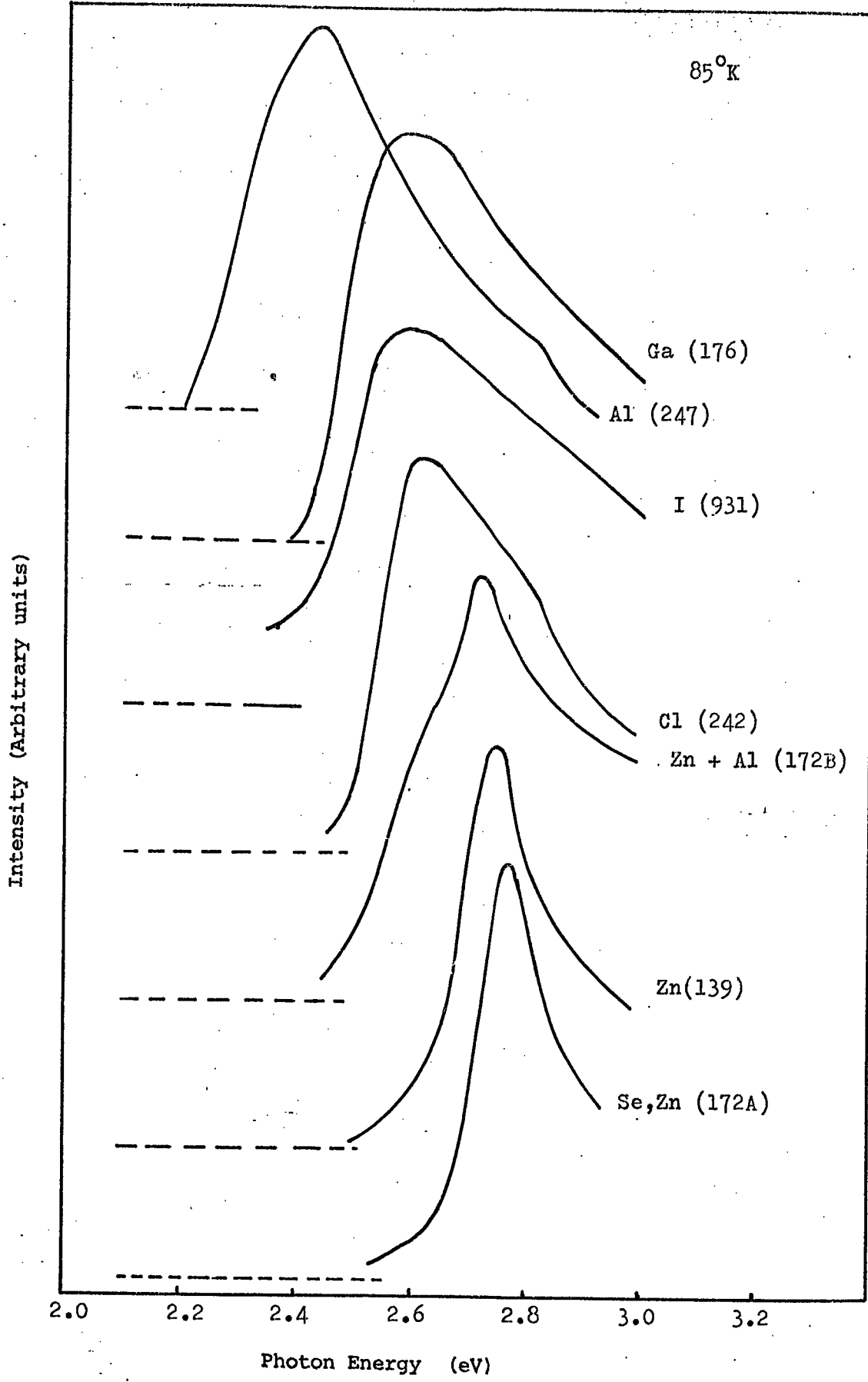


Fig. 6.18: Luminescence excitation spectra (at 80 K) for the orange band observed in the PL of Au-ZnSe diodes.

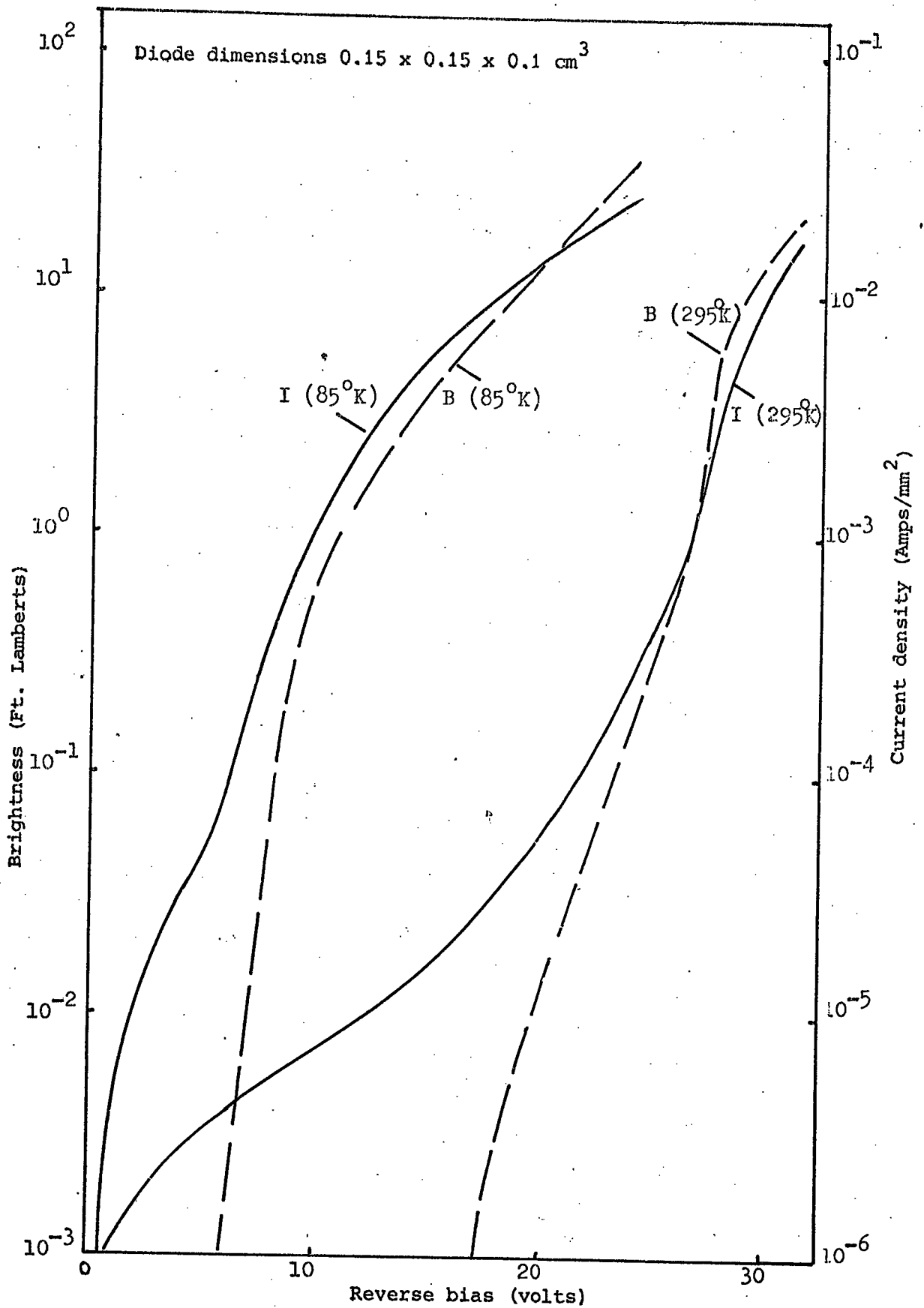


Fig. 6.19: Current/brightness characteristics as a function of applied bias in Au-ZnSe:Zn+Al, diode No.172B

Cl and No.931 containing I have already been recorded in Table 5.1

6.5.1 Forward bias EL and PL

(a) Brightness/current-voltage characteristics

The forward B/I-V characteristics obtained from the chlorine doped diode No.242 were similar to that of the aluminium doped diode (i.e. No.172B) shown in Figure 6.12. The light emission from this diode was poor at 295 K, but at 85 K a brightness of 40 ft-L was achieved. The characteristics of the iodine doped diode (No.931) are shown in Figure 6.20. From this diode a brightness of 20 ft-L was attained at 295 and 300 ft-L at 85 K with corresponding conversion power efficiencies of 2×10^{-4} and 10^{-3} % respectively. The brightness current variation followed the $B \propto i^n$ relation with $n = 1.6$.

(b) Spectral distribution

The FEL and PL emission spectra from the chlorine doped diode are illustrated in Figure 6.21. At 85 K, a single orange band was seen to peak at 2.08 eV (5950 Å) in FEL and 2.06 eV (6000 Å) in PL. Because of the poor emission intensity, the orange FEL emission spectrum could not be recorded at 295 K but the PL emission consisted of a broad orange band at 2.1 eV (5900 Å). The iodine doped sample also showed a single orange band in FEL and PL emission at 295 and 85 K (see Figure 6.22). The orange band was centred at 2.06 eV (6000 Å) at 295 and 2.04 eV (6080 Å) at 85 K in FEL and at 2.06 eV (6000 Å) at 295 and 2.02 eV (6120 Å) at 85 K in PL.

At 295 K, the orange band in the chlorine-doped diode was efficiently excited by photons with an energy of 2.55 eV (4850 Å). In the iodine-doped diode (see Figure 6.17), the same orange band was excited by 2.5 eV photons. At 85 K, the peak of the excitation band

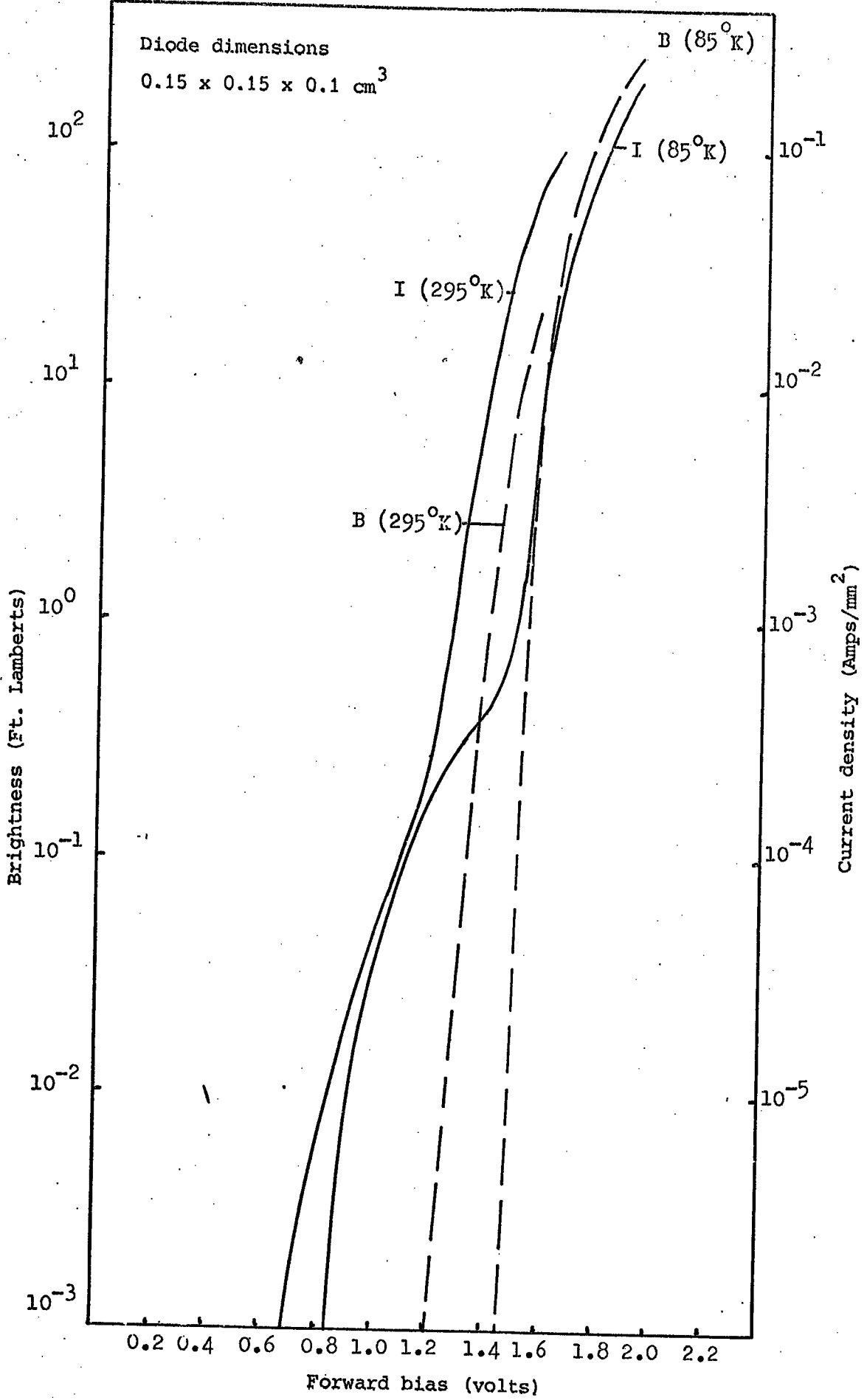


Fig. 6.20: Current/brightness characteristics as a function of applied bias in Au-ZnSe:I,Zn, diode No.931

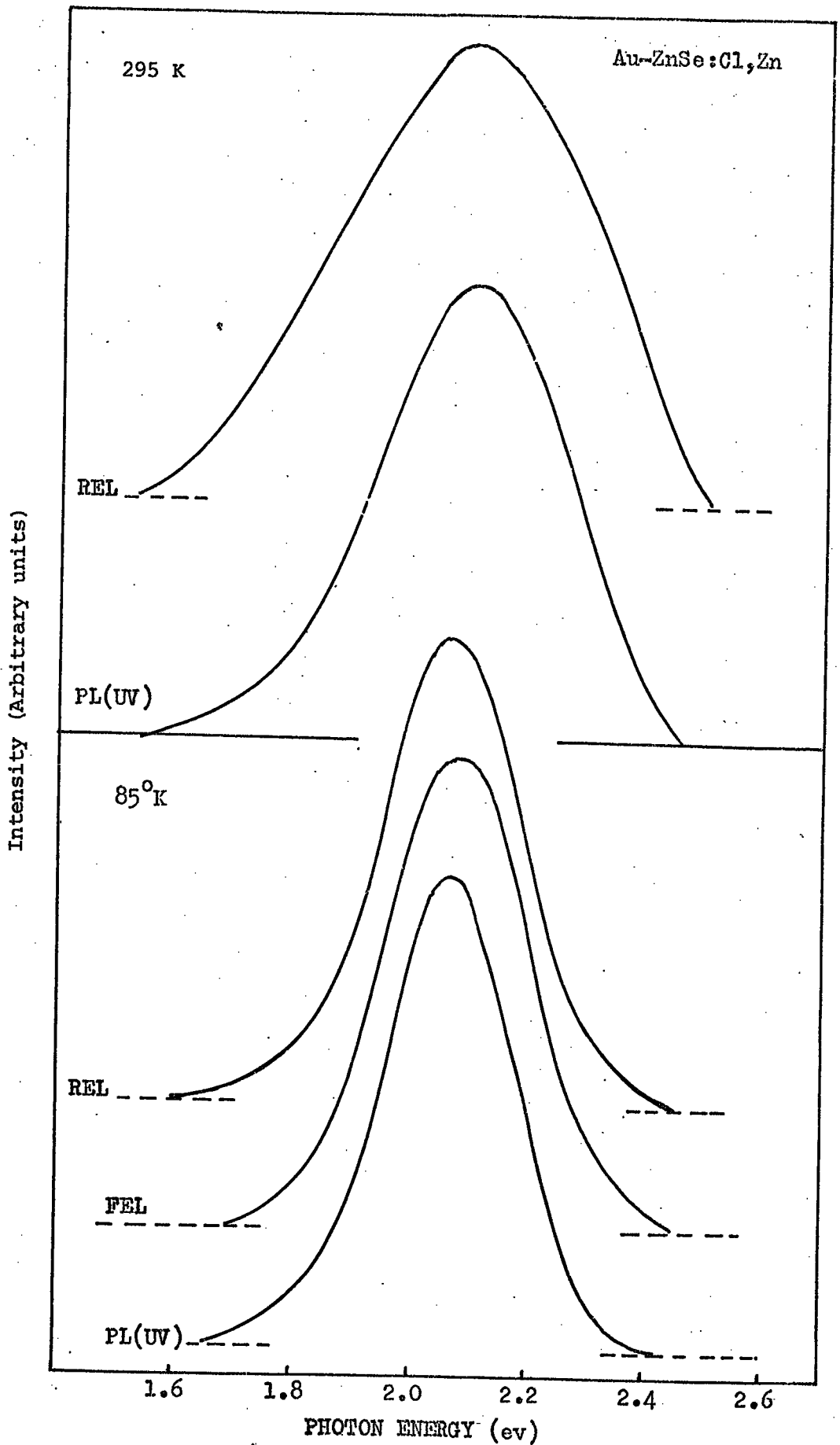


Fig.6.21: Reverse bias electroluminescence, Forward bias electroluminescence and Photoluminescence (excited by $UV = 3650 \text{ \AA}$) spectra on Au-ZnSe: Cl, Zn diode at 295 85°K .

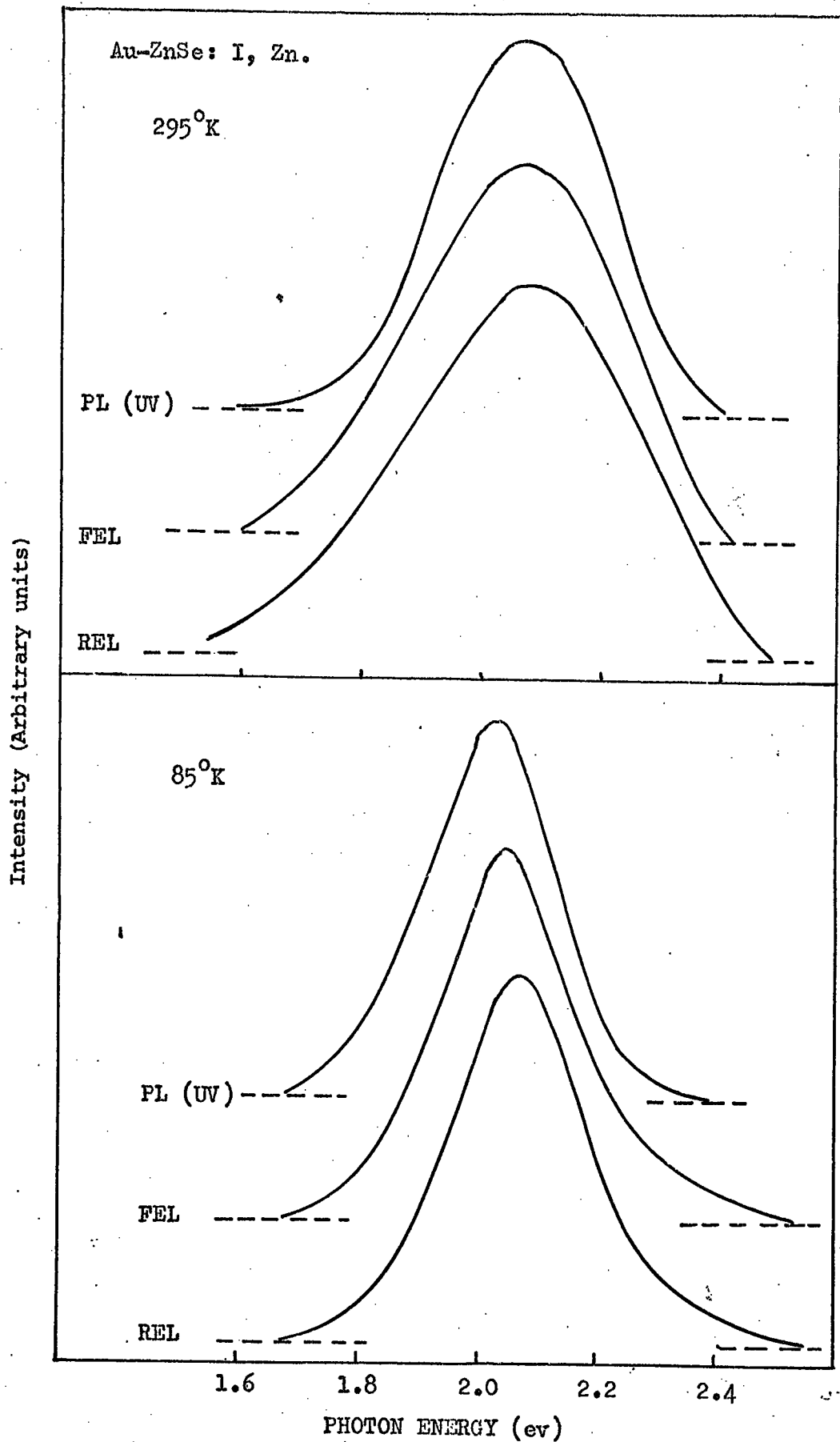


Fig. 6.22: reverse bias Electroluminescence, Forward bias Electroluminescence and Photoluminescence (excited by $UV = 3650 \text{ \AA}$) spectra on Au-ZnSe: I, Zn diode at 295° and 85°K.

shifted to higher photon energies of 2.61 eV (4750 Å) in diode No.242 and 2.59 eV (4790 Å) in diode No.931.

The temperature quenching of the orange band in FEL and PL in the chlorine doped sample is shown graphically in Figure 6.23. Two quenching energies of 14 meV and 360 meV were found.

6.5.2 Reverse bias EL

(a) Brightness/current-voltage characteristics

In reverse bias, the current and brightness of diode No.242 again varied roughly exponentially with voltage and a small avalanching effect occurred at biases greater than 15 V, (see Figure 6.24). The reverse B/I-V characteristics for the iodine doped sample are shown in Figure 6.25. In both diodes the brightness-current characteristics followed the $B \propto i^n$ relationship, with the value of n around 1.1 at 295 and 85 K. Brightnesses of 20 - 40 ft-L were achieved in these diodes with power conversion efficiencies of about 5×10^{-5} %. The brightnesses increased up to 100 - 200 ft-L at 85 K with slightly improved power efficiencies.

(b) Spectral distribution

The spectral distribution of the REL of these diodes is shown in Figures 6.21 and 6.22. The bands were slightly broader than in FEL and PL (see Table 6.3), but were located at the same photon energies.

Finally the temperature quenching of the orange band of the chlorine doped diode revealed two quenching energies of 14 and 360 meV (see Figure 6.23).

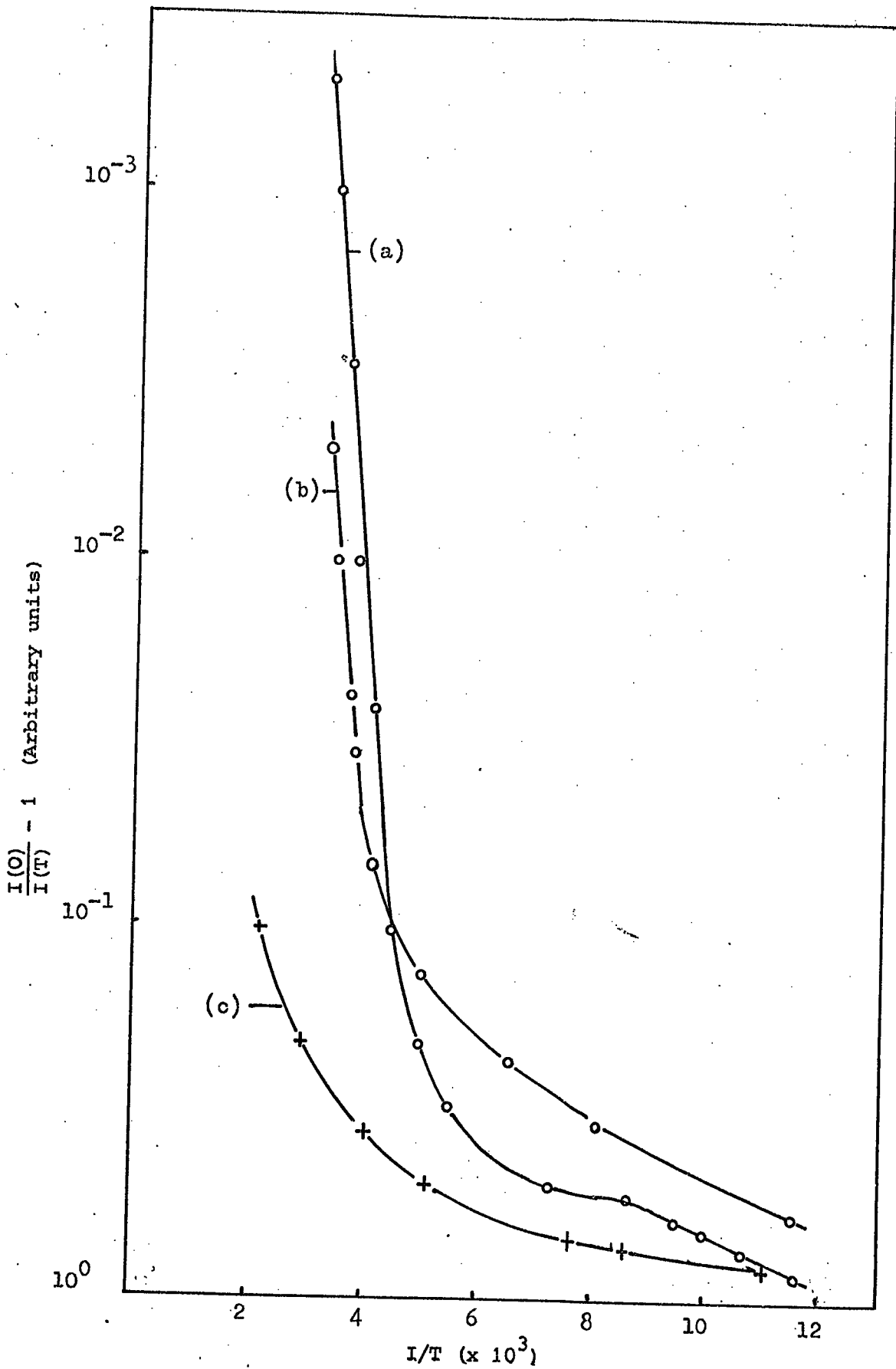


Fig. 6.23: The variation of the intensity of orange emission in (a) FEL, (b) REL and (c) PL in Au-ZnSe;Cl,Zn diode No. 242

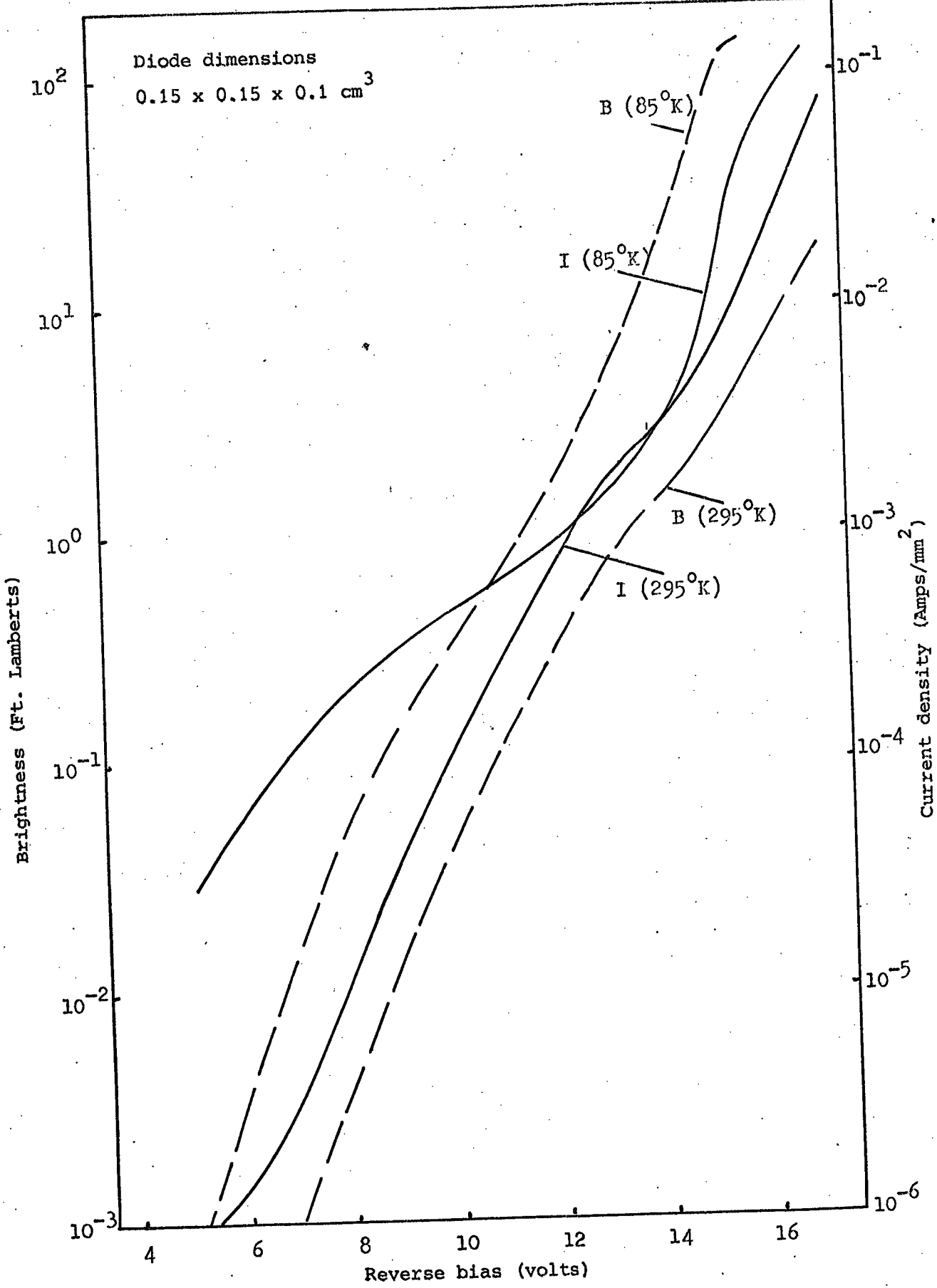


Fig. 6.24: Current/brightness characteristics as a function of applied bias in Au-ZnSe:Cl,Zn, diode No.242

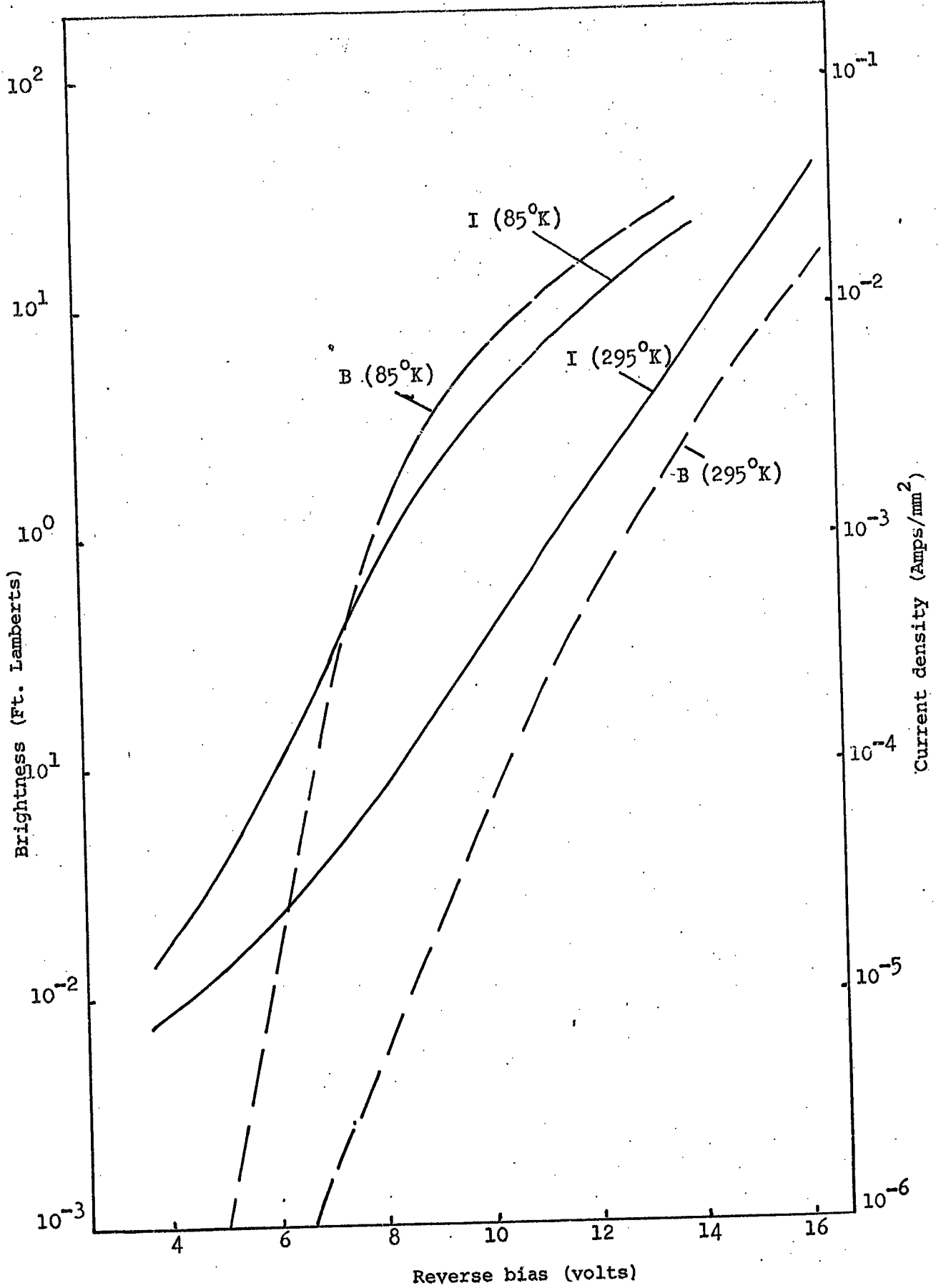


Fig. 6.25: Reverse current/brightness characteristics as a function of applied bias in Au-ZnSe:I,Zn, Diode No.931

Diode No.	Dopant	Temp. (°K)	FEL SPECTRA			PL SPECTRA			REL SPECTRA					
			Energy (eV)	Wave-length (Å)	Relative Strength	Band-Width (eV)	Energy (eV)	Wave-length (Å)	Relative Strength	Band-Width (eV)	Energy (eV)	Wave-length (Å)	Relative Strength	Band-Width (eV)
172A	Se,Zn	295	Infrared	?	Strong	?	1.931	6400	Medium	0.7	1.967	6300	Strong	0.94
		65	2.34	5300	Strong	0.15	2.34	5300	Strong	0.205	1.983	6250	Strong	0.92
			1.983	6250	Weak									
139	In,Zn	20	2.36	5250	Strong		2.36	5200	Strong		2.17	5700	Strong	
			2.01	6150	Weak		2.01	6150	Medium		2.38	5200	Strong	
		295	2.032	6100	Strong	0.55	2.066	600	Strong	0.46	2.066	6000	Strong	0.79
172B	Se,Zn+Al	65	2.083	5950	Strong	0.25	2.05	6050	Strong	0.24	2.04	6070	Strong	0.82
		20	2.34	5300	Shoulder		2.34	5300	Shoulder					
			2.08	5950	Strong		2.05	6050	Strong					
247	Zn,Al	295	2.066	6000	Strong	0.39	2.049	6050	Strong	0.41	2.066	6000	Strong	0.395
		85	2.032	6100	Shoulder	0.49	2.0	6200	Strong	0.31	2.032	6100	Strong	0.83
			2.233	5550	Strong		2.69	4610	Medium	0.75	2.233	5550	Strong	0.09
176	Ga,Zn		2.69	4610	Medium	0.086					2.690	4610	Medium	
		295	1.983	6250	Strong	0.39	1.967	6300	Strong	0.38	1.967	6300	Strong	0.45
		85	1.983	6250	Strong	0.22	1.983	6250	Strong	0.24	1.983	6250	Strong	
931	I,Zn		2.213	5600	Strong	0.17	2.213	5600	Strong	0.19	2.213	5600	Shoulder	
			2.695	4600	Medium	0.09	2.706	4580	Medium	0.85	2.69	4600	Weak	
		295	2.0	6200	Strong	0.52	2.0	6200	Strong	0.45	1.967	6300	Strong	0.72
242	Cl,Zn	85	2.156	5750	Strong	0.42	1.983	6250	Strong	0.31	2.083	5950	Strong	0.47
		295	2.066	6000	Strong	0.41	2.066	6000	Strong	0.34	2.066	6000	Strong	0.46
		85	2.039	6080	Strong	0.26	2.026	6120	Strong	0.26	2.025	6120	Strong	0.255
						2.1	5900	Strong	0.38	2.1	5900	Strong	0.51	
						2.06	6000	Strong	0.27	2.06	6000	Strong	0.28	

Table 6.3: The energy position and the band width at half height for deep centre (self-activated)

bands observed in FEL, PL and REL of Au-ZnSe diodes containing donors.

6.6 DISCUSSION

6.6.1 Mechanism for Electroluminescence

(a) Forward bias (injection) electroluminescence

Injection electroluminescence depends strongly on the efficient injection of minority carriers into the zinc selenide and their subsequent radiative recombination. Hole injection in Au-ZnSe diodes prepared on n-type material with no interfacial layers is negligible because the hole barrier which is defined as the energy bandgap minus the electron carrier is about $\phi_{\text{Bh}} \approx 1.3$ eV. However the inclusion of an insulating layer between the metal and the semiconductor allows the Fermi level to move towards the valence band and holes from the vicinity of the Fermi level in the gold can be injected into the semiconductor. This type of injection with consequent EL emission has been observed in wide gap semiconductors, including ZnSe by Fisher (1964), Fisher and Moss (1963) and more recently by Livingstone et al (1973). Similar observations have also been made using III-V semiconductors, for example in GaP by Card and Smith (1971) and Haeri and Rhoderick (1974). The fact that we have only been able to observe forward electroluminescence in Au-ZnSe diodes, in the presence of a relatively thick ($\geq 200 \text{ \AA}$) semi-insulating layer under the gold leads strong support to the basic model described above. The hole barrier height, ϕ_{Bh} , is calculated to be about 1.0 eV in Au-ZnSe diodes prepared on chemically cleaned surfaces. The hole injection efficiency, i.e. the fraction of the total current across the junction carried by holes, is low. This was estimated to be 10^{-5} for Au-ZnSe by Livingstone et al (1973). They also suggested that the hole injection efficiency had no strong temperature dependence. The similarities which we have observed in the thermal quenching of FEL and PL would indeed suggest that the intensity of the light output was largely determined by the radiative recombination efficiency rather than the hole injection efficiency. On the other hand, the light intensity is a measure

of the hole injection process. Therefore one might suggest that the voltage threshold for light emission is the bias necessary to align the valence band of ZnSe with the Fermi level in gold. This threshold voltage was found at 1.2 - 1.4 V at 295 K and 1.4 - 1.6 V at 85 K. If the minority injection and radiative recombination mechanisms were 100% efficient the luminance would be proportional to the square of the diode current, because of the two stage (bimolecular) recombination process. In our experiments the brightness varied with current as $B \propto i^{1.5}$. The variation is to be compared with similar variations ($B \propto i^{1.5}$) reported for the injection electroluminescence from $\text{Cu}_2\text{Se} - \text{ZnSe}$, p-n heterojunctions by Aven and Cusano (1964) and recently from phosphorous ion-implanted ZnSe p-n junction diodes by Park and Shin (1974).

The maximum brightness reached in FEL was about 20 ft-Lambert at 295 and 250 ft-Lambert at 85 K. This corresponds to light output powers of 0.25 and 3 μW at 295 and 85 K respectively. This should be compared with the light output power of about 1.2 μW obtained in phosphorous ion-implanted ZnSe p-n junction injection diodes.

The power efficiencies of the injection devices studied here were poor, i.e. typically of the order of $10^{-6} - 10^{-5}$ %. This is attributed partly to the extraction of electrons from the barrier region of the ZnSe into the gold. If the model suggested in the previous chapter for the Au-ZnO-ZnSe system (see Figure 5.21) is correct, the only barrier that could suppress electron extraction is that of the depletion layer. The barrier is expected to decrease and become flatter at higher applied biases, thus enhancing the extraction process, so that the luminance would decrease with increasing bias.

(b) Reverse bias EL

Reverse bias EL from Au-ZnSe Schottky diodes was reported recently by Allen et al (1972). They suggested that the electrons tunnel from the metal into semiconductor and are then accelerated in the high field of the depletion layer before exciting the luminescent centres or host lattice. Luminescence occurs following the subsequent recombination of the excited carriers. Our observations support this basic model. However, the indications are that in reverse bias, electrons are thermally activated over and also tunnel through the barrier in their passage into ZnSe (see Chapter 5). Impact excitation or ionization processes require electrons with kinetic energies of about 2 - 3 eV. The electric field of 10^5 V cm^{-1} or more which is present in the depletion region would be adequate to accelerate the electrons to the required energies. The lowest threshold for light emission in reverse biased Au-ZnSe diodes was about 2.5 V. Since impact excitation is a mono-molecular process the luminance would be expected to vary linearly with diode current. In practice this variation could again be expressed as $B \propto i^n$ with the value of n near 1.2. The sub linear variation observed at high current is attributed to joule heating effects. At room temperature a maximum brightness of about 100 - 150 ft-L was achieved with undoped and donor doped ZnSe. This would correspond a light output power of 1.2 - 1.8 μW and power efficiency of about $10^{-4} \%$.

6.6.2 Spectral Distribution of the Luminescence

(a) Exciton emission in forward biased Au-ZnSe diodes has been reported previously by Ryall and Allen (1973). They studied the emission in the range of temperatures from 85 to 300 K and attributed it to free exciton recombination. We have observed the exciton emission in FEL over the wider temperature range from 20 - 360 K and have found that the

exciton became bound to neutral donors, or acceptors, at temperatures below about 65 K.

In contrast with FEL, exciton emission was not observed in PL or in REL. It is possible that with injection electroluminescence (FEL) a higher concentration of injected electrons and holes is produced. Possibly injected holes increase the exciton recombination cross section. If this were so, then one would expect hole injection to play a greater role in exciton emission. Furthermore, one would expect the relative intensities (i.e. recombination cross sections) of exciton and pair emission to depend on the hole injection levels. However, experimentally the ratio of the intensities of edge and exciton emissions was found to be independent of the diode current.

Furthermore when the diodes (for example diode No.172A) were operated at low current levels, at 20 K, the intensity of the pair emission in FEL was about 30 times smaller than the intensity in PL for the same diode at the same temperature. However the exciton emission was still present in FEL but not in PL. Therefore the suggestion that the observation of exciton emission in FEL results from a higher density excitation may not be correct. Another possibility is that the band edges may play an important role. Exciton emission lies in a region of very strong absorption in ZnSe, i.e. of exciton self-absorption. The observed emission would emanate from exciton recombination very near the surface. So the surface properties of the semiconductor might well play an important part. Swank (1966) has found considerable band bending, with $V_{BO} \approx 0.58$ eV, at the free surface of ZnSe which was cleaved in vacuum. The magnitude of the band bending in chemically cleaned samples will be larger (see Chapter 5). The donor concentrations in the diode samples that showed exciton emission were of the order 10^{16} cm^{-3} . This together with a band bending of about 0.58, would lead to a localised

electric field of the order of $10^4 - 10^5 \text{ V cm}^{-1}$ at the surface of the ZnSe crystal. In PL the UV excitation would be absorbed to create free electrons and holes at the surface. But because of the high field, the free electrons and holes would be accelerated in opposite directions. Consequently the probability of free electrons and holes coming together to form excitons would be reduced. The absence of the exciton emission in the REL spectra would also support this suggestion. The situation in FEL is quite different. At those biases, where the exciton emission was observed, the bands would be completely flattened, so that in the absence of a strong electric field, injected electrons and holes can come together within one hole diffusion length to form excitons. This is also in good agreement with the observation that the exciton emission from FEL was localised around the gold contact. The observation in this laboratory of exciton emission in PL from insulating (as-grown) crystals of ZnSe would support the above suggestions since flat bands are expected in insulating ZnSe. It is concluded that exciton emission in conducting crystals of ZnSe can only be achieved by creating flat energy bands in the region of excitation. Exciton emission in PL using conducting crystals of ZnSe has been observed by Dean and Merz (1968) and Merz et al (1972), but they used a high power argon ion laser, as the exciting source. The changes that the energy bands of ZnSe may have undergone when such sources were used is not yet known. However, surface photovoltage measurements on other II-VI compounds, e.g. CdTe, CdS by Swank (1966) indicate that the bands are completely flattened at high light levels. This would suggest that a similar band flattening may have been achieved in conducting ZnSe.

(b) Pair Emission

The pair emission was observed in FEL, PL and in some diodes in REL. Edge emission in PL has been studied by various authors, namely

Iida (1968), Dean and Merz (1969), Chatterjee et al (1973) and Gezci and Woods (1975). Edge emission in FEL from Au-ZnSe diodes has been reported at liquid N₂ temperatures (see for example Ryall and Allen 1973). However the first detailed study of pair emission in forward biased Au-ZnSe diodes is presented in this work. The pair emission observed in FEL and PL is regarded as associated with bound to bound and free to bound recombination at 20 and 65 K respectively. With a diode containing no intentionally added impurities (i.e. No.172A), the pair emission in FEL and PL was similar and the ionization energies of the acceptor and donors involved with this edge emission were calculated to be 122 ± 2 meV and 26 ± 2 meV respectively. A small trace of a second pair emission was also observed in this diode involving acceptor and donor levels with ionization energies of 93 ± 2 meV and 31 ± 2 meV. With diodes containing indium (e.g. diode No.139) a single set of phonon-assisted bands was observed in FEL and is attributed to recombination between donor and acceptor levels. However two sets of pair emission bands were observed in PL, and were attributed to bound to bound and free to bound transitions involving the same donor-acceptor levels observed in FEL. The ionization energies of the donors and acceptors were found to be 30 and 107 ± 2 meV respectively. Gezci and Woods (1975) have studied the edge emission in PL in as-grown ZnSe crystals in this laboratory. They observed three different series of pair emission bands associated with donor-acceptor recombination and they suggested that two of these series were associated with random and preferential pairing of the same donors and acceptors, with an ionization energy of the acceptor of about 112 meV. They calculated the ionization energy of the acceptor responsible for the third donor-acceptor pair emission to be 122 meV. They also suggested that the acceptor-like impurity with ionization energy of 112 meV would be leached out by the heat treatment in molten zinc. However the

results obtained here, suggest that this acceptor-like impurity with an ionization energy in the range 120 - 130 meV was still present after the Zn treatment.

The investigation of the edge emission in crystals doped with donor impurities showed that the intensity of the edge emission in FEL and PL decreased gradually as the donor impurity content increased, see for example Figures 6.2, 6.8, 6.13 and 6.14. (The donor concentrations are given for those diodes in Table 5.1). No edge emission was observed in FEL or in PL from diodes with donor impurity concentrations greater than 10^{17} cm^{-3} . The interesting feature was that as the edge emission disappeared, the intensity of the self activated (orange) emission gradually increased. This means that the blue edge emission is quenched by the acceptor-like levels introduced together with the impurity donors leading to preferential recombination of carriers to give rise to the S.A. emission. Edge emission was also observed in the REL spectrum of a few of the diodes but its intensity was much weaker than that in PL or in FEL and it was much more localized.

(c) Deep Centre Emission

The self-activated (S.A.) and copper emission from zinc selenide in PL has been reported by Holton et al (1965), Iida (1968), Markowski et al (1969). Recently Jones and Woods (1974) studied the PL emission and excitation spectra of ZnSe crystals doped with copper or chlorine. They reported that at 85 K, the S.A. emission band was located at 2.01 eV (6150 Å) while the copper, red and green bands were located at 1.95 eV (6340 Å) and 2.34 eV (5300 Å) respectively. They stated that the peak of the S.A. band shifted towards higher photon energies while that of the copper red band shifted towards lower photon energies with increasing temperature. Jones and Woods also observed that the copper

red emission was excited in a band centred at 2.43 eV (5100 Å) while the S.A. emission was excited strongly in a band centred at 2.55 eV (4855 Å). With regard to the orange emission band observed in the present work, it would appear that excitation occurs in a narrow band with its maximum equal or just below the band gap energy. This is true for undoped diodes (No.172A) or for diodes with low donor concentration (i.e. in diodes No.172B and 139). However with diodes doped with donors (i.e. Cl, I) with densities of the order of 10^{17} cm^{-3} , a lower energy excitation process would seem to be active, resulting in a broad excitation band peaking around 2.6 eV. In general, the minimum observed in the spectral response of the short circuit photocurrent coincided with the maximum in the excitation band for S.A. emission. This may suggest that the excitation of the S.A. band occurs in a localised centre and ionization does not occur so that there is no contribution to the short-circuit photocurrent.

From the thermal quenching of the S.A. band in FEL and PL, two ionization energies were found. The smaller of about 14 - 30 meV is attributed to shallow donors, but no clear identification for the second ionization energy of about 180 meV (in the indium doped diode No.139) or 360 meV (chlorine doped diode No.242) is obvious. Apperson et al (1967) have observed an acceptor level with an ionization energy of about 190 meV. Similarly Iida (1968) obtained a value of 350 meV for an undoped crystal. However, the investigation of the luminescence and the electrical properties of a large variety of ZnSe crystals by Jones and Woods (1974,1976) led to the suggestion that these ionization energies may well be associated with deep donors. Furthermore, Jones and Woods have suggested that deep donor-acceptor pairs, (with donor ionization energies of 0.37 and 0.41 respectively) were responsible for the S.A. emission.

Following a study of the PL of as-grown crystals (Jones and Woods 1974), it was suggested that most of our crystals appeared to have been contaminated by copper (1 p.p.m.) during their growth. However in the present work the crystals were treated in molten zinc. This process removes copper from ZnSe (Aven and Woodbury 1962). However a small trace of copper may have been responsible for the broad red and green bands observed in the FEL, PL and REL emission spectra of the undoped diode No.172. The situation is complicated when S.A. emission and copper emission are present together. The orange bands observed in FEL, PL and REL lay in the range of energies from 1.93 eV (6400 Å) - 2.15 eV (5750 Å). This large variation in energy may have been due to a small amount of copper which remained in our diodes even after the heat treatment procedure. However the S.A. emission undoubtedly swamped any copper emission in diodes containing high donor impurity concentrations, i.e. in diodes with I or Cl with $N_d \geq 10^{17} \text{ cm}^{-3}$. Here it is concluded that the S.A. band lay at about 2.10 V (5900 Å). The FEL, PL and REL emission spectra in these diodes were virtually identical. However if the S.A. is weak then weak copper emission is partly superimposed on the S.A. emission band. The emission spectra obtained from diode No.247 is thought to be an illustration of such a super-position. The excitation spectra for the orange band in this diode showed a broad band peaking at about 2.4 eV (5180 Å) which is typical of copper doped samples (see Chapter 7). The net effect of this super-position was that the copper red and green bands shifted towards one another.

In general the emission bands in FEL, PL and REL were similar, although the production of hot electrons in REL causes broadening with long tails extending to the high energy end of the spectrum. However, if there is a concentration profile of luminescent centres at the surface

of the diode ($\sim 20 - 100 \mu\text{m}$) slight differences in the FEL, PL and REL spectra can be observed. For example in the case of the gallium doped diode No.176, there is about 0.2 eV difference between the FEL and PL emission bands at 85 K. The lower energy emission in PL is thought to be due to recombination near the surface, while the higher energies observed in FEL emission are thought to be associated with recombination in the bulk of the diode. The peak energy of the REL emission band lies between these two.

CHAPTER 7

ELECTROLUMINESCENCE IN ZnSe DOPED WITH LUMINESCENT CENTRES,

i.e. MANGANESE OR COPPER

7.1 INTRODUCTION

Manganese and copper are well-known as efficient PL activators in many materials, e.g. zinc sulphide, calcium halophosphate and willemite. In this work therefore these activators have been introduced into zinc selenide in an attempt to produce efficient electroluminescent diodes. Manganese as an activator has recently been used successfully in d.c. ZnS electroluminescent panels (Vecht et al 1969) and ZnSe electroluminescent diodes (Allen et al 1972, Özsan and Woods 1974). In this chapter, the electroluminescent properties of Schottky diodes formed on ZnSe crystals containing manganese or copper, or both, will be described. The luminescent emission was studied in both forward and reverse bias. The total light output was measured in diodes with dimensions of $0.15 \times 0.15 \times 0.1 \text{ cm}^3$ and the brightness expressed in terms of Ft -Lamberts. The light output was recorded as a function of applied bias and diode current. The PL excitation and emission spectra were also studied together with the REL and FEL spectra. In the figures illustrating the emission and excitation spectra, the intensities are in arbitrary units.

7.2 ELECTROLUMINESCENCE AND PHOTOLUMINESCENCE OF ZnSe CONTAINING MANGANESE

Zinc selenide crystals, containing manganese, were grown by the vapour phase or iodine transport methods (see Chapter 3). The most successful boules were grown from the vapour, in capsules with 1500 p.p.m. manganese chloride in the tail and 1% manganese in the charge. Atomic absorption analysis showed that the crystals grown by both methods contained about 1% manganese. The electroluminescent diodes produced from these two types

of crystal were found to give essentially similar results. It is therefore necessary to discuss only one type of electroluminescent diode and we shall describe that fabricated from vapour grown crystals. The crystal growth conditions and the heat treatment procedures used for crystal No.246 containing manganese have been listed in Table 5.1, and some of the electrical properties of some of the diodes cut from this crystal have already been described in Chapter 5.

7.2.1 Forward bias electroluminescence (FEL) and photoluminescence (PL)

(a) Brightness/current voltage characteristics

The forward B/I-V characteristics of Au-ZnSe:MnCl, Zn diodes were found to be similar to those diodes containing donor impurities which were described in Chapter 6. Again no FEL was observed from diodes produced on cleaved surfaces (e.g. diode No.246A).

The forward B/I-V characteristics of a ZnSe; Mn, Cl, Zn diode, prepared on a chemically cleaned chip, cut from boule No.246, are illustrated in Figure 7.1. The brightness and current were found to vary approximately exponentially with voltage over at least three orders of magnitude. The brightness-current characteristics obeyed the usual relation $B \propto i^n$ with n equal to 1.5 at 295 and 1.8 at 85 K. The brightness of 0.6 Ft-L at 295 K, and 40 Ft-L at 85 K correspond to power conversion efficiencies of $3 \times 10^{-6}\%$ and $6 \times 10^{-4}\%$ respectively.

(b) Spectral Distribution

The spectral distribution of the FEL and PL emissions measured at 295 and 85 K from a ZnSe:Mn,Cl diode No.246E, are shown in Figure 7.2. The FEL emission contained a single broad band (see Table 7.1) peaking at 2.11 eV (5880 Å) at 85 K and 2.08 eV (5950 Å) at 300 K. This FEL

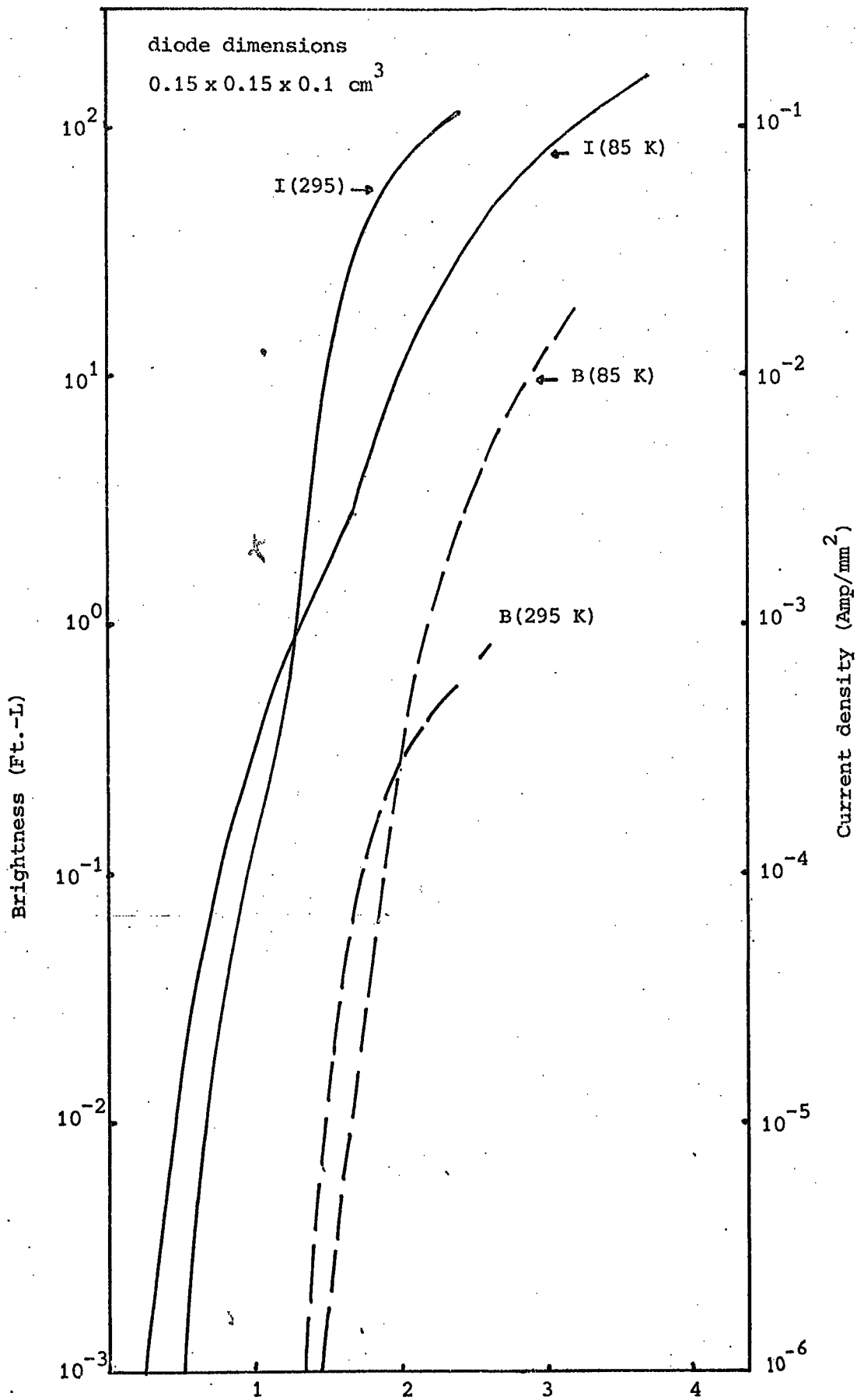


Figure 7.1: The forward brightness/current characteristics as a function of applied bias in ZnSe:Mn,Cl,Zn, diode No.246E

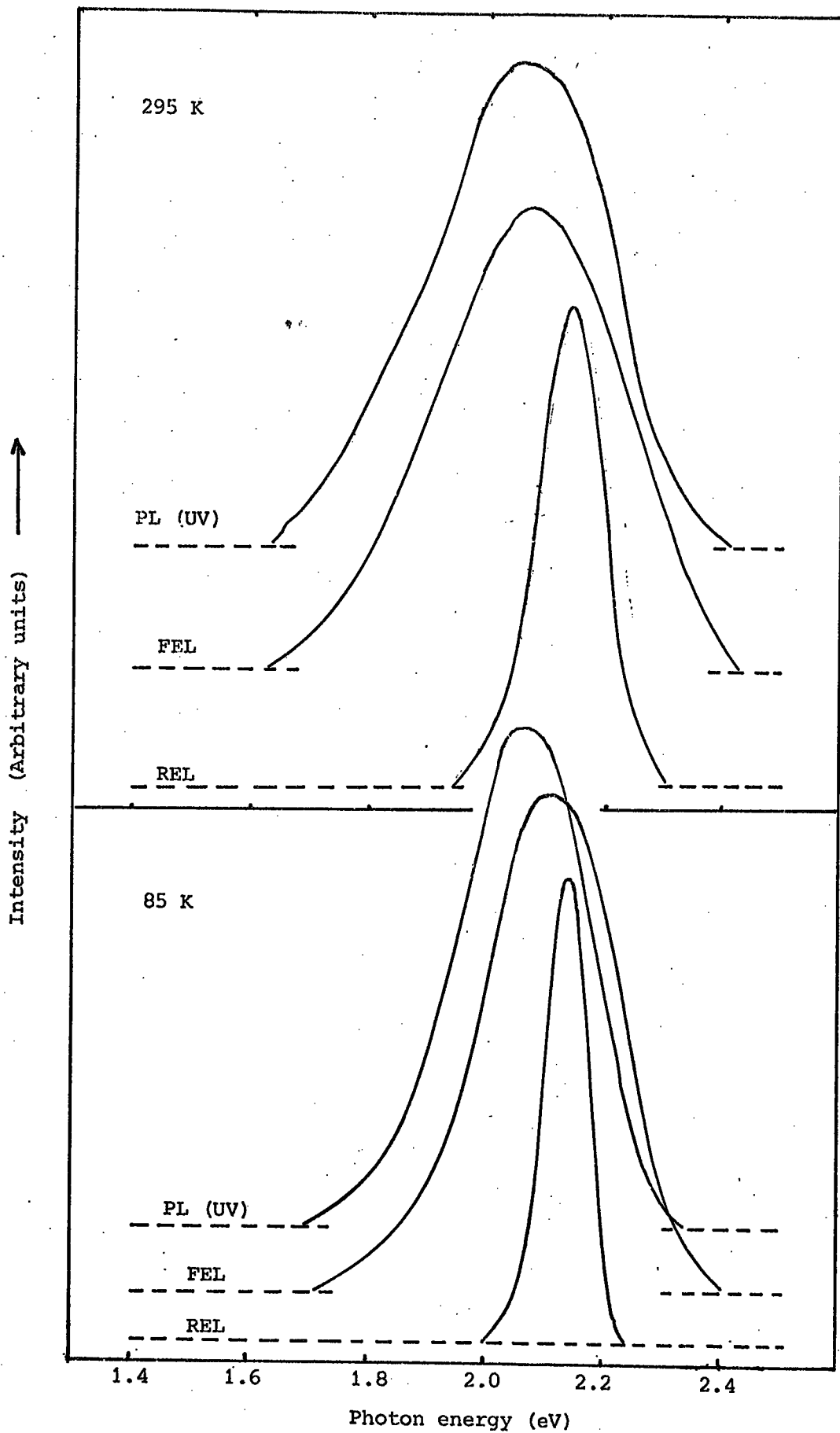


Figure 7.2: Spectral distribution for FEL, PL and REL emissions from ZnSe:Mn,Cl,Zn. Diode No. 246E

emission, in a manganese doped diode had its maximum at a slightly higher energy than that of the FEL emission observed in chlorine doped diodes (see Table 6.3).

The maximum of the PL emission (excited by UV radiation) was found at 2.05 eV (6050 Å) at 295 K and at 2.06 eV (6010 Å) at 85 K. At 295 K the PL excitation spectrum of the orange band showed a broad band peaking at about 2.38 eV (5200 Å) (see Figure 7.3). At 85 K the excitation spectrum contained two distinct bands at 2.45 eV (5065 Å) and 2.6 eV (4770 Å), see Figure 7.3. The excitation band at 2.45 eV was comparatively narrow and was not observed in any of our diodes which did not contain manganese. However the higher energy excitation band at 2.6 eV was observed in chlorine doped diodes (see Figure 6.18) and is attributed to the excitation of S.A. centres.

The PL excitation spectra, measured on some of our ZnSe:Mn,Cl,Zn diodes containing low concentrations of manganese, did not show the peak centred at 2.45 eV after heat treatment in molten zinc. The excitation spectra of these samples were similar to those of samples containing chlorine only.

7.2.2 Reverse bias Electroluminescence

(a) Brightness/current-voltage characteristics

The reverse B/I-V characteristics, at 295 and 85 K from a ZnSe:Mn,Cl,Zn diode prepared on a cleaved surface, are illustrated in curves (a) and (b), Figure 7.4 (295 K) and in curves (e) and (f) in Figure 7.4 (at 85 K) respectively. The reverse B/I-V characteristics of a second ZnSe:Mn,Cl,Zn diode (No.246B) prepared on a cleaved surface which was subsequently chemically etched are shown in curves (c) and (d) in Figure 7.4. In the preparation of diode No.246B, the gold layer was

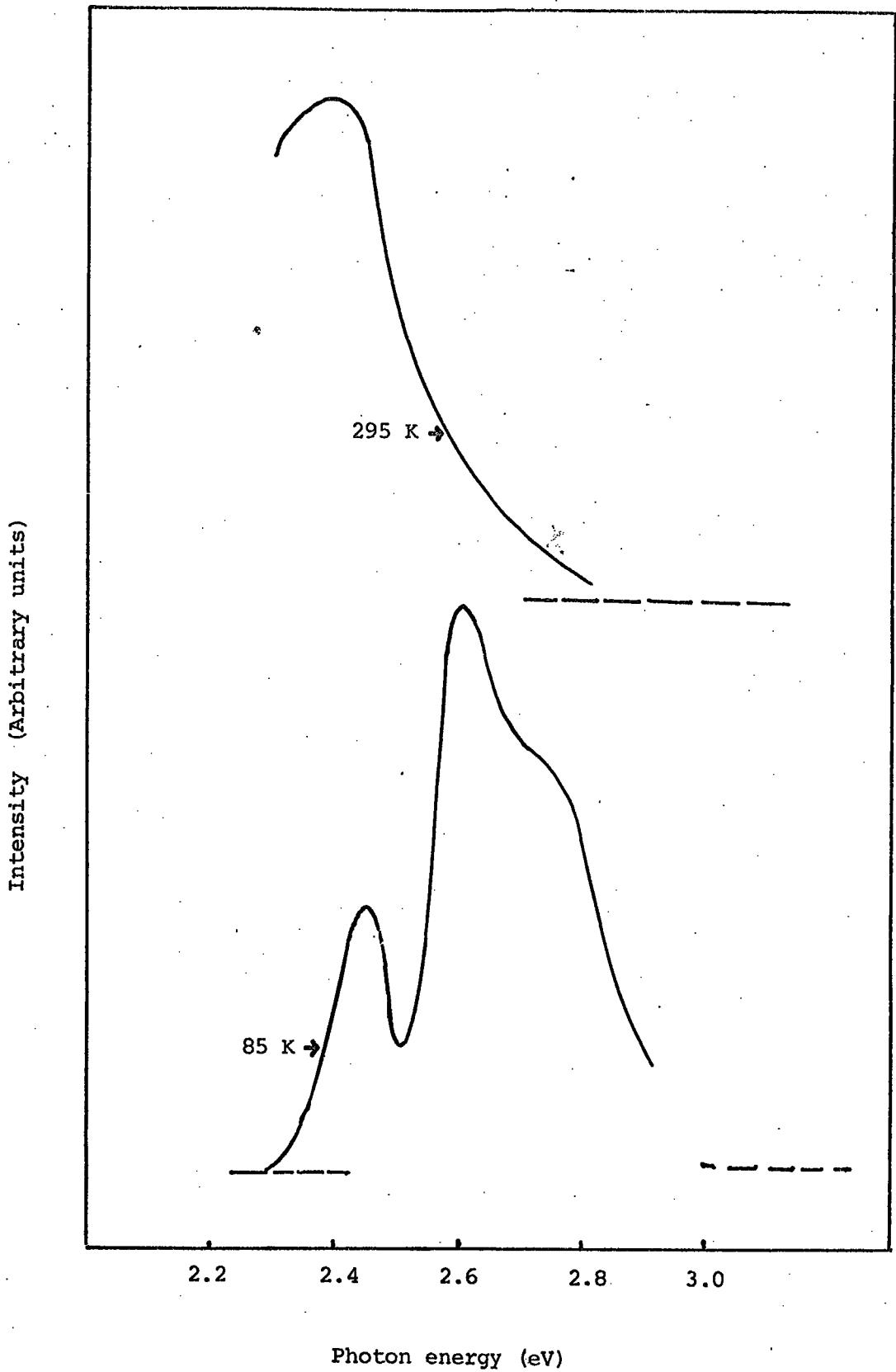


Figure 7.3: Luminescence excitation spectra for the yellow-orange band observed in PL in Au-ZnSe:Mn,Cl,Zn. Diode No.246E

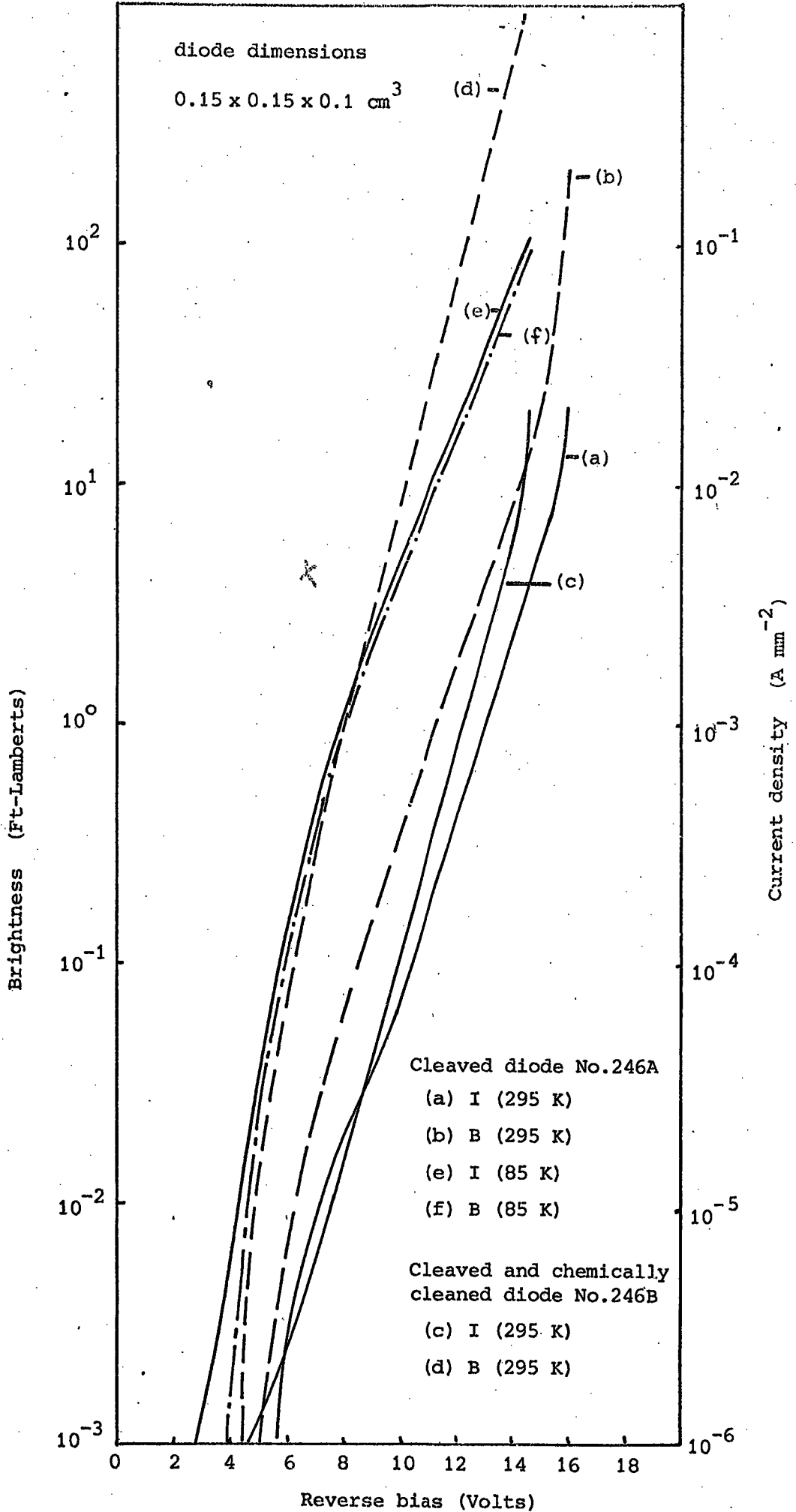


Figure 7.4: The reverse brightness/current variation as a function of applied bias in Au-ZnSe:Mn,Cl,Zn diode No.246E.

removed from the cleaved surface of the first diode, No.246A, and the chip was chemically etched prior to the redeposition of the gold contact.

With the cleaved diode (246A), the diode current increased rapidly at voltages below 8 V and then varied more or less exponentially with applied bias over three orders of magnitude of current. Similar behaviour was observed with the chemically cleaned diodes in which the leakage currents at low applied biases were more pronounced (not shown in Figure 7.4). With biases exceeding 15-16 V the current began to increase more rapidly than exponentially as an avalanche process developed. The B-V characteristics were almost parallel to I-V characteristics, at least at voltages higher than 8 V. The brightness increased more rapidly at low voltages, and it is meaningful to define a threshold for light emission which was usually found in the range 3.5-6 V. The light output increased with current according to the relation $B \propto i^{1.2}$. When the current density exceeded $5 \times 10^{-2} \text{ A mm}^{-2}$ the brightness began to decrease. This was thought to be due to local Joule heating. A maximum brightness of 200 Ft-L was measured for the cleaved diode No.246A, at 295 K, under which conditions the power conversion efficiency was $6 \times 10^{-4}\%$. At 85 K 100 Ft-L was obtained with a slightly lower power efficiency of $10^{-4}\%$. This was mainly due to the increased diode current at a given bias. The light output was much higher in diodes prepared on chemically cleaned surfaces. This is thought to be due to the formation of larger built in potential at the chemically cleaned surfaces (see Chapter 6.7). For example, maximum brightnesses of some 500 Ft-L were obtained for diode No.246S, and 800 Ft-L for diode No.246B leading to power conversion efficiencies of $1.9 \times 10^{-3}\%$ and $4 \times 10^{-3}\%$ respectively.

(b) Spectral distribution

The spectral distribution in REL was studied in large numbers of ZnSe diodes containing manganese. The emission consisted of a yellow band

Diode No.	Dopant	Temp (°K)	FEL Spectra				PL Spectra				REL Spectra			
			Energy (eV)	Wave-length (Å)	Relative Strength	Band-width (eV)	Energy (eV)	Wave-length (Å)	Relative Strength	Band-width (eV)	Energy (eV)	Wave-length (Å)	Relative Strength	Band-width (eV)
246	Mn,Cl	295	2.08	5950	Strong	0.34	2.05	6050	Strong	0.36	2.14	5780	Strong	00.13
		85	2.11	5880	Strong	0.27	2.06	6010	Strong	0.29	2.14	5780	Strong	0.09
165A	Cu Zn + Al	295	1.93	6400	Strong	0.36	1.95	6350	Strong	0.34	1.95	6350	Strong	0.36
			1.96	6300	Strong		1.96	6300	Strong	0.26	1.96	6300	Strong	
			2.19	5650	Shoulder		2.19	5650	Shoulder		2.19	5650	Shoulder	
			2.70	4580	Strong (zero-LO phonon)		2.70	4580	Strong (zero-LO phonon)		2.70	4580		
		65	2.67	4630	Medium (1-LO phonon)		2.67	4630	Strong (1-LO phonon)					
191	Mn,Cu,Cl Zn + Al		2.64	4685	Shoulder (2-LO phonon)		2.64	4685	Medium (2-LO phonon)		2.64	4685		
			2.615	4760	Weak (3-LO phonon)		2.615	4760	Shoulder (3-LO phonon)					
191	Mn,Cu,Cl Zn + Al	295					1.93	6400	Strong	0.27	1.93	6400	Strong	0.3
		85	1.93	6400	Weak		1.96	6300	Strong	0.23	1.96	6300		
											2.14	5780		

Table 7.1: The energy position and the band width at half height for the observed FEL, PL and REL emissions from ZnSe diodes containing manganese or copper or both.

with a maximum in the range 2.14 eV (5780 Å) - 2.1 eV (5900 Å). Some diodes emitted a peak at the low energy end of the above range, but these did not contain an additional band (at 2.45 eV) in their PL excitation spectra. It is considered therefore that they contained a low concentration of manganese. In contrast one of our diodes (No.246E), prepared from a boule containing 1% manganese, exhibited a room temperature REL emission band peaking at 2.14 eV (5780 Å) with a width at half height of 0.13 eV (350 Å). This width was much narrower than that of the FEL and PL emission bands observed in the same diode, (see Table 7.1). The REL emission was measured over the range 18-290 K at a constant reverse current of $3 \times 10^{-3} \text{ A mm}^{-2}$. The REL emission bands at 290 and 85 K are shown in Figure 7.2. The energy of the emission maximum remained virtually unchanged when the temperature was reduced to 18 K (see curve (a), Figure 7.5), but the band narrowed to a half width of 0.09 eV (240 Å) as the temperature was reduced to 100 K, and thereafter remained constant. A narrow band and the independence of its maximum with temperature are characteristic of the emission associated with transitions in localized manganese centres (see Chapter 2.3.4). To test whether the width of the emission band follows the relation given by equation 2.3.4 derived from the configurational coordinate model, (see for example Klick and Schulman, 1957), the square of the width of the band, $W^2(T)$, was plotted as a function of temperature T(K). According to equation 2.3.4, $W(T) \simeq W(0)$ and is independent of temperature at low temperatures. At high temperatures $W(T)$ should be proportional to $T^{1/2}$. The results plotted in curve (a), Figure 7.5 show that these conditions were obeyed. The slope of the straight line portion of the curves taken in conjunction with the value of $W(0)$ of 0.09 eV leads to a value of the phonon energy of 28 meV.

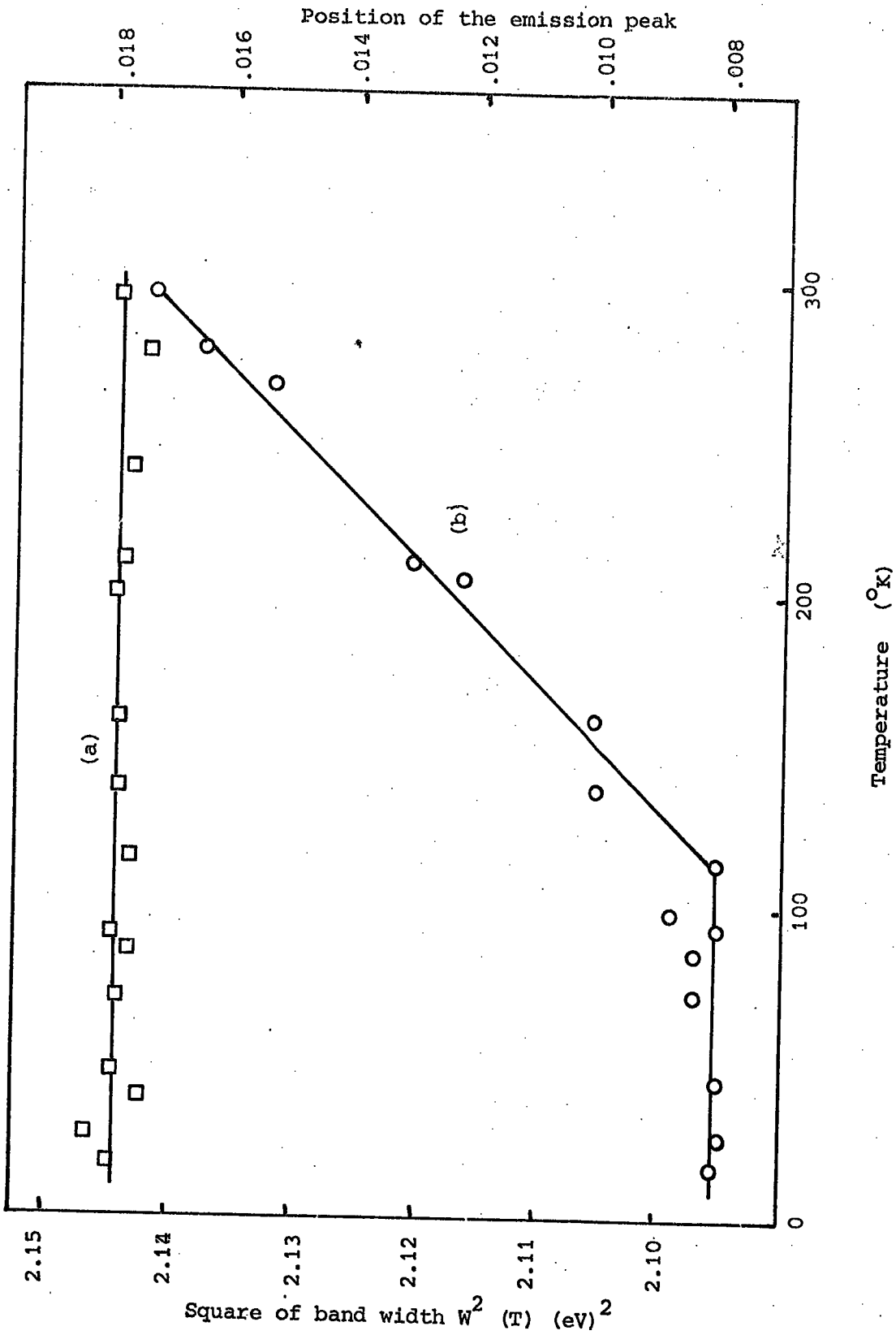


Figure 7.5: (a) Photon energy of the reverse EL emission maximum as a function of temperature for ZnSe:Mn,Cl,Zn. (b) Variation of the square of the width of the emission band at half height, $W^2(T)$, as a function of T.

7.2.3 Light output as a junction of temperature

In this section more detailed results for the temperature dependence of the light output from ZnSe:Mn,Cl,Zn diodes are given. The curves in Figure 7.6a show the variation of the light output with temperature for fixed current, in the cleaved diode (No.246A), and the chemically cleaned diode (No.246C). The variation of the applied bias required to sustain the fixed current is shown in Figure 7.6b. For temperatures below 260 K, the voltage at a fixed current changes almost linearly with temperature at a rate $\partial V/\partial T|_I$ of $1.6 \times 10^{-2} \text{ VK}^{-1}$ for the cleaved diode and $1.0 \times 10^{-2} \text{ VK}^{-1}$ for the chemically cleaned diode. At temperatures above 260 K, increasing voltage at fixed current leads to the avalanche region and $\partial V/\partial T|_I$ is very small. Clearly, the region where the light output increases with temperature in Figure 7.6a corresponds to the region where the voltage reaches the avalanching region in Figure 7.6b. This is further proof that impact excitation luminescence emission occurs in the localized manganese centres and that this process is strongly field dependent, but is temperature independent.

The temperature dependence (in fact a quenching) of the orange band in FEL and PL in this same diode was similar to that obtained from the diode (No.242) doped with chlorine only (see Figure 6.23). This result suggests that the FEL emission was substantially identical with S.A. emission.

7.2.4 Ageing of the light output in REL of ZnSe:Mn,Cl,Zn diodes

The effects of ageing on the electrical properties of some ZnSe:Mn,Cl,Zn diodes during prolonged d.c. operation were described in Chapter 5.9. In this section the effects of ageing in the reverse B-V characteristics and on the light output as a function of time will be described for diodes No.246A, 246B and 246C.

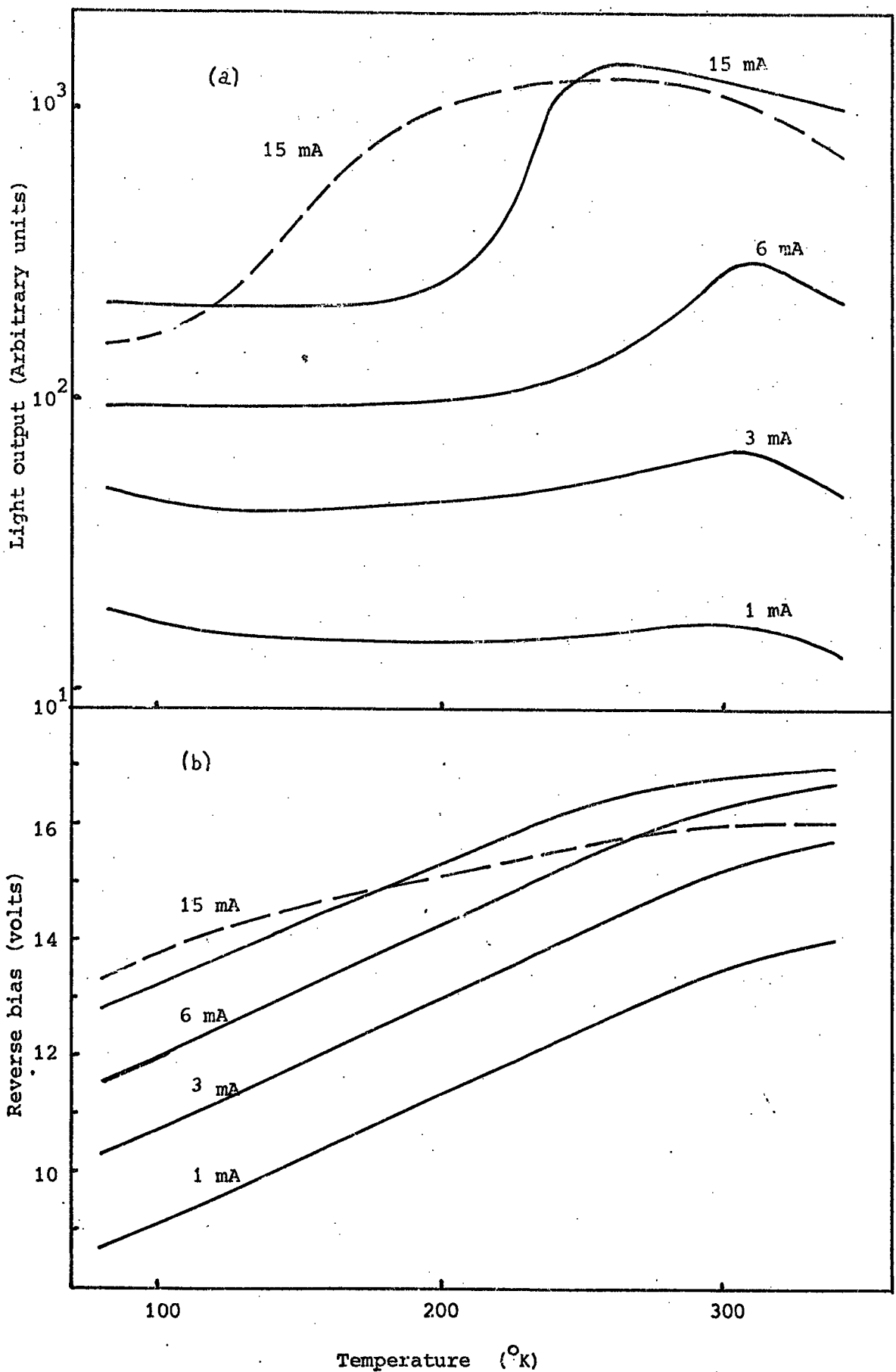


Figure 7.6: (a) The light output as a function of temperature, and (b) Reverse bias as a function of temperature; measured in Au-ZnSe:Mn,Cl,Zn diodes, operated at constant current (solid lines represent cleaved diode No.246A and broken lines represent chemically cleared diode No.246S)

The first diode examined was the cleaved one. The initial B-V characteristics were found to shift slightly to higher voltages, at least at biases greater than 9 V, after 350 and 1000 hours of operation at a constant current density of $1.5 \times 10^{-2} \text{ A mm}^{-2}$, see curves (2) and (3) in Figure 7.7. The initial brightness of 210 Ft-L increased steadily to 350 Ft-L after 1000 hours, see curve (a) in Figure 7.10. During this period the operating voltage rose from 16.06 V to 16.8 V, see curve (b) in Figure 7.10. The power conversion efficiency had almost doubled by the end of the ageing procedure. This behaviour is reminiscent of a slow forming process. The effect of ageing on some of the electrical parameters for this diode are listed in Table 5.3.

The B-V characteristics of the second diode (No.246B) which had been chemically etched, changed in an essentially similar way during 1000 hours operation. The B-V curve shifted almost parallel to themselves to higher applied biases during the ageing period, (see Figure 7.8). The initial brightness of 780 Ft-L increased to 860 Ft-L during 200 hours of operation at constant current ($1.5 \times 10^{-2} \text{ A mm}^{-2}$), see curve (c) in Figure 7.10. In this time the operating voltage rose from 14.5 V to 18.3 V. After this the brightness fell to 200 Ft-L after 1000 hours total operation in which the operating voltage increased further to 21.5 V (see curve (d), Figure 7.10). The power conversion efficiency decreased from an initial value of $4.3 \times 10^{-3} \%$ to $7.4 \times 10^{-4} \%$ after the total ageing time of 1000 hours. The changes in some of the device parameters during ageing are tabulated in Table 5.4. The effects of ageing on the B-V characteristics of the third diode (No.246S) are shown in Figure 7.9 and are similar to those of the other two diodes. The initial brightness of 280 Ft-L (see curve (c), Figure 7.10), increased to 500 Ft-L during the first 100 hours of constant current operation,

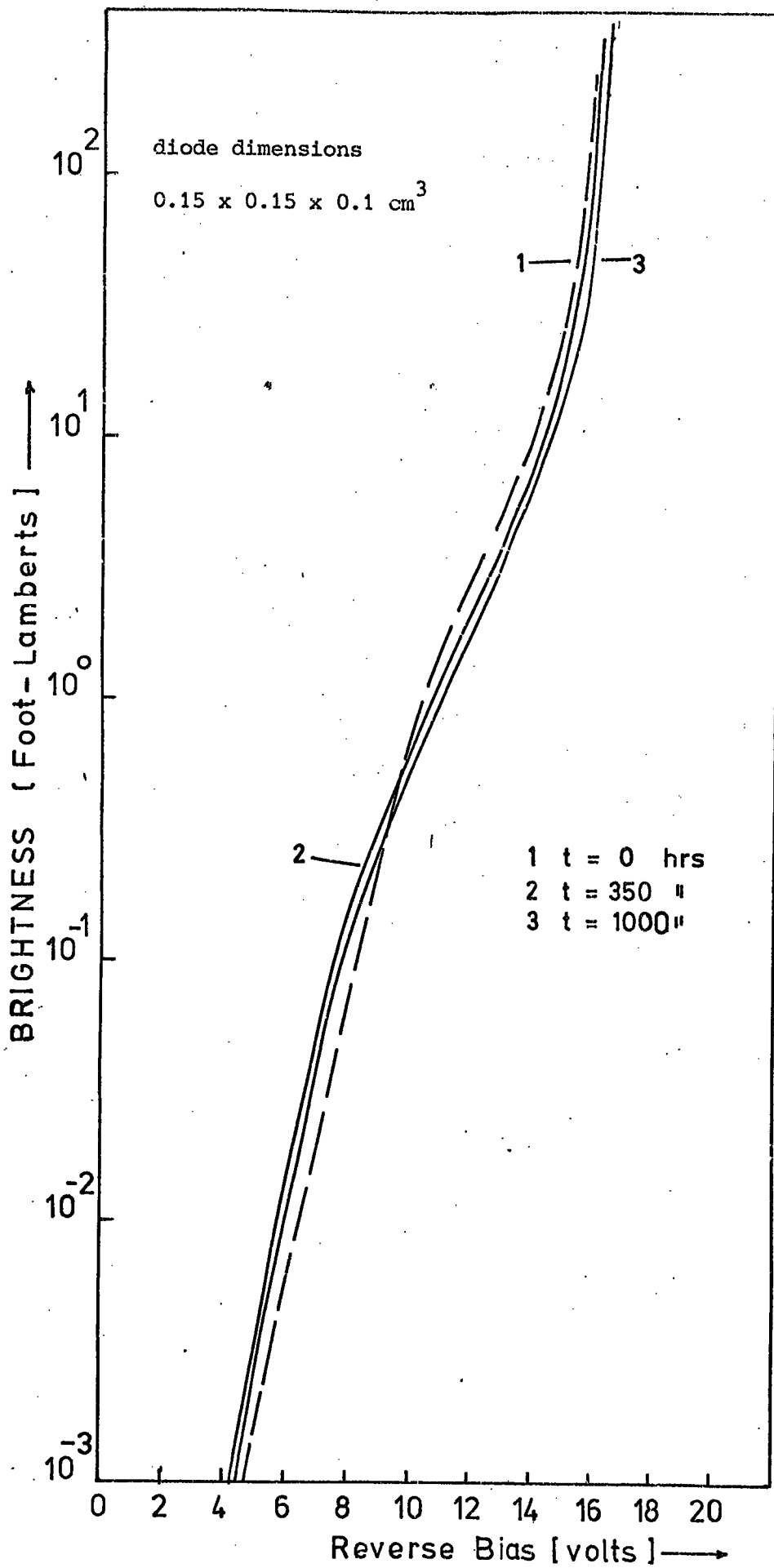


Figure 7.7: Ageing effect on Brightness — Voltage Characteristics for Au-ZnSe:Mn Diode prepared on cleaved surface.

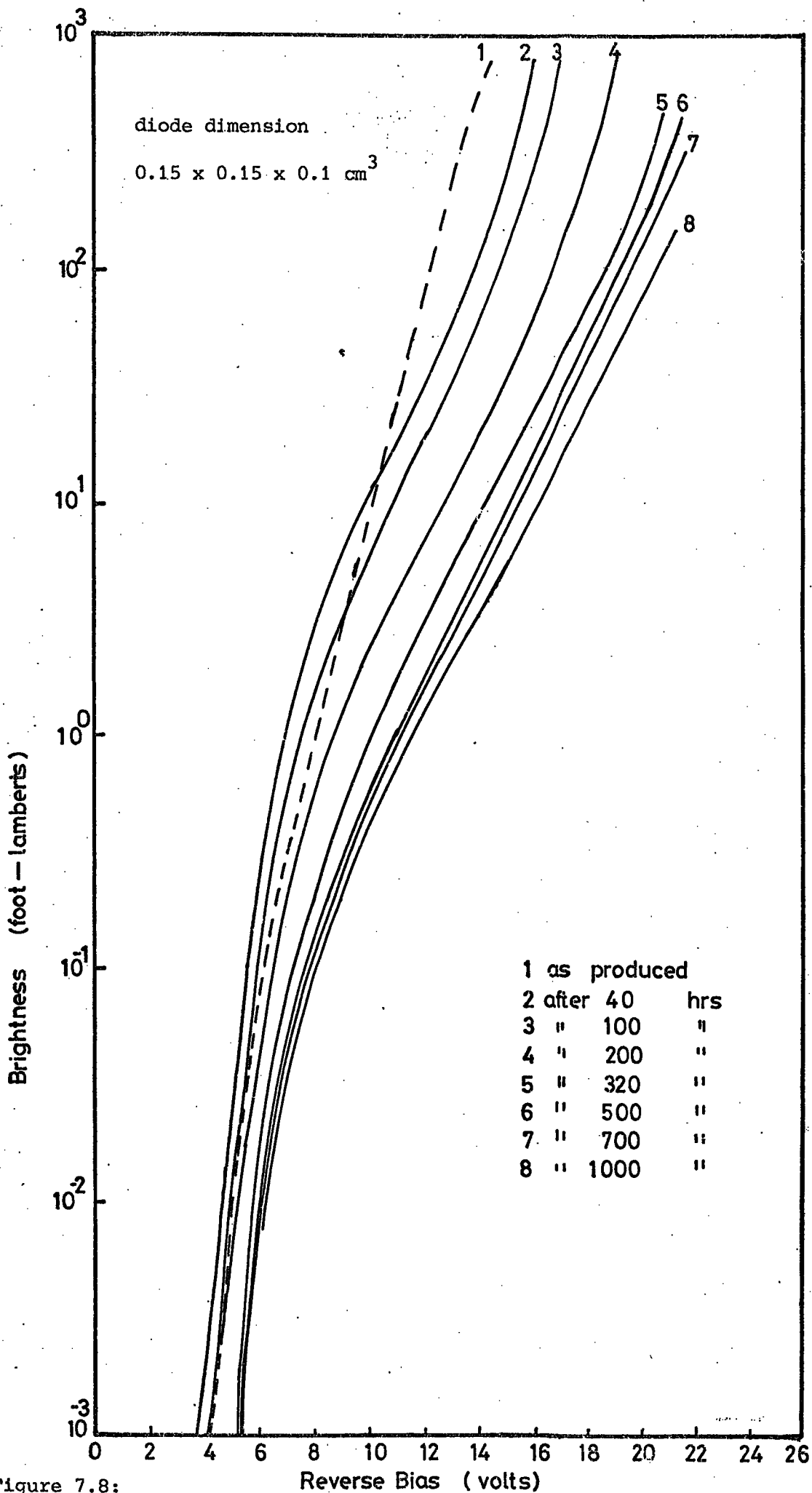


Figure 7.8:
Ageing effect on Brightness-Voltage Characteristics for Au-ZnSe:Mn diode prepared on chemically cleaned surface.

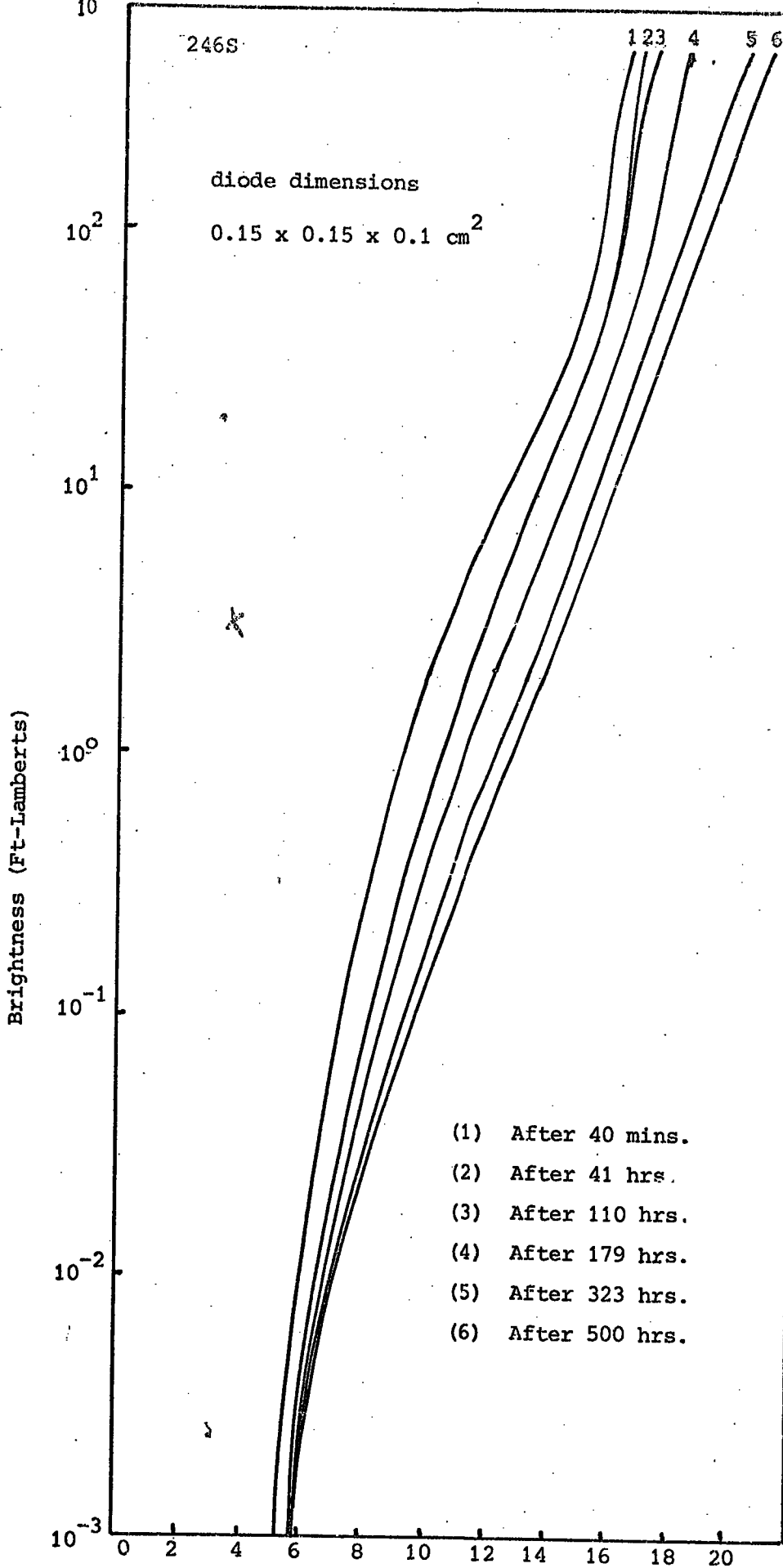


Figure 7.9: Ageing effect on brightness-voltage characteristics for Au-ZnSe:Mn,Cl,Zn, diode No.246S.

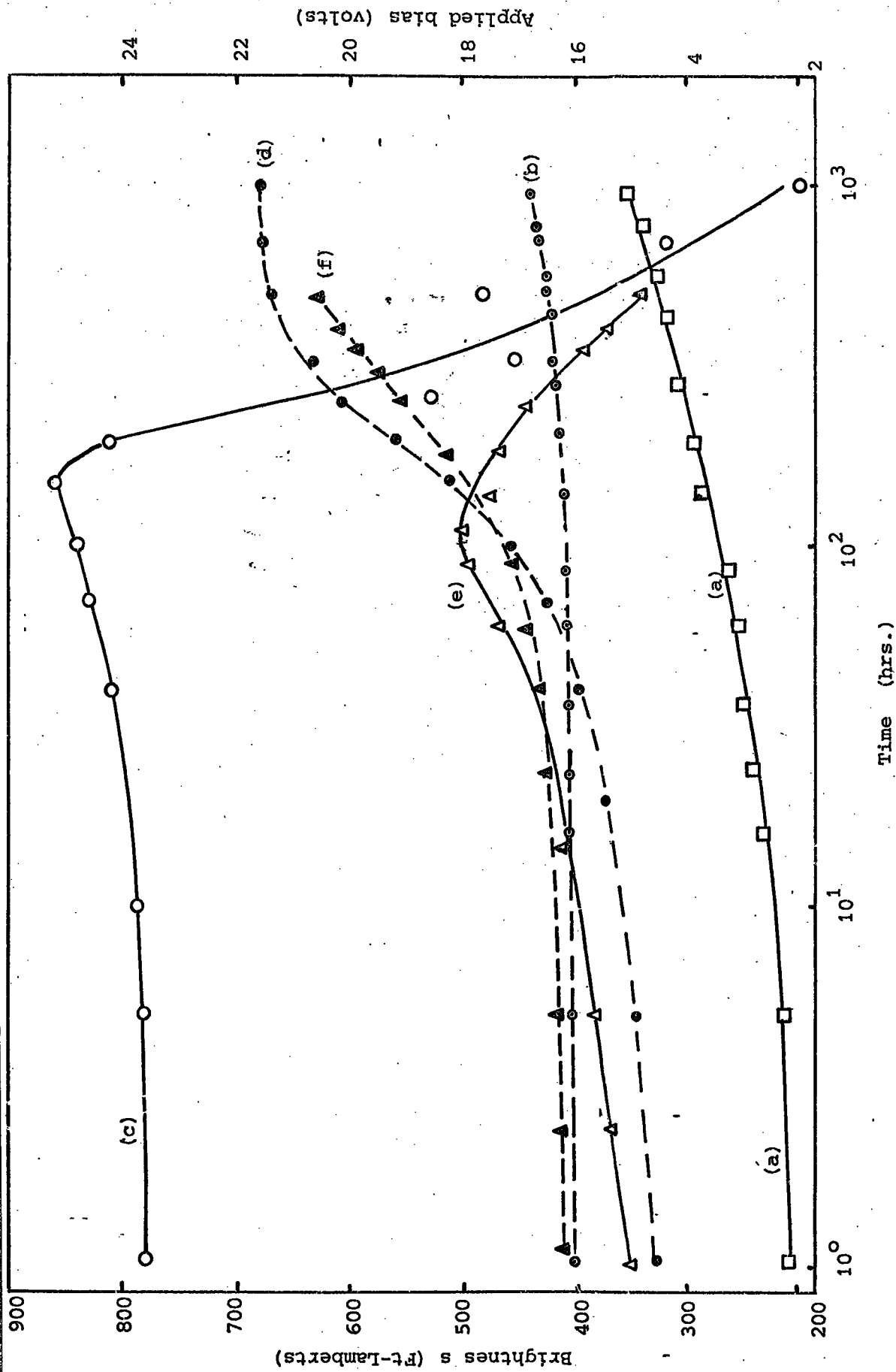


Figure 7.10: Solid curves represent the ageing in the light output of Au-ZnSe:Mn,Cl,Zn diodes with numbers (a) 246A, (c) 246B and (e) 246S. The broken lines show the change in the applied bias with time in diodes (b) 246A, (d) 246B and (f) 246S, respectively.

while the operating voltage increased from 16 V to 17.3 V, see curve (f) in Figure 7.10. Subsequently the brightness fell slowly to 340 Ft-L after 500 hours. The operating voltage, however, continued to increase to 20.1 V. The changes in the device parameters of this diode are tabulated in Table 5.5. Finally it should be mentioned that the fixed current densities of $1.5 \times 10^{-2} \text{ A mm}^{-2}$ at which the diodes were aged ensured that avalanching was occurring in all three diodes.

7.3 THE EFFECTS OF ADDING ALUMINIUM TO ZnSe:Mn,Cl DIODES

Recently, Allen et al (1972, 1973) reported a yellow electroluminescence from reverse biased Schottky diodes in ZnSe containing manganese and aluminium. They observed an emission band peaking at 2.10 eV (5900 Å) at room temperature which shifted slightly to 2.12 eV (5860 Å) at 100 K. In order to compare our results a little more closely with those of Allen et al, we have taken some of our crystals containing manganese and heated them for 7 days at 850°C in a molten mixture of zinc plus 20% aluminium. The resultant crystals were good semiconductors and the slopes of the $C^{-2} - V$ plots indicated that the uncompensated donor concentration was about 2-3 times higher than that obtained when similar crystals were heated in molten zinc only. Schottky diodes prepared from such crystals had properties similar to those described above, except that the highest luminances which could be achieved in reverse bias were slightly lower, of the order of 150 Ft-L, with power conversion efficiencies of $3 \times 10^{-4}\%$.

The other major difference was in the spectral distribution of the emission. The REL emission, at 300 K, consisted of a broad band at 2.07 eV (6000 Å) with a half width of 0.42 eV, see curve (1), Figure 7.11. There was a distinct shoulder in the red. The spectral distribution of

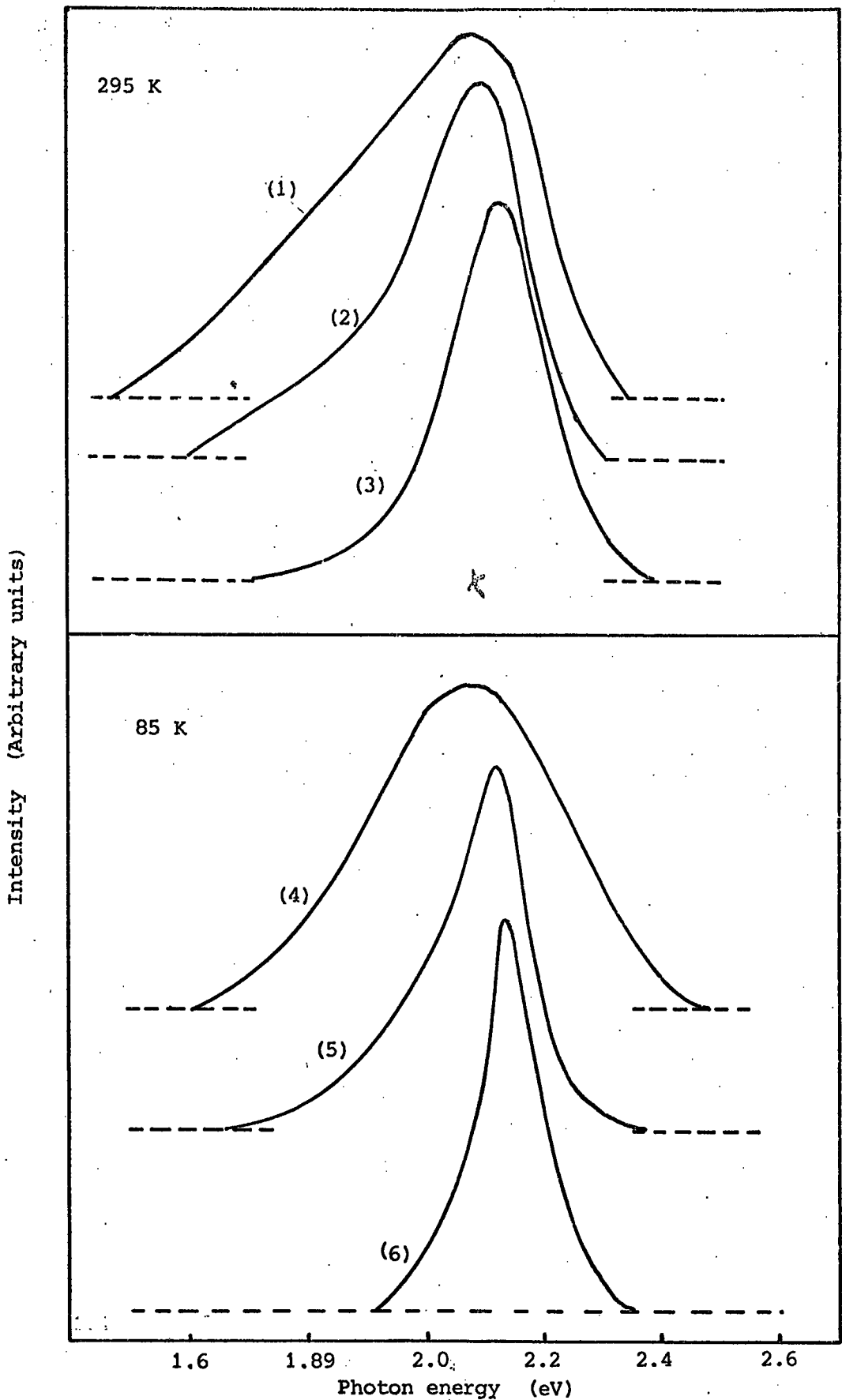


Figure 7.11: Spectral distribution of the REL in Au-ZnSe:Mn,Cl,Zn+Al diode, just after heating in molten zinc plus aluminium, (1) at 295 K, (4) at 85 K: After removing a 10 μm layer from the surface (2) at 295 K, (5) at 85 K: After removing further 10 μm layer (3) at 295 K, (4) at 85 K.

the REL emission was still broad (0.34 eV) at 85 K, with no change in the peak position (see curve (4), Figure 7.11). The FEL and PL emission bands, observed in this diode, both exhibited broad bands (0.35 eV) peaking at 2.066 eV (6000 Å) in FEL and 1.98 eV (6250 Å) in PL emission.

To determine whether the changed behaviour was attributable to diffused-in aluminium, the contacts were removed from this diode, and it was mechanically polished to remove approximately 10 µm from the surface to receive the gold electrode. The contacts were then remade in the usual way. The REL consisted of a comparatively narrow (0.23 eV) band peaking at 2.08 eV (5950 Å) at 295 K, see curve (2), Figure 7.11. The whole polishing and re-fabrication process was then repeated once more after which the REL spectral distribution was found to have narrowed further to 0.2 eV with a modified band maximum at 2.12 eV (5850 Å) at 295 K, see curve (3) in Figure 7.11. Curves 4, 5 and 6 in Figure 7.11 were measured at 85 K and correspond to curves 1, 2 and 3 which were measured at room temperature. The REL emission of the final diode, peaking at 5850 Å at 295 K and 5820 Å (with a band width of 0.17 eV) at 85 K, see curves (3) and (6), is very similar, although still somewhat broader, to that shown in Figure 7.2 for a ZnSe:Mn,Cl,Zn diode containing no aluminium. These results indicate that there was a concentration gradient of aluminium extending 20-40 µm into the original crystal, following the heat treatment in molten zinc and aluminium. The aluminium was directly responsible for the extended emission in the red, which was superimposed on the characteristic manganese emission.

7.4 ELÉCTROLUMINESCENCE AND PHOTOLUMINESCENCE IN ZnSe CRYSTALS DOPED WITH COPPER AND ALUMINIUM

When required, copper was introduced to zinc selenide crystals during the crystal growth procedure. For example, crystal No.165A was

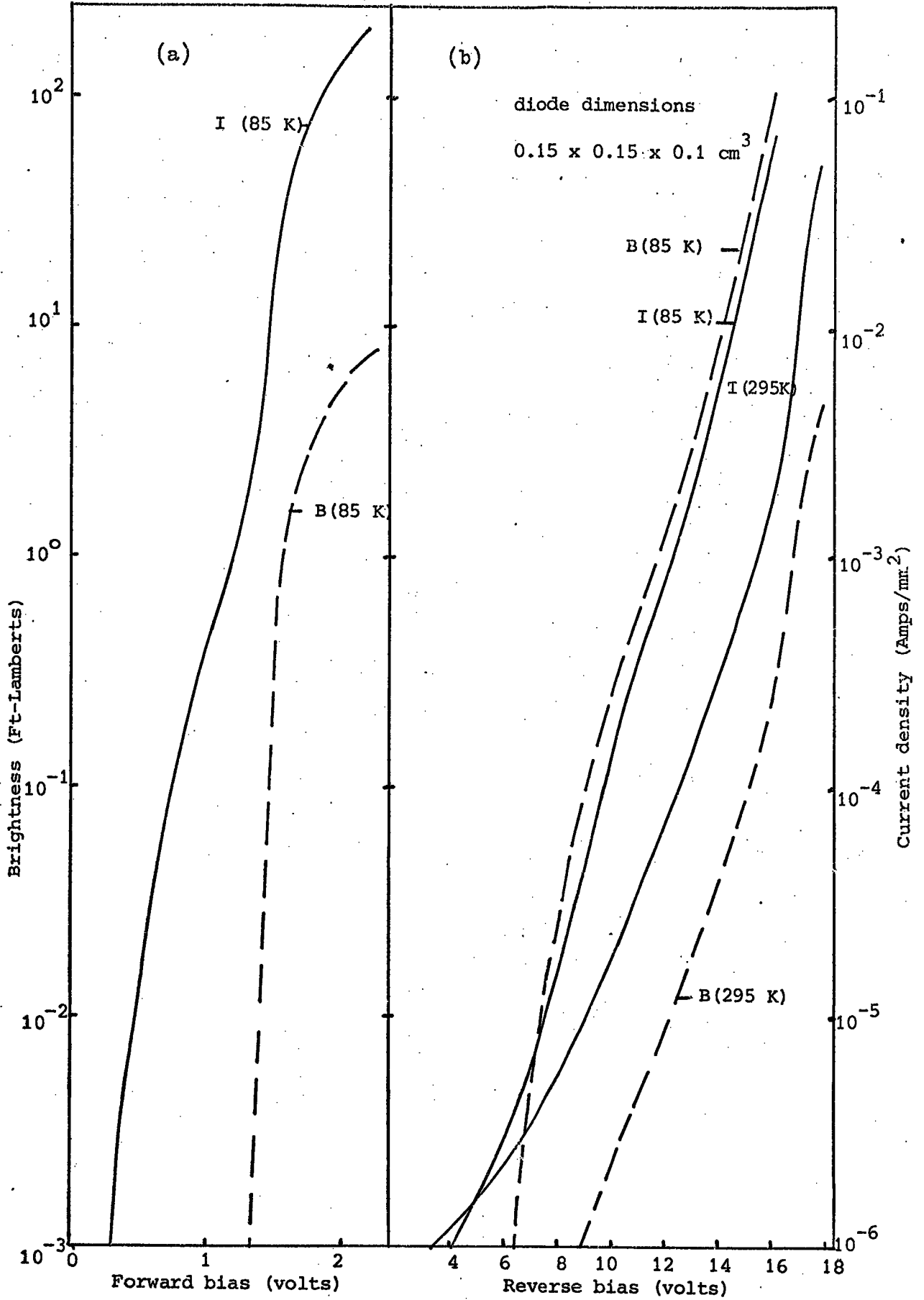


Figure 7.12: Brightness/current characteristics as a function of applied bias in Zn-ZnSe:Cu,Zn+Al, diode No.165A

grown with 100 p.p.m. copper selenide in the charge. To obtain conducting samples the crystal was heat treated in molten zinc plus 10% aluminium. The crystal growth parameters and details of the heat treatment administered to this sample have been recorded in Table 5.1. Some of the electrical parameters of Schottky diodes (e.g. diode No.165A) prepared on such crystals are also discussed in Chapter 5.

7.4.1 Forward electroluminescence and photoluminescence

(a) Brightness/current - voltage characteristics

The forward B/I-V characteristics, recorded at 85 K are illustrated in Figure 7.12a. Light emission was observed with a threshold of 1.3 V. The brightness current relation could be expressed in the form $B \propto i^{1.3}$ for biases greater than 1.4 V. This diode had a poor power conversion efficiency of about $2 \times 10^{-5}\%$ at a brightness of about 8 Ft-L at 85 K.

(b) Spectral distribution

The spectral distributions of the FEL and PL emissions were measured at 295 K and 65 K and are illustrated in Figure 7.13. The emission spectra at 65 K consisted of two parts, namely edge and deep centre emission. The edge emissions observed in FEL and PL were identical. An LO-phonon energy of 30.4 eV was again calculated from the equal energy separation of the phonon assisted bands (see Table 7.1). Assuming that this emission is of the free to bound type, and using an energy of 2.706 eV (4580 \AA) for the zero-phonon component, and 2.812 eV for the band gap energy, equation (2.3.3) gives an ionization energy of 111 meV for the acceptor involved in these transitions.

The deep centre emission, at 85 K, consisted of two bands with maxima lying at 1.96 eV (6300 \AA) and 2.2 eV (5650 \AA) both in FEL and PL.

Intensity (Arbitrary units)

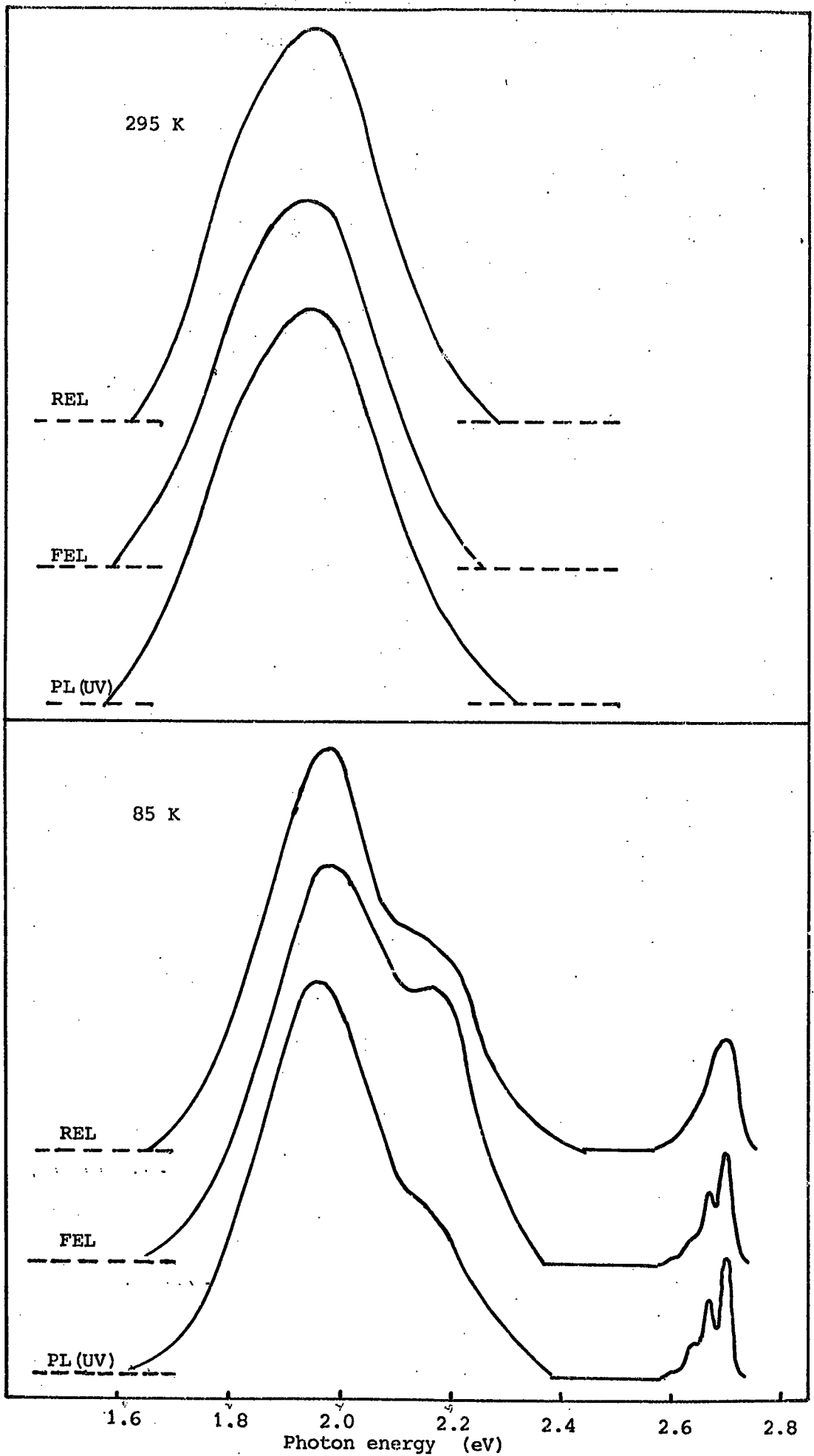


Figure 7.13: Spectral distribution for the REL, FEL and PL emissions from ZnSe:Cu,Zn + Al diode No.165A

At 295 K, both the FEL and PL emission exhibited a single broad band peaking at about 1.93 eV (6400 Å).

The luminescence excitation spectra of the red band in PL emission were recorded at 295 and 85 K and they are shown in Figure 7.14. Clearly the red emission is excited over a wide range of photon energies with a maximum efficiency at about 2.3 eV (5400 Å) at 295 K and at 2.38 eV (5200 Å) at 85 K respectively. A distinct shoulder was also apparent in these excitation spectra, at 2.63 eV (4700 Å) at 295 and 2.75 eV (4500 Å) at 85 K.

7.4.2 Reverse bias electroluminescence

(a) Brightness/current-voltage characteristics

The reverse B/I-V characteristics, at 295 and 85 K, are illustrated in Figure 7.12b. Both current and brightness varied roughly exponentially with voltage. At biases greater than 16 V, avalanching began. The B-I variations can again be expressed as $B \propto i^{1.2}$. Brightnesses of 100 Ft-L were achieved at 85 K with a power conversion efficiency of $10^{-4}\%$.

(b) Spectral distribution

The spectral distribution of the emission was found to be similar to that in FEL and PL, see Figure 7.13. The green and blue emissions in REL were found to be localized around the gold contact. Because of the poor emission intensity, the phonon side bands could not be observed in edge emission.

7.5 ELECTROLUMINESCENCE AND PHOTOLUMINESCENCE IN ZnSe CONTAINING MANGANESE, COPPER AND CHLORINE

Some crystals doubly activated with manganese and copper have also been investigated. The manganese and copper were introduced into zinc

Intensity (Arbitrary units)

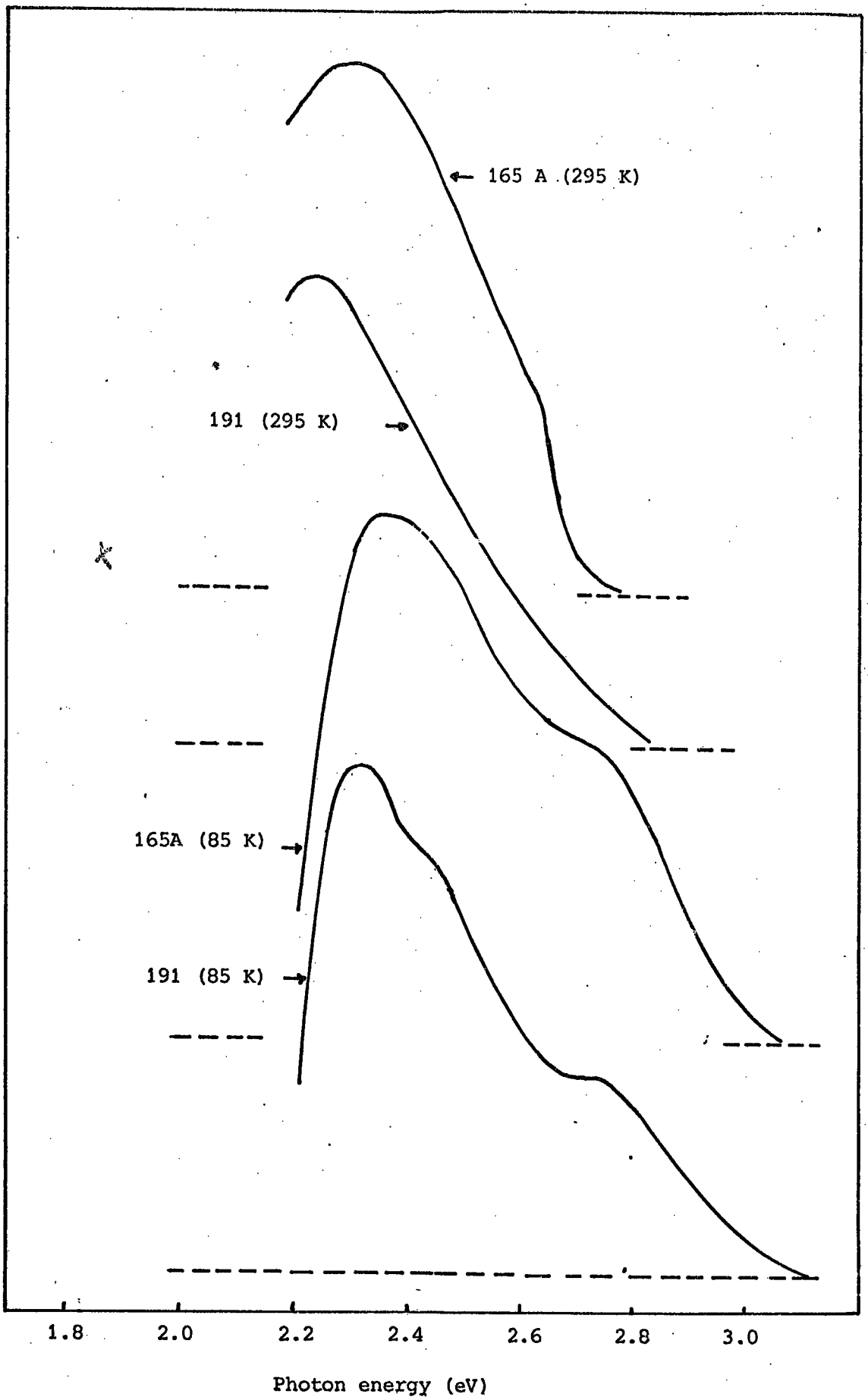


Figure 7.14: The luminescence excitation band of the red band in ZnSe;Cu,Zn + Al diode No.165A, and in ZnSe:Mn,Cu,Cl,Zn + Al, diode No.191

selenide during the growth procedure. For example the boule No.191 was grown from a capsule containing manganese chloride in the tail and 100 p.p.m. copper in the charge. In order to increase the conductivity of the as-grown crystal, the slices cut from the boule were heated in a molten mixture of zinc and 20% aluminium. The crystal growth parameter, and details of the heat treatment administered to these dice are tabulated in Table 5.1. The original yellowish colour of the dice were found to change to deep red after the heat treatment. However when the sides of one of the chips were polished and some 50 μm of the surface was removed, the original yellowish-orange body colour reappeared. The above mentioned dice, whether they had orange or red colours, were still quite good semiconductors. The Schottky barriers formed on these dice led to linear c^{-2} -V plots.

7.5.1 Forward bias electroluminescence and photoluminescence

(a) Brightness/current - voltage characteristics

The forward I-V characteristics of a ZnSe:Mn,Cu,Cl diode are shown in Figure 7.15. The forward current at a given bias was found to be almost one hundred times greater than that observed in any diode studied in this work. For example, at 295 K, a diode current density of $1 \times 10^{-1} \text{ A mm}^{-2}$ was obtained at a bias of 1.1 V. The I-V characteristics were exponential for biases exceeding 0.7 V. A poor light output of $5 \times 10^{-2} \text{ Ft-L}$ was observed at 1.4 V, at 85 K.

(b) Spectral distribution

No electroluminescence in forward bias was detected at room temperature, but at 85 K the FEL emission spectrum contained a band peaking at about 1.93 eV (6400 \AA). However a permanent record could not be made because the light output died out too quickly. The PL emission

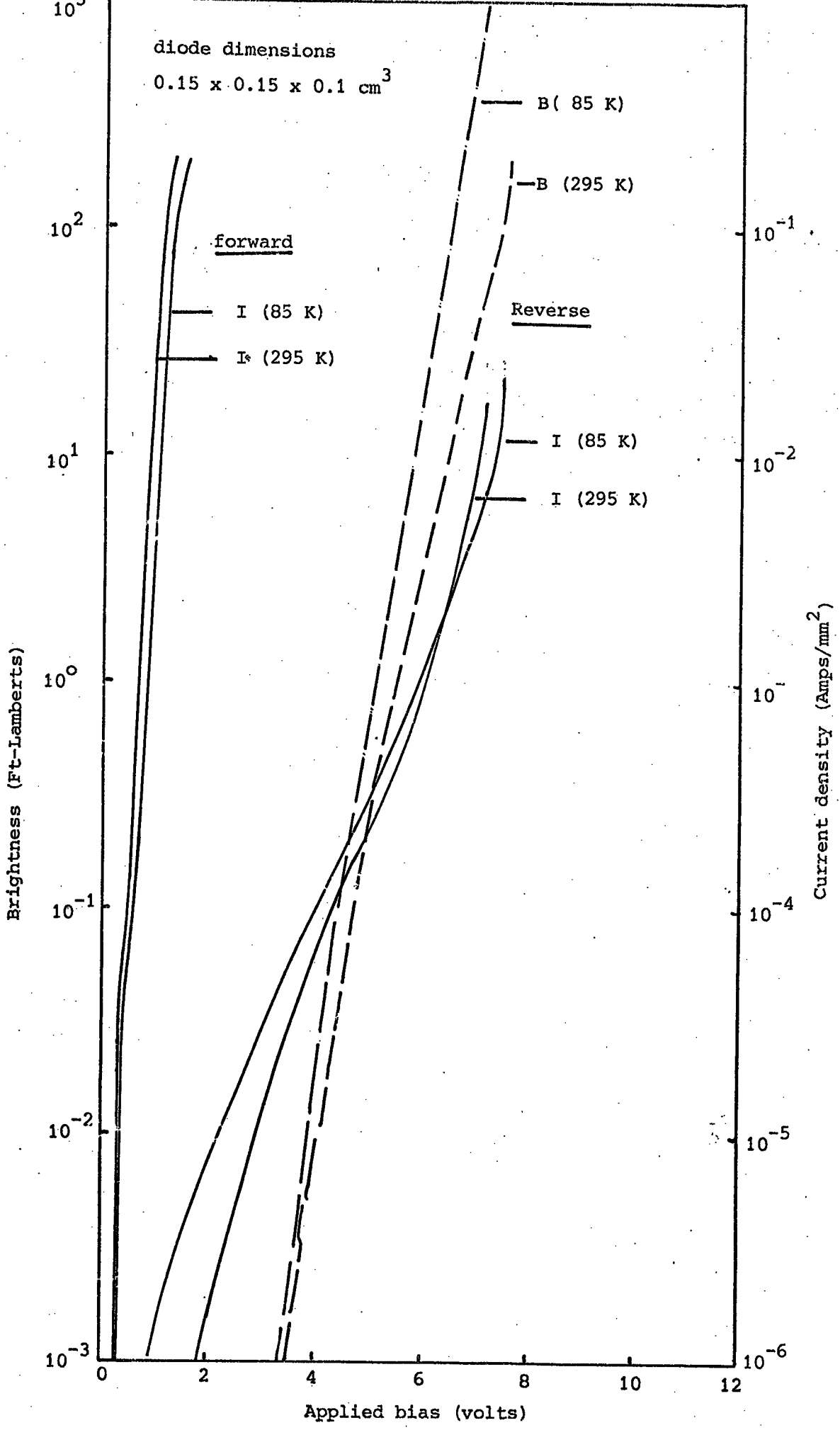


Figure 7.15: Brightness/current characteristics as a function of applied bias in Au-ZnSe:Mn,Cu,Cl,Zn+Al diode No.191

consisted of a single band peaking at 1.93 eV (6400 Å) at 295 K and 1.96 eV (6300 Å) at 85 K, see Table 7.1 and Figure 7.16.

The luminescence excitation spectra of the red band in PL were measured at 295 K and 85 K (see Figure 7.14). The red band was excited with a large range of photon energies with maximum efficiency at 2.25 eV (5500 Å) at 295 K. The maximum excitation at 85 K occurred at 2.31 eV (5350 Å) with a distinct shoulder at 2.75 eV (4500 Å). There was also a weak shoulder at about 2.46 eV (5040 Å) which is probably associated with manganese.

7.5.2 Reverse bias electroluminescence (REL)

(a) Brightness/current - voltage characteristics

The reverse current was found to flow at comparatively low applied biases in the ZnSe:Mn,Cu,Cl,Zn + Al diodes. Current densities of $2 \times 10^{-2} \text{ A mm}^{-2}$ were obtained at about 5 V in as-prepared devices. The initial I-V characteristics were stable with a weak light output. However, when the reverse bias was increased steadily the diode current started to decrease rapidly, but at the same time the light output increased drastically. This forming process continued for about 20 minutes before the B/I-V characteristics became fairly stable. They are illustrated in Figure 7.15.

The light emission first appeared at a threshold of about 3.5 V and the brightness increased nearly exponentially with applied bias over at least three orders of magnitude. Brightnesses of 200 Ft-L at 295 K and 2000 Ft-L at 85 K were achieved under which conditions the power conversion efficiencies corresponded to $1.5 \times 10^{-3}\%$ and $2 \times 10^{-2}\%$ respectively. The brightness-current characteristics in the avalanche regions follow the relation $B \propto i^{1.1}$.

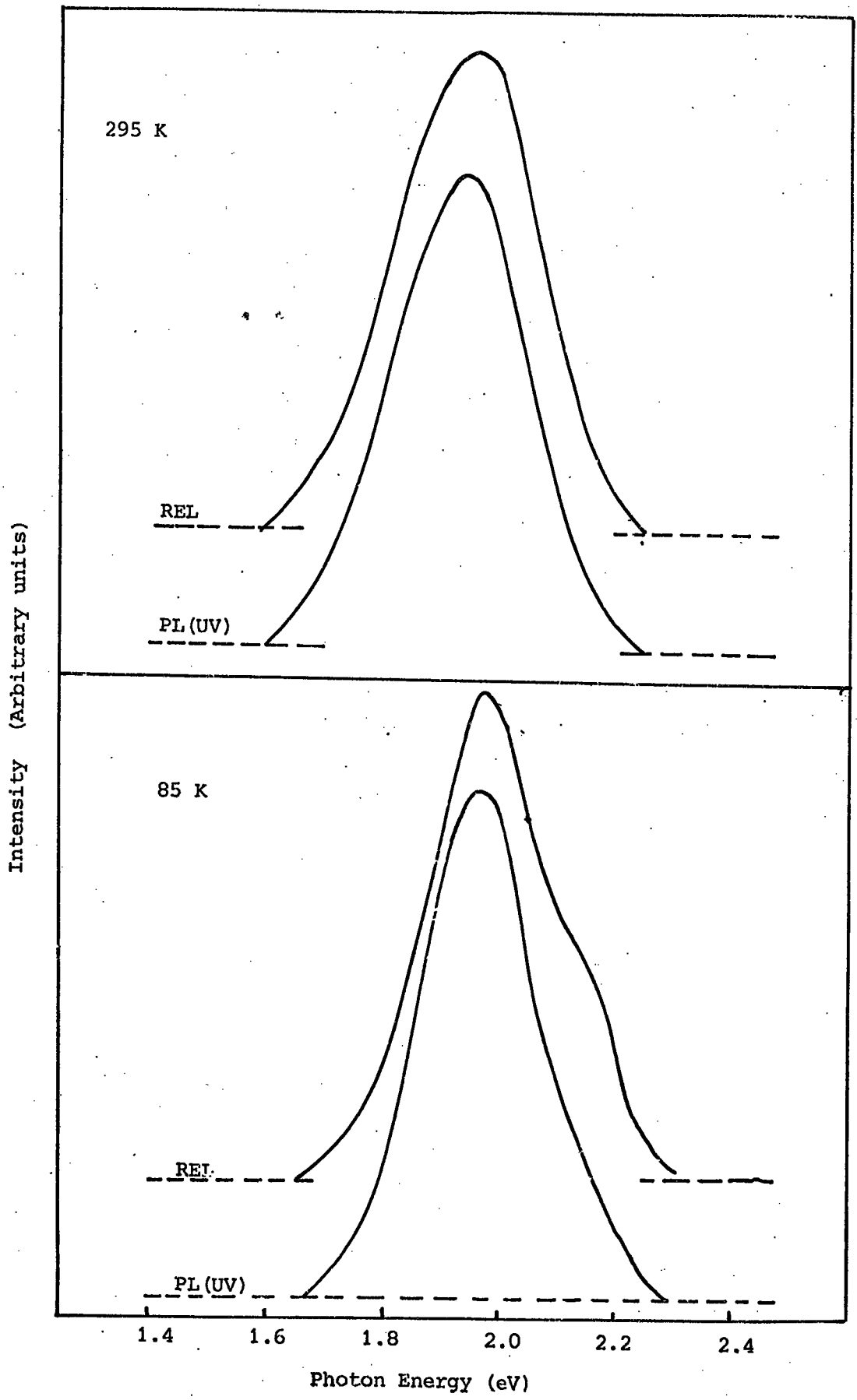


Figure 7.16: Spectral distribution for the REL and PL emission from Au-ZnSe:Mn,Cu,Cl,Zn+Al, diode No.191

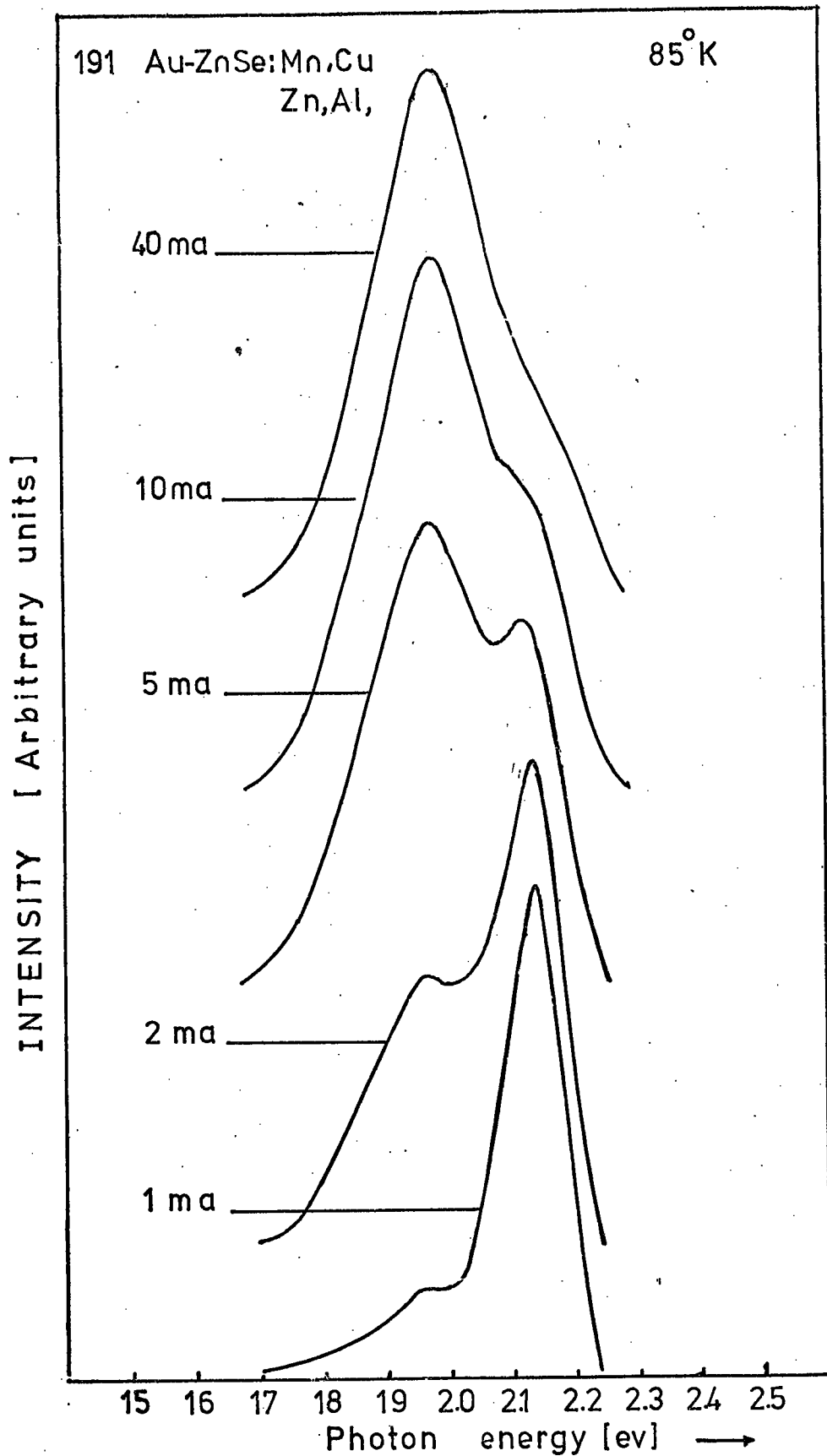


Figure 7.17: Reverse bias electroluminescence in Au-ZnSe:Mn,Cu,Zn,Al. diode as a function of diode current.

(b) The Spectral distribution

The spectral distribution of the REL emission of this diode operated at a high current density of $5 \times 10^{-2} \text{ A mm}^{-2}$, exhibited a single band peaking at 1.93 eV (6400 Å) at 295 K and at 1.96 eV (6300 Å) with a distinct shoulder at about 2.14 eV (5760 Å) at 85 K, see Table 7.1 and Figure 7.16. The visual effect was red. The spectral distribution of the REL emission, at 85 K, was found to change in shape at different diode current densities. When this diode was operated at lower current densities, the red band decreased in intensity as the shoulder in the yellow became more apparent (see Figure 7.17). At a density of $5 \times 10^{-3} \text{ A mm}^{-2}$, the REL emission spectrum consisted of two distinct bands with maxima at 1.97 eV (6270 Å) and 2.12 eV (5830 Å). As the diode current decreased further, the red band decreased in intensity and at current density of $1 \times 10^{-3} \text{ A mm}^{-2}$, the yellow band dominated the emission. The maximum of this yellow band was located at 2.14 eV (5780 Å) with a band width at half height of 0.01 eV (280 Å) and clearly this luminescence is almost certainly the characteristic manganese emission.

7.6 DISCUSSION

7.6.1 Mechanism for EL

The current transport mechanisms in reverse and forward biased ZnSe diodes doped with luminescence centres are obviously very similar to those observed in diodes containing substitutional donors. It follows, therefore, that the mechanisms of carrier injection and the excitation of luminescence are very similar to those already discussed in Chapter 6.6. In reverse bias, the dependence of brightness on current followed the relation $B \propto i^{1.2}$, suggesting strongly that hot electrons excite the luminescence centres by impact. In forward bias, however, minority

carrier injection is responsible for the observed luminescence. A brightness of 800 Ft-L (10^{-5} W), at a reverse bias of 14 V and current density of 1.5×10^{-2} A mm⁻², was achieved in the yellow region of the spectrum, from manganese doped devices. Inclusion of copper with manganese gave a red output with a brightness of 200 Ft-L at a reverse bias of 7.5 V and a current density of 2×10^{-2} A mm⁻². The magnitude of the light output in reverse bias was enhanced in the presence of an interfacial insulating layer, which is usually produced by the chemical etching procedure.

With one ZnSe:Mn,Cu,Cl,Zn+Al diode, No.191, the initial I-V characteristics exhibited comparatively high current levels at low applied biases. This may be a function of the lower barrier light as evidenced by the photoresponse measurements of Au-ZnSe diodes containing copper (see Figure 5.4). However these results are rather difficult to explain and will not be pursued here.

The interesting feature with ZnSe:Mn,Cu,Cl,Zn+Al diodes was that, as the reverse bias was increased from 3 V to 7.5 V, the initial high current density dropped quickly while the light output increased by an order of magnitude from 20 Ft-L to 200 Ft-L. This process was irreversible and is very similar to the process of "forming" reported in electroluminescent thin films (Plumb, 1971) and powdered layers of ZnS:Mn,Cu,Cl (Vecht, 1969). In the present work, this forming process has only been observed in single crystals of ZnSe containing Mn,Cu and Cl. The fact that the uncompensated donor concentration drops drastically from an initial value of 1.6×10^{17} mm⁻³ to 1×10^{16} mm⁻³ during forming, suggests the possibility of copper ionic migration in the high field of the depletion region affecting the electrical compensations.

A similar, but slower forming process has also been observed in the ZnSe diodes which contained manganese and no copper. This will be described in detail later.

7.6.2 Luminescence Transitions in Diodes containing Manganese

The optical absorption of ZnSe crystals containing manganese has been studied by Langer and Richter (1966). They observed three absorption bands, at 4.2 K, which were due to the tetrahedrally co-ordinated Mn^{2+} ion in ZnSe. The same bands were also observed by Jones and Woods (1973) who studied the luminescence excitation spectra of insulating crystals of ZnSe containing manganese. The absorption and luminescence excitation bands of Mn^{2+} are located at 2.30 eV (5300 Å), 2.45 eV (5060 Å) and 2.66 eV (4650 Å) at 85 K. These bands are associated with the ${}^6A_1 \rightarrow {}^4T_1$, ${}^6A_1 \rightarrow {}^4T_1$ and ${}^6A_1 \rightarrow {}^4T_2$, 4E transitions respectively. The characteristic yellow manganese emission is associated with the ${}^4T_1 \rightarrow {}^6A_1$ transition. The yellow emission from insulating ZnSe:Mn,Cl crystals lies at 2.12 eV (5860 Å) in PL.

Jones and Woods (1973) and Allen et al (1972,1973) who heated insulating ZnSe:Mn crystals in molten zinc to lower the resistivity were unable to detect the characteristic manganese emission in PL in the semi-conducting samples produced. Since optical absorption studies at helium temperatures (Jones and Woods, 1973) and Allen et al (1973) show that the characteristic bands and zero-phonon lines of substitutional Mn^{2+} are unaffected by the heating in molten zinc, it was concluded that the luminescence emission of Mn^{2+} would be quenched in the presence of free electrons by an Auger process. Allen et al (1973), also suggested that with ultraviolet excitation numerous free carriers would be generated to quench the manganese emission leaving the self-activated emission to be observed. In contrast they suggested that in REL, the emission originated from the depletion layer where the electron concentration is small, so that the manganese emission would then be dominant.

In the present work, the characteristic manganese emission was only detected in reverse biased zinc selenide diodes containing high concentrations of manganese ($\sim 1\%$). In these samples, manganese was found to emit a narrow band at 2.14 eV (5785 Å) with a width at half height of 0.13 eV (350 Å) at 300 K. The position of the band maximum remained virtually unchanged when the temperature was reduced to 18 K, but the band narrowed to a half width of 0.09 eV (240 Å).

In some of the diodes containing small concentrations (100 - 1000 p.p.m.) of manganese the characteristic emission was not often observed. The presence of foreign donors such as aluminium (see next section) can also give rise to complications. In general, a slight shift of the emission to longer wavelengths and the broadening of the emission band, as the diode current increased, is associated with the onset of the excitation of self-activated emission which increases intensity with increasing donor content. Copper impurities lead (see Section 7.6.5) to similar effects.

In ZnSe:Mn,Cl,Zn diodes the PL emission excited with ultraviolet light consisted of comparatively broad bands, peaking at about 2.06 eV (6010 Å). The manganese emission although quenched, was not totally quenched following the heat treatment in molten zinc. One illustration of this is provided by Figure 7.3, which shows the characteristic manganese excitation band from the 6A_1 ground state to the 4T_2 second excited state. The second broad peak at 2.6 eV is due to the excitation of the S.A. centres. Irradiation by uv, therefore, would excite both the manganese and S.A. centres together. However when the PL was excited by photon energies equal to the difference in energy of between the ground and second excited state of Mn^{2+} (i.e. by 2.43 eV photons), the resultant emission band became slightly narrower and peaked at 2.1 eV (5900 Å) but was still not wholly the characteristic manganese emission.

This is not surprising because it has been illustrated in Chapter 5, that the illumination of a diode in the second excitation band of Mn^{2+} would give rise to auto-ionization of electrons to the conduction band. Some of these free electrons would then recombine via S.A. or non-intentionally added copper centres, to contribute to the observed luminescence.

In forward bias the field of anode is too weak for impact excitation. However FEL emission peaking at 2.11 eV (5880 Å) is intermediate between that excited in PL and REL. The fact that some contribution from the manganese emission can be observed in forward bias suggests that the first excited state of Mn^{2+} lies beneath or close to the bottom of the conduction band, in order that the probability of capturing a thermal electron be finite. Allen et al (1973) have argued, relying largely on the work of Braun et al (1972) on photocapacitance of ZnSe, that the ground state of Mn^{2+} lies 0.6 eV above the valence band. As stated earlier in Chapter 5, our work suggests that the ground state of Mn^{2+} lies about 0.3 eV above the valence band. This locates the first excited state 4T_1 , just below and the second excited state, 4T_2 , just in the conduction band.

The overall situation therefore is clear, the emission observed from manganese doped crystals of zinc selenide may consist of the manganese or the S.A. emission or both. The relative proportions observed, manifested in the position and the width of the resultant band depend on the conditions of excitation. In reverse bias the manganese emission appears preferentially; in forward bias and in photoluminescence where the free carriers are plentiful and the S.A. centres are also excited, the manganese emission is reduced to a varying extent depending on the composition of the crystal.

7.6.3 The Effect of Doping ZnSe:Mn,Cl with Aluminium

When crystals doped with manganese were treated in molten zinc mixture of zinc and aluminium, the characteristic manganese emission was found to have been swamped after the in-diffusion of aluminium. Swank et al (1969) showed that aluminium diffuses into zinc selenide accompanied by zinc vacancies. As aluminium diffuses in, it may encourage any copper impurity present to take substitutional sites and become optically active. Traces of about 1 p.p.m. of copper have been observed in the as-grown ZnSe produced in the laboratory (Jones and Woods, 1974).

7.6.4 Luminescence Transitions in Copper Doped Samples

The photoluminescence emission bands in copper doped ZnSe samples are fairly well documented, see for example Halsted et al (1965), Iida (1969) and Jones and Woods (1974). In general copper-green, 2.34 eV (5300 Å) and copper-red, 1.95 eV (6350 Å), bands are present at 77 K. But the red band occurs alone at 300 K. The copper-green and copper-red bands in ZnSe are thought to be analogous to the copper-blue (4400 Å) and copper-green (5200 Å) bands in ZnS. There are at least two models to explain the copper emission in ZnSe. The first is a Schon-Klasens type scheme (see curve (a), Figure 2.4) in which a free electron recombines with a hole trapped at a Cu^+ ion. The second model is based on a pair emission scheme involving a shallower copper acceptor level of Cu^{2+} , and a donor level (see for example Jones and Woods, 1974). Both models have been tested by time resolved spectroscopy, for example by Fujiwara and Fukai (1966), who found a spectral shift, and Iida (1969) who did not. More recently Bryant and Manning (1974) found a shift in the peak position of copper emission using time resolved spectroscopy and suggested therefore that the copper emission is associated with the pair recombination. More recently Jones and Woods, (1974) have located the

Cu^+ and Cu^{2+} levels in ZnSe at 0.86 eV and 0.46 eV above the valence band.

In the present work, the REL, and PL and FEL emissions from a copper-doped ZnSe:Cu, Zn+Al diode contained similar bands. This would suggest that the radiative transitions involved in all three types of luminescence are identical. The copper-green and red bands peaked at 2.2 eV and 1.96 eV respectively. These bands seem to be displaced slightly towards one another. This is to be expected because these bands are superimposed on the S.A. emission band created by the in-diffusion of aluminium.

7.6.5 Luminescence Transitions in ZnSe:Mn,Cu,Cl,Zn+Al Diodes

The REL emission from Au-ZnSe:Mn,Cu,Cl,Zn+Al diodes exhibited both the manganese and copper-red emissions, but the copper-green band was not observed. The copper-red emission was found to be excited in a broad band peaking at 2.25 eV (5500 Å) at 300 and at 2.31 eV (5350 Å), with possible shoulders at 2.45 eV (5060 Å) and 2.75 eV (4500 Å) at 77 K. Now the high energy wing of the manganese emission which peaks at 2.14 eV can be shown to overlap the low energy side of the luminescence excitation band of the copper-red emission. It is possible therefore that the manganese emission can actually excite the copper-red emission either directly or by resonance energy transfer.

A resonance energy transfer process in reverse has been suggested before to explain the excitation of manganese in ZnS:Mn,Cu,Cl phosphors. Because of the greater band gap of ZnS, the luminescence excitation and emission bands for non-localized copper centres, occur at the relatively higher energies than in ZnSe. Therefore the copper-blue and green emissions in ZnS can excite the manganese ions directly or by a resonance transfer process.

In the present work, the possibility of radiative energy transfer between the manganese and copper centres in ZnSe:Mn,Cu was stimulated by the REL work. In reverse bias both the copper red and manganese emissions are expected to be excited by the impact of hot electrons in the depletion region. The REL emission spectra at 85 K (see Figure 7.17) show that the manganese centres were excited more efficiently at low diode currents. At higher currents, however, the copper-red emission increased at the expense of the manganese emission. One possibility is that the manganese emission is reabsorbed to enhance the copper-red emission. The observed brightness-current variation of $B \propto i^{1.1}$, at high current levels, would again suggest that impact excitation was the mechanism for the observed luminescence.

7.6.6 Ageing Effect in ZnSe:Mn,Cl,Zn Diodes

The maintenance of the light output of some of the reverse biased ZnSe:Mn,Cl,Zn diodes prepared on cleaved and chemically cleaned surfaces was investigated. The results, of course, have to be considered in conjunction with the effects of ageing on the electrical properties of the devices which were described in Chapter 5.9.

In general, the light output from cleaved diodes did not decrease but increased slowly during extended operating periods. This is in fact the result of a slow acting forming process. Similar forming processes were also observed in chemically cleaned diodes, but these occurred in a short period of a few hundred hours of constant current operation, after which time the light output fell drastically. The corresponding changes in the electrical characteristics and the device parameters (see Chapter 5.9), indicated that the thicknesses of the interfacial layers in both the cleaved and chemically cleaned diodes increased during prolonged operation. Another apparent change was the slight decrease

in the uncompensated donor concentration N_d . The rate of degradation of the electrical characteristics and the device parameters was faster in chemically cleaned diodes.

The changes in the device parameters during ageing were directly responsible for the observed changes in the light output. The changes in the device parameters were thought to have resulted from two effects in series, namely a change in the electrical properties of the depletion region, and changes in the electrical and physical properties of the interfacial layers. Here the apparent change in the depletion region manifested itself as a decrease in the uncompensated donor concentration. This is either due to ionic drift of the impurity ions in the high field depletion region, or to the production of compensating vacancies by hot electrons. A decrease in the uncompensated donor concentration without a considerable change in the barrier height at the junction, would increase the width of the depletion layer. Then the active region of the semiconductor, where the impact excitation of manganese centres occur, becomes wider. This in fact may explain the increasing light output observed in cleaved sample No.246A.

The situation in chemically cleaned diodes is slightly different. The comparatively high light output observed from these diodes is a result of higher built in fields. The built-in field at the Schottky junction of ZnSe diodes depends strongly on the surface preparation technique (see Chapter 5). In these diodes the uncompensated donor concentration decreases together with the barrier height, as deduced from measured C-V plots, so that no easy conclusion can be reached. However the decrease in the light output may be attributed to the decrease in the barrier height and the increase in the width of the interfacial layer. These all decrease the average field and the width of the active region in the semiconductor. The changes in the electrical properties of the interfacial layers are thought to be field induced.

CHAPTER 8

ELECTROLUMINESCENCE IN SOLID SOLUTIONS OF Zn(S,Se) CRYSTALS

8.1 INTRODUCTION

It is possible to vary the photon energy of the luminescence emission by alloying phosphors. In the present work zinc selenide and zinc sulphide were alloyed together in an attempt to produce red, yellow, green and blue light emitting diodes. In this chapter, the EL and PL emission from mixed crystals of zinc sulpho-selenide diodes, will be described. The mixed crystals studied were either nominally pure crystals or crystals doped with donors (e.g. iodine or aluminium or both) to stimulate the S.A. emission. The PL excitation spectra were also investigated. In the electroluminescent devices produced with mixed crystals, light was emitted for both directions of the applied bias.

8.2 SOME ELECTRICAL PROPERTIES OF Zn(S,Se) ELECTROLUMINESCENT DEVICES

8.2.1 Preparation of Schottky Barriers

Single crystals of $\text{ZnS}_x\text{Se}_{1-x}$ (where x represents the molar fraction of sulphur in the solid solution) were successfully grown in this laboratory using vapour phase or iodine transport methods (see Chapter 3). These mixed crystals were then annealed in molten zinc or in a molten mixture of zinc and 10% aluminium. Such treatment reduced the apparent resistivity as measured between two indium contacts, to the range $10 - 10^4 \Omega\text{cm}$. The details of the heat treatment administered to the various mixed crystals are tabulated in Table 8.1.

The successful preparation of Schottky barriers on $\text{ZnS}_x\text{Se}_{1-x}$ mixed crystals requires, among other things, the formation of satisfactory ohmic contacts, and indium metal was again used for this purpose. To obtain reasonable, ohmic contacts, on mixed crystals with sulphur

Crystal No.	Molar Composition %	Grown-in Impurities	Heat Treatment		
			Molten Elements	Temperature (C°)	Time (Hours)
225	ZnS _{0.6} Se _{0.4}	-	Zn	1000	430
249	ZnS _{0.2} Se _{0.8}	-	Zn + Al	850	240
241	ZnS _{0.6} Se _{0.4}	-	Zn + Al	900	260
944	ZnS _{0.6} Se _{0.4}	I	Zn	850	170
951	ZnS _{0.6} Se _{0.4}	I, Mn	Zn + Al	950	240
973	ZnS	I, Mn	Zn + Al	900	200
932	ZnSe	I	Zn + Al	850	240
940	ZnS _{0.13} Se _{0.87}	I	Zn + Al	850	170
943	ZnS _{0.2} Se _{0.8}	I	Zn + Al	850	290
947	ZnS _{0.35} Se _{0.65}	I	Zn + Al	850	192
952	ZnS _{0.52} Se _{0.48}	I	Zn + Al	850	290
954	ZnS _{0.57} Se _{0.43}	I	Zn + Al	900	170
956	ZnS _{0.67} Se _{0.33}	I	Zn + Al	900	240
958	ZnS _{0.80} Se _{0.20}	I	Zn + Al	900	240
961	ZnS _{0.92} Se _{0.08}	I	Zn + Al	900	240
962	ZnS _{0.98} Se _{0.02}	I	Zn + Al	1000	240
S2	ZnS	I	Zn + Al	1000	200

Table 8.1: The heat treatment conditions administered to ZnS_xSe_{1-x} crystals (x is the molar percentage of sulphur in the solid mixture).

contents up to at least 80% molar, it was necessary to increase the temperature of the indium in-diffusion process from 280°C in ZnSe to 400°C in $\text{ZnS}_{0.8}\text{Se}_{0.2}$. However it became increasingly difficult to prepare ohmic contacts on mixed crystals as the sulphur content increased beyond 80%. The I-V characteristics of some of the mixed crystals with symmetric indium contacts are illustrated in Figure 8.1. The characteristics were essentially the same when the bias was reversed. The characteristics were linear for ZnSe and remained linear for mixed crystals with sulphur contents at least up to 30%. With some of the mixed crystals with sulphur concentrations between 40-80%, the characteristics were reminiscent of those expected for single carrier, space-charge-limited currents in insulators where the I-V variation can be expressed by a relation of the form $i \propto V^n$ with n equal to 1 at low voltages, changing to 2 at higher voltages. An illustration of this is provided by curve (c) in Figure 8.1 for the mixed diode No.954 and in curve (d) for diode No.241 (see Table 8.1 for the compositions). As the sulphur content increased further, i.e. to 92%, sample No.961, the I-V characteristics obeyed an $i \propto V^n$ relation again with the values of n equal to 1, 2 and then 9-10, see curve (e) in Figure 8.1. In the ZnS:I,Zn+Al sample, regions with n equal to 1 or 2 were not observed in the range of current (lowest 10^{-6} Amp mm^{-2}) studied here. However the recorded I-V characteristic at biases greater than 10 V can be expressed approximately as $i \propto V^{15}$.

The ohmic behaviour of all the crystals was also tested at 85 K, and it was observed that the I-V characteristics in most of the mixed crystals containing more than 30% sulphur, obeyed a relation of the form $i \propto V^n$ with regions where n is equal to 1, 2 and 9-10.

Schottky barrier devices were prepared on crystals to which two ohmic indium contacts had been reasonably successfully applied (see

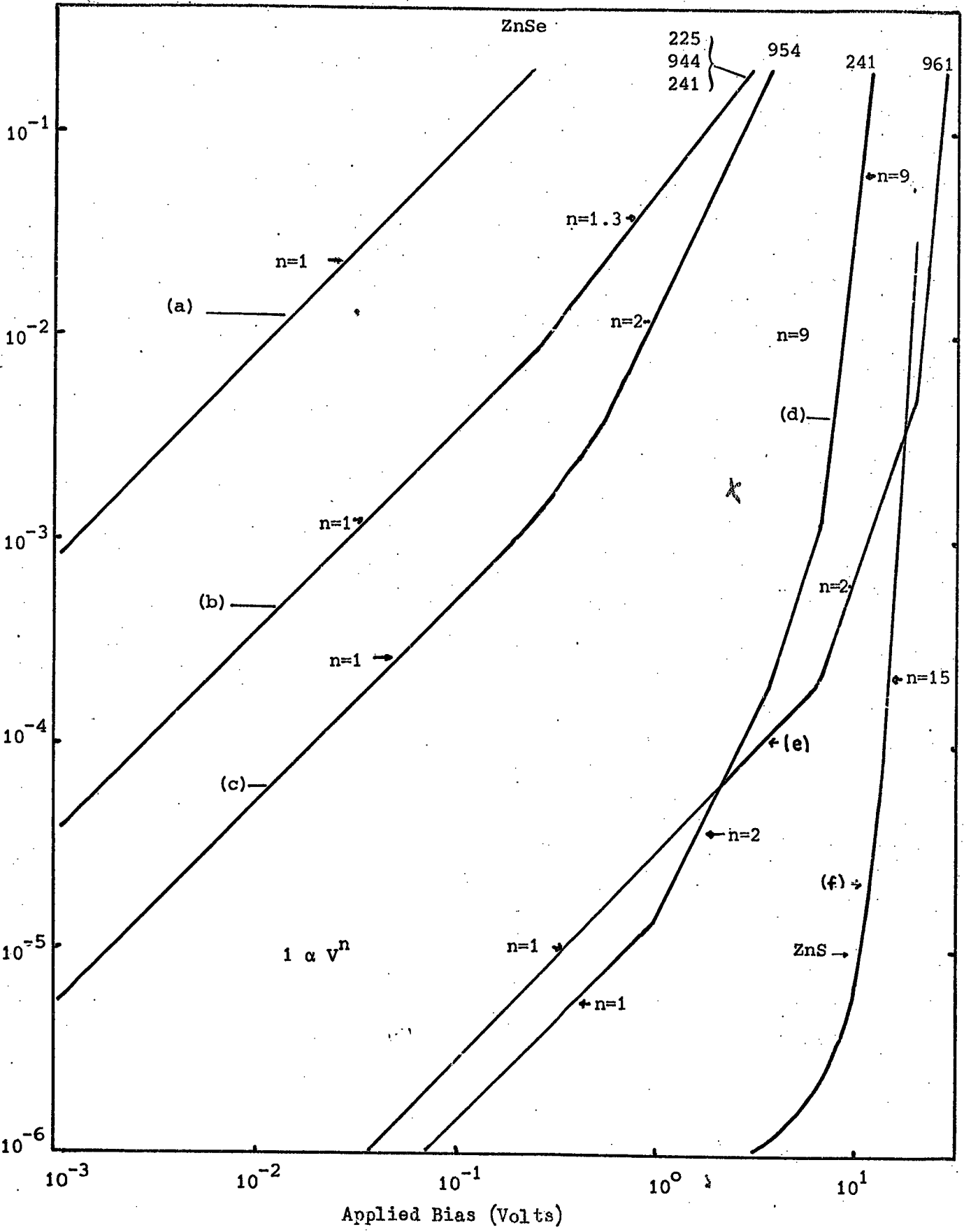


Figure 8.1: The I-V characteristics of ZnS_xSe_{1-x} crystals with symmetric indium contacts. (See Table 8.1 for the compositions).

curve (b) in Figure 8.1). One of the indium contacts was removed and gold electrodes (1 mm^2 in area) were then evaporated on to chemically etched surfaces. The I-V characteristics obtained from such $\text{Au-ZnS}_x\text{Se}_{1-x}$ diodes were found to be rectifying and will be described later.

8.2.2 Photoresponse and C-V measurements

The short-circuit photocurrent in $\text{Au-ZnS}_x\text{Se}_{1-x}$ Schottky diodes was investigated in the range of photon energies $0.8 \text{ eV} \leq h\nu \leq 3.7 \text{ eV}$. The junction was illuminated through the large surface which carried the gold electrode. Typical spectral distributions are illustrated in Figure 8.2. The low energy photothreshold can again be treated as a measure of the electron barrier height and some results are listed in Table 8.2. With photon energies equal to or greater than the energy band gap, electron-hole pairs are created in the depletion layer and these are responsible for the large increase in photocurrent at higher photon energies. The magnitude of the photocurrent decreased steadily as the sulphur content increased. With diodes containing up to 80% sulphur, the sign of the photocurrent at 295 K was positive over the whole range of photon energies studied. However when the sulphur concentration exceeded 80% the photocurrent at low photon energies was often observed to change its sign. One example of this can be seen in the photocurrent of the Au-ZnS:I,Zn+Al device at 295 K in Figure 8.2. Similar behaviour was also observed at 85 K with most of the $\text{Au-ZnS}_x\text{Se}_{1-x}$ diodes with sulphur concentrations larger than 30%, see lower curves in Figure 8.2. The reversal of the photocurrent may be attributed to the non-ohmic indium contact presenting a second barrier on ZnS. This will be discussed later in Section 8.5.

The short-circuit photocurrents in some $\text{Au-ZnS}_x\text{Se}_{1-x}$ diodes containing manganese were also investigated. An interesting feature

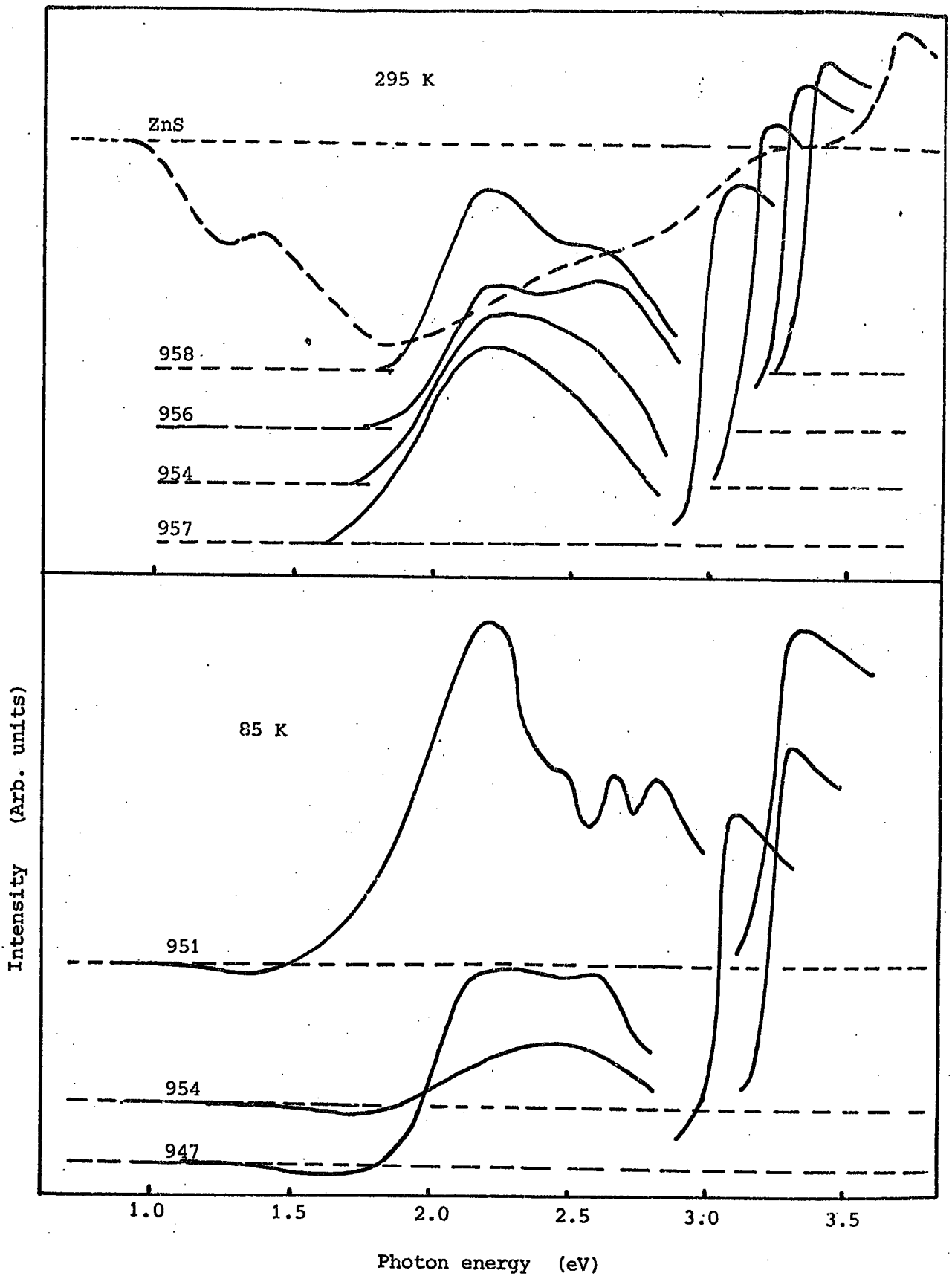


Figure 8.2: The spectral distribution of short circuit photocurrent recorded on some of the $\text{Au-ZnS Se}_x \text{1-x}$ diodes (see Table 8.1 for the impurity contents and composition).

Diode	Composition	Phototreshold ϕ_{Bn} (ph)	ϕ_{Bn} (C-V)	Uncompensated donor concentration N_d ($\times 10^{17}$)
932	ZnSe:I,Zn+Al	1.59	1.9	1.3
940	ZnS _{0.13} Se _{0.77} :I,Zn+Al		2.35	2.6
943	ZnS _{0.2} Se _{0.8} :I,Zn+Al		2.2	0.56
952	ZnS _{0.5} Se _{0.5} :I,Zn+Al		1.75	0.34
954	ZnS _{0.6} Se _{0.4} :I,Zn+Al	1.8	3.6	6.1
956	ZnS _{0.67} Se _{0.33} :I,Zn+Al	1.86	-	-
958	ZnS _{0.8} Se _{0.2} :I,Zn+Al	1.82	2.0	1.1
S1	ZnS:I,Zn+Al	0.95 (In)	4.5	0.24
225	ZnS _{0.6} Se _{0.4} :Zn	1.75	2.45	0.04
241	ZnS _{0.6} Se _{0.4} :Zn+Al	1.79	2.45	0.33
951	ZnS _{0.6} Se _{0.4} :I,Mn,Zn		3.7	0.026

Table 8.2: Some of the device parameters obtained from phototreshold and C^{-2} -V plots on some of the Au-ZnS_xSe_{1-x} diodes.

of the spectral response measured at 85 K of the photocurrent of the Au-ZnS_{0.6}Se_{0.4}:I,Mn,Zn diode No.951 is shown in Figure 8.2. This is the set of small maxima occurring at 2.48 eV (5000 Å), 2.65 eV (4670 Å) and 2.82 eV (4400 Å). Such maxima were not observed in any of the mixed crystal diodes of the same composition which did not contain manganese. The maxima were found to correspond to the PL excitation bands observed in the same sample, see later.

The C-V characteristics of Au-ZnS_xSe_{1-x} diodes were recorded at 200 kHz in the dark. Most of the resultant C⁻²-V plots were straight lines, see Figure 8.3. The voltage intercepts lay in the range 2.0 - 3.5 V for diodes with sulphur contents up to 80%. These values are higher than those obtained from photothreshold measurements and can be attributed to the presence of insulating layers between the gold and the sulpho-selenides. An attempt was also made to estimate the approximate uncompensated donor concentrations of our diodes. It was assumed that the dielectric constant would vary linearly with composition from 9.1 in ZnSe to 8.5 in ZnS, as the sulphur concentration increased. The donor concentrations were then calculated from the slopes of the C⁻²-V plots using equation 2.4.7. Some of the results are recorded in Table 8.2.

In mixed crystals with sulphur contents in excess of 80% the C⁻²-V plots deviated from straight lines and became slightly concave upwards at low applied biases. This is thought to be due to voltage being dropped at the indium contact as well as the gold, which would cause a decrease in the slope of the C⁻²-V plot and an increase in the voltage intercept. This is illustrated for an Au-ZnS:I,Zn+Al-In diode in Figure 8.3. Clearly the calculation of N_d from such plots will be slightly in error. At 85 K the extrapolated intercept for most of the Au-ZnS_xSe_{1-x} diodes shifted to higher voltages. This is also thought

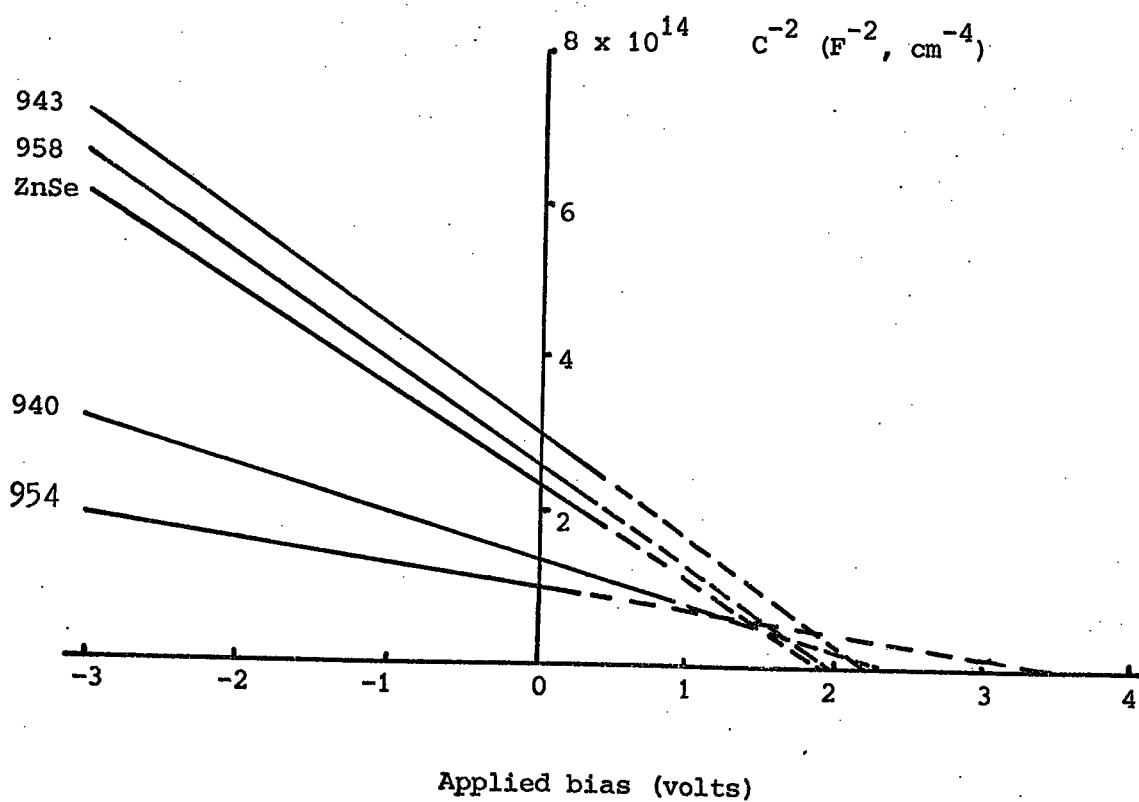
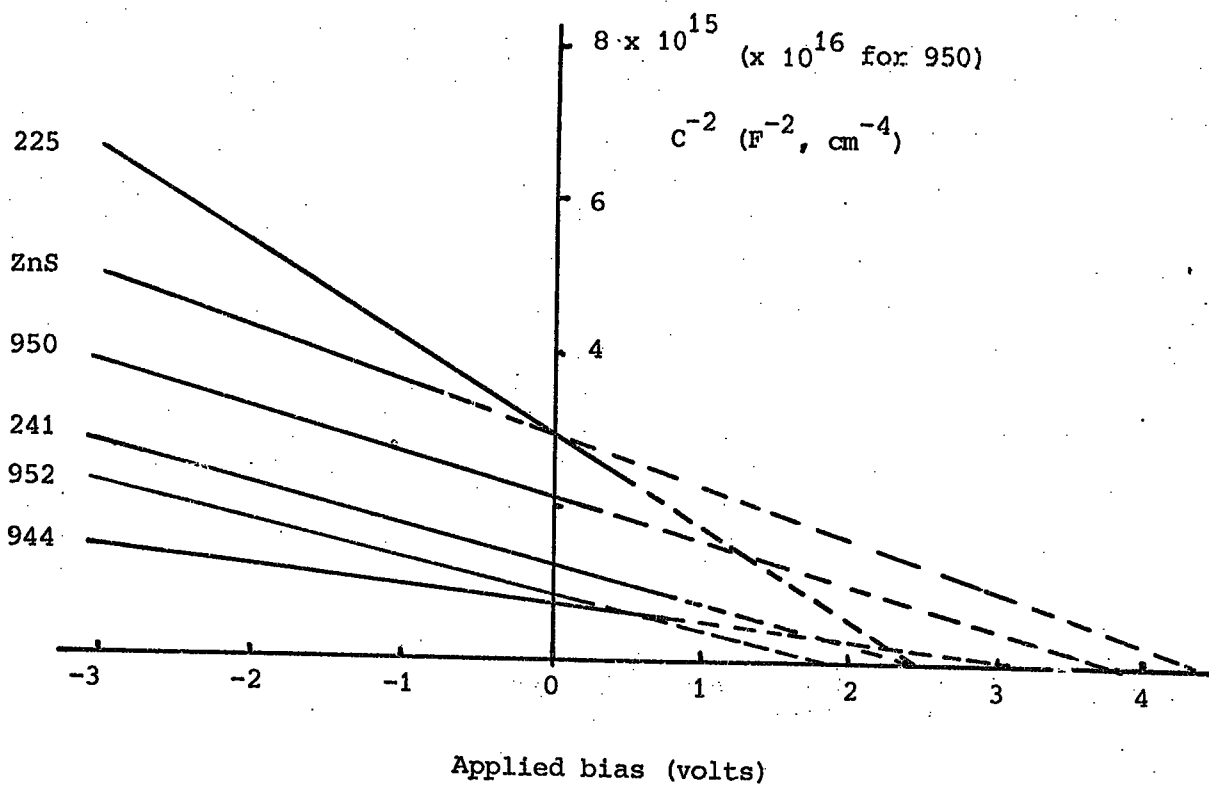


Figure 8.3: $C^{-2} - V$ plots obtained from some of the $\text{Au-ZnS}_{x}\text{Se}_{1-x}$ diodes. (See Table 8.1 for the compositions).

to be due to the non-ohmic behaviour of the indium contact which is more pronounced at low temperatures.

8.3 EL AND PL IN $ZnS_x Se_{1-x}$ MIXED CRYSTALS

8.3.1 Nominally pure $ZnS_x Se_{1-x}$ crystals

The EL and PL from nominally pure ZnSe crystals has been described previously in Chapter 6. In this laboratory, the nominally pure mixed crystals could only be grown successfully using the vapour method when sulphur compositions did not exceed 60%, see Cutter et al 1976. To prepare EL and PL devices these nominally pure mixed crystals were treated in molten zinc. The heat treatment conditions used with one such crystal (No.225) are listed in Table 8.1. An approximate uncompensated donor concentration of about $4 \times 10^{15} \text{ cm}^{-3}$ was calculated from the $C^{-2} - V$ plot.

The I-V characteristics measured on an $Au-ZnS_{0.6}Se_{0.4}:Zn$ diode showed rectification. The B/I-V characteristics obtained from this diode are illustrated in Figure 8.4. The forward I-V and B-V characteristics recorded at 85 K were roughly exponential. At the highest current densities the forward B/I-V curves appeared to saturate. This was due to the limitation of the current by the series differential resistance of the device. The reverse B/I-V characteristics were displaced to rather high applied biases, but once again the variation of B and I with V at 295 K was nearly exponential. In both forward and reverse bias brightness varied with the current as $B \propto i^{1.3}$. The brightness of 2 Ft-L observed in reverse bias at 295 K corresponds to a conversion power efficiency of $7 \times 10^{-6} \%$.

The spectral distributions of the FEL, REL and PL emissions recorded at 300 and 85 K are illustrated in Figure 8.5. At room temperature both REL and FEL emission spectra exhibited a broad band centred near 2.0 eV (6200 Å). However, the PL emission was much narrower

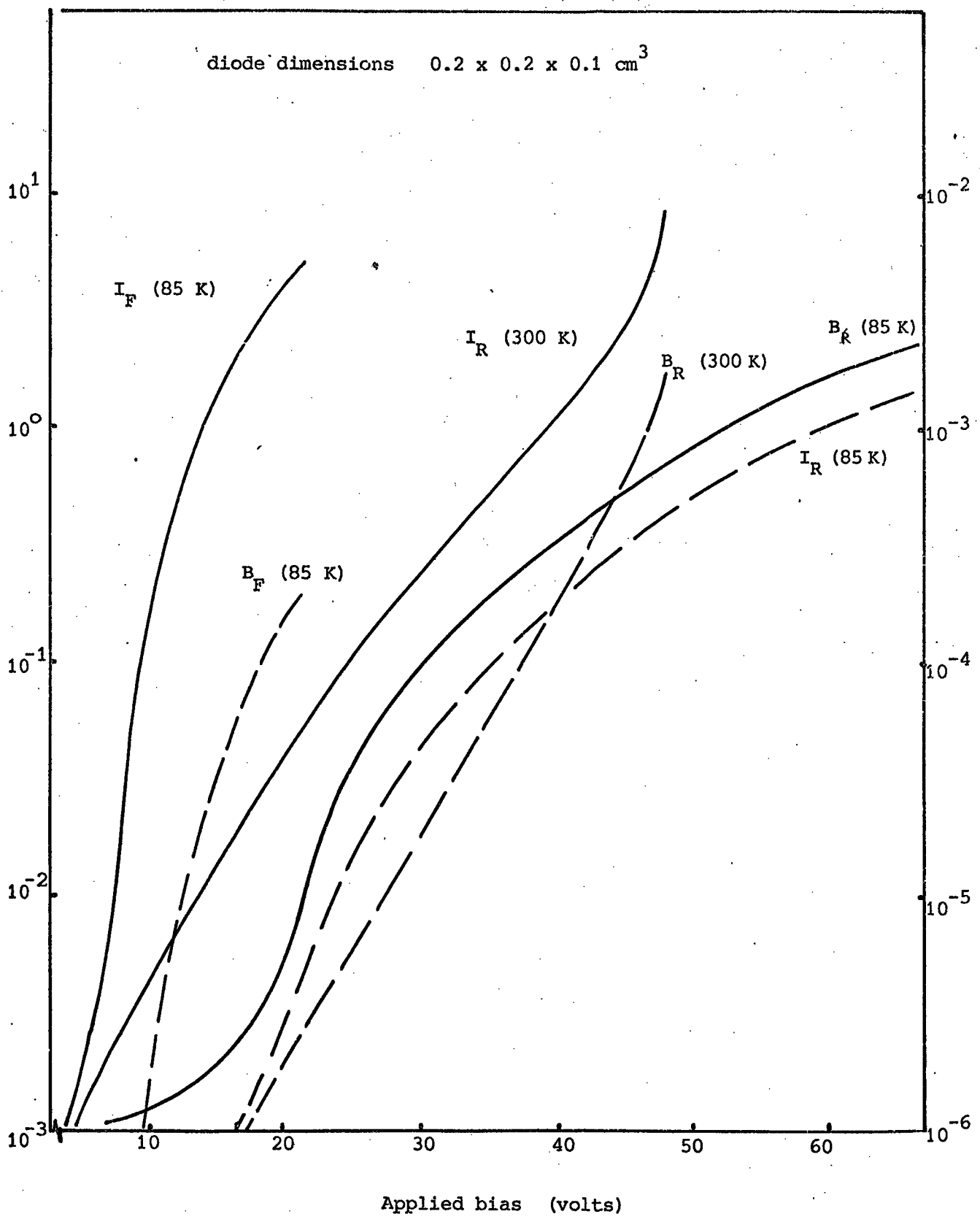


Figure 8.4: The variation of brightness and current as a function of applied bias in $\text{Au-ZnS}_{0.6}\text{Se}_{0.4}:\text{Zn}$, diode No.225

Intensity (Arb. Units)

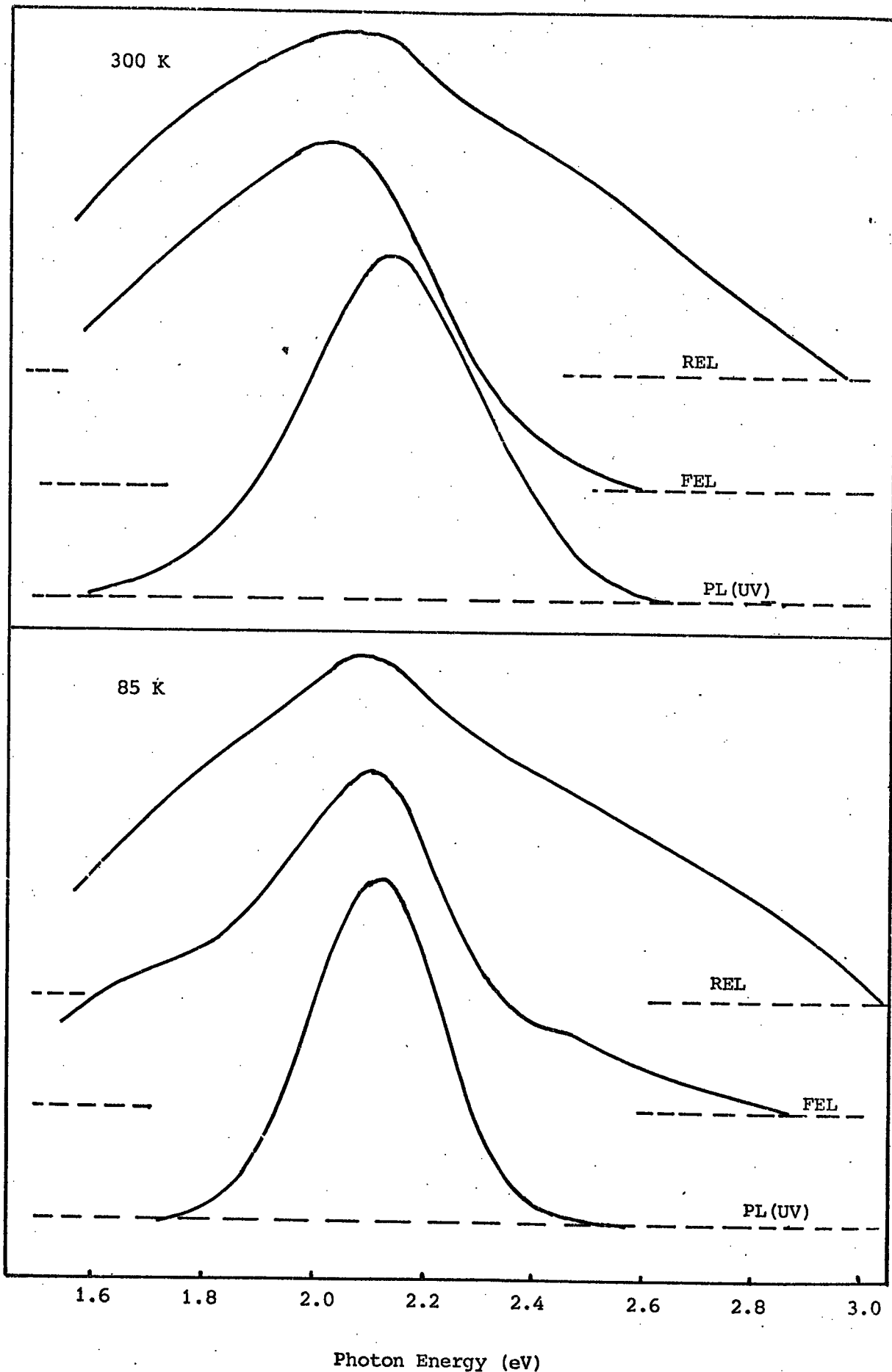


Figure 8.5: The spectral distribution of FEL, REL and PL recorded at 300 and 85 K on $\text{Au-ZnS}_{0.6}\text{Se}_{0.4}:\text{Zn}$, Diode No.225.

(see Table 8.3) with a peak position at the slightly higher energy of 2.12 eV (5850 Å). At 85 K, both the FEL and PL emission were centred at 2.1 eV (5900 Å). The REL emission band was still broad, but the FEL emission exhibited distinct shoulders in the red (~1.7 eV) and in the green (~2.45 eV). The PL emission band at 85 K was still narrower than the electroluminescence bands. The excitation spectra of the yellow PL emission band of this and other diodes are illustrated in Figure 8.6. Efficient excitation of the yellow band occurred in a broad band with a maximum at 2.88 eV (4300 Å) at 295 and 2.95 eV (4200 Å) at 85 K.

8.3.2 Mixed crystals doped with aluminium or iodine

Mixed crystals containing aluminium were obtained by annealing vapour grown crystals in a molten mixture of zinc and aluminium. Of this group of diodes two, namely Au-ZnS_{0.2}Se_{0.8}:Zn+Al (No.249) and Au-ZnS_{0.6}Se_{0.4}:Zn+Al (No.241) will be described. Mixed crystals containing iodine were grown by the chemical transport method where iodine was used as the transporting agent. In this group, only one crystal (No.944), with the composition ZnS_{0.6}Se_{0.4} was examined. Details of the heat treatment given to these crystals are given in Table 8.1. Some of the device parameters can be found in Table 8.2.

A variety of different metal contacts were investigated on the ZnS_{0.6}Se_{0.4}:Zn+Al, crystal No.241. EL was produced in dice (0.2x0.2x0.1 cm²) equipped with symmetrical indium contacts (1 mm² in area). Such devices emitted green light equally for both polarities of applied d.c. bias. Curve (a) in Figure 8.7 shows a typical I-V characteristic while curve (b) depicts the brightness, B, as a function of V. With the opposite polarity the characteristics were essentially similar. When the I-V characteristics were plotted on a log-log scale, see curve (d)

Intensity (Arb. units)

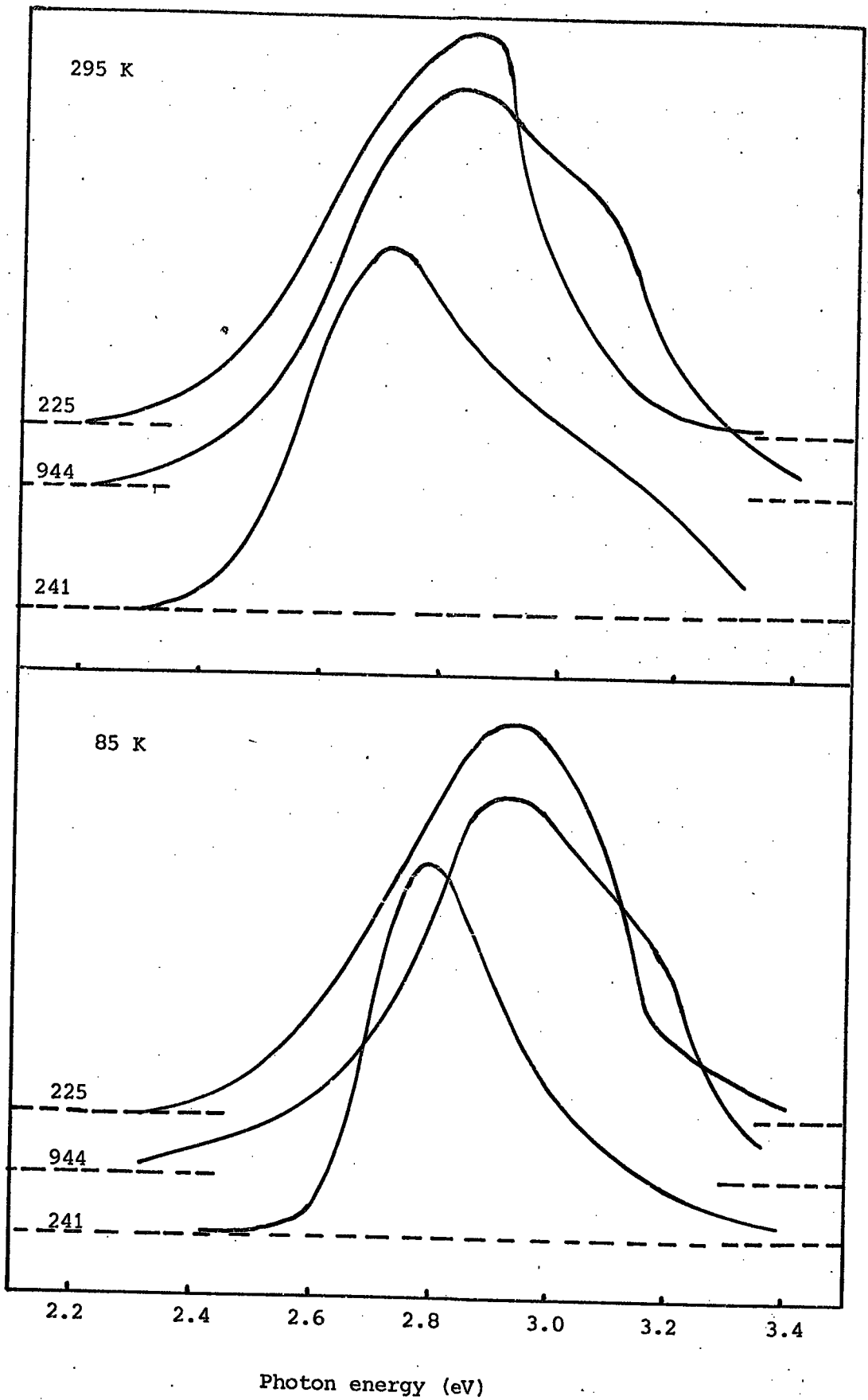


Figure 8.6: The excitation spectra for the yellow band observed in PL of diodes No. 225, 944 and 241 (see Table. 8.1 for impurity content and composition of these diodes).

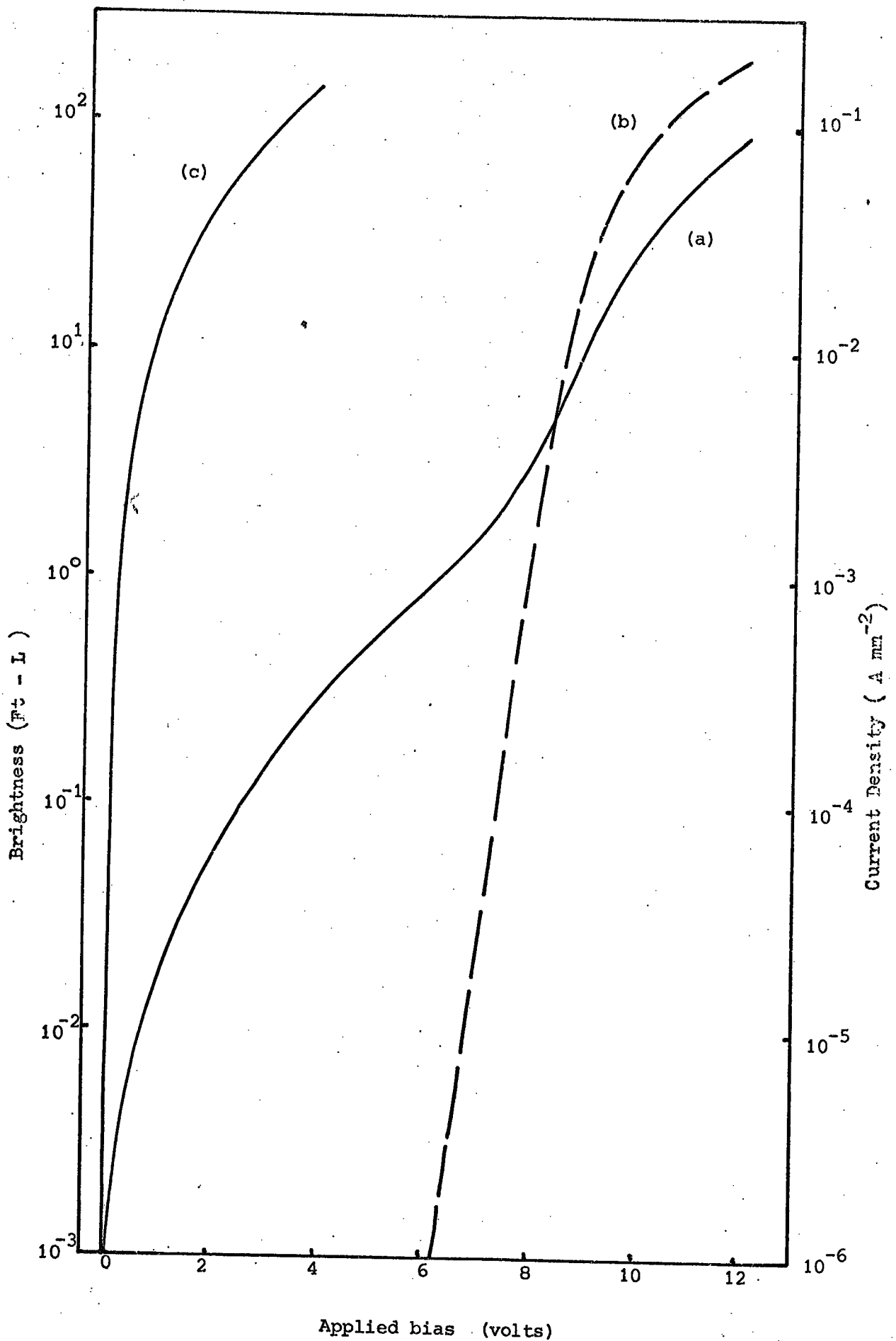


Figure 8.7: (a) I-V characteristics of a $ZnS_{0.6}Se_{0.4}$ die with symmetrical indium contacts, (b) B-V characteristics, (c) I-V characteristics after removing a $50\ \mu m$ layer from each large area face.

in Figure 8.1, the variation obeyed the relation $I \propto V^n$ with n equal to 1, 2 and 9. The region where $n = 9$ was dominant at biases higher than 6 V. This voltage (6 V) was also the threshold for the onset of the EL emission. The variation of the brightness in this region is embodied in the relation $B \propto I^{0.9}$, which strongly suggests that the mechanism for EL is impact excitation. The brightness reached a value of 200 Ft-L with a bias of 11 V. This corresponds to a conversion power efficiency of $2 \times 10^{-4}\%$. At this stage it was discovered that the resistivity of this die was not uniform throughout its thickness. When layers approximately 50 μm thick were removed by mechanical polishing from each of the large area faces and symmetric indium contacts were reapplied, the I-V characteristics shifted to lower applied biases, see curve (c) in Figure 8.7. When this curve was replotted on log-log scale the variation was found to consist of two regions of the form $I \propto V^n$, with n equal to 1 and 1.3 (see curve (b) in Figure 8.1). No EL was observed. However, when such a die was equipped with one indium contact and one evaporated gold contact (1 mm^2 in area), a Schottky diode resulted. In reverse bias, the EL was quite intense. Curve (a) of Figure 8.8 shows the reverse I-V characteristic and curve (b) the B-V characteristic. With this arrangement a luminance of 200 Ft-L was obtained with a five-fold increase in the conversion power efficiency over the first device to $1 \times 10^{-3}\%$. Although no EL in forward bias was detected at 295 K, it was readily observed at 85 K. However, at this reduced temperature the REL was much more intense, see curves (d) and (e), Figure 8.8, reaching a luminance of 1000 Ft-L with a power conversion efficiency of $4 \times 10^{-3}\%$.

To determine the uncompensated donor concentration for the resistive layers formed on the surface of the dice after the heat treatment, the resistive layer was removed from one face and an ohmic contact

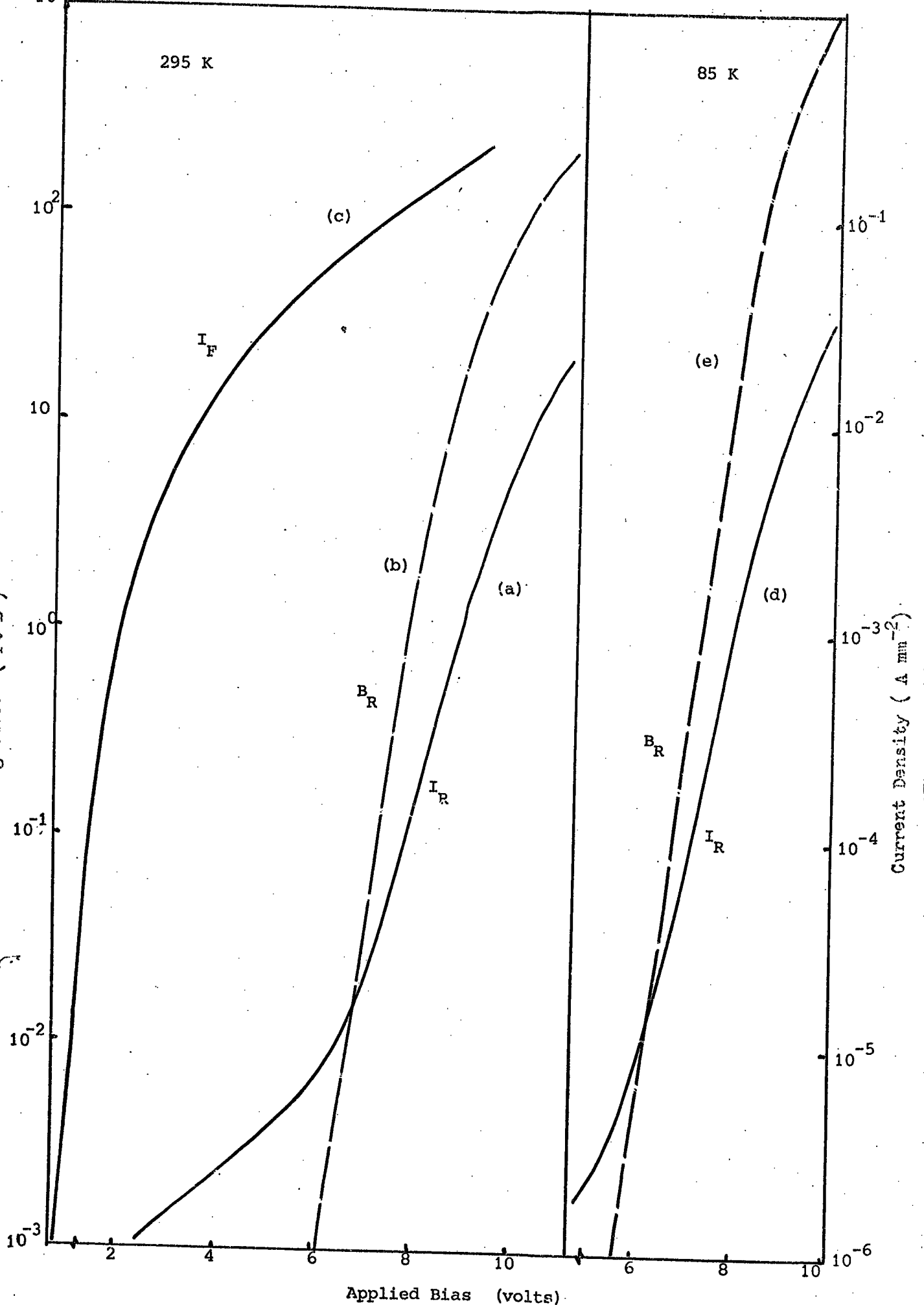


Figure 8.8: (a) Reverse I-V, (b) Reverse B-V, (c) Forward I-V characteristics at 293 K and (d) Reverse I-V, (e) Reverse B-V characteristics at 85 K, recorded on Au-ZnS_{0.6}Se_{0.4}:Zn+Al, Diode No.241.

was applied. A gold electrode was then evaporated on to the opposite face with its resistive layer, to form a blocking contact. The $C^{-2} - V$ plots obtained from such devices were linear and the uncompensated donor concentrations, calculated from the slope, were between 10^{11} and 10^{14} cm^{-3} . A Schottky barrier was also formed on the dice with compositions $\text{ZnS}_{0.2}\text{Se}_{0.8}$ from boule No.249. EL was observed in both forward and reverse bias again. Light output with a brightness of 80 Ft-L in the orange was observed in reverse bias with a power conversion efficiency of $8 \times 10^{-5} \%$.

The forward and reverse B/I-V characteristics were also recorded for the $\text{Au-ZnS}_{0.6}\text{Se}_{0.4}:\text{I,Zn}$ diode No.944, at 295 and 85 K. see Figure 8.9. Both the brightness and the current, in forward and reverse biases varied almost exponentially with applied voltage. The variation of brightness with current obeyed the relation $B \propto i^n$ with n equal to 1.6-1.7 in forward and 1.1-1.2 in reverse bias. The threshold for light emission was about 1.5 V at 295 and 4.4 V at 85 K. A brightness of 10^{-2} Ft-L observed at 295 K under forward bias corresponds to a power conversion efficiency of $10^{-6} \%$. The light output in reverse bias at 295 K was slightly better with 20 Ft-L corresponding to a power efficiency of $2.4 \times 10^{-5} \%$.

The spectral distributions of the EL and PL emissions from diodes Nos.249,241 and 944, are illustrated in Figures 8.10, 8.11 and 8.12 respectively. In diode No.249, both the FEL and REL emissions exhibited a yellow-orange band at room temperature, peaking around 2.05 eV (6050 Å). The PL emission was slightly displaced to 2.1 eV (5900 Å). All these bands shifted to higher energies on cooling (see Table 8.3). In diode No.241, the light was emitted in a broad band in REL, which was centred at 2.27 eV (5450 Å) at 295 K, and which shifted to 2.34 eV (5300 Å) at 85 K. The FEL emission was similar to the REL. The PL emission was

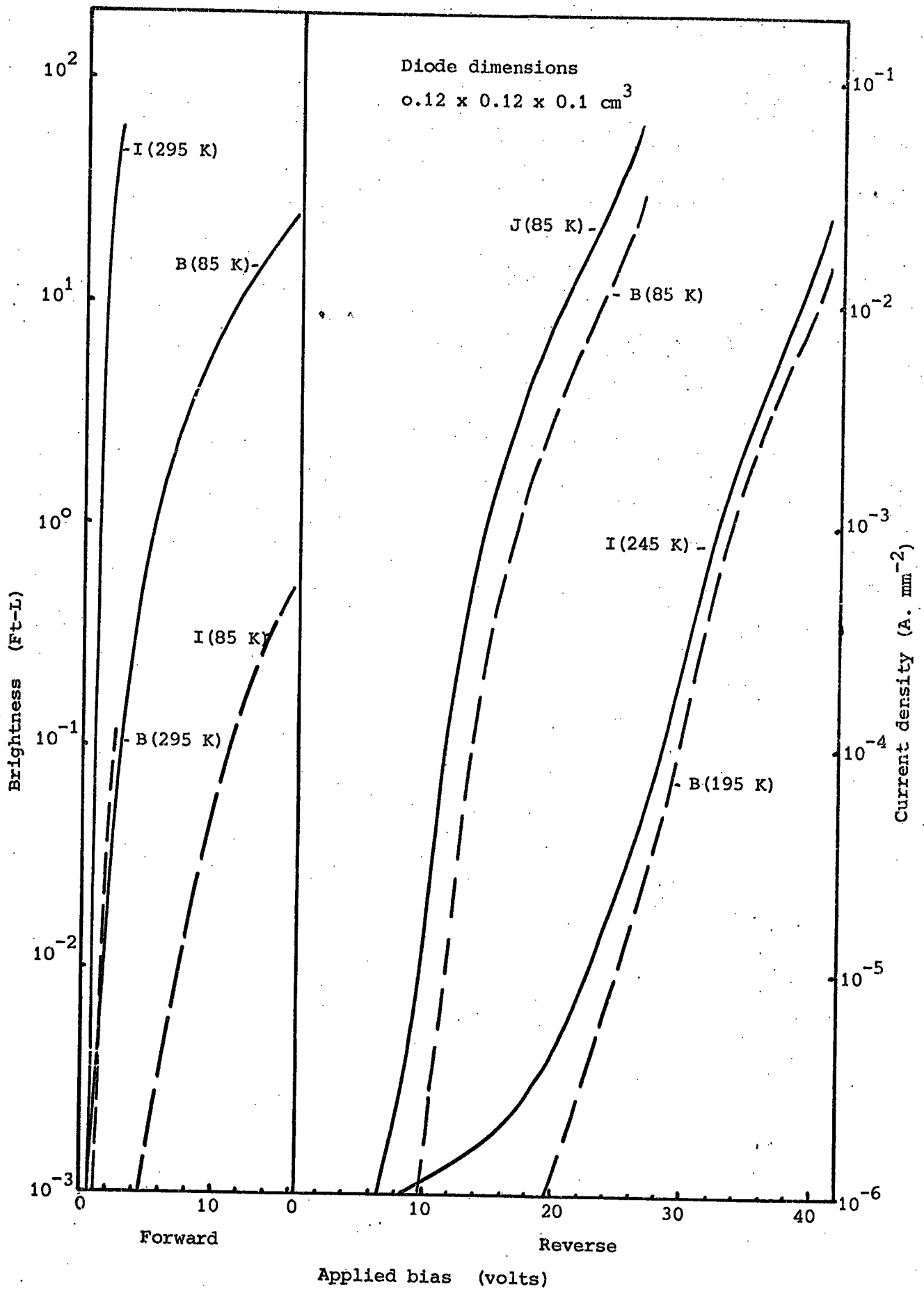


Figure 8.9: The variation of brightness and current as a function of applied bias in Au-ZnS_{0.6}Se_{0.4}:I,Zn, Diode No.944

Intensity (Arb. units)

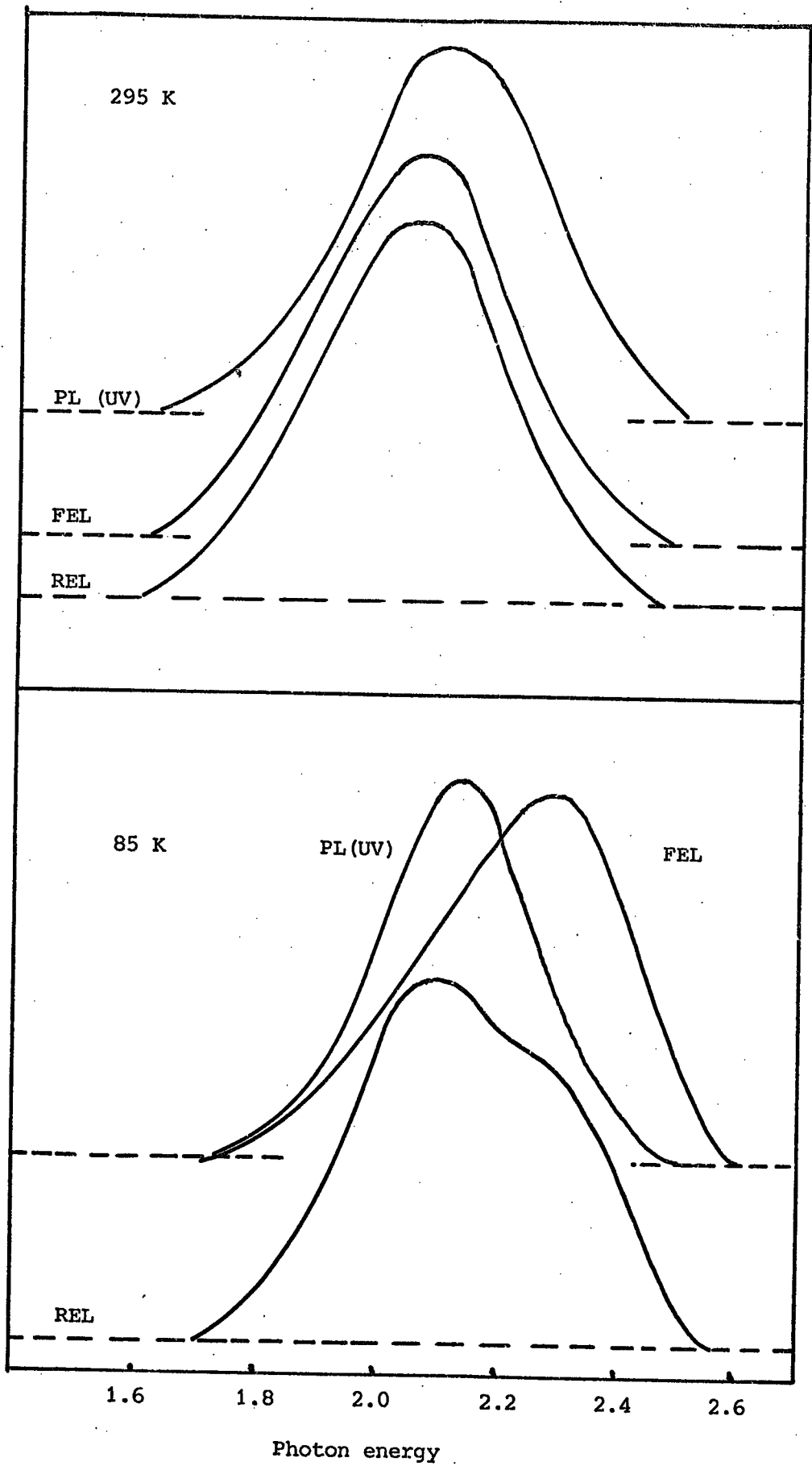


Figure 8.10: Spectral distribution for FEL, REL and PL emission recorded on $\text{Au-ZnS}_{0.2}\text{Se}_{0.8}:\text{Zn+Al}$, Diode No.249 at 295 and 85 K.

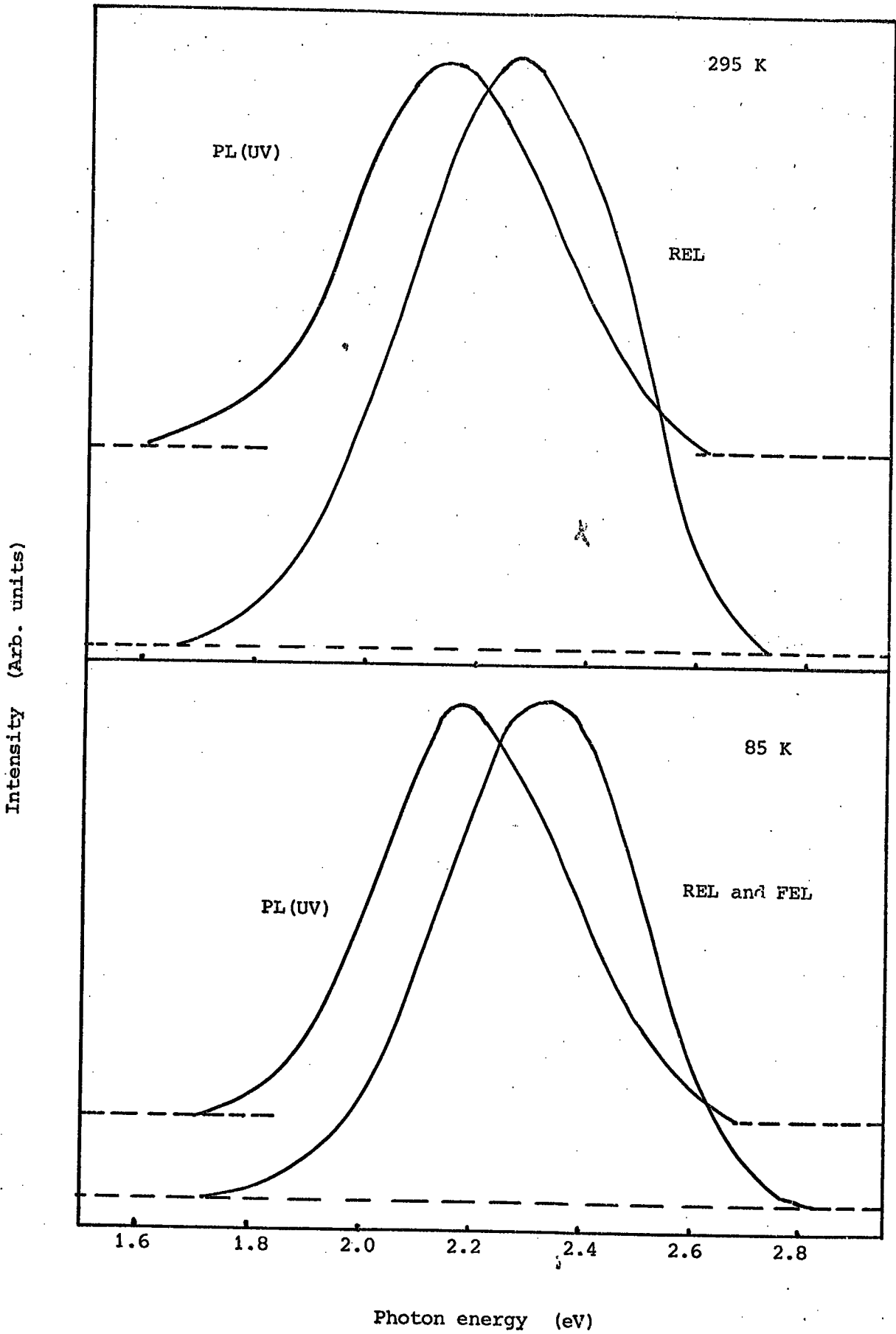


Figure 8.11: Spectral distribution for FEL, REL and PL(UV) emissions recorded from $\text{Au-ZnS}_{0.6}\text{Se}_{0.4}:\text{Zn+Al}$, Diode No.241 at 295 and 85 K.

Intensity (Arb. units)

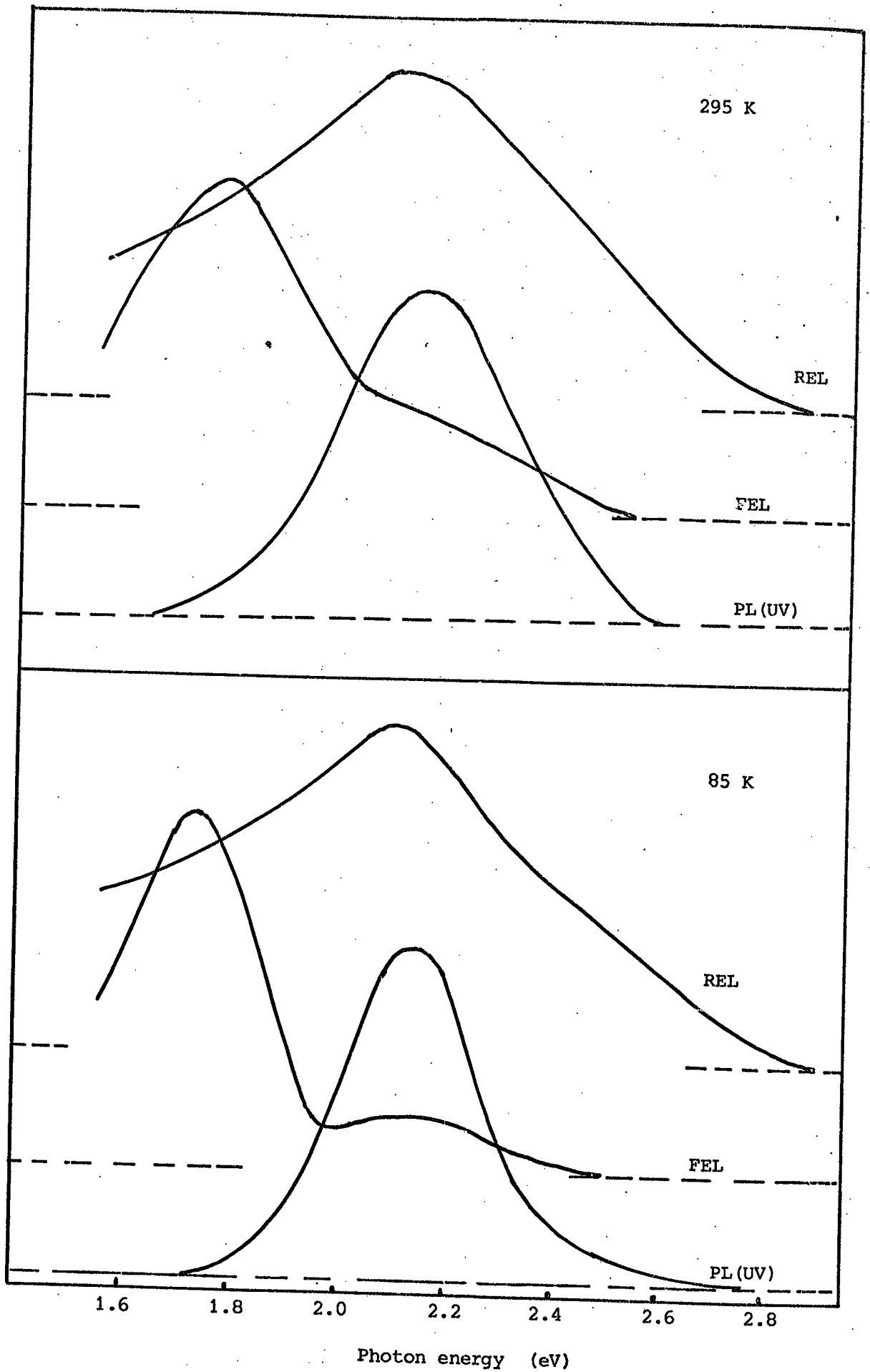


Figure 8.12: Spectral distribution for FEL, REL and PL(UV) emissions recorded on $\text{Au-ZnS}_{0.6}\text{Se}_{0.4}:\text{I,Zn}$, Diode No.944.

slightly different and was centred at 2.14 eV (5800 Å) at room temperature. It shifted to slightly higher energies, i.e. 2.17 eV (5700 Å) at 85 K. With diode No.944, the FEL and REL emissions showed different features. The FEL at 295 K consisted of a red band centred at about 1.77 eV (7000 Å) with a long shoulder on the high energy side of this band. The REL emission however was a broad (see Table 8.3) band centred at about 2.1 eV (5900 Å). At 85 K, the red band in FEL shifted to lower energies to 1.72 eV (7200 Å) and another peak centred at 2.14 eV (5800 Å) appeared in the yellow. In PL at 295 K however a single broad band in the yellow was observed (see Table 8.3) centred at 2.14 eV (5800 Å). This did not shift in energy when the temperature was reduced to 85 K. Finally, the PL excitation spectra for the yellow band observed in diodes No.241 and 944 are illustrated in Figure 8.6. The excitation bands were broad, with maximum efficiency occurring at 2.88 eV (4300 Å) for diode No.944 and 2.72 eV (4550 Å) for diode No.241 respectively at room temperature. A shoulder at about 3.1 eV (4000 Å) was also apparent in both spectra. At 85 K, both excitation bands shifted to higher energies with a maximum excitation occurring at 2.95 eV (4200 Å) in diode No.944 and 2.82 eV (4400 Å) in diode No.241.

8.3.3 Mixed Crystals doped with Iodine and Aluminium

The EL and PL emission was investigated for these crystals over the whole range of compositions. The aluminium was introduced into these crystals, which were grown by the iodine transport technique, by heating them in a molten mixture of zinc and 10% aluminium, see Table 8.1. The device parameters are recorded in Table 8.2.

The B/I-V characteristics of the Au-ZnSe:I,Zn+Al diode No.932 are illustrated in Figure 8.13. The shapes of the I-V and B-V curves in forward and reverse bias were similar to those of any other ZnSe diode

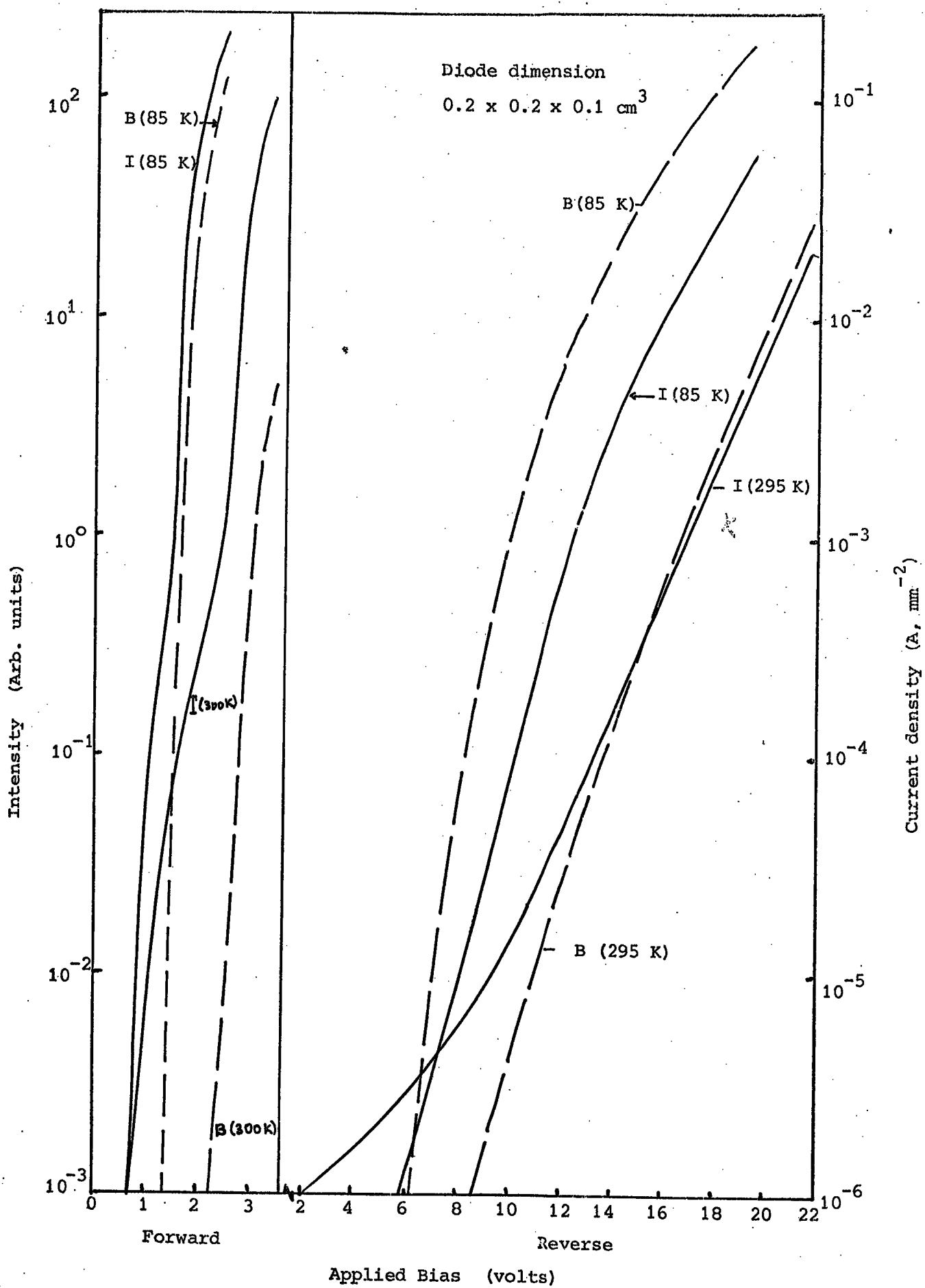


Figure 8.13: The variation of brightness and current as a function of applied bias in Au-ZnSe:I,Zn+Al, Diode No.932

Diode No.	Temp. (K)	FEL EMISSION			REL EMISSION			PL EMISSION		
		Energy (eV)	Wave-length (Å)	Band-width (eV)	Energy (eV)	Wave-length (Å)	Band-width (eV)	Energy (eV)	Wave-length (Å)	Band-width (eV)
225	295	2.0	6200	0.61	2.0	6260	0.95	2.12	5850	0.37
	85	2.1	5900	-	2.1	5900	0.9	2.12	5850	0.27
249	295	2.05	6050	0.39	2.05	6050	0.38	2.1	5900	0.38
	85	2.3	5400	0.9	2.1 2.3	5900 5400	-	2.14	5800	0.3
241	295	-	-	-	2.27	5450	0.47	2.14	5800	0.42
	85	2.34	5300	0.4	2.34	5300	0.42	2.175	5700	0.4
944	295	1.77 2.12	7000 5850	0.4 -	2.1	5900	0.8	2.14	5800	0.42
	85	1.7 2.14	7200 5800	0.3 0.36	2.1	5900	0.89	2.14	5800	0.3
951	295	2.12	5830	0.18	2.12	5830	0.19	2.12	5840	0.22
	85	2.12	5850	0.13	2.12	5850	0.14	2.1	5900	0.17
973	295	2.12	5850	0.17	2.12	5860	0.22	2.1	5880	0.24
	85	2.12	5840	0.14	2.12	5850	0.20	2.08	5950	0.18
932	295	2.05	6050	0.4	2.06	6000	0.40	2.05	6050	0.34
	85	2.15	5700	0.47	2.03	6050	0.36	2.03	6100	0.26
940	295	2.05	6050	0.40	2.06	6000	0.53	2.05	6050	0.32
	85	2.17 2.3	5700 5400	- -	2.06	6000	0.46	2.06	6000	0.34
943	295	2.1	5900	0.45	2.06	6000	0.50	2.06	6000	0.39
	85	2.17 2.3	5700 5400	- -	2.1	5900	0.50	2.07	5950	0.3
947	295	2.06	6000	0.43	2.1	5900	0.50	2.09	5920	0.41
	85	2.17 2.32	5700 5350	- -	2.21	5600	0.60	2.12	5820	0.36
952	295	2.15	5750	0.43	2.1	5900	0.60	2.12	5850	0.40
	85	2.17 2.34	5700 5300	- -	2.22	5600	0.57	2.14	5800	0.42
954	295	2.214	5600	0.77	2.1	5900	0.88	2.20	5650	0.51
	85	2.17 2.38	5700 5200	- -	2.38	5200	0.47	2.21	5600	0.43
958	295	1.82 2.3	6800 5400	- -	2.214	5600	0.9	2.25	5500	0.50
	85	2.38	5200	0.60	2.34	5300	0.5	2.28	5400	0.51
961	295	1.82 2.33 2.65	6800 5350 4650	- - -	2.3	5400	1.05	2.42	5100	0.56
	85	2.58	4800	0.8	2.53	4900	0.34	2.47	5000	0.53
962	295	2.43	5100	0.57	2.38	5200	0.8	-	-	-
	85	2.63	4700	0.68	2.7	4600	0.68	2.52	4900	0.35
S2	295	2.63	4700	0.53	2.4	5150	0.6	2.52	4900	0.58
	85	2.75	4500	0.48	2.78	4450	0.52	2.56	4840	0.5

Table 8.3: The peak position energies and the band width at half height of FEL, REL and PL(UV) emission bands recorded from ZnS_xSe_{1-x} diodes. (See Table 8.1 for the impurity contents and compositions of the mixed crystals).

described in earlier chapters. The brightness-current characteristics obeyed the $B \propto i^n$ relation with n equal to 1.5 in forward, and 1.03 in reverse bias. A maximum brightness of 30 Ft-L was achieved at 295 K with a conversion power efficiency of $7 \times 10^{-5}\%$.

As the sulphur concentration was increased the forward B/I-V characteristics shifted towards higher biases, although reverse biases to pass similar current levels were still below 20 V. One such example is illustrated by the curve in Figure 8.14 for the Au-ZnS_{0.6}Se_{0.4}:I,Zn+Al diode No.954. The forward B/I-V characteristics were similar to those of diode No.944 with the same composition but with no aluminium. The brightness varied almost exponentially with applied bias. At the highest current levels, saturation effects were observed in the B/I-V characteristics which were due to the limitation of the diode current by the series resistance of the device. However no such saturation was observed at 85 K. The reverse B/I-V characteristics would appear to have shifted to lower applied biases compared with those of diode No.944 (see Figure 8.9).

A poor brightness of 7 Ft-L only was obtained at 295 K with a power efficiency of $2 \times 10^{-5}\%$. As the sulphur concentration was increased beyond 80%, the forward B/I-V characteristics shifted towards higher applied biases and no saturation was observed. This is attributed to the non-ohmic behaviour of the indium contact at these compositions.

The B/I-V characteristics obtained from an Au-ZnS:I,Zn+Al device are illustrated in Figure 8.15. There was a threshold of about 11 V for the onset of forward EL at room temperature (the indium negative), and there was then a rapid increase in both brightness and current with increasing applied bias. At 85 K, the threshold for FEL was around 8 V. With increasing bias both the brightness and current increased at first rapidly and then less rapidly at biases between 12-16 V. Beyond 16 V the current began to increase more rapidly than exponentially, as an

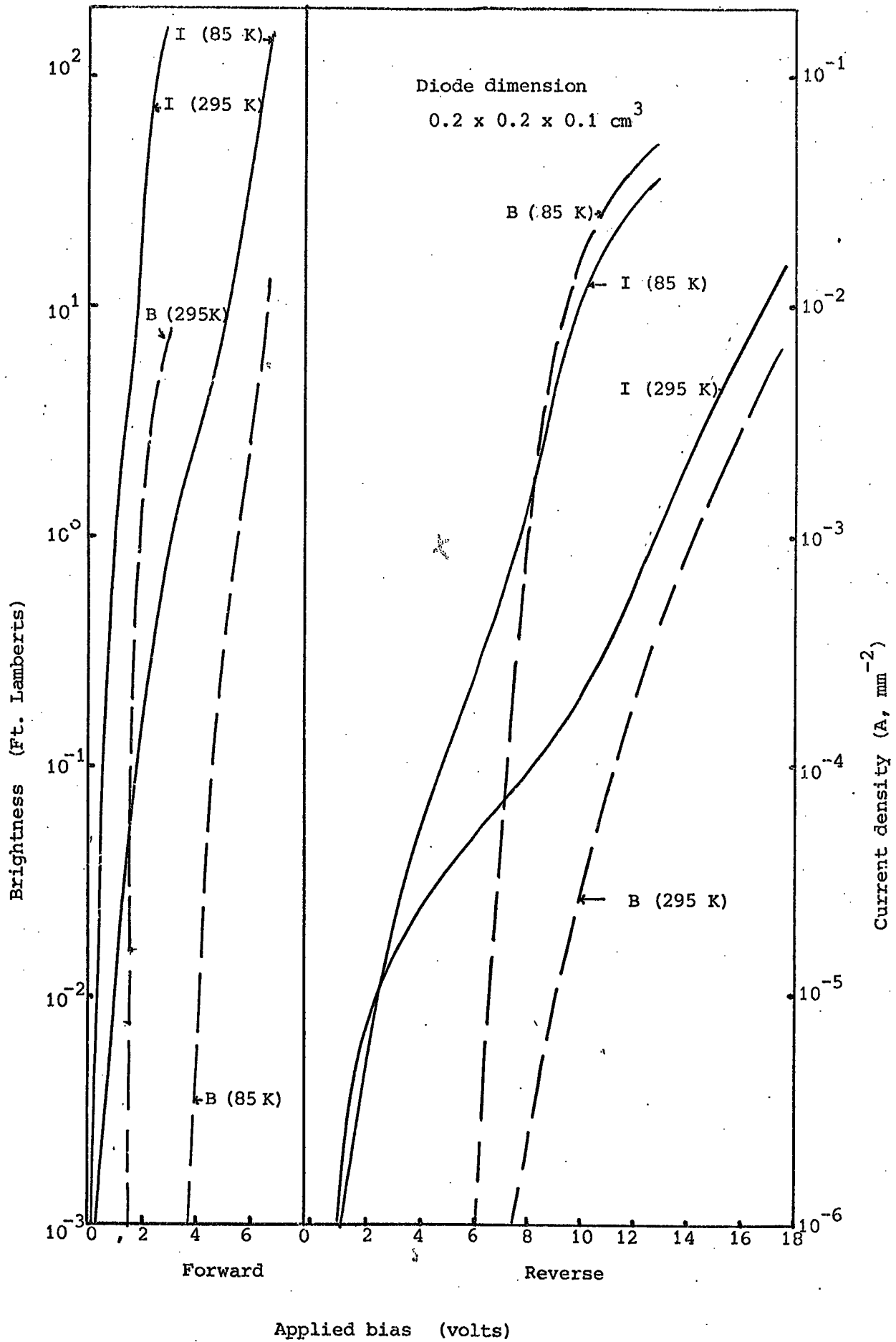


Figure 8.14: The variation of brightness and diode current as a function of applied bias in Au-ZnS_{0.6}Se_{0.4}:I,Zn+Al Diode No. 954.

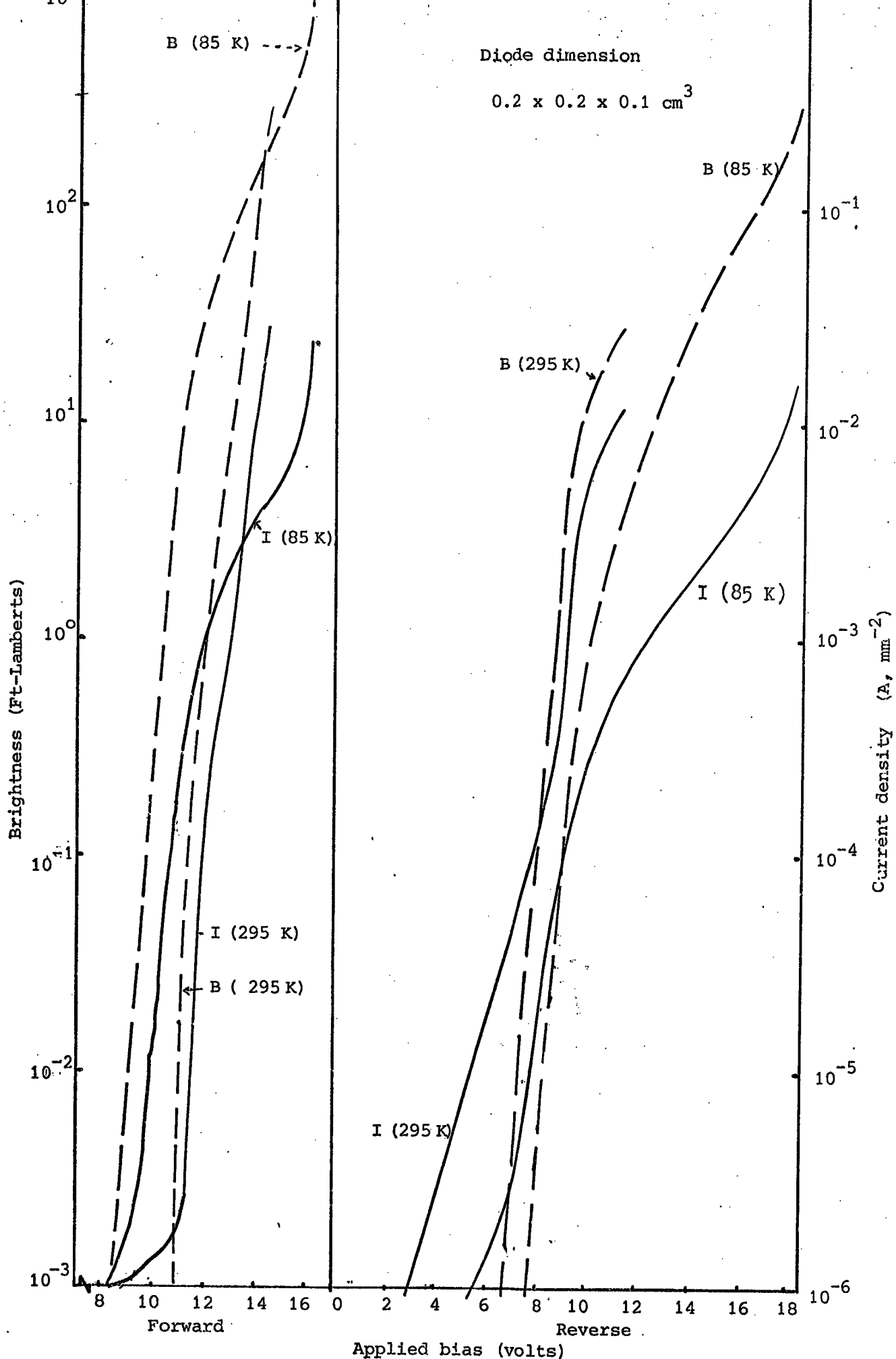


Figure 8.15: The variation of brightness and current as a function of applied bias in Au-ZnS:I,Zn+Al-In , Diode No.S2

avalanche process developed. The brightness-current variation obeyed a relation of the form $B \propto i^{1.05}$ at both 295 and 85 K. Brightnesses of 300 Ft-L at 295 K and 1000 Ft-L at 85 K with an input power around 400 m W corresponded to conversion power efficiencies of about $9 \times 10^{-4}\%$ at 295 K and $3.1 \times 10^{-3}\%$ at 85 K. The reverse I-V characteristics contained some leakage currents at low applied biases. The voltage threshold for observable REL emission was between 6 and 8 V. The B-I characteristics could again be described by a relation of the form $B \propto i^{1.05}$. However the reverse brightnesses of 30 Ft-L at 295 and 300 Ft-L at 85 K corresponded to conversion power efficiencies of $2.4 \times 10^{-4}\%$ and $1.1 \times 10^{-3}\%$ respectively.

The spectral distribution of the FEL, REL and PL emissions of the mixed crystals containing iodine and aluminium were also measured. The spectral distributions of the FEL emissions of the various devices are illustrated in Figure 8.16. The FEL spectra obtained from the Au-ZnSe:I,Zn+Al diode No.932, exhibited a single broad band (see Table 8.3) centred at 2.05 eV (6050 Å). The wavelength of the FEL emission did not change significantly in mixed crystals containing sulphur up to 40 molar percent, but with higher sulphur content shifted gradually to higher energies with increasing band width (see Table 8.3). At the ZnS end the FEL consisted of a blue emission peaking at 2.63 eV (4700 Å). It is interesting to note that the blue FEL emission in ZnS shifts to a green FEL emission at 2.43 eV (5100 Å) when as little as 2% ZnSe is added to ZnS. At 85 K, the FEL spectra of Au-ZnS_xSe_{1-x} devices were all slightly displaced to high photon energies (see Figure 8.17). The emission in ZnSe consisted of a yellow band at 2.17 eV (5700 Å) with a distinct shoulder in the green. The yellow emission band was also seen in mixed crystals with sulphur concentrations up to 60%, and its photon energy was not greatly dependent on the sulphur content. However the green emission

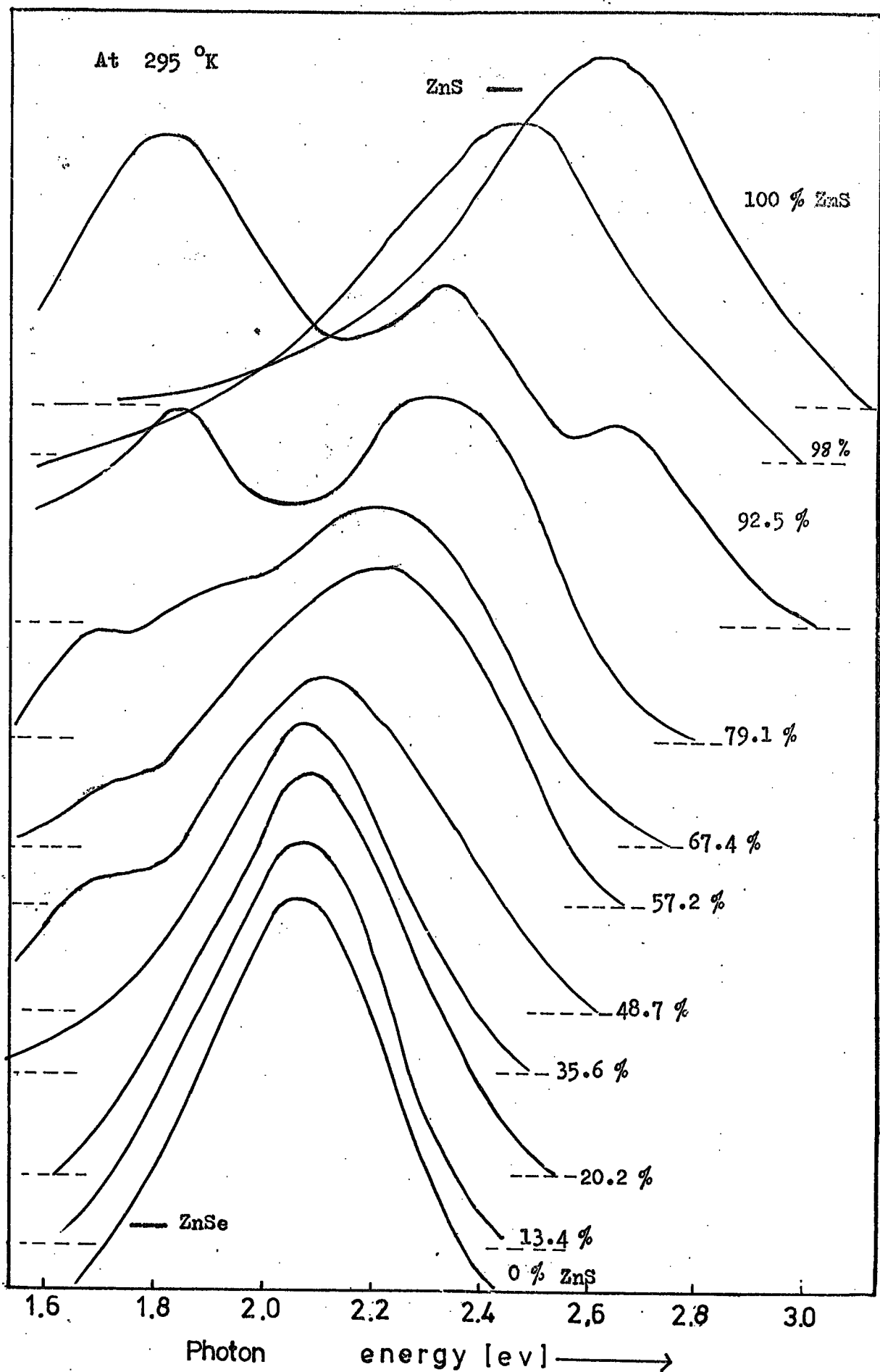


Figure 8.16: Forward-bias electroluminescence spectra of $\text{ZnS}_x\text{Se}_{1-x}$:I,Zn,Al. crystals

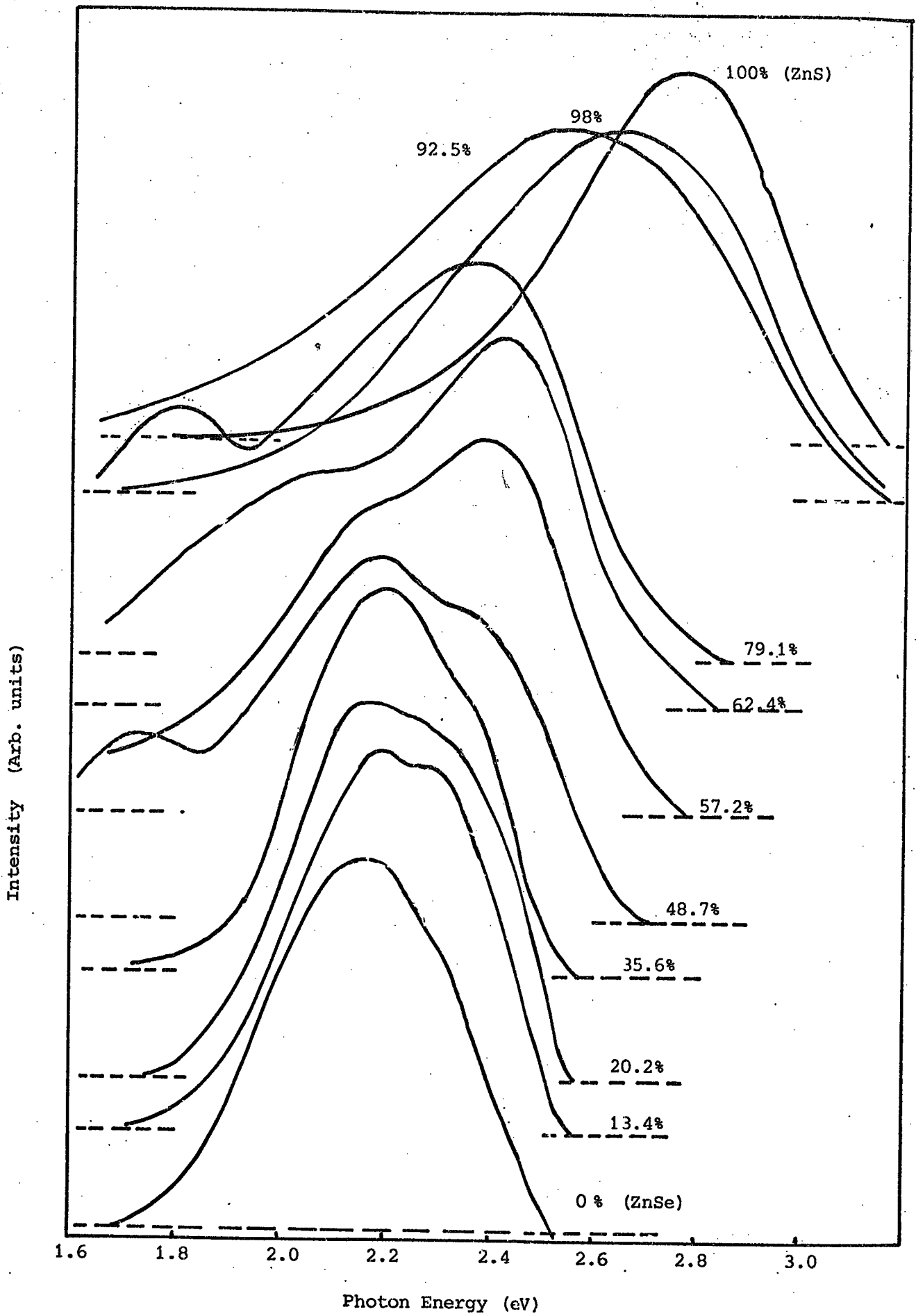


Figure 8.17: Forward bias EL spectra in $\text{Au-ZnS}_x\text{Se}_{1-x}:\text{I,Zn,Al}$ crystals recorded at 85 K.

band in ZnSe was found to increase in intensity and did shift to higher energies as the sulphur concentration increased. At the composition $\text{ZnS}_{0.6}\text{Se}_{0.4}$ the FEL emission consisted of a broad band in the green at 2.38 eV (5200 Å) with a shoulder in the yellow at 2.17 eV (5700 Å). There was a small additional band in the red, peaking at 1.72 eV (7200 Å). For crystals with increasing sulphur concentrations beyond 60% the yellow emission band disappeared gradually as the green band shifted to higher energies up to 2.75 eV (4500 Å) at 100% ZnS. The energies of the FEL emission bands from mixed crystals at intermediate compositions are listed in Table 8.3, and their variation with composition is illustrated in Figure 8.20.

The spectral distributions of the REL emission at 295 K from mixed crystals are illustrated in Figure 8.18. The REL emission consisted mainly of a yellow band centred at about 2.06-2.1 eV (6000-5900 Å) in crystals with sulphur concentrations up to 70% and then shifted gradually to higher energies to 2.4 eV (5150 Å) at the ZnS end. At 85 K the peak position of the REL emission shifted gradually to higher energies as the sulphur concentration increased (see Figure 8.19 and Table 8.3). The REL emission band from ZnS was located at about 2.78 eV (4450 Å). The variation of the peak position of the REL with composition can be seen in Figure 8.20.

The PL emission of $\text{ZnS}_x\text{Se}_{1-x}:\text{I,Zn,Al}$ crystals was recorded at 295 K and 85 K (see Figures 8.21 and 8.22, and Table 8.3). The orange emission typical of ZnSe diodes gradually shifted to higher energies as the sulphur concentration increased, see Figure 8.27. The rate of shift of the peak position to higher energies again was much more rapid for compositions with sulphur concentrations in excess of 70%. The PL emission from $\text{ZnS}:\text{I,Zn,Al}$ was centred at 2.53 eV (4900 Å) at 295 and 2.55 eV (4850 Å) at 85 K.

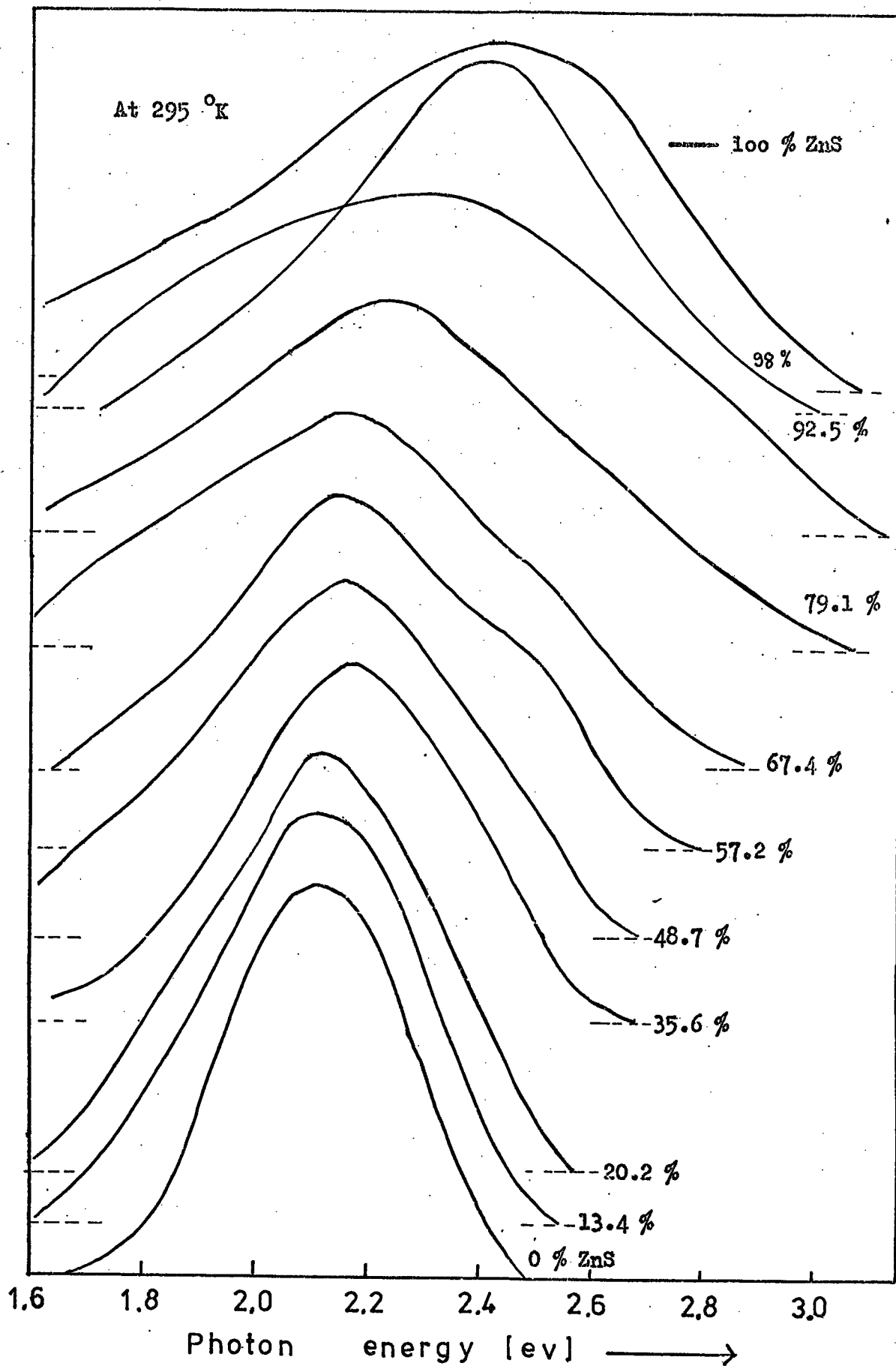


Figure 8.18: Reverse-bias electroluminescence spectra of $\text{ZnS}_x\text{Se}_{1-x}$ crystals

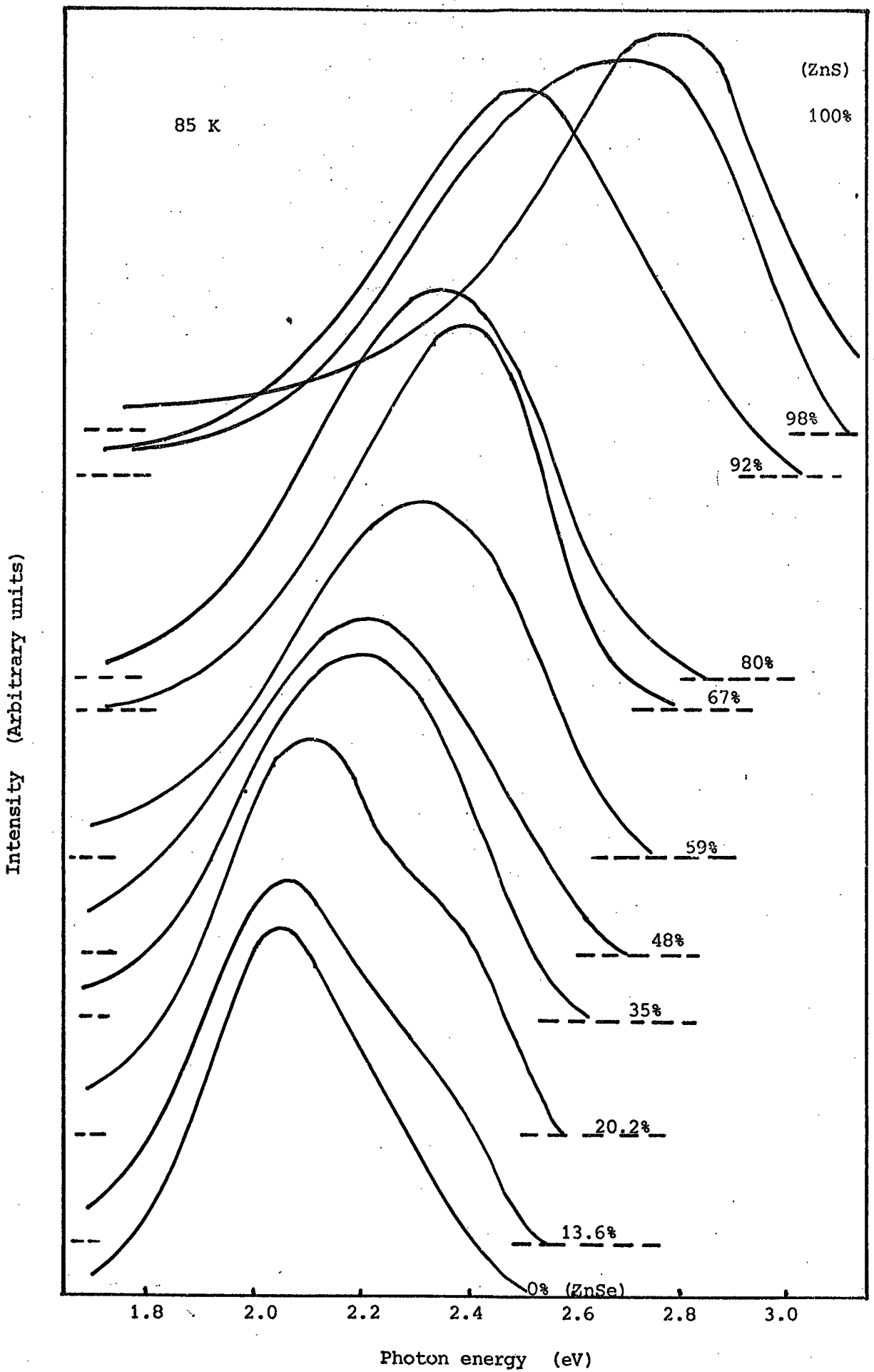


Figure 8.19: Reverse bias EL spectra of $\text{Au-ZnS}_x\text{Se}_{1-x}$; I, Zn, Al diodes at 85 K.

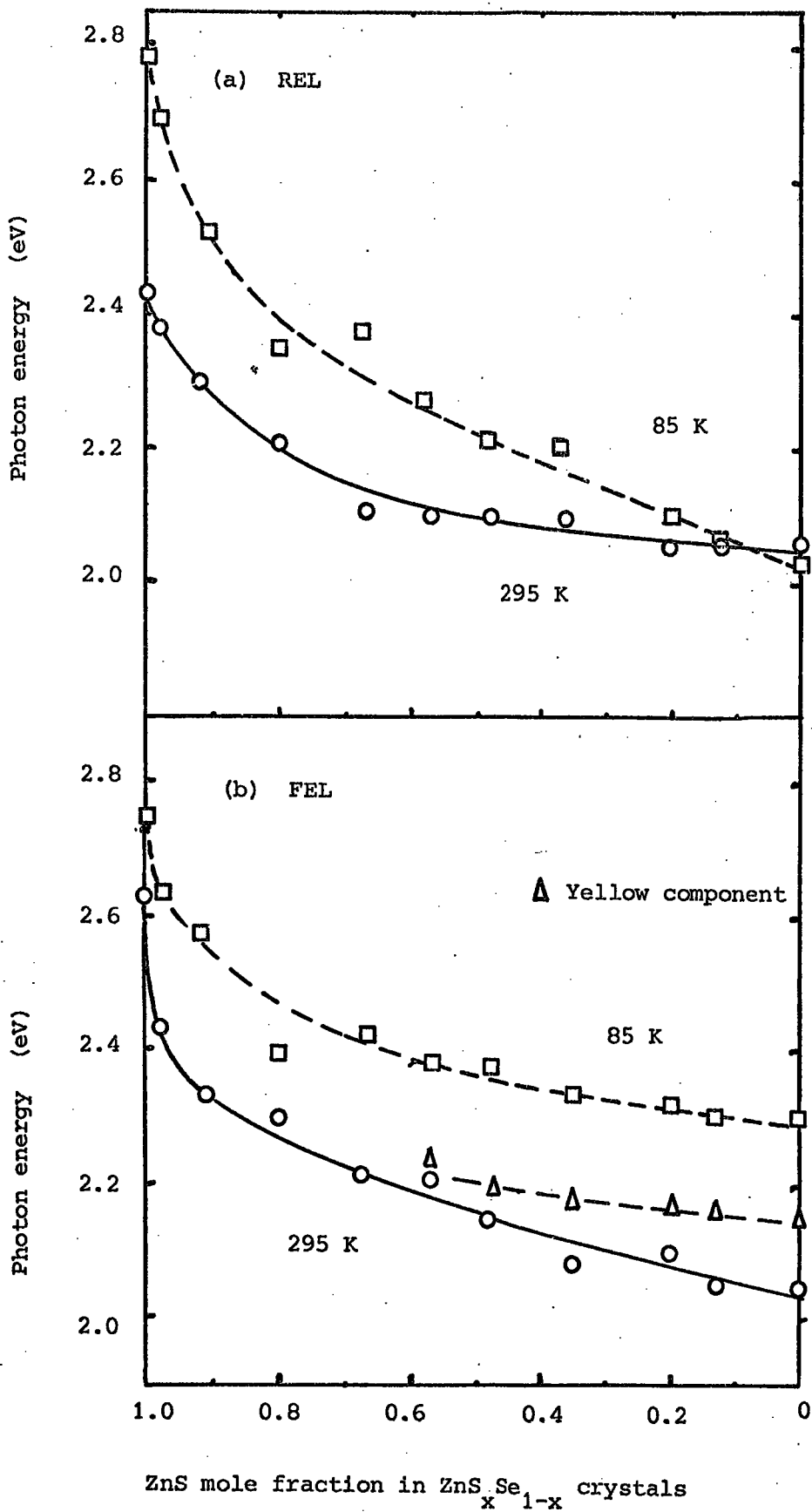


Figure 8.20: The energy peak position of the REL and FEL emissions as a function of ZnS mole fraction of $\text{Au-ZnS}_x\text{Se}_{1-x}:\text{I,Zn,Al}$ diodes.

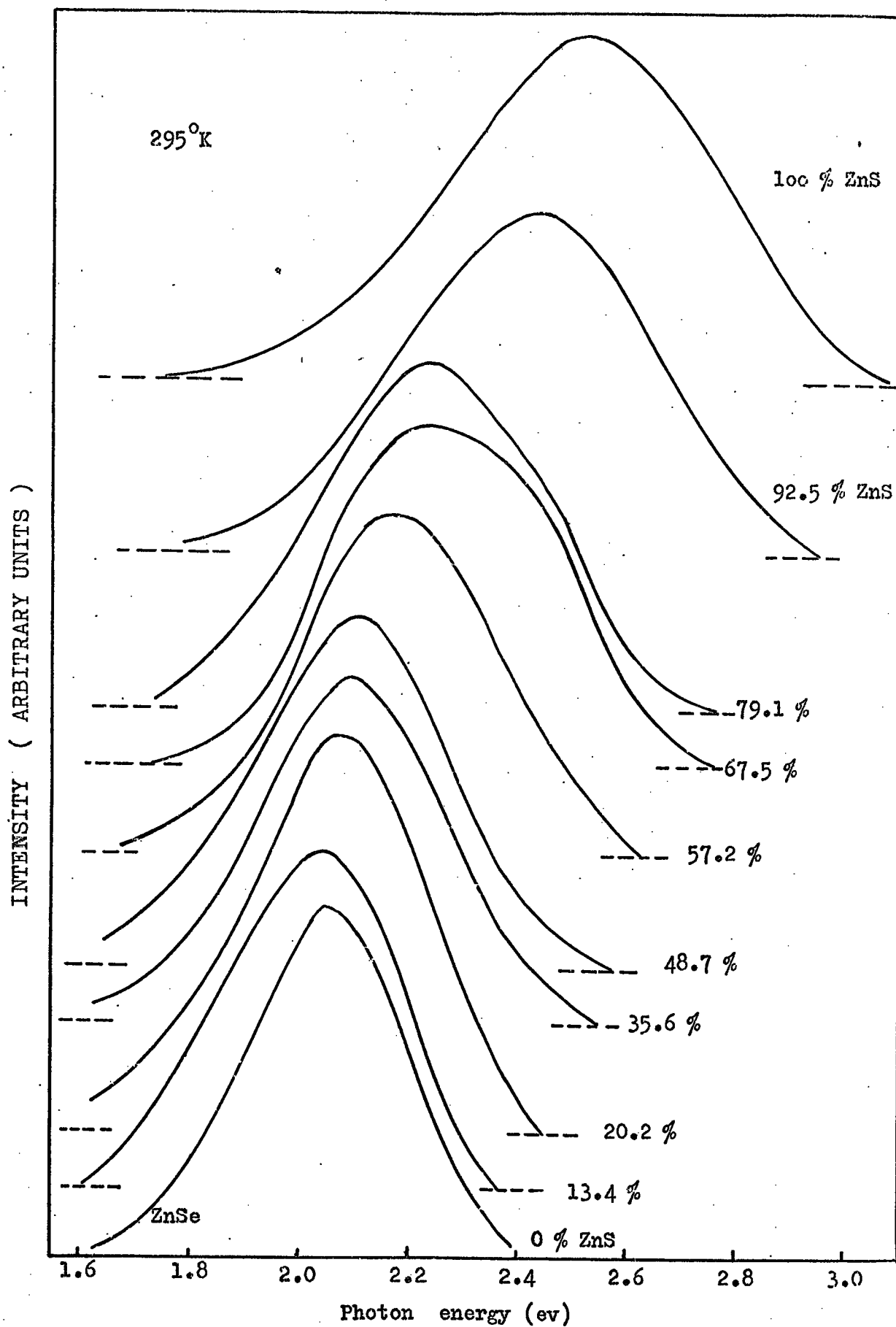


Figure 8.21: Photoluminescence spectra under 3650 Å excitation

of ZnS_xSe_{1-x} ; I,Zn,Al crystals. at 295°K

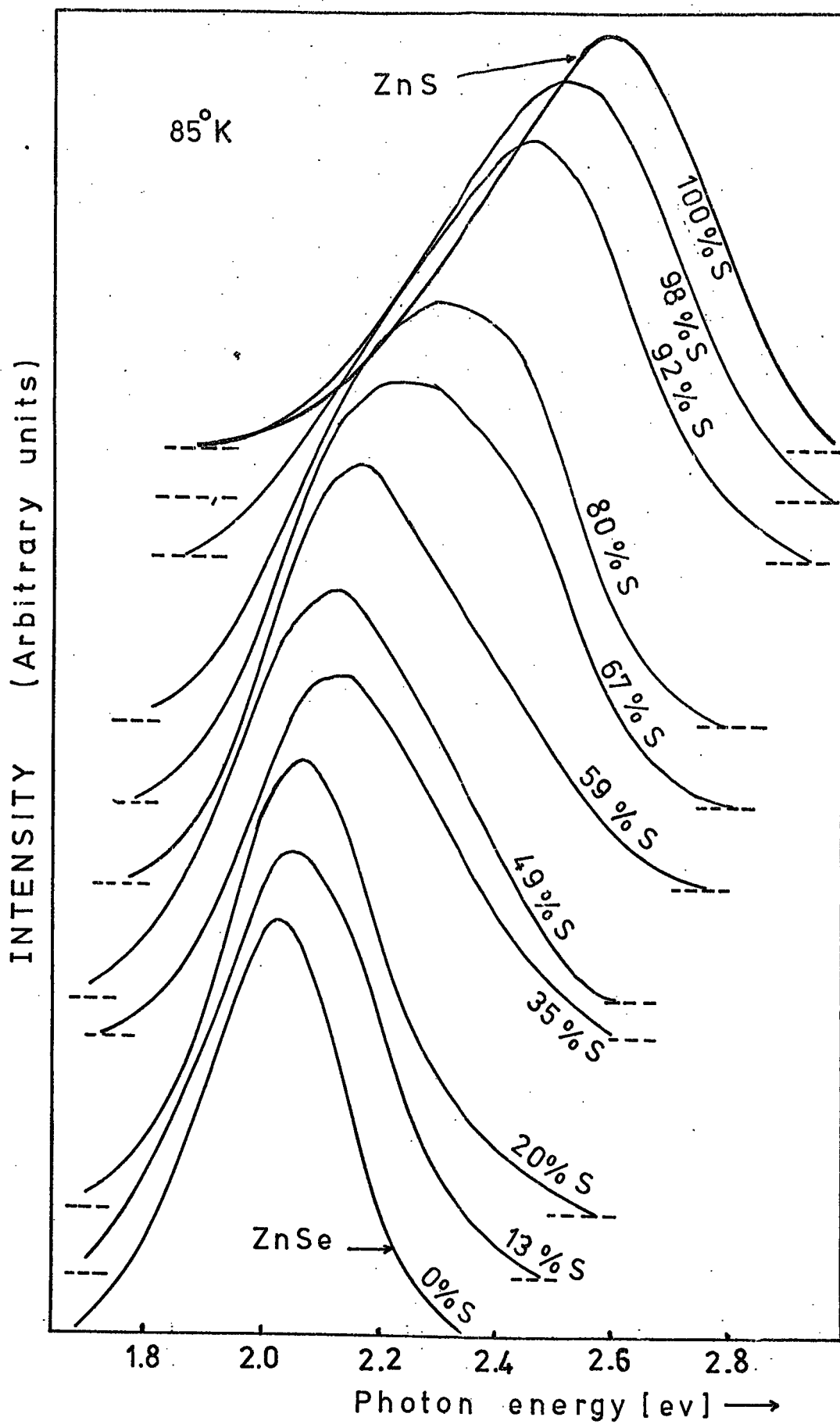


Figure 8.22: Photoluminescence spectra under 3650\AA excitation of $\text{ZnS}_x\text{Se}_{1-x}$, Zn, Al. crystals. at 85°K

The PL excitation spectra were also studied and were measured by monitoring the emission in three distinct bands, namely the orange-yellow at 2.06 eV (6000 Å), the green at 2.3 eV (5300 Å) and the blue at 2.53 eV (4900 Å). The luminescence excitation spectra of the orange-yellow emission are illustrated in Figures 8.23 and 8.24. The efficient excitation of the yellow band in mixed crystals occurred at photon energies well below that of band gap. The excitation spectra of the green band at 295 K could only be detected for crystals with sulphur concentrations exceeding 50%, see Figure 8.26, and for whole range of compositions at 85 K, see Figure 8.27. Similarly the excitation spectra of the blue emission could only be obtained for crystals with sulphur concentrations over 90% at 85 K. The result can best be illustrated in curves showing the variation of the peak energy of the excitation spectra against composition in Figure 8.27.

8.3.4 Mixed Crystals containing Manganese as a Luminescent Centre

The EL and PL emission from ZnSe diodes doped with manganese has been described in detail in Chapter 7. Here the EL and PL emission from a Au-ZnS_{0.6}Se_{0.4}:I,Mn,Zn+Al diode No.951 and a Au-ZnS:I,Mn,Zn+Al-In device No.973 were studied. The uncompensated donor concentration calculated from the straight line C^{-2} -V plot obtained at 295 K, on diode No.950 (see Figure 8.3) was $2.6 \times 10^{15} \text{ cm}^{-3}$. However comparable information could not be obtained for the ZnS device which showed a constant capacitance of about $7 \times 10^{-9} \text{ F cm}^{-2}$ irrespective of the bias. The B/I-V characteristics from these two devices are shown in Figure 8.28. The reverse B/I-V characteristics obtained from both diodes exhibited exponential regions at low applied biases, and saturation occurred at the highest current levels. Maximum brightnesses of 4 Ft-L and 40 Ft-L observed in the two devices (Nos. 951 and 973) in reverse bias

INTENSITY (ARBITRARY UNITS)

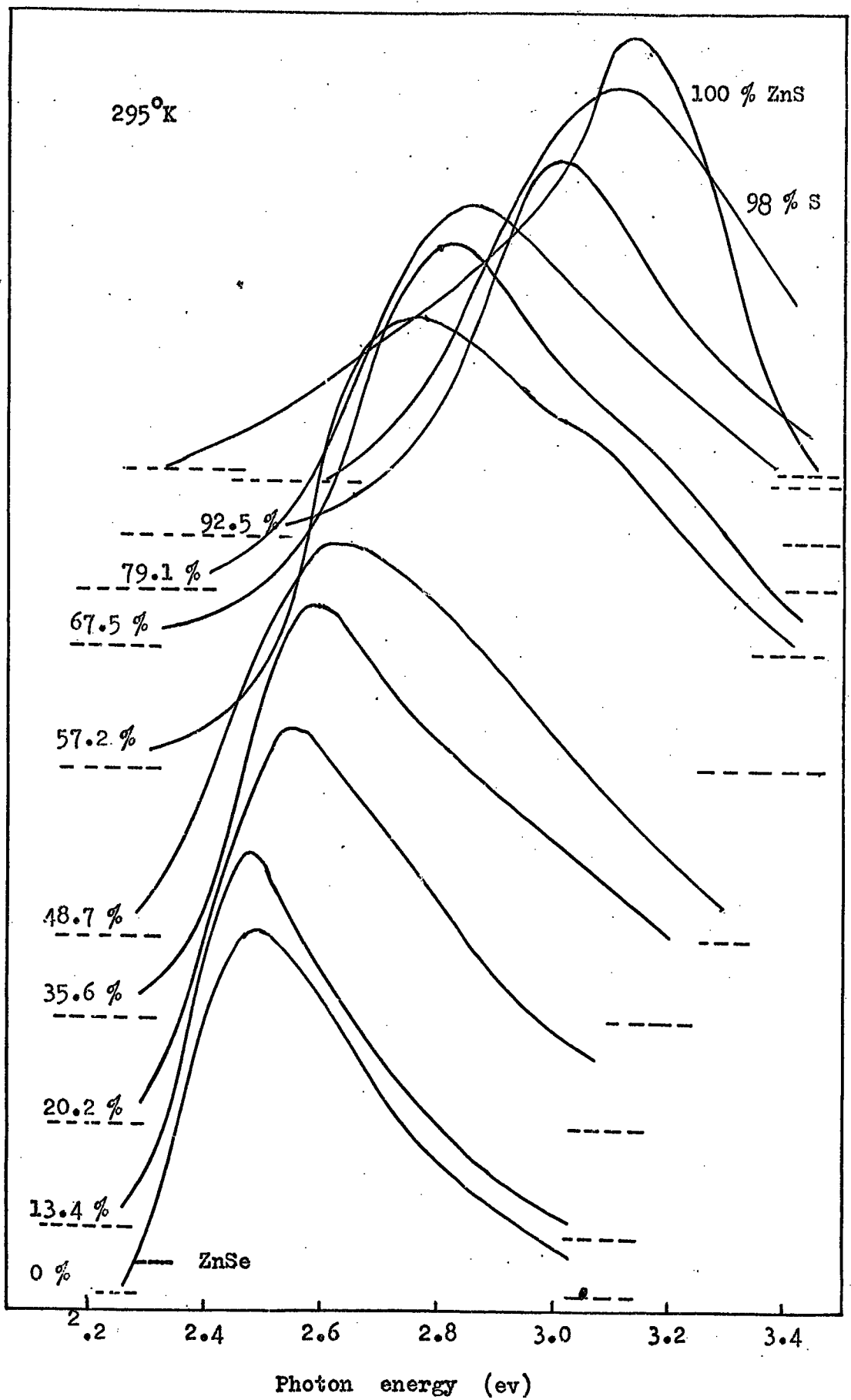


Figure 8.23: Excitation spectra of $\text{ZnS}_x\text{Se}_{1-x}$: I,Zn,Al crystals monitored to a band at 6000 \AA at 295°K .

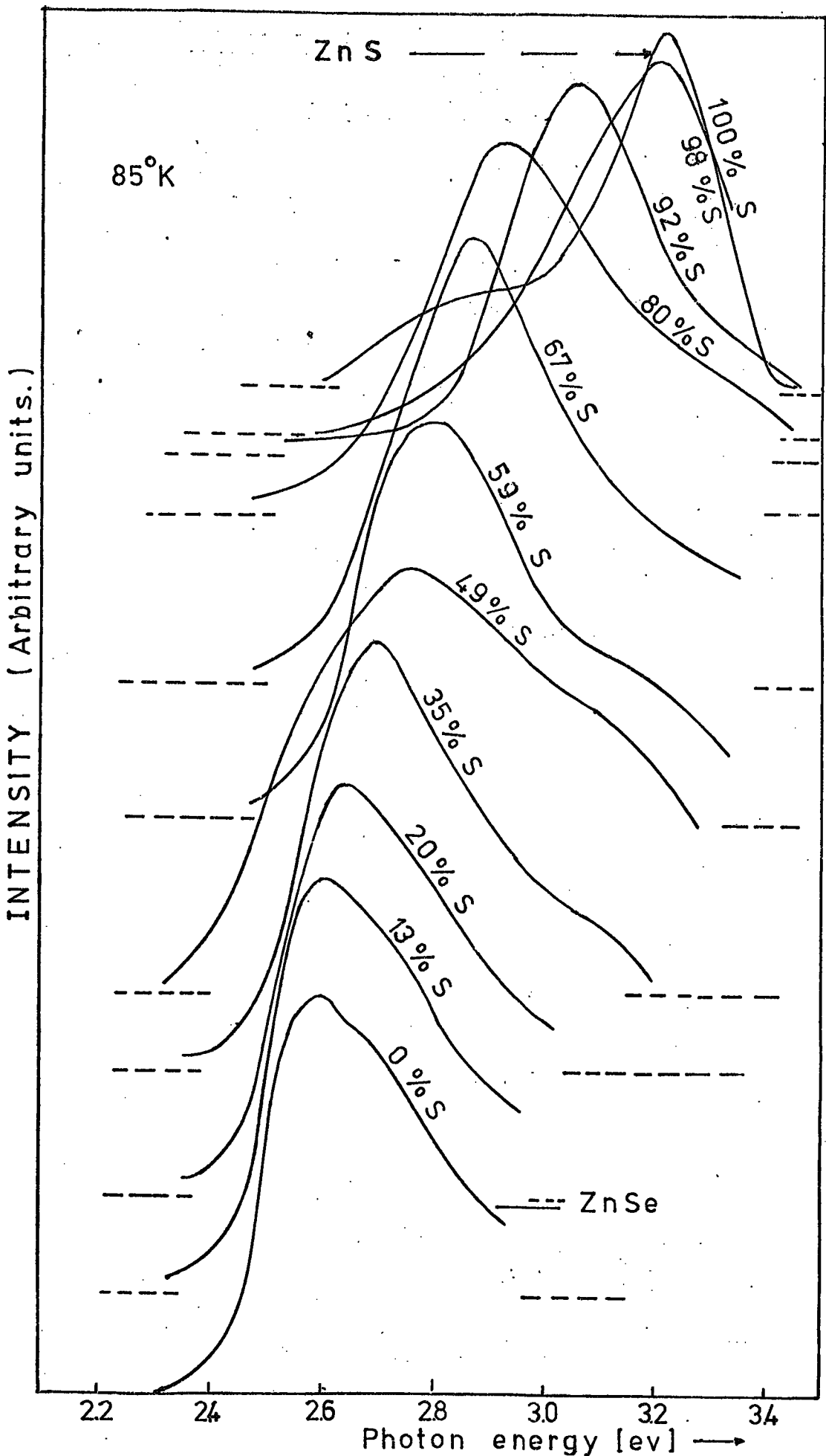


Figure 8.24: Excitation spectra of ZnS:Se :I,Zn,Al crystals monitored to band at 6000 \AA at 85°K

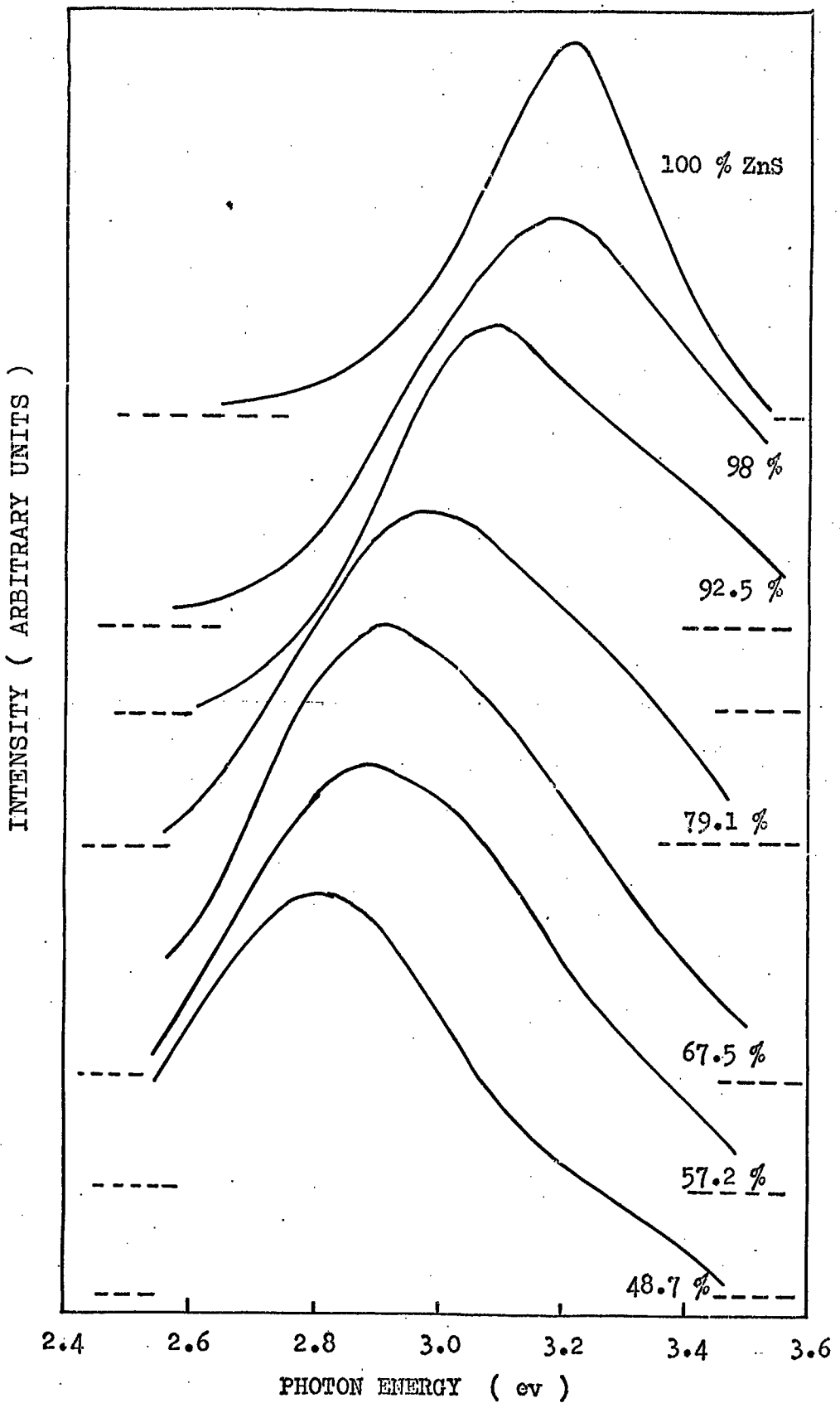


FIG. 8.25: Excitation spectra of $\text{ZnS}_x\text{Se}_{1-x}:\text{I}$ crystals monitored to a band at 5300 \AA at 295°K .

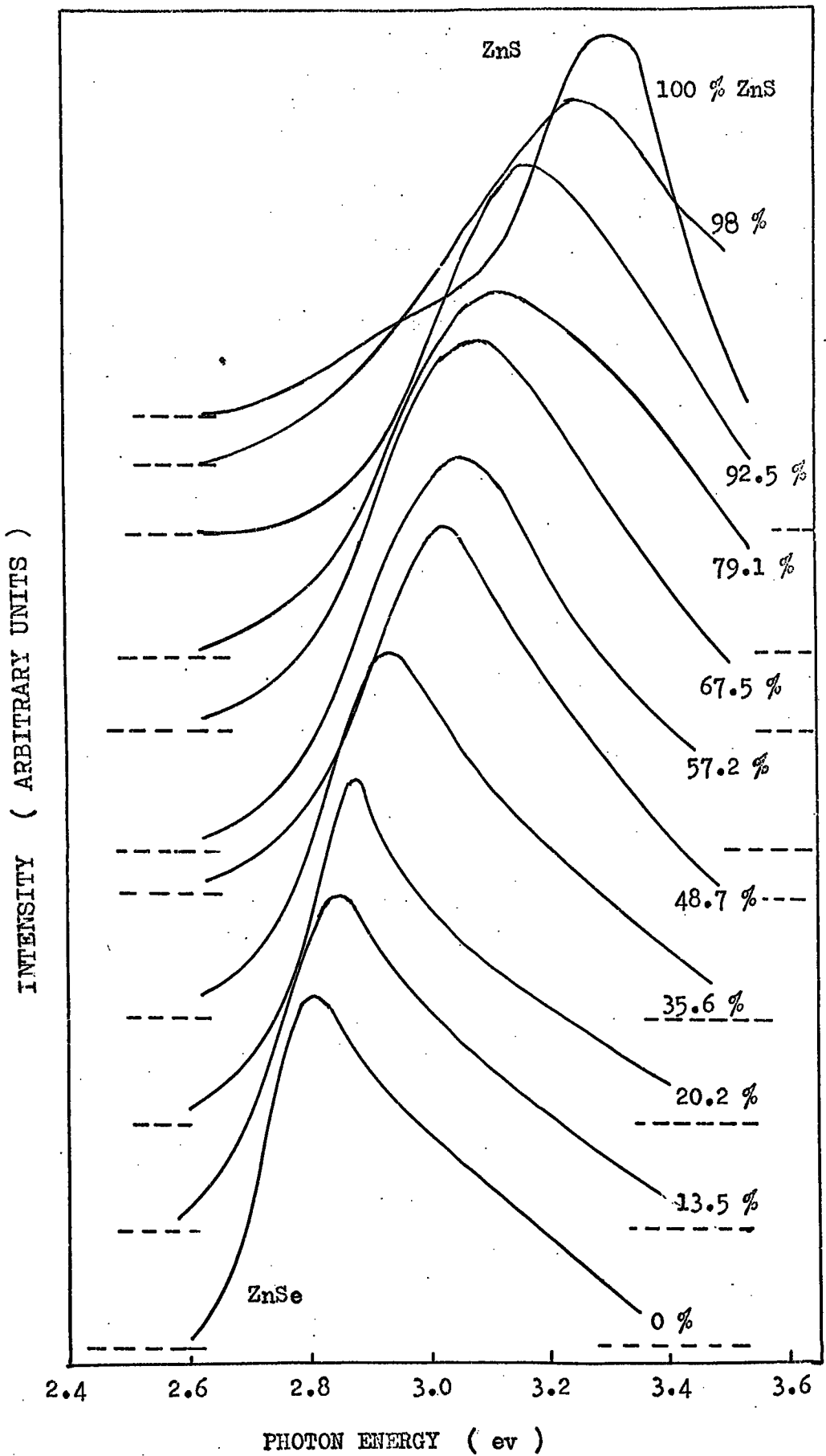


FIG 8.26: Excitation spectra of ZnS Se_{1-x} : I, Zn, Al crystals monitored to a band at 5300 Å, at 85°K.

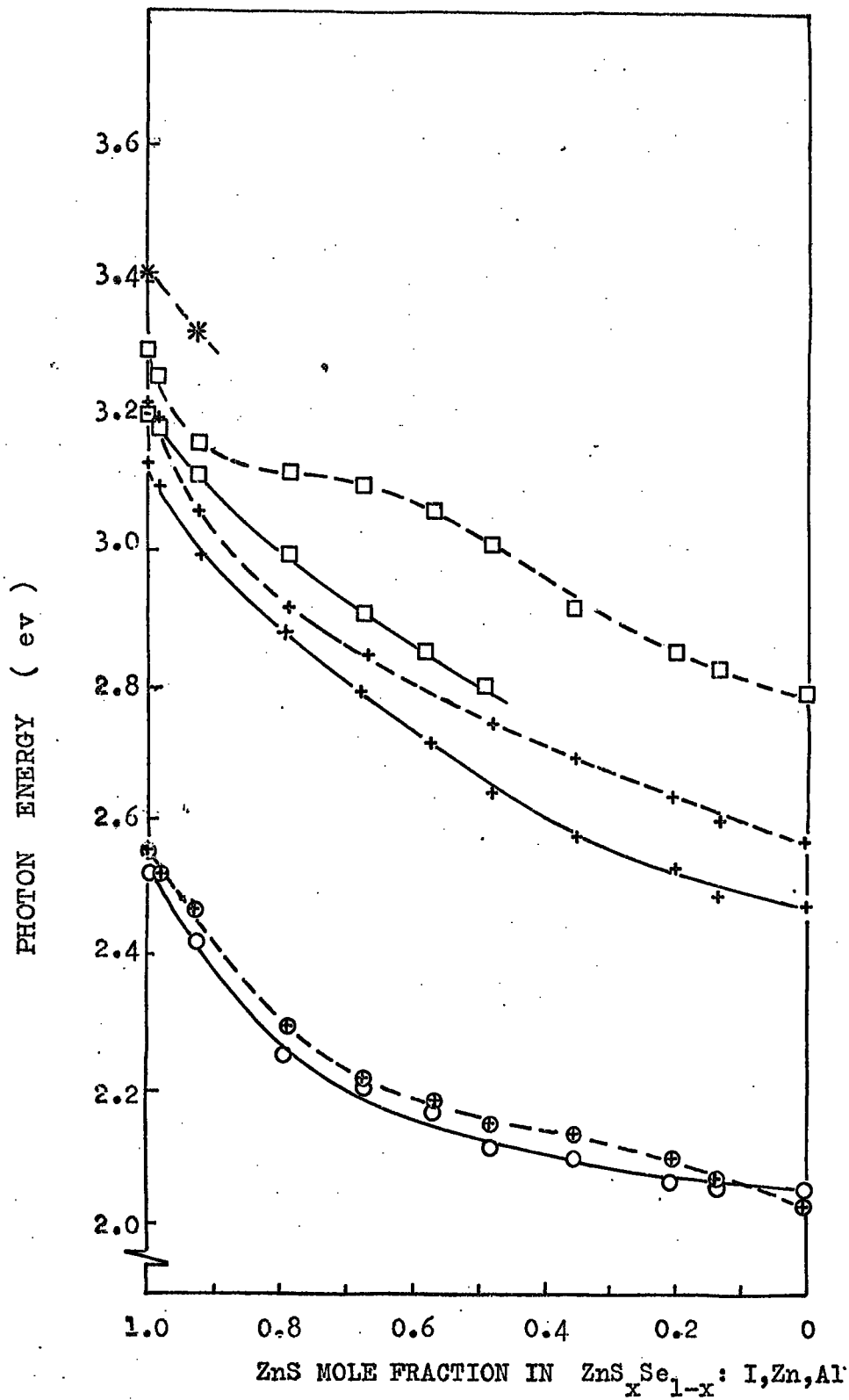


FIG 8.27: THE EMISSION AND THE EXCITATION SPECTRA OF $ZnS_xSe_{1-x}: I$ CRYSTALS HEATED IN MOLTEN ZINC AND ALUMINUM. PHOTOLUMINESCENCE —○—○— AT 295°K, —⊕—⊕— AT 85°K . EXCITATION SPECTRA MONITORED TO BANDS; 6000 Å; —+—+— AT 295°K AND —++—++— AT 85°K, 5300 Å; —□—□— AT 295°K AND —□—□— AT 85°K, 4900 Å; —*—*— AT 85°K

corresponded to power conversion efficiencies of $2 \times 10^{-5}\%$ and $4 \times 10^{-5}\%$. In forward bias (indium negative), brightnesses and currents varied almost exponentially with voltage at low applied biases but when the biases exceeded a certain value, i.e. 20 V in diode No.950, and 35 V in device No.973, the brightness and current began to increase very rapidly as an avalanche process developed. The brightnesses of 50 Ft-L in diode No.950 and 100 Ft-L in device No.973 corresponded to power conversion efficiencies of $3.4 \times 10^{-5}\%$ and $2 \times 10^{-4}\%$.

The spectral distributions for the EL and PL emissions obtained from these two diodes are illustrated in Figure 8.29. Both diodes exhibited the characteristic manganese emission band in electroluminescence. The emission was almost the same as in ZnSe:Mn which was not unexpected. The PL, REL and FEL emission bands from the two devices were located at 2.12 eV ($5830 \text{ \AA} - 5860 \text{ \AA}$) at 295 K with a slightly narrower band width in FEL. The position of the maximum EL emission did not change on cooling, although a slight shift in PL emission to lower energies was often observed. The peak positions and the band widths of these emissions are tabulated in Table 8.3.

The excitation spectra of the PL emission from mixed crystals containing manganese are illustrated in Figure 8.30 together with an excitation spectrum obtained from a resistive sample of ZnSe:Mn. The excitation spectra in these samples contained a series of narrow bands resulting from the transitions from the ground (6A_1) to the first (4T_1) second (4T_2) and third (${}^4A_2, {}^4E$) excited states of the Mn^{2+} ion. The first excitation band, centred at about 2.3 eV (5370 \AA) is at almost the same energy in all these mixed crystals. However the photon energy of the second and the third excitation bands shifts to slightly higher energies as the selenium is replaced by sulphur. The peak position of the excitation bands are tabulated in the inset of Figure 8.30.

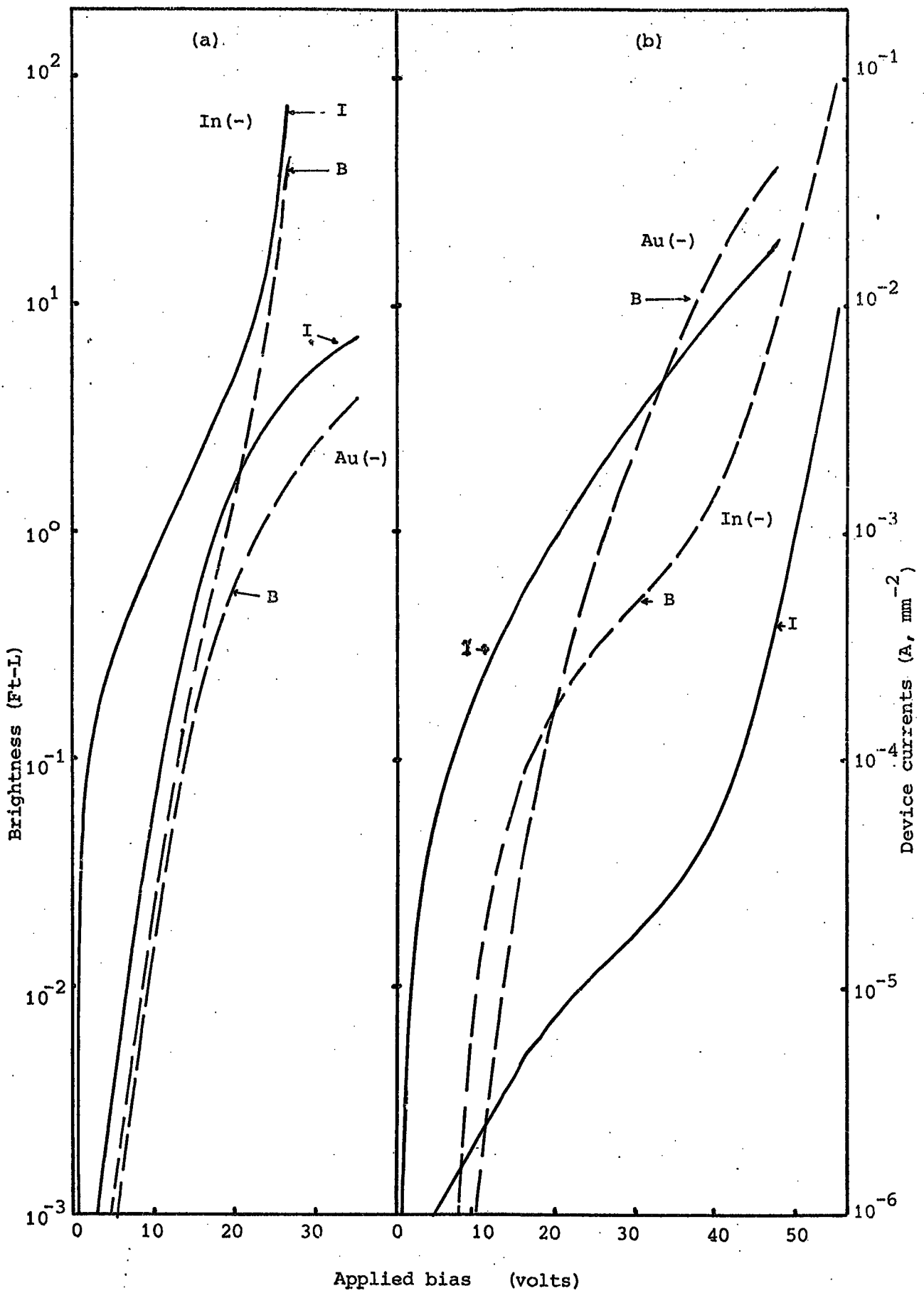


Figure 8.28: Brightness/current variation as a function of current in (a) Au-ZnS_{0.6}Se_{0.4}:I,Mn,Zn+Al and (b) in Au-Zns:I,Zn+Al-In devices at 295 K.

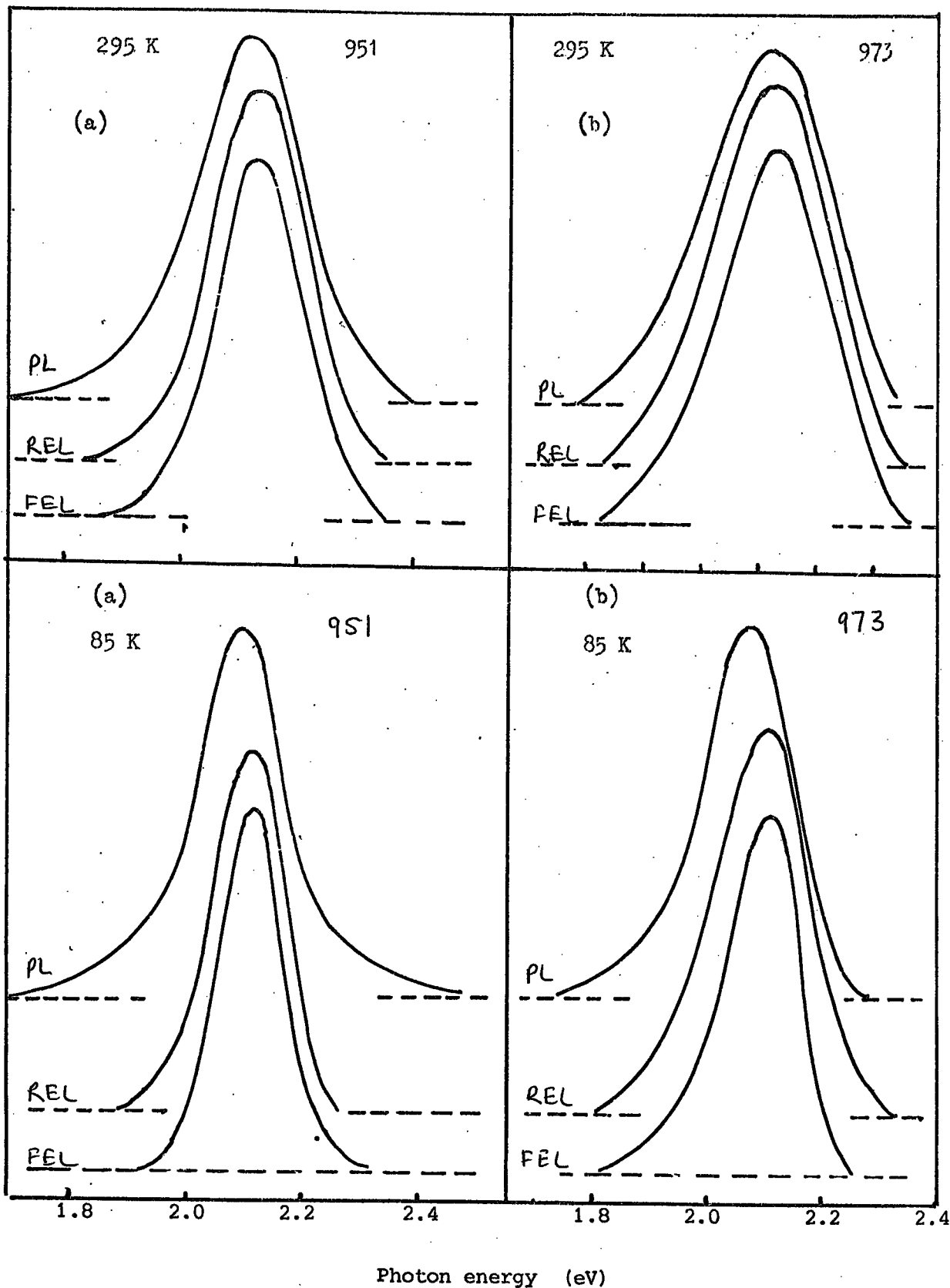


Figure 8.29: Spectral distribution for the FEL, REL and PL(UV) emissions in
 (a) $\text{Au-ZnS}_{0.6}\text{Se}_{0.4}:\text{I,Mn,Zn+Al}$, (Diode No.951) and
 (b) $\text{Au-ZnS}:\text{I,Mn,Zn+Al-In}$ (Device No.973) devices.

INTENSITY (Arb. Units)

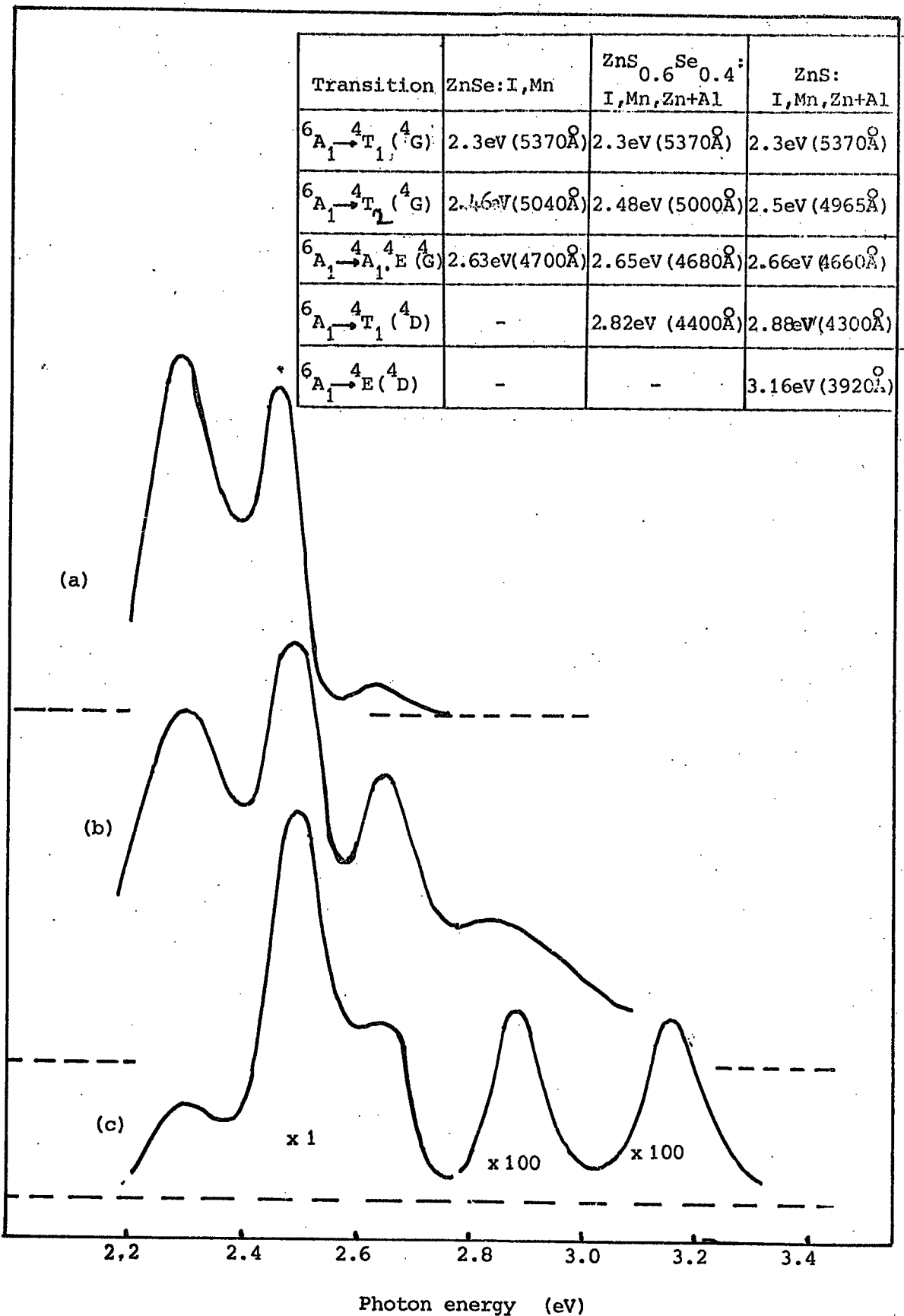


Figure 8.30: Spectral distribution of the PL excitation spectra in (a) Resistive ZnSe:I,Mn, (b) Au-ZnS_{0.6}Se_{0.4}, I,Mn,Zn+Al diode No.951, (c) Au-ZnS:I,Mn,Zn+Al device No.973, recorded at 85 K. The inset shows the photon energy of the peaks of the excitation bands.

8.4 THE MAINTENANCE OF Zn(S,Se) DIODES

Most of the light emitting devices produced on mixed crystals of zinc sulpho-selenide, have exhibited a deterioration in brightness similar to that observed in ZnSe diodes. Thus when the diodes were operated at a constant current for several hours, the intensity of the EL first increased and then decreased slowly. During this time the applied bias increased continuously. These processes occurred at a much faster rate than those observed in ZnSe diodes. The decay of the REL was irreversible for most of the mixed diodes with reasonable ohmic contacts. However in some mixed crystal devices which showed EL for both directions of the applied bias (i.e. devices with non-ohmic indium contacts), the decay process was much slower. Furthermore, applications of the bias in one direction bias offset slightly the decay effects produced by similar biases in the opposite direction. This again may have been due to ionic movement in the high field regions of the bulk.

8.5 DISCUSSION

8.5.1 Electrical Properties

The electrical properties of EL diodes prepared on $\text{ZnS}_x\text{Se}_{1-x}$ mixed crystals are strongly dependent on whether ohmic contacts can be obtained on these materials. Kaufman and Dowbor (1974) have studied the mechanisms of the formation of ohmic contacts to $\text{ZnS}_x\text{Se}_{1-x}$ crystals. Although they did not describe detailed I-V characteristics of their devices, they suggested that indium and most of the indium alloys dissolve the $\text{ZnS}_x\text{Se}_{1-x}$ so that upon cooling a layer is deposited on the conducting crystal which makes the ohmic contact. In short, a liquid-phase epitaxial layer is grown from the zinc chalcogenides

dissolved in liquid indium. In the present work, the resistivities of mixed crystal dice, after heat treatment in a molten mixture of zinc and aluminium, were often found to be non-uniform. It appears that a low donor concentration in the surface layers of a die was associated with our procedure for removing it from the molten mixture of zinc and aluminium. During this process there was a period of about 10 minutes during which the dice were at elevated temperatures in the vapour rather than in the melt. No successful ohmic contacts were put on any such dice (see curve (d), Figure 8.1) using indium metal. However after removal of the resistive surface layers by mechanical polishing satisfactory ohmic contacts could readily be formed on conducting dice. Another important parameter in the preparation of ohmic contacts was the temperature. With mixed crystals containing sulphur concentrations higher than 30%, the temperature needed to obtain ohmic behaviour was well in excess of 350°C . At such temperatures the rate of zinc vacancy in-diffusion from the surface would be quite significant. The result would be to convert the surface regions of the mixed crystals to highly compensated insulating layers. In the present work the observation of one-carrier SCL currents in some of the devices with two symmetric indium contacts would strongly support the suggestions that insulating layers were formed under the indium contacts. The formation of insulating films during the fabrication of the indium contact was not controllable. In fact forming ohmic contacts on nominally pure mixed crystals was much easier than forming them on mixed crystals containing both iodine and aluminium.

The spectral distribution of the short circuit photocurrent in some of the Schottky diodes on mixed crystals was similar to that in ZnSe diodes. The low energy threshold was taken as a measure of the height of the barrier formed by gold in mixed crystals. Typically the barrier

height was around 1.8 eV when the gold had been deposited on to chemically cleaned crystals with sulphur concentrations around 60%. A minimum also occurred at photon energies just below the band gap. This minimum occurred over a slightly broader range of photon energies in the mixed crystals and it shifted to higher energies as the sulphur concentration increased. It was again noticeable that these minima corresponded to maxima in the PL excitation spectra. As with ZnSe, the fact that no contribution to the photocurrent was observed for photon energies which excite the S.A. centres to luminescence, would suggest again that these centres are highly localized.

The short circuit photocurrent in the Au-ZnS_{0.6}Se_{0.4}:I,Mn,Zn+Al diode No.951 exhibited an interesting feature, namely the series of maxima at photon energies of 2.48 eV (5000 Å), 2.65 eV (4680 Å) and 2.82 eV (4400 Å). These three maxima do correspond to the luminescence excitation bands of Mn²⁺ ions in the same crystal (see Figure 8.30). However the luminescence excitation band at 2.3 eV (5370 Å) was not reflected in the spectral response of the photocurrent. This again, as in ZnSe, would suggest that the electrons raised to the first excited state are not ionized to the conduction band, while in contrast, electrons in the second third and fourth excited states are. This implies that the ground state of the Mn²⁺ ion in ZnS_xSe_{1-x} crystals is associated with the conduction rather than valence band of the sulpho-selenides. This is not surprising, because if II-VI compounds can be approximately considered to be ionic the conduction band is derived from the energy bands of the cations and the valence bands from those of the anions. A variation of the composition of the host material from ZnSe to ZnS means that there is a variation in the energy of the valence band while that of the conduction band remains constant. Since an Mn²⁺ ion replaces a cation, it follows that its energy levels may also be controlled by the

conduction band in Zn(S,Se) solid solutions, and hence its ground state would remain parallel to the conduction band at a depth a little less than the energy of the second excited state.

Some of the EL devices prepared on mixed crystals with sulphur concentrations exceeding 80% exhibited a reversal of the direction of the photocurrent at some photon energies below the band gap. It is suggested that this is due to the non-ohmic behaviour of the indium contact which would tend to form a barrier. The Au-ZnS:I,Zn+Al-In device (see dashed curve in Figure 8.2) is a typical example. Assuming that the barrier created at the indium non-ohmic contact is slightly lower than that created under the gold electrode, then low energy photons would travel through the bulk of the ZnS to be absorbed in the indium and the resultant photo-excited electrons would be emitted into the ZnS. The low energy threshold was about 0.95 eV which provides a measure of the barrier height at non-ohmic indium metal. At higher photon energies the electrons would also be photo-excited into the ZnS from the gold electrode. Therefore the total photocurrent would be the sum of the two photo-excited components drifting in opposite directions. In our samples, the negative direction of the photocurrent, i.e. from In contact into ZnS, at low photon energies may be attributable to the fact that the indium contact was slightly larger than the gold dot. At photon energies larger than 3.3 eV most of the photons would be absorbed at the front surface of the dice. At photon energies a little less or equal to the band gap (≈ 3.6 eV), the free electron-hole pairs are generated within the depletion layer under the gold contact and are responsible for the rapid increase in the photocurrent in the opposite direction.

The C^{-2} - V plots for sample diodes which had reasonable ohmic contacts were found to be straight lines. From the slopes, the uncompensated donor concentrations of the mixed crystals were calculated to

be in the range $10^{15} - 10^{17} \text{ cm}^{-3}$. The voltage intercept, V_i , however was higher than the corresponding values of the photo-thresholds. This again was due to the presence of semi-insulating films, under the gold, formed during the chemical etching procedure. The width of the semi-insulating layer was estimated to be around 300-400 Å, using Cowley's theory (1967).

The forward I-V characteristics of most of the Schottky diodes with reasonably satisfactory ohmic contacts were approximately exponential. The forward characteristics shifted slightly to higher applied biases as the sulphur concentration in the mixed crystals increased. This may have been due to the increase in the barrier height in the metal-insulator-semiconductor junction with increasing sulphur concentration. Again, the larger leakage currents at low voltage and the onset of hole injection at high forward bias, makes it difficult to understand the current transport mechanism in these devices. The reverse I-V characteristics were also influenced strongly by the semi-insulating layer between the gold and the mixed crystals. The nearly exponential variation at high current levels might suggest that tunneling currents are operative at high applied fields. However the overall picture of current transport across these junctions is by no means clear.

8.5.2 Mechanism of EL

In Schottky devices formed on chemically cleaned dice the barrier heights were around 1.6-1.8 eV. This together with the calculated uncompensated donor concentration of about $10^{15} - 10^{17} \text{ cm}^{-3}$, would give rise to a value of $\left| \mathcal{E}_{\text{max}} \right|_{V=0}$ of about 10^5 V cm^{-1} or more in the depletion region. Therefore in reverse bias when the electrons are injected into semiconductor either by thermal activation over, or tunnelling through the barrier, they accelerate in the high field region and achieve sufficient energies to impact excite the S.A. or

characteristic luminescence (i.e. Mn^{2+}) centres and the EL emission observed. In forward bias, the chemically deposited semi-insulating layer under the gold is believed to enhance the injection of holes into the mixed crystal and EL is then observed following the recombination of free electrons and holes. In some diodes the $B \propto i^n$ relation with n equal 1.5 - 1.6 was obeyed in the forward direction, supporting the suggestion of hole injection. With some devices, especially those formed on mixed crystals grown by vapour transport, the application of two symmetric indium contacts on to a die with resistive layers on its skin led to good EL emission being obtained. The mechanism of the EL in such devices is difficult to explain. However there may be some sort of a $n-n^+$ junction present in the bulk of the crystal with resistive layers close to the surface. The strength of the field in the $n-n^+$ junction would strongly depend on the difference of the work function in both the n or n^+ regions. The built in potential in this junction is believed to lie mostly in the n^+ region and the magnitude of the built-in potential can be roughly thought to be the difference in the energy of Fermi levels in the n and n^+ regions. The strength of the electric field in this junction is probably too small to initiate an impact excitation process. It is possible that there are some shallow donor levels in the mixed crystals, some of which are thermally ionized, while slightly deeper donor levels are not. It is suggested that these second deep donor levels can be ionized in the presence of a sufficiently large electric field. Lanczos (1930,1931) calculated that a field of $7 \times 10^5 \text{ V cm}^{-1}$ was necessary to ionize atomic hydrogen from the state $n = 5$ which is 0.54 eV deep. The nature of the donor levels in mixed crystals has not been studied fully but it is reasonable to assume that they lie in the energy range from 0.03 eV (in ZnSe) to 0.1 eV (in ZnS, see for example Kukimoto et al, 1968) so that field ionization would be

possible at lower fields. Therefore on application of the bias, the field strength in the depletion region in the n^+ region would increase until it reached a level when the deeper donor levels start to empty by field ionization. This increases the built-in potential and hence the field in the n^+ region increases. This chain reaction allows the field to increase to a level where injected electrons are accelerated to sufficient energies to excite the luminescent centres by impact.

At low applied biases the current will be limited by the thin resistive surface n -layers. But as the field increases in the n^+ depletion region the electrons tunnel through this thin layer and reach the n^+ region where they are accelerated to energies high enough for impact excitation and eventually for ionization of the lattice. Then an even more rapid increase in the current is observed.

This model can also be used to explain the mechanism of EL in the Au-ZnS-In devices. In reverse bias (gold negative) the field in the ZnS may well be enhanced by the field ionization of shallow donors. However in the forward direction (indium negative), an $n-n^+$ junction may form under the indium contact. As the bias increases a similar field emission of deep donor impurities could be responsible for the luminescence under the indium contact. At even higher biases light also originated from the anode. This is not surprising because at these biases, hole injection from the gold into the ZnS through a thick semi-insulating interfacial layer could readily occur.

8.5.3 Luminescent transitions involved in ZnS_xSe_{1-x} diodes

The PL emission spectra of $Zn(S,Se)$ phosphors containing sulphur have been studied by several authors, e.g. Leverenz (1950), Klasens (1953)

and Morehead (1963). All these authors varied the S/Se ratio in a few big steps from ZnS to ZnSe and all agree that the gradual increase in the selenium concentration in the Zn(S,Se) system causes a gradual and steady change of the copper green emission in ZnS to a copper red emission in ZnSe. A corresponding investigation of the copper blue emission has been carried out by Halsted et al (1965), and they also suggested a steady shift from blue (in ZnS) to green (ZnSe). Lehmann (1966) observed both blue (2.79 eV) and green (2.35 eV) bands in ZnS:Cu,Cl phosphors which shifted to the green (2.34 eV) and red (1.95 eV) bands in ZnSe respectively. Lehmann (1967) had also investigated the SA emission from Zn(S,Se):halides in PL. He observed the blue SA emission in ZnS at 2.61 eV. When 1% sulphur was replaced by selenium, the green band at about 2.3 eV appeared as a shoulder. The blue band then decreased in intensity and the green band shifted to lower energies to 2.0 eV in ZnSe. Ozawa and Hersch (1973) have studied the PL emission from Zn(S,Se):I single crystals. The results they obtained from as-grown crystals annealed in molten zinc were similar. They found that the blue SA emission in ZnS jumped to green when a small quantity of sulphur was replaced by selenium. The luminescence transition for the SA emission was suggested by Lehmann (1967) to be of the Schon-Klasens type

The PL emission spectra of our mixed crystal diodes were also examined. In diodes with both iodine and aluminium impurities, the orange PL emission of ZnSe changed to yellow steadily as the sulphur concentration in the mixture was increased, see Figure 8.27. This situation did not change appreciably until the sulphur content exceeded 70%, when there was a more rapid shift to higher photon energies. To achieve a good green emission in PL it is necessary to have 80% sulphur in the solid solution. However to obtain a blue emission one needs as much as 90% sulphur in the mixture. One interesting feature is that

the SA emission in ZnSe shifts to lower energies on cooling, whereas this shift is in the opposite direction for almost all the other compositions in the mixed crystals. As the sulphur concentration is increased, the PL emission bands become broader and the high energy tails of the emission extended to progressively higher energies, although no shift in the low energy tails was observed, see Figures 8.21 and 8.22.

In REL the same general pattern appeared with slight differences of detail. The orange REL emission in ZnSe:I,Zn.Al shifted to higher energies slowly as the sulphur concentration increased. The REL emission bands were rather broad compared with the PL bands. At 295 K the REL maxima occurred at slightly lower photon energies than in PL. However at 85 K the peak energies were well in excess of those of the PL emissions, see Figure 8.20 and 8.27. The blue (2.63 eV) FEL emission in the Au-ZnS:I,Zn+Al-In device at 295 K jumped to green (2.43 eV) when as little as 2% of sulphur was replaced by selenium, thereafter the green band shifted gradually to yellow and then to orange as the selenium concentration in the mixture was increased gradually. At 85 K, the FEL emission from most of the mixed diodes exhibited two distinct bands in the yellow and green regions. The FEL emission was yellow (2.15 eV) in ZnSe:I,Zn+Al diodes with a slight shoulder in the green. Replacing about 13% of selenium with sulphur causes both yellow (2.15 eV) and green (2.3 eV) bands to appear. As the sulphur concentration was increased the green band shifted to higher energies slightly and the net result is that the overall emission band became very wide. This situation did not change appreciably until the sulphur content exceeded 60% when there was a rapid shift from green to blue emission, see part (b), Figure 8.20.

The luminescence of manganese doped mixed crystals was similar to that obtained with ZnSe:Mn. The EL in both $\text{ZnS}_{0.6}\text{Se}_{0.4}:\text{I,Mn,Zn+Al}$ and $\text{ZnS}:\text{I,Mn,Zn+Al}$ was contained in a comparatively narrow band at 2.12 eV. This emission corresponded to the ${}^4\text{T}_1 - {}^6\text{A}_1$ transition.

The PL emission in $\text{ZnS}_{0.6}\text{Se}_{0.4}:\text{I,Mn,Zn+Al}$ and $\text{ZnS}:\text{I,Mn,Zn+Al}$ devices exhibited slightly broader bands. This may be due to the contributions of the yellow SA emissions in these crystals. The interesting features of the EL and PL emission spectra of these diodes were that no green or blue SA emissions were observed. This may be because the manganese excitation bands lie in the green and blue regions of the spectrum (see Figure 8.30) and the green and blue SA emission bands in these materials could actually be used to excite manganese centres directly. Finally, the luminescence excitation spectra of mixed crystals containing manganese (see Figure 8.30) exhibited no shift in the position of the first excited state as the sulphur concentration increased. However there was a slight shift to higher energies with the second, third and fourth excited states. This would mean that the crystal field in cubic $\text{ZnS}_x\text{Se}_{1-x}$ crystals may have an effect on the second, third and the fourth excited states of Mn^{2+} ions, but not on the first one (${}^4\text{T}_1$).

CHAPTER 9

CONCLUSION

9.1 SUMMARY OF RESULTS

The aim of the research reported in this thesis was to investigate whether electroluminescent devices could be prepared on single crystals of ZnSe, ZnS and Zn(S,Se) in an attempt to produce red, yellow, green and blue light emitting diodes.

Cubic ZnSe crystals containing added impurities such as Mn, Cu, Al, Ga and Cl were grown successfully using a vapour phase technique. This method could only be used to grow single crystals of $\text{ZnS}_x\text{Se}_{1-x}$ with values of x up to 0.6 at least. However homogeneous and single crystals of $\text{ZnS}_x\text{Se}_{1-x}$ were grown successfully for all compositions using the iodine transport technique. Manganese was also introduced successfully into mixed crystals grown by iodine transport and the results proved successful.

The production of electroluminescent diodes involved the treatment of the crystals of interest in molten zinc or in a molten mixture of zinc and aluminium. This process reduced the resistivity of the crystals to the range 1-1000 ohm cm. Most of the electroluminescent devices studied here were in the form of Schottky barrier diodes. The rectifying contact was deposited on a cleaved or chemically cleaned surface of a crystal by vacuum evaporation of gold. Ohmic contacts to ZnSe were provided by indium metal. Indium metal also provided satisfactory ohmic contacts to $\text{ZnS}_x\text{Se}_{1-x}$ crystals with compositions with values of x up to 0.8. However it became increasingly difficult to prepare indium ohmic contacts on mixed crystals containing higher sulphur concentrations.

The electrical properties and the device parameters of the ZnSe diodes were studied in detail. Nearly ideal Schottky barriers were

formed on cleaved surfaces of ZnSe crystals. The long wavelength threshold of the short-circuit photocurrent gave a direct measure of the barrier height in the Au-ZnSe system. The value of the barrier height was 1.36 eV in cleaved and 1.63 eV in chemically etched surfaces. The values of the barrier heights obtained from plots of C^{-2} against V were higher than values obtained from the photothresholds, and this was taken to indicate that a semi-insulating layer existed between the gold and semiconductor. Measurements of the equivalent parallel conductance of the ZnSe, MIS diodes have shown that the density of surface states lying near the middle of the band gap of zinc selenide is very low, at about 10^{10} states $\text{cm}^{-2} \text{eV}^{-1}$, some 1.36 eV below the conduction band in cleaved crystals. One result of the low density of surface states in ZnSe, is that straight forward C-V measurements do not introduce serious error into the derived values of the uncompensated donor concentrations provided that the measurements are made at sufficiently high ($f \geq 200$ kHz) frequencies. It should also be emphasized that the magnitude of the surface state densities reported here is totally inadequate to pin the Fermi level at the free surface of ZnSe; a density of about 10^{13} states $\text{cm}^{-2} \text{eV}^{-1}$ would be required for that purpose. Mead (1966) has observed that the barrier heights formed by the deposition of various metals on to ZnSe and ZnS in u.h.v. showed a linear variation with the difference in electronegativities between zinc and the metal in question. Clearly no pinning of the Fermi level, by surface states occurred and this is taken to indicate that surface states were virtually non-existent in the middle of the band gaps of ZnSe and ZnS. This of course is in complete agreement with our observation on ZnSe. Using Cowley's (1966) theory, the width of the interfacial semi-insulating layer was found to be about 14 \AA for cleaved diodes and about 200 \AA or more in chemically cleaned diodes.

The forward current-voltage characteristics obtained from cleaved and chemically cleaned ZnSe diodes showed that the transport process was mainly governed by thermionic emission over the barrier. However the reverse bias current-voltage characteristics were somehow obscured by the presence of the interfacial layers. The results would suggest that in reverse bias the electrons are injected into ZnSe both by thermal activation and by tunnelling through the barrier.

The electrical properties and device parameters for $\text{ZnS}_x\text{Se}_{1-x}$ electroluminescent devices were also studied. The photothreshold values of the barrier height for chemically etched Au- $\text{ZnS}_x\text{Se}_{1-x}$ diodes were somewhat higher than in ZnSe at around 1.8 eV for Au- $\text{ZnS}_{0.6}\text{Se}_{0.4}$. Again higher values of V_i measured from the C^{-2} -V plots indicated the presence of a semi-insulating interfacial layer of about 300 Å thick between the gold and the sulpho-selenide. Although current-voltage characteristics were studied the presence of interfacial layers, and leakage currents, and the difficulty in producing perfect ohmic contacts made it difficult to understand the actual current transport mechanism at the junction.

The injection EL observed in forward biased junctions was involved with the hole injection across thick (≥ 200 Å) interfacial layers into ZnSe or $\text{ZnS}_x\text{Se}_{1-x}$ at the anode. Edge emission, namely exciton and pair emission has been studied in FEL and PL from ZnSe diodes. The exciton emission was only observed in FEL and did not appear in REL and PL (UV). This suggests that the exciton emission in conducting ZnSe samples can only be achieved with flat energy bands at the surface of the semiconductor. The study of exciton emission in the temperature range from 20 - 360 K has indicated that excitons became bound to neutral donors or acceptors at temperatures below 65 K. At high temperatures they remain free. 'Blue' EL from ZnSe, at room temperature, was thus achieved in the form of bright spots localized around the anode,

resulting from free exciton emission. Donor-acceptor pair emission was also observed in FEL and PL at low temperatures. The sum of the donor and acceptor ionization energies ($E_a + E_d$) involved in these transitions was calculated to be around 139 - 147 meV.

The intensity of the edge emission in FEL and PL from crystals doped with donor impurities decreased gradually as the impurity content increased, and the blue edge emission was replaced by the yellow-orange SA emission. The SA emission in ZnSe is located at about 2.1 eV (5900 Å). Some confusion may arise when small quantities of unintentionally added copper centres are present together with the SA centres. However the SA emission undoubtedly swamped any copper emission in our ZnSe diodes containing high donor impurity concentrations (i.e. $N_d \geq 10^{17} \text{ cm}^{-3}$). In general the SA emission bands excited in three different ways, namely FEL, PL(UV) and REL, were similar, although the production of hot electrons in REL causes broadening with long tails extending to the high energy end of the spectrum.

The SA emission in $\text{ZnS}_x\text{Se}_{1-x}$ diodes was also investigated. The results obtained in PL and FEL indicate that the yellow-orange SA emission in ZnSe shifted gradually to green and then to blue as the selenium was replaced by sulphur. There are some indications that the yellow emission in ZnSe shifts only slightly, but the green band in ZnSe shifts to higher energies gradually as the sulphur content is increased. This suggestion is supported by the luminescence excitation spectra. The REL emission spectra were found to be broader than FEL and PL emission spectra in mixed crystal diodes. This broadening is probably attributable to hot electrons.

The optimum composition for a green emitting (5450 Å) device in mixed crystals was $\text{ZnS}_{0.6}\text{Se}_{0.4}$. Reverse biased Schottky barrier

devices gave a brightness of 200 Ft-L with a power conversion efficiency around $1 \times 10^{-3}\%$. However to obtain a blue emitting device the sulphur concentrations needed in the mixture were in excess of 90%. With blue (4800 Å) emitting ZnS devices, a maximum brightness of 300 Ft-L was achieved at a conversion power efficiency around $10^{-3}\%$. A mechanism, involving impact excitation at the cathode (stimulated by the field ionization of shallow electron traps) in series with hole injection through an interfacial layer at the anode was suggested to be responsible for the electroluminescence in the sulphur-rich devices.

Luminescent centres such as manganese or copper, or both, were also introduced into ZnSe crystals. An optimum brightness of 800 Ft-L, with a conversion power efficiency approaching to $10^{-2}\%$ was obtained from reverse biased ZnSe:Mn diodes. The characteristic manganese emission in EL lay at 5785 Å. From the variation of the half width of the Mn⁺⁺ band with temperature a phonon energy of 28 meV was found for the lattice interaction with the manganese ion. This was slightly lower than the LO phonon energy of about 31 meV. The emission from ZnSe:Mn diodes may consist of manganese or SA emission or both. In reverse bias the manganese emission appears preferentially. However in forward bias EL and in photoluminescence where free carriers are plentiful, Auger de-excitation can occur (Allen et al 1973, Jones and Woods 1973) and the SA emission is then observed. Manganese, as a luminescent centre, was also introduced into $\text{ZnS}_x\text{Se}_{1-x}$ and ZnS crystals. The EL and PL emission again exhibited the characteristic yellow manganese emission at 5830 - 5860 Å. Brightnesses up to 100 Ft-L were obtained from these devices. The short-circuit photocurrent obtained from $\text{ZnS}_x\text{Se}_{1-x}:\text{Mn}$ diodes suggested that the ground state of the Mn²⁺ ion may be tied to the conduction band of the mixed crystals, with the first excited 4T_1 (4G)

state close, and slightly below the conduction band. Furthermore the luminescence excitation spectra of these crystals suggest that the cubic crystal field of $\text{ZnS}_x\text{Se}_{1-x}$ although not affecting the first excited state 4T_1 (4G) does affect the second 4T_2 (4G), third ${}^4A_1, {}^4E$ (4G) and fourth excited states slightly.

Introduction of copper into ZnSe as a luminescent centre leads to a red emission in both EL and PL. However a red output at 6400 Å at an optimum brightness of 200 Ft-L was achieved in reverse biased ZnSe:Cu,Mn,Cl diodes. The conversion power efficiencies of these red emitting diodes were around $1.5 \times 10^{-3}\%$.

Finally several ZnSe:Mn diodes have been run in reverse bias on life test for periods up to 1000 hours. The results obtained show that two major physical changes occur: the width of the semi-insulating layer increases and the uncompensated donor concentration in the barrier region decreases. It is clearly shown that the changes in the device parameters which take place during ageing are responsible for the observed changes in the light output. In conclusion it must be emphasized that the increase in the light output and power conversion efficiency of a cleaved diode over 1000 hours operation demonstrates that electro-luminescent ZnSe:Mn diodes can be made to last for lengths of times which practical applications would demand. Even the performance of the etched diodes is promising since they were driven very hard on life test, were not encapsulated and still had a brightness of 200 Ft-L after 1000 hours.

9.2 Future Work

In order to understand and identify the mechanisms involved in the various luminescence processes, time resolved spectroscopy would be invaluable. Pair recombination for example can be recognized by a shift in the wavelength of the emission with time after the excitation pulse.

A study of electroluminescent diodes, described in this thesis, by time resolved spectroscopy should be experimentally rather simple to carry out.

Although exciton emission was observed in few of the ZnSe diodes, it might be of interest to investigate the exciton emission further at low temperatures to determine the energy depths of such shallow donors as Cl, I, Al, Ga, In and acceptors such as Cu, Ag, Au etc.

With regard to the electrical measurements, the presence of a semi-insulating layer between the gold and the selenide in etched diodes was found to have a crucial effect. The physical and electrical changes in this interfacial layer were the principal reason for the change in EL light output during prolonged operation. It may be of interest if some other insulators with known physical and electrical properties (i.e. SiO₂, Y₂O₃ etc.) are deposited between the gold and the selenide.

The electroluminescent devices formed on the mixed ZnS_xSe_{1-x} crystals gave promising results in the quest for green and blue light emitting diodes. However their electrical properties could not be investigated in detail. Firstly, a detailed study of the formation of perfect ohmic contacts on these crystals is needed. Secondly Hall effect measurements to study the bulk mobilities would be valuable in determining the current transport mechanisms.

The studies of the luminescent emission and excitation spectra on ZnS_xSe_{1-x}:Mn diodes could be extended to lower temperatures (4 K) to determine the phonon side bands involved with the characteristic luminescent transitions taking place in localized Mn²⁺ ions.

Finally the photo-capacitance technique can be a valuable tool with which to study the deep lying impurity centres in Schottky barriers on ZnS_xSe_{1-x}.

REFERENCES

- Addamiano A and Dell P A (1957) J. Phys. Chem. Vol.61 pp120
- Aigrain P. and Balkanski M (1961) Selective Constants Relative to Semiconductors Perm. Press Paris
- Allen J W (1964) Proc. 7th Int. Conf. Phys. of Semicon. Paris pp.781-86
- Allen E T and Crenshaw J L (1912) Am. J. Sci. Vol. 34 p.310
- Allen J W, Livingstone A W and Turvey K (1972) Sol. St. Electron 15 1363
- Allen J W, Ryall M D and Wray E M (1973) Phys. Stat. Sol. (A) 17 K101
- Andrews J M and Lepsetter M P (1970) Sol. St. Electron. 13 1011
- Apperson J, Vorobiov Y and Garlick G F J (1967) Br. J. Appl. Phys. 18 389
- Arizumi T and Hirose M (1969) Japan J. Appl. Phys. 8 749
- Atalla M M (1966) Proc. Munich Symp. on Microelectronics Munich Oldenburh pp.123-57
- Aven M (1965) Appl. Phys. Lett. 7 146
- Aven M (1967) II-VI Semiconducting Compounds ed. D G Thomas New York Benjamin pp.1232-59
- Aven M (1971) J. Appl. Phys. 42 3 p.1204
- Aven M (1973) J. Luminescence 7 195
- Aven M, Marple D T F and Segal B (1961) J. Appl. Phys. Suppl. 32 2251
- Aven M and Woodbury H H (1962) Appl. Phys. Lett. Vol.1 No.3 p.53
- Aven M and Segal B (1963) Phys. Rev. 130 81
- Aven M and Cusano D A (1964) J. Appl. Phys. 35 3 606
- Aven M and Halsted R E (1965) Phys. Rev. 137 228A
- Aven M and Mead C A (1965) Appl. Phys. Lett. 7 8

- Aven M and Prener J S (Edits.) (1967) Physics and Chemistry of
II-VI Compounds North Holland Pub. Co.
- Azano S and Nakao Y (1964) J. Appl. Phys. Japan 3 137
- Bardeen J and Shockley W (1950) Phys. Rev. 80 72
- Berg A A and Dean P J (1972) Proc. IEEE 60 156
- Bergstresser T K and Cohen M L (1967) Phys. Rev. Vol. 164 p.1069
- Berlincourt D, Jaffe H and Shiozawa L R (1963) Phys. Rev. 129 1009
- Bethe H A (1942) MIT Radiation Lab. Report 43-12
- Beserman R and Balkanski (1971) Phys. Stat. Solidi 44 535
- Biter W J, Indradev and Williams F (1969) J. Phys. Chem.
Sol. 30 503
- Bjerkeland H and Holweck I (1972) Phys. Norv. 6 139
- Blount G H, Fisher M W, Morrison R G and Bube R H (1966)
J. Electrochem. Soc. 113 690
- Braun S, Grimmeis H G and Allen J W (1972) Phys. Stat. Solidi
(a) 14 527
- Brooks H (1955) Advances in Electronics and Electron Phys. 7 156
- Bryant F J and Manning P S (1974) J. Phys. Chem. Sol. 35 97
- Bundel A A, Guretskaya Z I and Noskova M N (1961) Optics and
Spect. 11 352
- Burr K F and Woods J (1971) J. Cryst. Growth Vol.9 p.183
- Card H C and Rhoderick E H (1971) J. Phys. D. Appl. Phys. 4 1589
- Card H C and Smith B L (1971) J. Appl. Phys. 42 5863
- Cardona M (1961) J. Appl. Phys. Suppl. 32 2151
- Chan F N and Park Y S (1964) Bull. Am. Phys. Soc. (2) Vol.9 p.296
- Chatterjee P K, Rosa A J and Streetman B G (1973) J. Luminescence
8 176
- Chistyakov I D and Krucceanu E (1961) Rev. Phys. Vol.6 p.211
- Clark L and Woods J (1968) J. Cryst. Growth Vol.3 p.127

- Cohen M L and Bergstresser T K (1966) Phys. Rev. 141 p.789
- Consigny R L and Madigan J R (1970) Sol. Stat. Electron. 13 113
- Conwell E M and Weisskopf V F (1950) Phys. Rev. 77 388
- Cowley A M (1966) J. Appl. Phys. 37 8 3024
- Crowell C R, Spitzer W G, Howarth L E and Labate E E (1962)
Phys. Rev. 127 2006
- Crowell C R and Sze S M (1966) Sol. St. Electron. 6 445
- Crowell C R and Rideout V L (1969) Sol. St. Electron. 12 89
- Cullity B D (1967) Edit. The elements of x-ray diffraction
Addison-Wesley Pub. Co.
- Curie G and Curie D (1960) J. Phys. Rad. Vol.21 p.127
- Cutter J R and Woods J (1975) J. Phys. D. Vol.8 p.314
- Cutter J R, Russell G J and Woods J (1976) J. Cryst. Growth 32 179
- Dean P J and Merz J L (1969) Phys. Rev. 178 3 1310
- Destriau G (1936) J. Chem. Phys. 33 587
- Devlin S S (1967) Phys. and Chem. of II-VI Comp. ed M Aven and
J S Prener North Holland Pub. Co. Ltd. Ch.11
- Dexter D L and Seitz F (1952) Phys. Rev. 86 964
- Dexter D L, Klick O C and Russell G A (1955) Phys. Rev. Vol.100
No.2
- Dietz R E, Hopfield J J and Thomas D G (1961) J. Appl. Phys.
32 10 2282
- Erginsoy C (1950) Phys. Rev. 79 6 1013
- Ewles J (1938) Proc. Roy. Soc. A Vol.167 p.34
- Fischer A G (1958) Z. Naturforsh Vol.13a p.2549
- Fischer A G (1959) Electrochem. Soc. Vol.106 No.9 p.838
- Fischer A G (1964) Phys. Lett. 12 313
- Fischer A G (1964) Radiative Recombination in Semiconductors p.259
Dunod Paris

- Fischer A G (1966) 'Electroluminescence in II-VI Compounds'
Luminescence of Inorganic Solids P Goldberg Edit. Acad. Press
New York pp.541-602
- Fischer A G and Moss H I (1963) J. Appl. Phys. 34 2112
- Fitzgerald A G, Mannami M, Pogson E H and Yoffe A D (1966)
Phil. Mag. 19 197-200
- Fowler R H (1931) Phys. Rev. 38 45
- Fukuda Y and Fukai M (1967) J. Phys. Soc. Japan 23 902
- Fuller M L (1929) Phil. Mag. Vol.8 p.658
- Fujiwara S and Fukai M (1966) J. Phys. Soc. Japan 21 1463
- Georgobiani A N and Steblin V I (1967) Sov. Phys. Semiconductor
1 772
- Gezci S (1973) Ph.D. Thesis University of Durham
- Gezci S and Woods J (1972) J. Mat. Sci. 7 603
- Gezci S and Woods J (1975) J. Luminescence 10 267
- Gill R W A and Rothschild S (1960) Enlarges Abst. Electrochem.
Soc. Electronics Div.9 72
- Gol'dman A G, Korolko B N and Lysenko S F (1968) J. Appl.
Spectroscopy 8 6 571
- Goodman A M (1963) J. Appl. Phys. 34 2 329
- Green L C, Reynolds D C, Czyzak S J and Baker W M (1958)
J. Chem. Phys. Vol.29 p.1375
- Grimmeis H G (1974) Proc. Con. on Metal-Semicon. Contacts
Inst. of Phys. 22 3
- Gross E F, Permogrow S A and Razbirin B S (1966) Fiz. tverd.
tela 8 1483. Sov. Phys. Sol. Stat. 8 1180 (1966) : J. Phys.
Chem. Sol. 27 1647 (1966)

- Haeri S Y and Rhoderick E H (1974) 'Metal-Semiconductor Contacts'
84 Inst. of Phys. Con. Ser. No.22
- Halsted R E, Lorentz M R and Segal B (1961) J. Appl. Chem. Sol.
22 109
- Halsted R E and Aven M (1965) Phys. Rev. Lett. 14 64
- Halsted R E, Aven M and Coghill H G (1965) J. Electrochem. Soc.
112 177
- Harrison W A (1956) Phys. Rev. Vol.101 3 903
- Hartmann H (1960) Fortschr. Mineral Vol.38 p.185
- Hartmann H (1962) Phys. Stat. Sol. Vol.2 p.585
- Heiland M and Mollwo H (1959) Sol. Stat. Phys. Vol.8 p.191
- Henisch H K (1957) 'Rectifying Semiconductor Contacts' (Oxford
Clarendon)
- Henisch H K (1962) Electroluminescence Pergamon Press Oxford
- Herring C (1954) Phys. Rev. 96 1165
- Hite G E, Marple D T F, Aven M and Segal B (1967) Phys. Rev.
156 p.850
- Holton W C, Wit M. De and Estle T L (1965) Int. Symp. Luminescence
(Karl Theimig K G Munich) p.454
- Howarth D J and Sondhemier E H (1953) Proc. Roy. Soc. (London)
219 53
- Iida S (1968) J. Phys. Soc. Japan 25 1 177
- Iida S (1969) J. Phys. Soc. Japan 26 5 1140
- Indradev and Garlick G F J (1967) Brit. J. Appl. Phys. 18 1
- Ivey H F (1963) Electroluminescence and related effects, Advances in
Electronics and Electron Physics Suppl.1 L. Manton Edit.
Academic Press New York
- Jones G (1973) Ph.D. Thesis University of Durham

- Jones G and Woods J (1973) J. Phys. D. Appl. Phys. 6 1640
- Jones G and Woods J (1974) J. Lumin. 9 389
- Jones G and Woods J (1976) to be published
- Kane E O (1957) J. Phys. Chem. Sol. 1 249
- Kaufman R G and Dowbar P (1974) J. Appl. Phys. 45 10 4487
- Klasens H A (1946) Nature 158 306
- Klasens H A (1953) J. Electrochem. Soc. 100 72
- Klick C C (1953) Phys. Rev. Vol.89 No.1 p.274
- Klick C C and Shulman J H (1957) Sol. St. Phys. 5 97
- Kroger F A (1940) Physica Vol.7 p.1
- Kukimoto H, Shionoya S, Koda T and Hioki R (1968) J. Phys. Chem. Sol. 29 935
- Kurik M V (1967) Phys. Lett. 24 A 742
- Lambe J J and Klick C C (1955) Phys. Rev. 98 5 909
- Lanczos C (1930) Z. Phys. 62 518
- Lanczos C (1931) Z. Phys. 68 204
- Langer D and Ibuki S (1965) Phys. Rev. 128 A 809
- Langer D W and Richer H J (1960) Phys. Rev. 146 2 554
- Larach S (1953) J. Chem. Phys. Vol.21 p.756
- Larach S, Shrader R E and Stocker C F (1957) Phys. Rev. Vol.6 p.211
- Larach S and Shrader R E (1959) R.C.A. Rev. 20 532
- Lehmann W (1966) J. Electrochem. 113 5 449
- Lehmann W (1967) J. Electrochem. Soc. 114 1 83
- Lempicki A, Birman J, Samelson H and Neumark G (1961) Proc. Inter. Conf. Semiconductor Phys. Prague (1960) pp.768-770
- Leverenz H W (1950) An introduction to luminescence of solids Wiley New York (1950)
- Livingstone A W, Turvey K, and Allen J W (1973) Sol. Stat. Electron. 16 351
- Lohovec K, Accando C A and Jamgochian E (1951) Phys. Rev. 83 603

- Lohovec K, Accando C A and Jamgochian E (1953) Phys. Rev. 89 20
- Lorenz M R (1967) Aven and Prener (1967) Chap. 1
- Lossev O V (1923) Telegrafija i telefornia 18 61
- Mandel G (1964) Phys. Rev. 134 A. 1073
- Markovskii L Ya, Mironov I A and Ryzhkin S Yu (1969) Opt. and Spectrosc. 27 84 and Bull. Acad. Sci. U.S.S.R. Phys. Ser. (USA) 33 (1968)
- Marple D T F (1964) J. Appl. Phys. 35 1879
- Martin P G (1970) M.Sc. Thesis University of Durham
- McClure D S (1963) J. Chem. Phys. 39 2850
- Mead C A (1965) Phys. Lett. 18 218
- Mead C A (1966) Sol. Stat. Electron. 9 1023
- Merz J L, Kukimoto H, Nassau K and Shiver J W (1972) Phys. Rev. B 6 545
- Morehead F F (1963) J. Phys. Chem. Sol. 24 37
- Morehead F F (1967) 'Electroluminescence in II-VI compounds' Phys. and Chem. of II-VI compounds M. Aven and J S Prener Edits. North Holland Amsterdam
- Motossi F, Leutwein K and Schmid G S (1966) Z. Naturforsch 21 A461
- Mott N F (1940) Electronic Process in Ionic Crystals N F Mott and R W Gurney (Oxford U.P.) Ed. (1957) p.221
- Narita S (1960) J. Phys. Soc. Japan 15 128
- Narita K, Watanave H and Wada M (1970) Jap. J. Appl. Phys. Vol.9 p.1278
- Nelson J B and Riley D B (1945) Proc. Phys. Soc. 57 160
- Nicollian E H and Goetzberger A (1967) The Bell Sys. Tech. J. V. XLVI 6 1055
- Nitsche R (1960) J. Phys. Chem. Sol. 17 163

- Orgel L E (1955) J. Chem. Phys. Vol.23 No.6 p.1004
- Ozawa L and Hersh H N (1973) J. Electrochem. Soc. 938
- Özsan M E and Woods J (1974) J. Appl. Phys. Lett. 25 489
- Özsan M E and Woods J (1975) Sol. Stat. Electron. 18 519
- Padovani F A and Stratton R (1966) Phys. Rev. Lett. 16 1202
- Park Y S, Geesner C R and Shin B K (1972) Appl. Phys. Lett. 21
- Park Y S and Shin B K (1974) J. Appl. Phys. 45 3 1444
- Park Y S and Shin B K (1974) J. Appl. Phys. 45 3 74
- Parmenter R H (1955) Phys. Rev. V. 100 p.573
- Pashinkin A S, Tishchenko G N, Korneeva I V and Reyzhenko R N
(1960) Krystallografiya Vol.5 p.261
- Pauling L (1960) The nature of the chemical bond 3rd Edt.
Cornel U.P. New York
- Pedrotti L S and Reynolds D C (1960) Phys. Rev. Vol.120 No.5 p.1664
- Piper W W (1953) Phys. Rev. 92 23
- Piper W W and Williams F E (1952) Phys. Rev. 87 151-2
- Piper W W and Polish S J (1961) J. Appl. Phys. Vol.32 p.1273
- Plumb J L (1971) Jap. J. Appl. Phys. 10 3 326
- Prener J S and Williams F E (1956) J. Chem. Phys. 25 361
- Prener J S and Weil D J (1959) J. Electrochem. Soc. 106 409
- Ray B (1969) Edit. II-VI Compounds Pergamon Press
- Reinberg A R, Holton W C, M. de Wit and Watts R K (1971) Phys.
Rev. B3 410
- Reynolds D C and Czyzak S J (1950) Phys. Rev. Vol.79 p.543
- Reynolds D C, Pedrotti L S and Larson O W (1961) J. Appl. Phys.
32 10 2250
- Rhoderick E H (1969) The third Sol. Stat. Con. Exeter
- Rhoderick E H (1970) J. Phys. D. Appl. Phys. 3 1153

- Rhoderick E H (1972) J. Phys. D 5 1920
- Rhoderick E H (1974) Proc. on Metal Semiconductor Contacts
Inst. of Phys. 22 3
- Rodé D L (1970) Phys. Rev. B. 2 10 4036
- Roth W L (1967) Aven and Prener (1967) Chap. II
- Rothschild S (1963) J. Electrochem. Soc. 110 28
- Round H J (1907) Electr. Wld. 19 307
- Russell G J Private Comm.
- Ryall M D and Allen J W (1973) J. Phys. Chem. Sol. 34 2137
- Samelson H (1961) J. Appl. Phys. Vol.32 pp.309-317
- Samelson H (1962) J. Appl. Phys. Vol.33 p.1779
- Schön M (1941) Z. Phys. 119 463
- Schottky W (1938) Natanwiss V 26 p.843
- Schottky W and Spenke E (1939) Wiss. Veroff. Siemens Werke 18 225
- Segal B (1967) Phys. and Chem. of II-VI Compounds Edit. M Aven and
J S Prener North Holland Publ Co. p.41
- Seitz F (1939) Trans Faraday Soc. Vol.35 p.74
- Shionoya S, Era K and Washizawa Y (1966) J. Phys. Japan 21 1624
- Skinner B J and Barton B (1960) Amm. Mineralogist Vol.45 p.612
- Smith R W (1955) Phys. Rev. 100 760
- Smith R W (1957) Phys. Rev. 105 900
- Spenke E (1958) Electronic Semiconductors New York : McGraw-Hill
- Stringfellow G B and Bube R H (1968) Phys. Rev. 171 903
- Stukel D J, Euwena R N and Collins T C (1969) Phys. Rev. 179 740
- Suzuki A and Shionoya S (1971) J. Phys. Soc. Japan V 31 No.5
p.1445
- Swank R K (1966) Phys. Rev. 153 3 p.844
- Swank R K, Aven M and Devine J Z (1969) J. Appl. Phys. 40 1 89

Sze S M, Crowell C R and Kahing D (1964) J. Appl. Phys. 35 2534

Sze S M (1969) Edit. Phys. Semiconductor Devices J Wiley & Sons
New York

Thomas D G and Hopfield J J (1962) Phys. Rev. V 128 p.2135

Turvey K and Allen J W (1973) J. Phys. C. Sol. Stat. Phys. 6 2887

Van Gool W (1961) Philips Res. Reports Suppl. No.3

Vecht A, Werring N J, Ellis R and Smith P J F (1969) Brit. J.
Appl. Phys. D 2 2 953

Wagner C (1931) Phys. Z 32 641

Wheeler R G and Miklosz J C (1964) Proc. 7th Int. Conf. on Phys.
of Semicond. ed M. Hulin p.873

Williams F E (1953) J. Phys. Chem. Vol.57 p.776

Williams R (1962) Phys. and Chem. of Sol. 23 1057

Woodbury H H and Aven M (1962) 7th Int. Conf. Phys. Semicond.
Paris 1964

Yu P W and Park Y S (1973) Appl. Phys. Lett. 22 7 345

Zook D (1964) Phys. Rev. 136 869

